R-09-04

Strategy for thermal dimensioning of the final repository for spent nuclear fuel

Harald Hökmark, Margareta Lönnqvist, Ola Kristensson
Clay Technology AB

Jan Sundberg, Geo Innova AB

Göran Hellström, Neoenergy

December 2009

Svensk Kärnbränslehantering AB
Swedish Nuclear Fuel
and Waste Management Co

Box 250, SE-101 24 Stockholm
Phone +46 8 459 84 00

ISSN 1402-3091
SKB Rapport R-09-04

Strategy for thermal dimensioning of the final repository for spent nuclear fuel

Harald Hökmark, Margareta Lönnqvist, Ola Kristensson
Clay Technology AB

Jan Sundberg, Geo Innova AB

Göran Hellström, Neoenergy

December 2009

Summary

The present report describes a strategy for dimensioning the KBS-3 repository such that the bentonite buffer temperature does not exceed 100°C for any canister deposited at either of the two sites considered for the repository. For both sites, Forsmark and Laxemar, thermal site descriptions exist /Back et al. 2007, Sundberg et al. 2008a, b/. The thermal site descriptions give the rock thermal conductivity and the heat capacity of the different rock domains identified at the sites. For each rock domain, there are distributions of the parameter values on different scales and models for their spatial variability.

The strategy is focused on layout step D2 for which a set of design premises has been specified, e.g. the spacing between tunnels is fixed at 40 m and the initial canister power is set at 1,700 W for all canisters. In addition, there should not be any optimization of the layout, i.e. the canister spacing should be set to the same value everywhere in each rock domain such that the temperature criterion is met for every canister.

The hottest canisters will be those deposited in dry deposition holes in low-conductivity rock in central parts of the deposition areas. The dimensioning parameter is, therefore, the peak buffer temperature in such deposition holes. The problem of calculating the peak buffer temperature in any deposition hole can be resolved into two, largely independent, problems:

1. Calculating the temperature difference between the wall of the deposition hole and the hottest point of the buffer. For dry deposition holes that point will be found at the top of the canister.
2. Calculating the rock wall temperature.

Local buffer/canister solution

A reference evolution of the temperature difference between the rock wall and the hottest buffer point is established by using typical laboratory-scale parameter values of the buffer heat transport properties and properties of open air-gaps combined with field-data from a well instrumented and dry deposition hole in the Prototype Repository at Äspö HRL. The temperature difference can be resolved into two components, both practically independent of the rock properties:

- The temperature drop across the annular space between rock wall and the buffer inner boundary at canister mid-height.
- The net effect of the transport resistance across the air-filled gap between the canister surface and buffer inner boundary and the difference between the top and mid-height canister surface temperatures.

Rock wall temperature and peak buffer temperature

There are two independent methods of rock wall temperature calculation: An analytical and a numerical one. In both methods the rock wall temperature depends on the layout (i.e. canister spacing) and on the rock thermal properties, whereas the details of the conditions in the interior of the deposition holes are unimportant. The peak buffer temperature is found by adding the temperature difference between the wall of the deposition hole and the hottest point of the buffer (the reference evolution) to the rock wall temperature. The most important aspects of the two methods can be summarized as follows:

- The analytical solution can be used for fast and efficient investigations of the thermal evolution of the repository on all scales in time and space.
- The analytical solution can be used to establish nomographic spacing-temperature charts, based on peak temperatures calculated from hundreds of spacing-conductivity combinations.
- The analytical solution does not take the spatial variation of the rock thermal properties into account. Therefore, the use of the analytically obtained nomographic spacing-temperature charts cannot provide more than reasonable approximations, or first guess values, of the spacing required to ensure that the 100°C criterion is met.

- The numerical method takes spatial variations and autocorrelations in the thermal properties, as described in the rock domain thermal models, into account. As opposed to the analytical method, the temperature influence from the backfilled tunnel above the deposition holes is accounted for. It is also possible to account for the temperature dependence in thermal properties.

Margins

There are uncertainties in input data as well as systematic over and underestimates associated with both the local canister/buffer solution and the calculation of the rock wall temperature. Therefore, the dimensioning of the repository, i.e. establishing canister spacing for the different rock domains at a given site, must be made with a margin to the 100°C threshold. The margins presented in the report are conditioned for the numerical method.

In total, the margin adds up to 3.8–6.3°C depending on the thermal conductivity of the rock. The largest individual uncertainty, about 3°C, is related to the heat transport in the interior of the deposition hole.

Strategy – layout step D2

The issue is to determine the canister spacing for the different rock domains. The following steps should be taken to ensure that the temperature criterion is met (cf. flowchart in Figure Su-1):

- The margin to the 100°C threshold temperature is determined (steps 2 and 3 in outline flowchart).
- A nomographic chart (Figure Su-2) is established for the rock domain (step 4 in outline flow-chart) by use of the analytical solution.
- A first guess value of the effective dimensioning domain conductivity is made based on the thermal conductivity distribution suggested for the rock domain on the 5 m scale (step 5 in outline flowchart). The best guess is a value picked from the low conductivity tail (usually 0.1–2 percentile) of the conductivity distribution established for the rock domain.
- A trial canister spacing corresponding to the best guess conductivity is obtained from the nomographic chart (step 5 continued).
- A large number of stochastic realisations of the spatial distributions of the thermal conductivity and heat capacity in the whole rock domain are produced in the thermal site descriptive model (step 6 in outline flowchart).
- A finite difference model of a centrally located tunnel in the rock domain being considered is generated. The spacing is set at the trial value (step 7 in outline flowchart).
- Numerous simulations of the maximum buffer temperature are generated with the numerical model. The simulations are based on a selection of domain model realisations where the concentration of cells with low thermal conductivity around the central canisters is maximized (step 7 continued).
- If the numerical modelling verifies that the maximum peak temperature matches the criterion (with account of the margin for the rock domain), the trial spacing can be established as the reference spacing in the given rock domain. If not, there may be a need to repeat the simulations with modified canister spacing (step 8 in outline flowchart).

Optimization

The strategy described here for the dimensioning of Layout D2, does not include any optimization, i.e. the canister spacing is set schematically to ensure that the 100°C criterion will always be met for central canisters deposited in completely dry deposition holes in worst-case low-conductivity rock. However, the majority of the canister positions will be in volumes of rock that dissipate heat much more efficiently than the low-conductivity rock that controls the layout decisions. There are also hundreds of positions near the tunnel ends that would get buffer temperatures lower than the threshold, regardless of the local heat transport conditions. This means that there is significant room for layout optimizations.

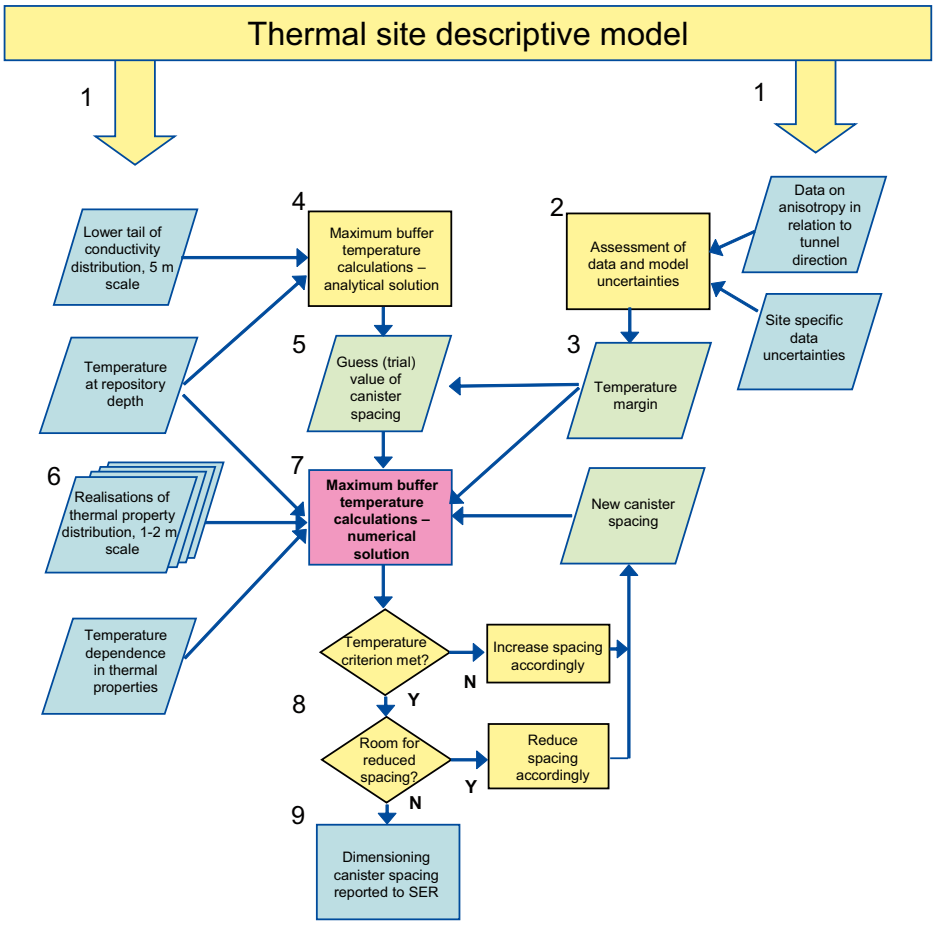

Figure Su-1. *Dimensioning strategy flowchart.*

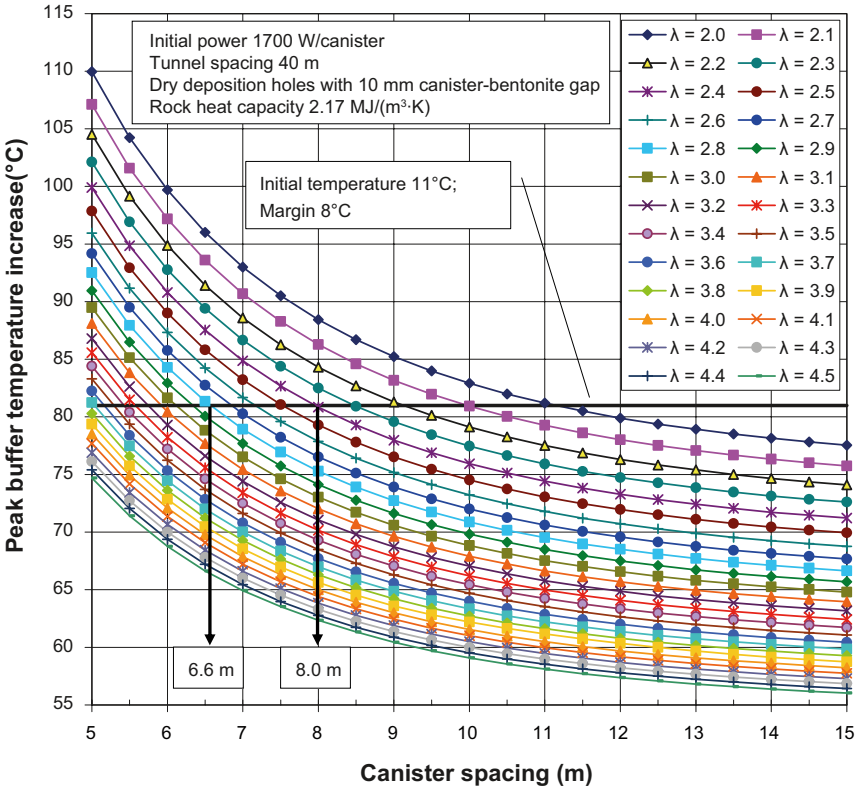

Figure Su-2. *Nomographic spacing-temperature chart.*

One possibility to prepare for an optimization would be to reduce the tunnel spacing and increase the dimensioning minimum canister spacing correspondingly. The canister spacing can then be modified as the construction work progresses and detailed information on the local conditions is obtained.

In addition to spacing modifications, there will be the possibility of controlling and planning the canister production (i.e. the power distribution among the canisters) in order to take advantage of high conductivity positions, tunnel end effects and near-field design improvements.

Sammanfattning

Den föreliggande rapporten beskriver strategin för att dimensionera ett KBS-3-slutförvar så att den maximala bufferttemperaturen inte överskrider 100°C för någon kapsel deponerad på någon av de två platser som kan komma ifråga för slutförvaret. För båda platserna, Forsmark och Laxemar, finns termiska platsbeskrivningar /Back et al. 2007, Sundberg et al. 2008a, b/. De termiska platsbeskrivningarna ger värmeledningstal och värmekapacitet för de olika bergdomäner som identifierats på platserna. För var och en av domänerna anges fördelningar av parametervärden på olika skalor samt modeller för de rumsliga egenskapsvariationerna.

Strategin har fokuserats på Layout D2, för vilken det finns ett antal förutbestämda designkriterier, exempelvis att avståndet mellan tunnlar skall vara 40 m och att den initiella kapseleffekten hos alla kapslar skall vara 1,700 W. Ingen optimering av layouten skall göras, dvs. kapselavståndet i en given bergdomän skall sättas till samma värde överallt så att temperaturkriteriet uppfylls för alla kapslar.

De varmaste kapslarna är de som deponeras i torra deponeringshål i lågkonduktivt berg i de centrala delarna av deponeringsområdena. Den dimensionerande parametern är därför den maximala buffert-temperaturen i sådana deponeringshål. Beräkningen av den maximala bufferttemperaturen i ett god-tyckligt deponeringshål kan delas upp i två, i stort sett, oberoende problem:

1. Beräkning av skillnaden mellan bergväggstemperaturen och temperaturen hos bufferten i den varmaste punkten. I torra deponeringshål kommer den punkten att vara vid kapseltoppen.
2. Beräkning av bergväggstemperaturen.

Inre buffert/kapsellösning

En referensutveckling av temperaturskillnaden mellan bergväggen och den varmaste bentoniten upprättas med användning av typiska laboratoriebestämda parametervärden på värmeledningsegenskaperna hos spalter och buffert, i kombination med fältdata från ett välinstrumenterat torrt deponeringshål i Prototypförvaret i Äspö HRL. Temperaturskillnaden kan delas upp i två komponenter, som är oberoende av bergets egenskaper:

- Temperaturfallet över det cylindriska utrymmet mellan bergvägg och buffertens inre rand vid kapselns höjdcentrum.
- Nettoeffekten av transportmotståndet i den luftfyllda spalten mellan kapselytan och buffertens inre rand samt skillnaden i yttemperatur mellan kapselns topp och höjdcentrum.

Bergväggstemperatur och bufferttemperaturmaximum

Det finns två oberoende sätt att beräkna bergväggstemperaturen – ett analytiskt och ett numeriskt. I båda fallen beror bergväggstemperaturen på layouten (dvs. kapselavstånd) och bergets värmeledningsegen-skaper, medan detaljer i förhållandena i det inre av deponeringshålen är oväsentliga. Den maximala bufferttemperaturen erhålls genom att addera temperaturskillnaden (referensutvecklingen) mellan bergväggen och den varmaste punkten i bufferten till bergväggstemperaturen. De viktigaste aspekterna av de två metoderna kan sammanfattas på följande sätt:

- Den analytiska lösningen kan användas för att snabbt och effektivt beskriva den termiska utvecklingen hos förvaret på alla skalor, i både tid och rum.
- Den analytiska lösningen kan användas för att upprätta kapselavstånd-temperatur-nomogram baserade på maxtemperaturer som beräknats för hundratals kombinationer av kapselavstånd och värmeledningstal.
- Den analytiska lösningen tar inte hänsyn till spatiella variationer i bergets värmeledningsegenskaper. De analytiskt framtagna nomogrammen kan därför inte ge mer än rimliga approximationer, eller första uppskattningar, av de kapselavstånd som behövs för att säkerställa att 100°C-kriteriet uppfylls.

- Den numeriska metoden tar hänsyn till spatiella variationer och spatiella autokorrelationer i både värmeledningstal och värmekapacitet enligt beskrivning i de termiska modellerna för bergdomänerna. I motsats till den analytiska metoden, tar den numeriska modellen hänsyn till effekter av den återfyllda tunneln ovanför deponeringshålen. Det är dessutom möjligt att ta hänsyn till temperaturberoendet hos de termiska egenskaperna.

Marginaler

Det finns osäkerheter samt systematiska över- och underskattningar associerade med både den lokala kapsel-/buffertlösningen och beräkningen av bergväggstemperaturen. Dimensioneringen av förvaret, dvs. att ta fram kapselavstånd för de olika bergdomänerna på en given plats, måste därför göras med marginal till temperaturkriteriet på 100°C. Marginalerna som presenteras i rapporten är optimerade för den numeriska metoden.

Den totala marginalen är 3.8–6.3°C beroende på bergets värmeledningsegenskaper. Den största individuella osäkerheten (omkring 3°C) är relaterad till värmetransporten i det inre av deponingshålet.

Strategi – Layout D2

Syftet är att bestämma kapselavstånd i de olika bergdomänerna. Följande steg skall tas för att säkerställa att temperaturkriteriet blir uppfyllt (se flödesschemat i Figur Sa-1):

- Marginalen till temperaturkriteriet (100°C) bestäms (steg 2 och 3 i flödesschemat).
- Ett nomogram (Figur Sa-2) tas fram för bergdomänen med hjälp av den analytiska lösningen (steg 4 i flödesschemat).
- En gissning av bergdomänens effektiva dimensionerande värmeledningstal görs baserat på fördelningen av värmeledningsegenskaperna på 5 m-skalan i bergdomänen (steg 5 i flödesschemat). Det gissade värdet tas från lågkonduktivitetssvansen (vanligen i 0.1–2-percentilen) av den fördelning som upprättats för domänen.
- Ett kapselavstånd motsvarande det gissade effektiva dimensionerande värmeledningstalet för domänen tas fram med hjälp av nomogrammet (steg 5 fortsatt).
- Ett stort antal stokastiska realiseringar av värmeledningtalets och värmekapacitetens spatiella fördelning produceras i modellen för den termiska platsbeskrivningen för att beskriva variabiliteten i hela bergdomänen (steg 6 i flödesschemat).
- En finit-differensmodell av en centralt belägen tunnel i den aktuella bergdomänen tas fram. Kapselavståndet sätts till det värde som tagits fram med hjälp av nomogrammet (steg 7 i flödesschemat).
- Ett stort antal simuleringar av den maximala bufferttemperaturen genereras med hjälp av den numeriska modellen. Beräkningarna baseras på ett urval av bergdomänrealiseringar där koncentrationen av celler med lågt värmeledningstal runt de centrala kapslarna i den finita-differensmodellen är maximerad (steg 7 fortsatt).
- Om de numeriska modellerna kan verifiera att den maximala bufferttemperaturen uppfyller temperaturkriteriet (med hänsyn till marginalen för den givna bergdomänen) kan detta kapselavstånd användas som referens för den givna bergdomänen. Om inte, kan det finnas behov av att göra om modelleringen med korrigerat kapselavstånd (steg 8 i flödesschemat).

Optimering

I den beskrivna strategin för dimensioneringen av Layout D2 ingår inte någon optimering, dvs. kapselavstånden sätts på ett schematiskt sätt så att temperaturkriteriet på 100°C alltid håller för centralt placerade kapslar deponerade i fullständigt torrt berg med sämsta tänkbara värmeledning. Majoriteten av kapselpositionerna kommer dock att finnas i berg med betydligt bättre värmeledning än den som styr layoutbeslutet. Det finns även hundratals kapselpositioner i slutet på deponeringstunnlarna där den maximala bufferttemperaturen kommer att bli lägre än designvärdet oavsett de lokala värmeledningsegenskaperna. Detta innebär att det finns stort utrymme för optimering av layouten.

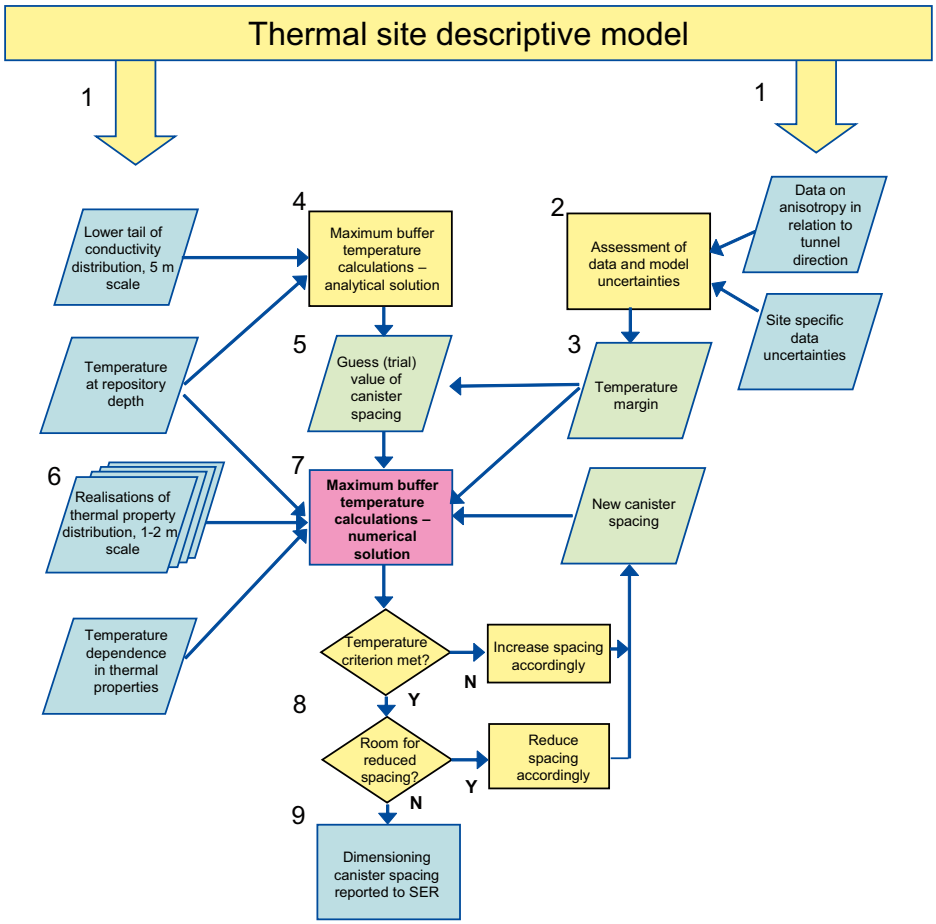

Figur Sa-1. *Flödesschema för dimensioneringsstrategin.*

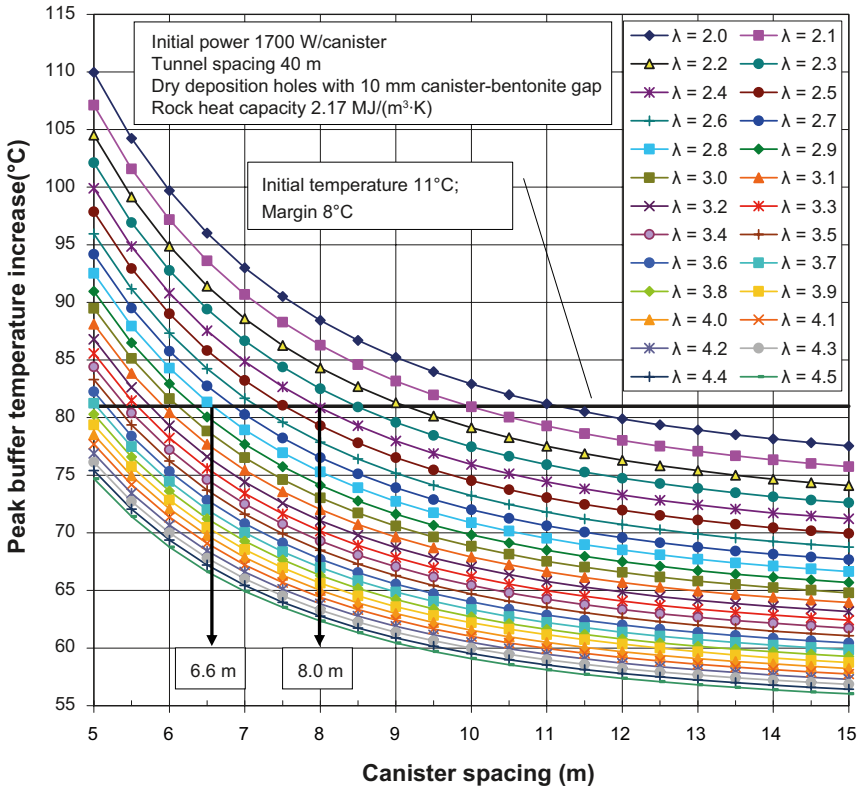

Figur Sa-2. *Nomogram för kapselavstånd-temperatur.*

En möjlighet att förbereda för en optimering är att minska tunnelavståndet och öka det dimensionerande minsta kapselavståndet. Under det fortlöpande konstruktionsarbetet kan sedan kapselavståndet modifieras allteftersom mer detaljerad information om de lokala egenskaperna blir tillgänglig.

Utöver avståndsmodifikationer, kommer det att finnas möjligheter att kontrollera och planera kapselproduktionen (dvs. kapslarnas effektfördelning) för att dra fördel av kapselpositioner i högkonduktivt berg och i tunnelslut, och av förbättringar av närfältsdesignen.

Contents

1 Introduction and background

1.1 General

In the Swedish KBS-3 concept for geological disposal of spent nuclear fuel, copper canisters with a cast iron insert containing the fuel are surrounded by bentonite clay for isolation and mechanical protection /SKB 2006/. The canisters are deposited in vertical deposition holes in the floor of horizontal tunnels at 400 to 700 m depth below ground surface in crystalline rock. The heat generated by the spent nuclear fuel will increase the temperature of all components of the KBS-3 repository: fuel, canisters, engineered barriers, deposition tunnel backfills, tunnel seals, top seal below ground surface, arrangements for sealing off investigation boreholes and the host rock itself.

For the engineered barrier, i.e. the bentonite buffer surrounding the canisters, the peak temperature must not exceed 100ºC for any of the deposition holes. This temperature limit will be one important factor when deciding on the repository layout, i.e. on the distance between deposition holes and between deposition tunnels. Figure 1-1 shows, as an example, a plan view of the outlines of one of the layout options preliminary considered for the Forsmark site /Brantberger et al. 2006/. The insets show schematics of the KBS-3 repository, with access ramp, system of transport and deposition tunnels, geometry of an individual deposition tunnel and an individual deposition hole.

1.2 Objectives

1.2.1 Primary objective

The primary objective of the present work is to form a strategy for the thermal dimensioning of the nuclear waste repository, i.e. for determining the tunnel and canister spacing for a KBS-3 repository at either the Forsmark or Laxemar site with due account of the rock thermal properties (including their spatial variability) reported for the two sites. The focus here is establishing guidelines for layout step D2 with the tunnel spacing fixed at 40 m and the initial canister power fixed at 1,700 W for all canisters. The near-field is assumed to be designed according to the reference given in /SKB 2010a, b, d/. For step D2

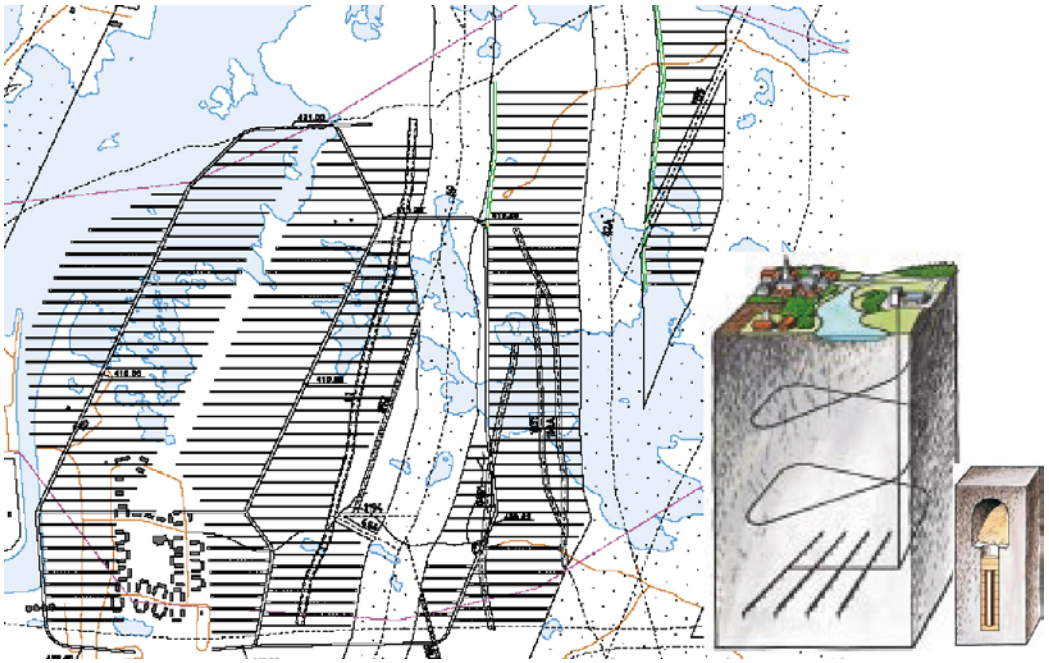

Figure 1-1. *Plan view of preliminary Forsmark layout option /Brantberger et al. 2006/. Insets show part of the tunnel system at repository depth and schematics of the near-field geometry /SKB 2006/.*

there should not be any optimization of the layout, i.e. the canister spacing should be set at the same value everywhere within each rock domain, meaning that the domain values with the lowest effective conductivities will determine the domain canister spacing. In order to make efficient use of the rock volume in step D2, it is essential that this spacing is determined with as much as rigor as possible. This means that:

1. the methods of peak canister temperature calculation must be clearly described and verified and
2. that all uncertainties are accounted for and translated into carefully calculated margins.

The points above are two sub-objectives pertaining to layout step D2 and correspond to the main body of this report.

In the layout work to follow step D2, it will be required that possibilities of optimization are utilized. Given the conductivity distributions described in the thermal site descriptive models for Forsmark and Laxemar, it is, for instance, clear that a large majority of the canisters will be deposited in rock with properties that would allow for significantly smaller canister spacing than the general D2 spacing. A third sub-objective to the main strategy issue is to:

3. Identify possibilities for optimization in following layout steps.

1.2.2 Secondary objective

A secondary objective is to provide references for SR-Site process reports. The handling of thermal processes in the geosphere, buffer, tunnel backfill, tunnel plugs, top seals, central area, borehole seals and bottom plate should be based on the most recent and updated understanding of the thermal evolution in the near-field and far-field, i.e. the one developed for the purpose of the primary objective. Therefore, the calculation methods are demonstrated and applied beyond the ranges in time and space required for the dimensioning strategy purpose.

1.3 Thermal dimensioning of the repository

1.3.1 General

The present report outlines a strategy for dealing with the thermal dimensioning of the repository that ensures that the 100ºC buffer temperature criterion will be met for all canisters and, at the same time, ensures an efficient use of the rock volume. The report is intended to be used as a basis for the thermal dimensioning of Layout step D2 presented in the Site Engineering Reports for the Forsmark and Laxemar sites. The strategy must be general enough that it can be applied, i.e. translated into layout instructions, in both Site Engineering Reports. The layout instructions will vary between the different rock domains identified at the sites such that the hottest canisters in each domain will determine the minimum canister spacing in that individual domain. These canisters will be found in deposition holes that are:

1. Completely dry. Since there is no water uptake and buffer swelling in dry holes, the initial gap between canister and buffer is not closed or reduced. This gives a high heat transport resistance and high canister temperatures. The bentonite blocks and the pellets-filled annular space between the blocks and the walls of the deposition holes remain in the initial, unsaturated state with initial low values of the heat transport parameters. This, too, will tend to give high canister temperatures.
2. Located in the central parts of the deposition areas, i.e. with several neighbour canisters in all directions. This results in higher canister temperatures compared to the conditions in the peripheral parts of the repository.
3. Located in volumes dominated by low conductive rock. Low conductive rock surrounding an individual canister will tend to increase the contribution from that particular canister to its own temperature and, depending on the size of the volume, also the contribution from nearby canisters.

For layout step D2 it will be assumed that all three conditions apply, at least for a number of canisters. The canister spacing will be set accordingly in the entire rock domain being considered, irrespective of the conditions that apply for other canisters. For layout D2 there is no way to make efficient use of the rock volume other than to ensure that that spacing is not unnecessarily large. In following layout

steps, possibilities of optimization, i.e. ways of taking advantage of the much more favourable conditions that will apply for the majority of the canisters, will be explored.

The main focus of this report is establishing a method for defining the layout D2 canister spacing. There are also general descriptions of the large-scale thermal evolution of the repository. These are needed to demonstrate general understanding of the thermal problem, for instance regarding the importance of the deposition sequence and conditions around the edges of the repository, and to show that the tunnel-scale canister spacing work is consistent with that understanding.

The strategy required at the time of this report regards a one-layer repository. Most of the elements and methods of the one-layer strategy outlined here: e.g. near-field representation, assessment of uncertainties and account of spatial variability in the rock mass, would be practically identical for a two-layer repository. Additional parameters to be considered would be the vertical layer-to-layer distance, the layer order and the time-lag between the two deposition campaigns.

1.3.2 Design premises

Layout D2

The strategy for the thermal dimensioning (distances between deposition holes and tunnels) for layout D2 shall be based of the following requirements and conditions forming the design premises /SKB 2009/:

1. Maximum allowed peak temperature in the bentonite buffer in all deposition holes; 100°C.
2. Maximum thermal canister power: 1,700 W.
3. Distance between deposition tunnels: c-c = 40 m.
4. Distance between deposition holes: c-c $\geq$ 6 m.

Optimization of the layout shall not be performed but different possibilities to optimize the repository shall be discussed.

Near-field design

The near-field description given in Chapter 3 is an example based on the design given in /SKB 2010a, b, d/. While all results presented here are based on that description, the strategy does not depend on the details of it.

1.3.3 Principles of peak buffer temperature calculation

Being able to calculate the peak buffer temperature for the hottest canisters is obviously a key issue. Figure 1-2 shows the principles of the temperature calculations made here.

1. Calculation of the rock wall temperature, taking into account the spatial variability in thermal rock properties.
2. Calculation of the temperature difference between the rock wall and the canister/bentonite interface at the top of the canister (hottest buffer point in dry deposition holes).
3. Addition of the rock wall temperature and the temperature difference to get the bentonite temperature at the hottest point.

For dry deposition holes, the 10 mm clearance between canister and bentonite blocks will remain open and the 50 mm pellets-filled gap between bentonite blocks and rock wall will remain unsaturated. The heat transport resistance of these gaps will tend to raise the temperature of the canister surface and the bentonite that is actually in direct contact with the canister, i.e. the bentonite on top of and below the canister. Knowing the canister power and assuming typical parameter values of the heat transport properties of the gaps and the buffer, it is possible to establish a reference evolution of the total difference $\Delta T_{tot}(t)$ between the rock wall temperature at canister mid-height and the temperature at the top of the canister. This reference evolution is independent of the rock properties. Adding the difference to the rock wall temperature $T_{wall}(t)$ at canister mid-height will give the maximum bentonite temperature.

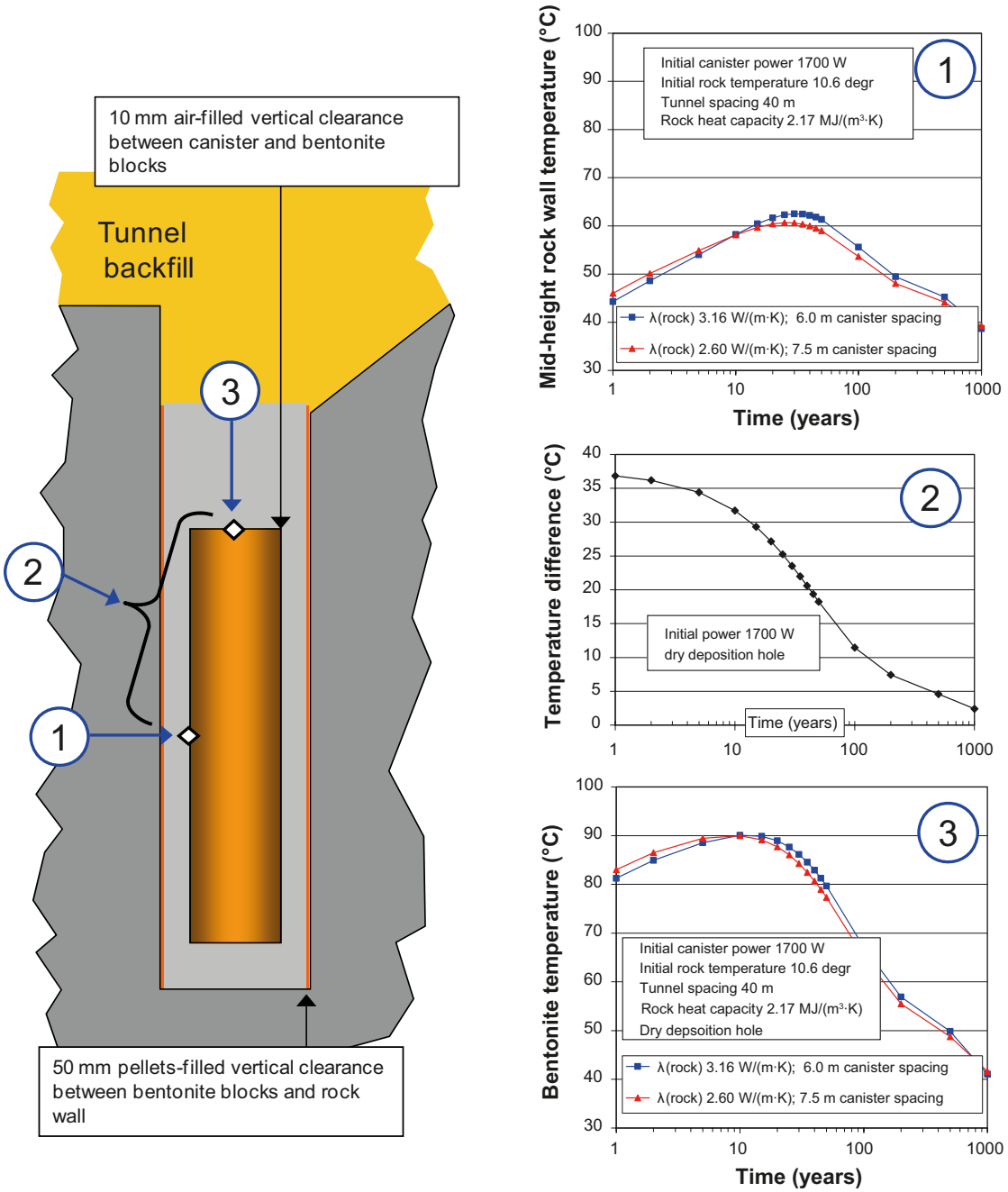

Figure 1-2. *Principle of peak buffer temperature calculation. The rock wall temperature at canister mid-height (1) is added to the temperature difference (2) between rock wall and the top of the canister to find the maximum bentonite temperature (3). The difference (2) is due to the heat resistance over buffer and gaps (local solution) whereas the rock wall temperature (1) depends on layout and rock thermal properties. The example curves shown here were calculated by use of the analytical method described in Chapter 4.*

Calculating the rock wall temperature at canister mid-height is a much more complicated problem. For the idealized case of homogenous rock with one distinct value of the thermal conductivity (and the heat capacity), an analytical solution can be used to find the rock wall temperature as function of the canister and tunnel spacing (cf. e.g. /Claesson and Probert 1996, Hökmark and Fälth 2003/). In the real case of heterogeneous rock, it is necessary to take the spatial variability of the thermal conductivity and the heat capacity into account. For this reason, a numerical method has been developed (see chapter 5) that takes the spatial variability and the anisotropy in the geology directly into account, i.e. with automatic inclusion of all scale aspects.

In the strategy described in this report, the analytical solution is used for preliminary spacing estimates and the numerical solution is used to modify and finally establish the spacing. Both methods of peak buffer temperature calculation include the same reference evolution of the difference $\Delta T_{tot}(t)$ between rock wall temperature and the bentonite temperature at the canister top. An outline of the strategy is given in the next section.

1.3.4 Outline of strategy for design step D2

The point of departure for the dimensioning of repository is the thermal site descriptive model established for the site being considered /Back et al. 2007, Sundberg et al. 2008a, b/. The site model gives, for instance, the distribution of thermal properties, their spatial variability (based on the geological site model) and the in-situ temperatures. The strategy of the thermal dimensioning is pictured schematically in Figure 1-3 and summarized as follows:

1. Data is recovered from the thermal site descriptive model.
2. Model and data uncertainties are assessed. Parts of these uncertainties are based on site model data.
3. A temperature margin to the 100°C criterion is determined and the corresponding temperature threshold (the maximum allowed calculated peak temperature) is established (see chapter 6).
4. Based on the initial temperature at the projected repository depth (site descriptive model data), a guess value picked from the low conductivity tail of the conductivity distribution (site model data) and the reference thermal evolution of the deposition hole interior, the peak temperature as function of the canister spacing is obtained by use of the analytical solution (see chapter 4). The value picked from the low conductivity tail should empirically correspond to the 0.1–2 percentiles.
5. Applying the uncertainty margin gives the maximum allowed calculated peak temperature and the associated analytically obtained spacing. This spacing is used as a first trial value in the following.
6. A large number of stochastic realisations of the thermal property distribution applying for the rock domain being considered have been produced in the site descriptive models (tunnel-scale rock volumes large enough to hold a number of canister positions). A selection of these realisations provides the property distribution input to the numerical peak temperature calculations.
7. Numerical Finite Difference models (see chapter 5) of one tunnel with a number of canisters in the central parts of a repository, based directly on the property distribution of the selected rock domain realisations, are generated. To reduce the number of thermal analyses, the realisations are ranked and the worst case realisations, i.e. those having the lowest conductivity in the central parts, are picked for thermal simulations. Canisters are spaced according to the analytically obtained trial value. The models are analyzed thermally to find the peak buffer temperature.
8. If the highest peak temperature does not match the threshold, i.e. 100°C minus the margin, the spacing needs to be modified and then checked numerically using the same set of rock domain realisations.
9. The spacing is approved as the dimensioning rock domain spacing and reported as such in the Site Engineering Report (SER).

The strategy described above does not include any measures to optimize the layout, i.e. to take advantage of the significantly better heat transport conditions found around the majority of the canisters than around the hottest canisters. Such measures are discussed along with a more complete strategy description in Chapter 7. The strategy is used for design step D2. However, the main elements of the strategy can, with small modifications, be used in later design steps.

1.3.5 Application of the temperature criterion

All results presented in the following are based on strict but schematic application of the temperature criterion. The hottest bentonite will be found at the canister top for the hottest canisters, i.e. those with an open gap around the cylindrical periphery as shown in Figure 1-2. The temperature threshold is therefore compared here (point 8 in scheme described in Figure 1-3) with the temperature calculated at the copper/bentonite interface at the top. For the reference canister design /SKB 2010b/, this part of the buffer is, however, hydraulically and mechanically shielded by flanges (cf. Chapter 2) and does not contribute to the isolation or protection of the canister. From this point of view, it would be more relevant to exclude this part of the buffer and compare the threshold with the bentonite temperature a couple of centimetres above the interface. This is discussed in the uncertainty section (Chapter 6).

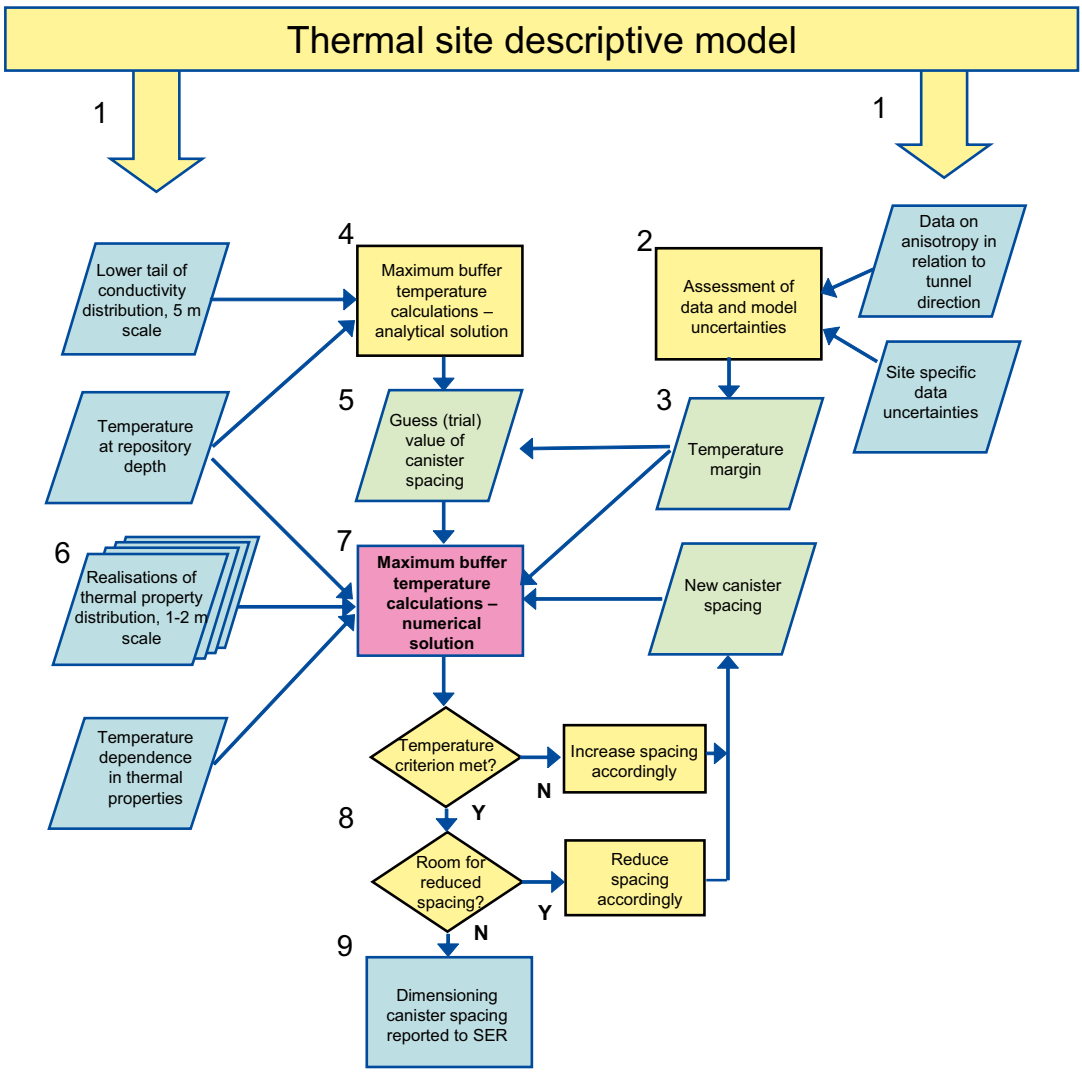

Figure 1-3. *Schematic description of the strategy for thermal dimensioning of the repository. Possible optimization measures are not included in the scheme.*

Theoretically, it cannot be excluded that small parts of the buffer will get into direct contact with the hottest parts of the canister surface, i.e. around mid-height. At the time of installation, the gap will be uniform as indicated in Figure 1-2, cf. /SKB 2010a/, but if buffer fragments detach later, these could get temperatures a few degrees higher than the calculated peak buffer temperature. This possibility is not considered here; if the contact area is small, the consequences for the buffer function would be small, if there is a large contact zone this would break the thermal isolation of the canister and bring the canister temperature down.

1.3.6 Data input

Rock

The heat transport properties of the host rock are obviously important to the temperature levels reached in all repository components, irrespective of the repository layout. Due to the low permeability of crystalline rocks, heat transport in the repository host rock can be approximated to take place by conduction only, i.e. neglecting convection /Thunvik and Braester 1991, Hartley et al. 2006/. Thermal site descriptive models, based on direct and indirect determinations of the thermal conductivity and heat capacity of the different rock types found at SKB's two sites Forsmark and Laxemar, have been developed as an aid to plan for the dimensioning of the repository /Back et al. 2007, Sundberg et al. 2008a, b/. The thermal site models give descriptions of how the thermal conductivity varies within and between the rock types found at the sites and of the spatial correlation of the thermal conductivity within the geologically defined rock domains. The site model also gives the ground temperature at repository depth.

Deposition hole interior

Bentonite thermal properties data are derived from /Börgesson et al. 1994/. Properties of the pellet slot are based on observations from the Prototype Repository /Goudarzi and Johannesson 2006/. Properties, i.e. the effective conductivity, of the open canister-bentonite gap is based on tabulated values of hot air conductivity, on direct copper surface emissivity measurements /Appendix C/ and on expressions valid for the radiant heat transfer between parallel surfaces of different temperatures /Bird et al. 2002/.

1.4 This report

This report describes the process indicated in the flowchart shown in Figure 1-3. The main body regards the calculation of the key parameter: the peak temperature at the top of a canister in a dry deposition hole.

The heat load, i.e. the number of canisters, the initial canister power and the decay characteristics, is an input to all temperature calculations on all scales. In the near-field, the shape and size of individual canisters also become important. The representation of the heat load is described in Chapter 2.

The internal solution, i.e. the heat transport in the interior of a dry deposition hole is, to a large extent, independent of the host rock properties and the repository layout (uncertainties are handled in Chapter 6). Chapter 3 describes the reference evolution suggested here for the temperature difference between the rock wall and the top of the canister (cf. Figure 1-2). The reference evolution is based on laboratory-scale data and on temperature measurements performed in a dry and well-instrumented deposition hole in the Prototype Repository at Äspö HRL. However, that particular Prototype Repository hole cannot, even if it is categorized as dry, be trusted to represent a maximally dry KBS-3 deposition hole. Therefore the relevance of the reference evolution and the need for margins are evaluated by comparison with results from calculations based on independent estimates of the heat transport properties of the different materials (gaps, bentonite blocks and pellets). There are two appendices relevant to Chapter 3: Appendix A (Code_Bright one-canister analyses) and Appendix C (Emissivity of copper from electron beam welds). The most relevant results from the appendices are, however, found in the main text.

To find the peak buffer temperature, the temperature difference between rock wall and bentonite as described in Chapter 3 must be added to the rock wall temperature (cf. Figure 1-2). Two ways of doing this are described:

- Adding the difference to analytically calculated rock wall temperatures (Chapter 4).
- Adding the difference to numerically calculated rock wall temperatures (Chapter 5).

The analytical way (Chapter 4) is fast and based on idealized assumptions of the rock heat transport properties. It captures the thermal evolution of the repository rock mass on all scales in time and space, which is demonstrated in the beginning of the chapter. The governing equations are presented. Thousands of results of peak buffer temperature calculations for different assumptions regarding the rock heat transport properties and the repository layout are generated and compiled in nomographic spacing-temperature charts. The analytical solution is also applied to demonstrate differences in peak buffer temperature between central and peripheral deposition holes and the effects of distributing deposition over time. The analytical solution cannot account explicitly for the spatial variability of the rock heat transport properties. However, knowing the distribution of the rock thermal conductivity reasonable guess values of the dimensioning rock thermal conductivity (picked from low conductivity tail of the distribution in the 5 m scale) can be used to estimate the approximate canister spacing required to meet the 100°C criterion. There are two appendices relevant to this chapter: Appendix B: Anisotropy in the analytical solution and Appendix D: Accounting for spatial variability in the analytical solution. The analytical approach described in Appendix D takes the distribution of rock thermal properties into account in an approximate way, but does not account for spatial correlations.

The Finite Difference numerical method (Chapter 5) is the tool used to finally establish the canister spacing. The input to the model is a selection of 3D realisations picked from a large set (typically 500–1,000) produced within the site descriptive modelling work. The realisations describe the distribution and

spatial variability of the thermal conductivity within the rock domain. The numerical method and model (including the procedure of selecting relevant 3D realisations) is described, a validation of the model is performed and the numerical method is compared with an independent numerical code and the analytical method. Examples are given of applications to cases with site data (property distributions and spatial property correlations).

Uncertainties and margins, identified and quantified in Chapters 3, 4 and 5 are summarized and evaluated in Chapter 6.

The strategy as outlined in Figure 1-3 is established and described in Chapter 7.

The main conclusions are listed in Chapter 8.

2 Heat load

2.1 Heat decay

The power of each individual canister decays at a rate that depends on the fuel burn-up and on the interim storage time, i.e. the time elapsed between discharge and deposition. The power used as example input to the calculations presented in this report is given by the exponential expression below. The expression is fitted to data given for SVEA96 fuel (BWR fuel of 38MWd/kgU burn-up /SKB 1999/) to give the normalized power *P(t)* after about 37 years of interim storage /Fälth and Hökmark 2006/.

$$P(t) = \sum_{i=1}^{7} a_i \exp(-t / t_i) \qquad 2\text{-}1$$

Here t is time in years after deposition and t_i are time constants. The coefficients a_i are shown in Table 2-1. The seven-exponential expression is valid for 20,000 years and more. To capture just the first 30 or 40 years of decay, it would be sufficient to fit the power data to two exponentials.

To match the intended target initial power (see next section), each canister will contain a mix of fuel assemblies of different age and burn-up. Figure 2-1 shows normalized power data of BWR and PWR fuel for two interim storage assumptions. Here, the BWR and PWR data are from /Håkansson 2000/. The exponential expression appears to be an adequate approximation and is used as an example throughout this report although there are now updated decay energy data /SKB 2010c/. None of the basic conclusions depend, however, on the details of the decay function.

Table 2-1. Time constants and coefficients of exponential power expression.

i	t_i [years]	a_i [–]	i	t_i [years]	a_i [–]
1	20	0.060147	5	2,000	0.025407
2	50	0.705024	6	5,000	–0.009227
3	200	–0.054753	7	20,000	0.023877
4	500	0.249767			

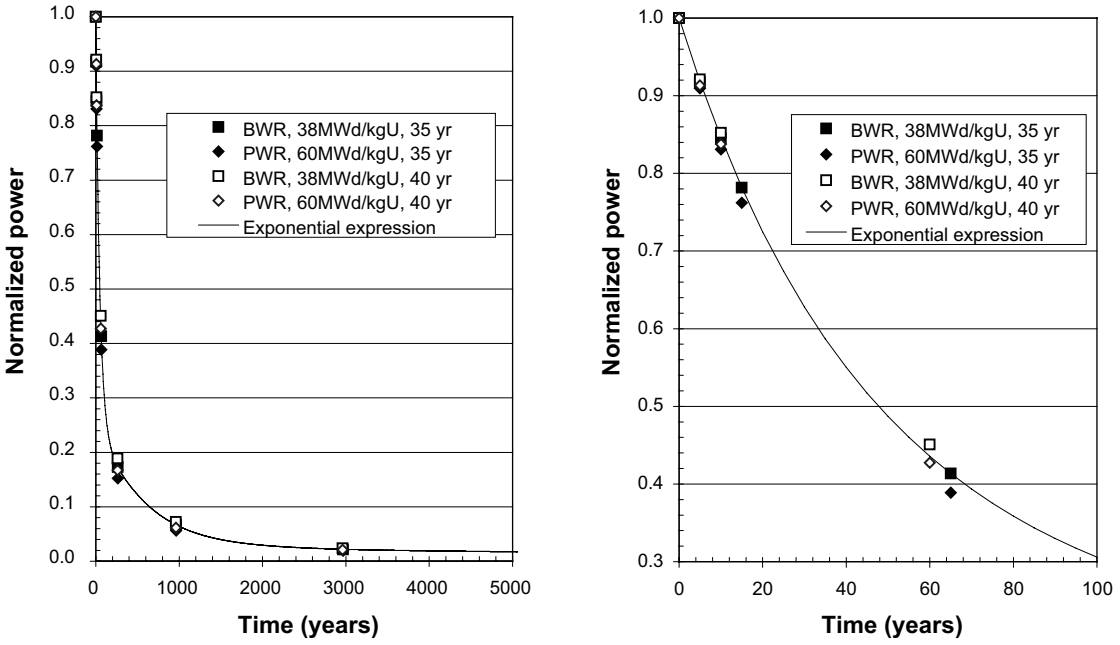

Figure 2-1. *Normalized heat power of 35 and 40 year-old BWR and PWR fuel with burn-up 38 MWd/kgU and 60 MWd/kgU, respectively, compared with the exponential expression. Decay energies from /Håkansson 2000/.*

Figure 2-2 shows normalized power data based on the updated radionuclide inventory calculations /SKB 2010c/. As far as BWR and PWR fuel is concerned, the exponential expression appears to describe the energy decay very satisfactory, at least for the first 30 years following deposition. About 0.2% of the BWR fuel assemblies will contain MOX fuel with a burn-up of 50 MWd/kgU /SKB 2010c/, which fits the exponential expression well for a mininum of 15 years. Assemblies containing MOX of less burn-up (e.g. 30MWd/kgU, cf. Figure 2-2, right) will not occur other than by way of exception and must be handled as such once the amounts are known.

In conclusion, the exponential power expression will be sufficient and adequate for the dimensioning issue and is used without exceptions throughout in this report.

2.2 Initial power

For layout D2, the canister power at the time of deposition must not exceed 1,700 W.

In reality it will not be possible to select and combine fuel assemblies such that all canisters will have exactly the 1,700 W target initial power. At some point there will be an excess of high-power assemblies or low-power assemblies. Some canisters will potentially have to be left with one or more empty assembly slots in order not to exceed the target initial power. At the time of this report it is not clear how many canisters would be affected and what the final power distribution among the canisters will be. An optimization possibility may be to allow for the power to exceed 1,700 W in some canisters and deposit these in selected positions.

In all calculations and examples in this report, the initial canister power is set at the value fixed for layout step D2, i.e. 1,700 W.

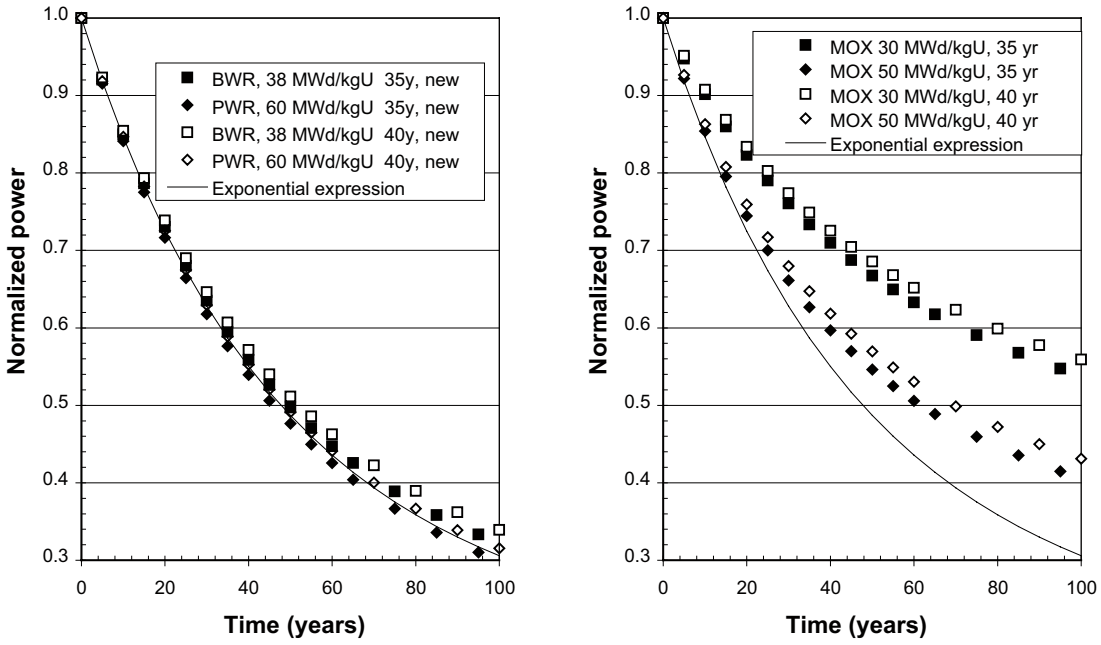

Figure 2-2. *Exponential expression compared with normalized heat power based on updated decay energy calculations. Left: Ordinary BWR and PWR fuel of different age and different burn-up. Right: MOX fuel of different age and different burn-up. Decay energies from /SKB 2010c/.*

2.3 Canister

The heat-generating spent fuel is contained in cylinder-shaped canisters. For the calculations presented here, the dimensions are as shown schematically in Figure 2-3. Two design options are considered: with and without flanges. The flange option is the reference one /SKB 2010b/. The copper shell is assumed to be 50 mm thick and to have standard tabulated thermal properties (Appendix A). The thermal properties of the steel insert are adjusted here to account for the cavities (Appendix A). The fuel assemblies emit heat in proportion to the relative burn-up, i.e. at a lower rate in the end-sections. In the one-canister models analyzed here, this has been accounted for in an approximate way (Appendix A).

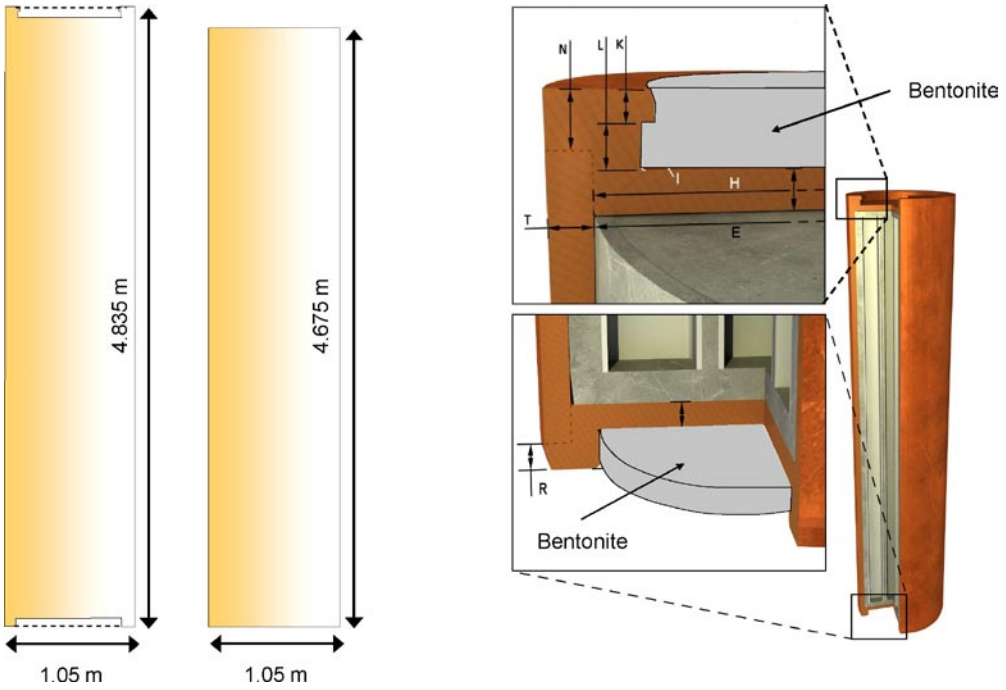

Figure 2-3. *Left: Schematic view of KBS-3 canister (two design options). Right: Bottom and lid for design option with flanges (from /SKB 2010b/). The space shielded by the flanges is filled with bentonite buffer with properties approximately as those of the bentonite surrounding the canisters /SKB 2010a/.*

3 Local canister/buffer solution

3.1 General

The difference between the rock wall temperature at canister mid-height and the bentonite temperature at the canister/bentonite interface (cf. Figure 1-2) can be divided in two components:

- The temperature drop across the annular space between the rock wall and the buffer inner boundary at canister mid-height. This barrier space is composed of highly compacted bentonite blocks (inner main part) and bentonite pellets (outer 50 mm).
- The gap effect. The air-filled 10 mm gap between the canister surface and buffer inner boundary will tend to isolate the canister and increase the canister surface temperature. Hot air has a thermal conductivity of about 0.03 W/(m·K), but because of radiant heat transport across the gap, the effective conductivity $\lambda_{g(eff)}$ will be slightly higher. The resulting temperature drop across the air-filled space is denoted ΔT_g in the following. The bottom and top parts of the canister surface have somewhat lower temperatures than the mid-height surface. Because of the high copper thermal conductivity the difference ΔT_c will be small. The gap effect is defined here as the net effect of the transport resistance across the air-filled gap and the difference between the top and mid-height surface temperatures.

The notations below are used in the following:

$\Delta T_1(t)$	Temperature drop across the bentonite buffer at canister mid-height
$\Delta T_2(t)$	The gap effect (= $\Delta T_g - \Delta T_c$)
$\Delta T_g(t)$	Temperature drop across the air-filled canister-bentonite gap
$\Delta T_c(t)$	Difference between canister mid-height and canister top copper surface temperature
$\Delta T_{tot}(t)$	Total difference between mid-height rock wall temperature and the bentonite temperature at the canister top (= $\Delta T_1(t) + \Delta T_2(t)$)
ϕ	Ratio between canister surface flux at mid-height and average surface flux
$\lambda_{b(eff)}$	Effective thermal conductivity of buffer (block and pellets at canister mid-height)
$\lambda_{g(eff)}$	Effective thermal conductivity of open canister-bentonite gap

In this chapter, a model for calculating $\Delta T_{tot}(t)$ in dry deposition holes is described. To find the peak buffer temperature, $\Delta T_{tot}(t)$ must be added to the rock wall temperature at canister mid-height (cf. Figure 1-2). The model gives a reference evolution which is based on best estimations of the thermal properties of the materials in the interior of the deposition holes and of the effects of open gaps. Data and model uncertainties associated with the calculation of $\Delta T_{tot}(t)$ are evaluated at the end of the chapter.

3.2 Temperature drop across the bentonite buffer

3.2.1 Model

A few days after deposition the heat transport in the interior of the deposition hole has become virtually independent of the canister and buffer heat capacities /Hökmark and Fälth 2003/. Due to the small width/height ratio of the annular buffer space, the axial component of the heat flux can be ignored at canister mid-height, meaning that the mid-height, quasi steady-state, heat flux $q(r;t)$ can be approximated to be perfectly radial:

$$q(r,t) = q(t) \cdot \frac{R_0}{r} \qquad 3\text{-}1$$

Here R_0 is the canister radius and $q(t)$ is the canister surface heat flux at canister mid-height. The temperature gradient within the buffer at time t is given by:

$$\frac{dT(t)}{dr} = \frac{q(r,t)}{\lambda_{b(eff)}} \qquad 3\text{-}2$$

Here $\lambda_{b(eff)}$ is the effective buffer conductivity (blocks and pellets). Setting $q(r,t)$ as in Equation 3-1, integrating Equation 3-2 between $r = R_1$ (buffer inner radius) and $r = R_2$ (deposition hole radius) gives the temperature drop $\Delta T_1(t)$ at time t across the buffer:

$$\Delta T_1(t) = \frac{q(t)}{\lambda_{b(eff)}} \cdot R_0 \cdot \ln(R_2 / R_1) \qquad 3\text{-}3$$

The flux across the buffer space is not completely determined by the local canister as suggested by Equation 3-3. Neighbour canisters give flux contributions that don't cancel out even if the deposition geometry is perfectly regular. The effect is however small (around 1% for 6 m canister spacing, cf. Appendix A, and even smaller if the spacing is larger) and is conservatively ignored here. The horizontal heat flux at canister mid-height $q(t)$ scales with the average surface flux:

$$q(t) = \phi \frac{Q(t)}{A} \qquad 3\text{-}4$$

Here A is the total canister surface area and $Q(t)$ is the canister power. For dry deposition holes without moisture uptake and swelling, the heat transport properties in the near-field can be assumed to remain as at the time of installation, meaning that the flux ratio ϕ can be approximated to be constant over time.

3.2.2 Reference evolution – assessment of data

Geometry

The canister radius R_0 is set at 0.525 m /SKB 2010b/.

The buffer inner radius R_1 is set at 0.535 m, i.e. with 10 mm clearance between the canister surface and the bentonite blocks /SKB 2010a/.

The deposition hole radius R_2 is set at 0.875 m /SKB 2010d/.

Canister surface heat flux

The canister power $Q(t)$ (cf. Equation 3-4) is assumed to be as described in Chapter 2 and the area is set at A = 17.663 m^2 (radius 0.525 m and height 4.83 m). The surface flux is not evenly distributed over the surface. It is higher around the more efficiently cooled edge regions than at mid-height, meaning that the mid-height/average flux ratio ϕ is less than 1. Figure 3-1 (left) shows how the horizontal flux varies along the height of a canister in the Prototype Repository /Kristensson and Hökmark 2007a/. The mid-height flux appeared to be about 92% of the average canister surface flux, in keeping with results of FLAC2D calculations reported by /Hökmark and Fälth 2003/, cf. Figure 3-1 (right).

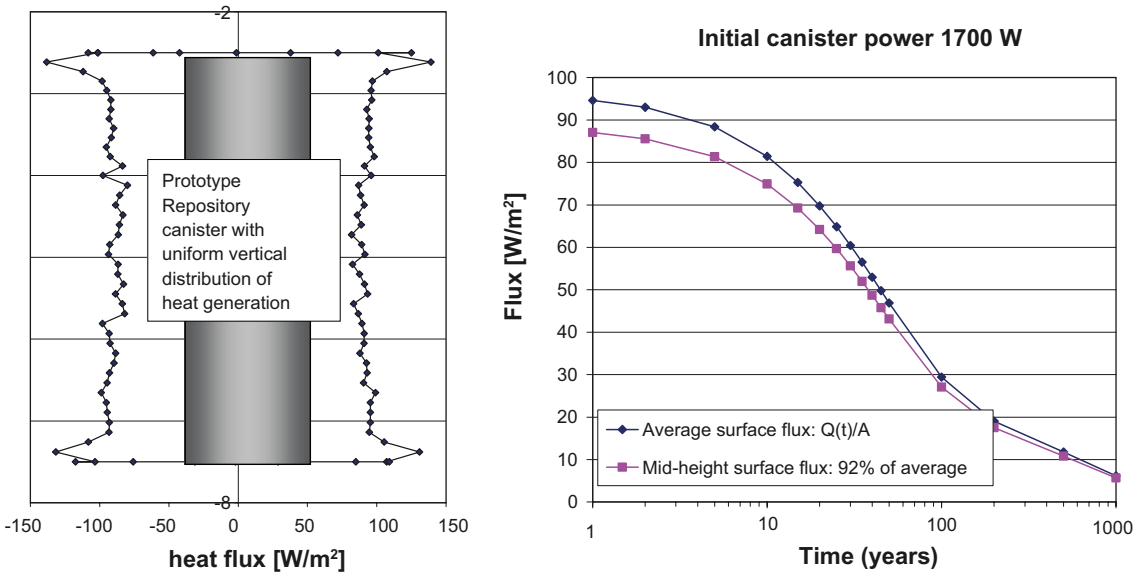

Figure 3-1. *Left: Horizontal surface flux at different heights calculated for a Prototype Repository canister Right: Canister surface heat flux as function of time.*

The surface flux ratio ϕ is not a fixed quantity, but depends on the rock thermal conductivity, the details of the heat transport in the deposition hole and in the backfilled tunnel, and on the conditions in the interior of the canister (effects of cavities in steel insert and distribution of heat load, i.e. burn-up, along the fuel assemblies). If there is an insulating air-filled gap between the canister surface and the surrounding bentonite blocks, there will be an additional redistribution of the heat output, i.e. the mid-height flux will be further reduced. Figure 3-2 shows Code_Bright results obtained for a number of assumptions regarding the rock conductivity and the properties of the 10 mm insulating air-filled gap (cf. Appendix A). Note that the flux profiles are different from the one shown in Figure 3-1 for the Prototype Repository canister. This is due to a different and more realistic representation of how the heat generation is distributed along the height of the canister. The effective air gap conductivities tried here are based on different assumptions regarding the radiant heat transfer across the gap (cf. following sections). For the dimensioning gap assumption (effective gap conductivity $\lambda_{g(eff)}$ = 0.04 W/(m·K)) the flux ratio ϕ ranges between 88% and 90% for the fixed moisture content cases pictured in Figure 3-2, cf. Table 3-1.

At a distance of 2 m below and above mid-height the flux is even smaller than at mid-height. Taking effects of moisture redistribution into account gives 85% to 87% for the case with λ_{Rock} = 2.5 W/(m·K), cf. Appendix A. For the reference evolution, it is judged that ϕ = 87% is a relevant estimate, i.e. $q(t)$ is given by:

$$q(t) = 0.87\frac{Q(t)}{17.66} = 0.04926 \cdot Q(t) \ \text{(W/m}^2\text{)} \qquad 3\text{-}5$$

Effective buffer conductivity – general

If there is water uptake from the surrounding rock or from the backfilled tunnel, the effective buffer conductivity $\lambda_{b(eff)}$ will increase over time. For the reference evolution considered here, the water uptake and the associated $\lambda_{b(eff)}$ increase are conservatively ignored. Therefore, the assumption made here is that the properties of the blocks and pellets do not change after deposition.

Moisture movements that take place without supply of water, e.g. thermally induced moisture redistribution and loss of moisture from the buffer to the backfill, will impact the thermal conductivity in all parts of the buffer. The net effect on $\Delta T_1(t)$ (and $\Delta T_{tot}(t)$) cannot be assessed using Equation 3-3 and mid-height $\lambda_{b(eff)}$ estimates, since Equation 3-3 is valid only if the conditions can be approximated to be radial symmetric. Instead, the effects of a worst case drying scenario (completely dry deposition hole located in a completely dry tunnel section backfilled with high-suction material) are evaluated in the end of this chapter using results from Code_Bright finite element T-H models.

For the reference evolution, the issue is to establish a reasonably realistic value of the effective conductivity of the buffer, i.e. of the annular space between the air-filled gap and the rock wall. The mid-height effective conductivity $\lambda_{b(eff)}$ is given by:

$$\lambda_{b(eff)} = \frac{\lambda_{pellets} \cdot \lambda_{block} \cdot \ln\left(R_2 / R_1\right)}{\lambda_{pellets} \cdot \ln\left(R_{bp} / R_1\right) + \lambda_{block} \cdot \ln\left(R_2 / R_{bp}\right)} \qquad 3\text{-}6$$

Here R_{bp} is the radius of the block/pellets interface.

Figure 3-3 shows the total effective buffer conductivity as a function of the pellet slot conductivity for a number of block conductivity assumptions. For the reference evolution, without any moisture supply or redistribution, the geometry and the properties do not change after installation, i.e. they will remain as shown in the top part of the figure. Values of the block conductivity λ_{block}, the pellet slot conductivity $\lambda_{pellets}$ and the total effective buffer conductivity $\lambda_{b(eff)}$ are assessed in following sections.

Bentonite block conductivity

Figure 3-4 shows laboratory-determined bentonite block conductivities as function of saturation /Börgesson et al. 1994/.

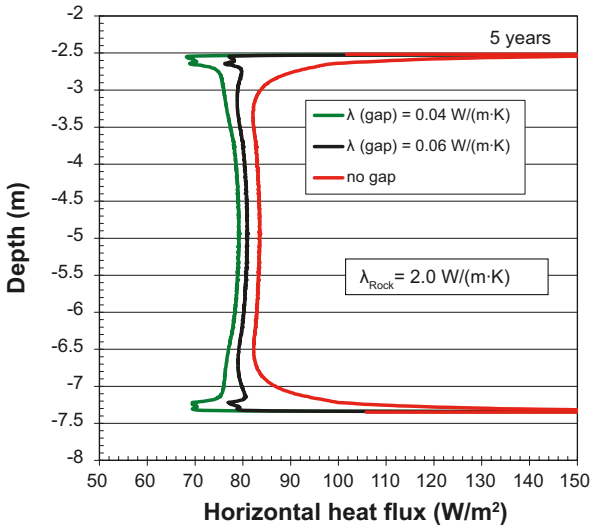

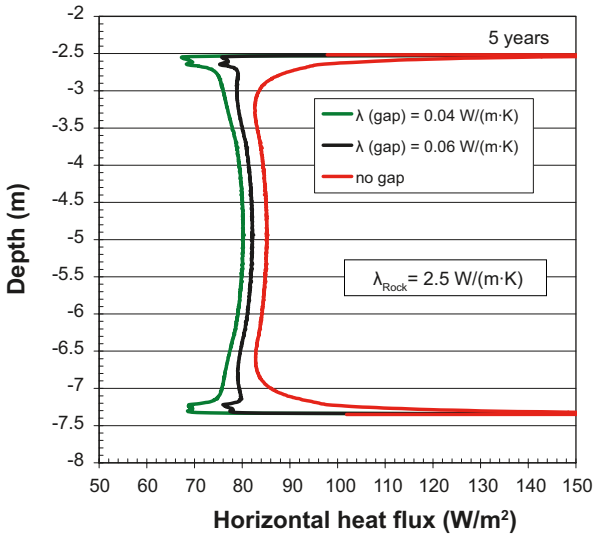

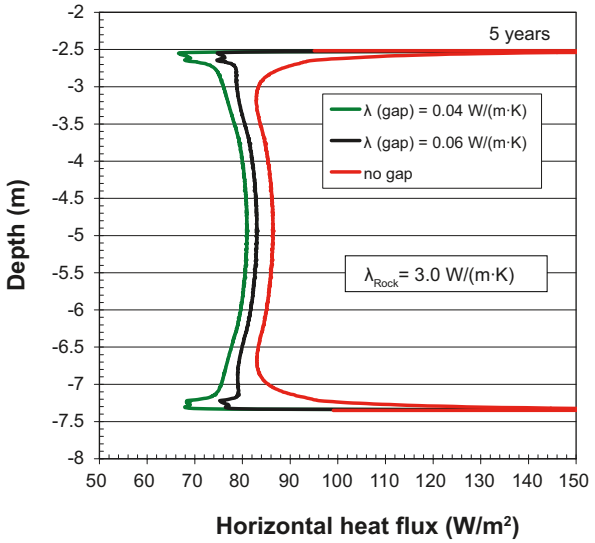

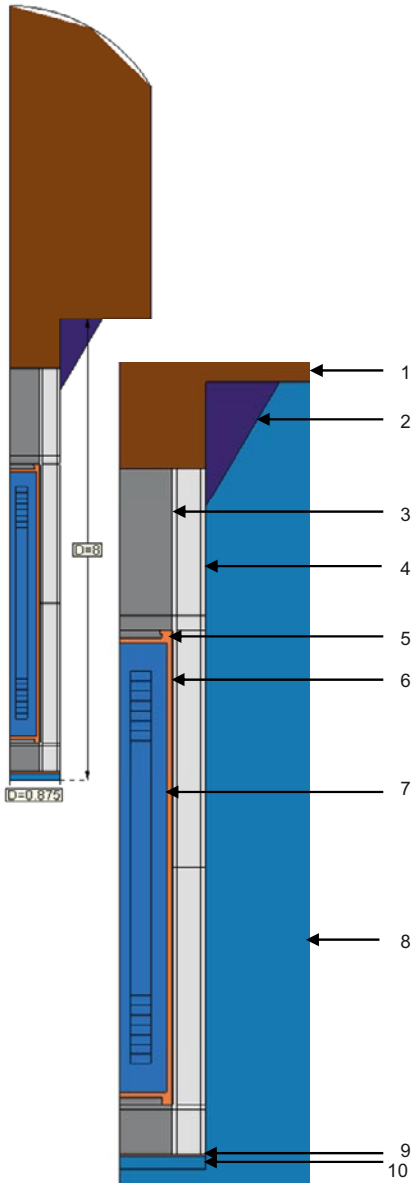

1. Backfill
2. Wedge
3. Bentonite, top and bottom
4. Bentonite, incl. Pellets
5. Copper
6. Gap
7. Cast iron
8. Rock
9. Copper plate
10. Concrete pedestal

Figure 3-2. *Left: Horizontal surface heat flux for different assumptions regarding the effective gap thermal conductivity. Right: Geometry of central part of axisymmetric Code_Bright model.*

Table 3-1. Mid-height/average flux ratios for cases shown in Figure 3-2. Values in parentheses apply 2 m above and below mid-height.

	Percent of average canister surface flux after 5 years at canister mid-height (+2m/–2m)		
	λ_{Gap} = 0.04 W/(m·K)	λ_{Gap} = 0.06 W/(m·K)	No gap
λ_{Rock} = 2.0 W/(m·K)	88.2 (87.6/87.7)	90.2 (90.2/90.4)	93.1 (95.9/96.3)
λ_{Rock} = 2.5 W/(m·K)	89.4 (87.7/87.7)	91.6 (90.2/90.3)	95.0 (95.6/95.9)
λ_{Rock} = 3.0 W/(m·K)	90.3 (87.8/87.7)	92.6 (90.2/90.2)	96.5 (95.3/95.6)

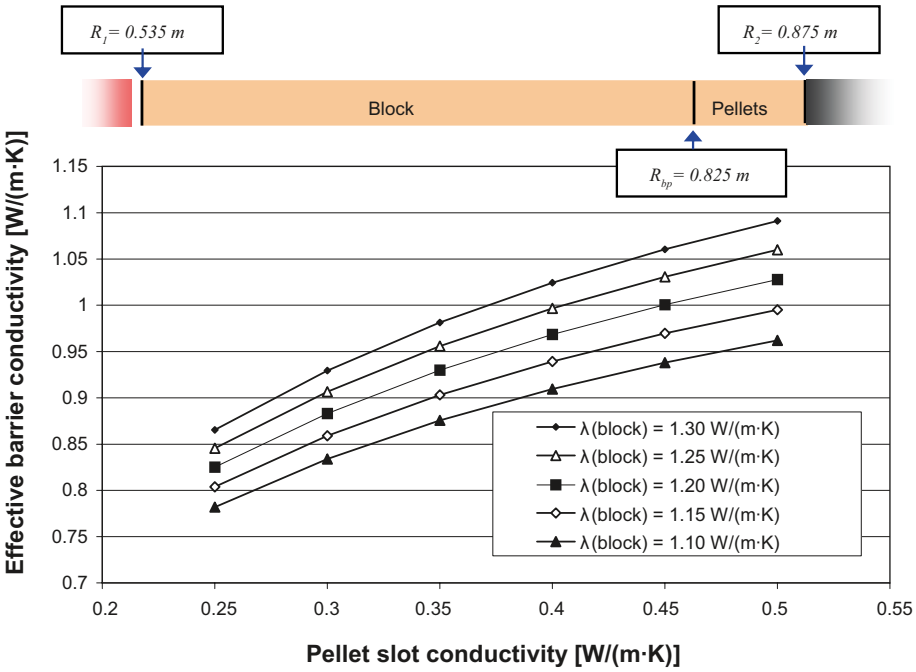

Figure 3-3. Effective buffer conductivity as a function of the pellet slot conductivity for a number of block thermal conductivity assumptions.

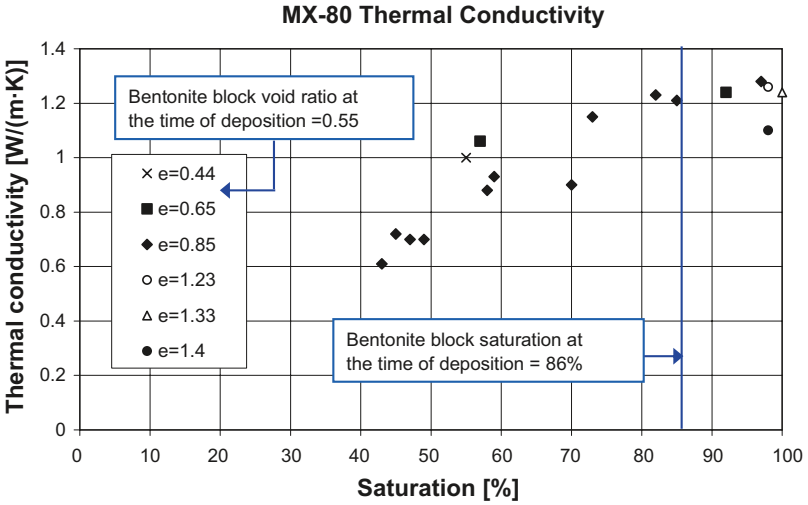

Figure 3-4. Thermal conductivity as function of saturation for MX80 bentonite blocks of different void ratios. At the time of deposition, bentonite blocks will have a thermal conductivity of a little more than 1.2 W/(m·K). Data from /Börgesson et al. 1994/.

For the case used as reference in this report KBS-3 blocks are assumed to have a void ratio of about 0.55 and an 85% degree of saturation. This is in keeping with the blocks installed in the Prototype Repository, but may be revised in the future reference design. The void ratio and saturation indicate that the block conductivity should be a little more than 1.2 W/(m·K) at the time of deposition.

The data plotted in Figure 3-4 suggest that the saturation must drop below about 65% for the conductivity to be lower than 1.0 W/(m·K). In the 80–100% saturation range, the thermal conductivity appears to be less sensitive to saturation variations. These laboratory-scale results have been verified in the field: the thermal conductivity of the canister mid-height bentonite blocks in the full-scale Prototype Repository experiment has been determined to be above 1.25 W/(m·K) for wet as well as for dry deposition holes /Kristensson and Hökmark 2007b/.

Pellet filling conductivity

Heat transport across the porous pellet filling is a combination of conduction, radiant heat transfer, convection and evaporation/vapour diffusion/condensation and cannot easily be determined in laboratory-scale experiments. Figure 3-5 shows equipment and results from a study by /Sugita et al. 2003/, performed on pellets of Kunigel sodium bentonite with a dry density of 1,000 kg/m^3. For the reference case considered here, the pellet filling is assumed to have a dry density of about 1,100 kg/m^3 and an initial water content of about 13%. This is in keeping with the installation conditions in the Prototype Repository. The right part of Figure 3-5 indicates that this would give a pellet slot conductivity of about 0.1–0.2 W/(m·K). In KBS-3 deposition holes, there will be not only pure conduction, but also effects of evaporation/condensation, radiation and convection, meaning that field-scale conductivities should be a bit higher. In addition, the higher pellet density in the Prototype Repository would mean that the conductivity is slightly higher than the laboratory results obtained for Kunigel pellets.

In the following section the pellet slot conductivity is assessed (along with the total effective buffer conductivity) from observations made in field-scale tests.

Total effective buffer conductivity assessed from large-scale field test

The large-scale Prototype Repository experiment at Äspö HRL offers a possibility to assess values of the effective pellet slot conductivity and the effective buffer conductivity $\lambda_{b(eff)}$. Figure 3-6 shows buffer temperatures as a function of radial distance from the canister axis measured in a particularly dry deposition hole /Goudarzi and Johannesson 2006/. These measurements were conducted 50 days after test start. At this instance of time, relative humidity sensor readings indicated that no detectable water uptake had taken place anywhere in that particular hole. This means that the buffer heat transport conditions pictured in Figure 3-6 are probably representative of dry KBS-3 deposition holes. The measured temperatures are compared with theoretical radius-temperature relations obtained using a few hypothetical combinations of block and pellet conductivities. Each of the combinations shown

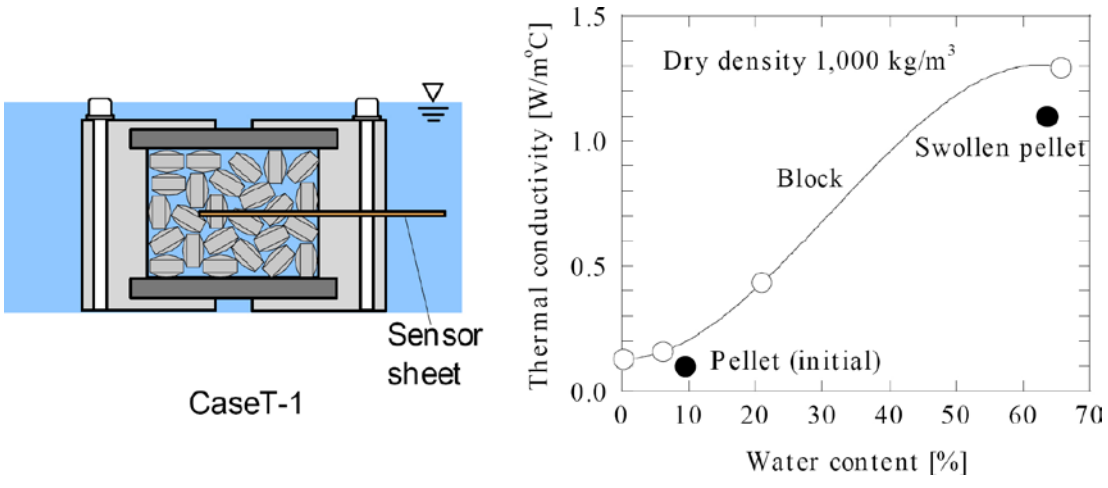

Figure 3-5. *Test setup and results from lab-scale pellets study. From /Sugita et al. 2003/.*

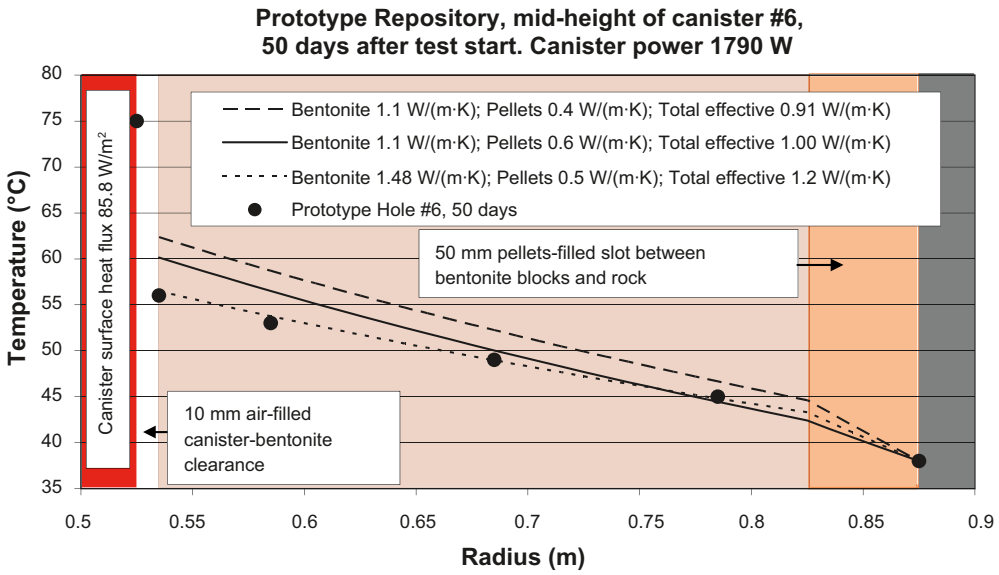

Figure 3-6. *Thermocouple readings compared with theoretical distance-temperature relation obtained assuming mid-height heat flux being 87% of average surface heat flux. Best match is for the dotted line.*

in Figure 3-6 corresponds to a value of the total effective buffer conductivity $\lambda_{b(eff)}$. The best match corresponds to a total effective buffer conductivity of almost 1.2 W/(m·K). This is on level with the block conductivity values and is possibly an overestimate. Yet the surface heat flux has been reduced to account for the flux distribution around the canister and additional redistribution effects caused by the open gap (cf. previous section). The total canister heat load has been verified by comparison between calculated and measured rock temperatures /Kristensson and Hökmark 2007a/. A possible explanation of the low temperature gradient across the bentonite buffer found in Figure 3-6 is that the canister is not perfectly centred in the hole and that the flux is unevenly distributed around the periphery.

Figure 3-7 shows the same prototype data, but here the canister heat flux has been arbitrarily reduced such that the slope of the temperature curves in the bentonite block section agrees with typical laboratory values of the block thermal conductivity.

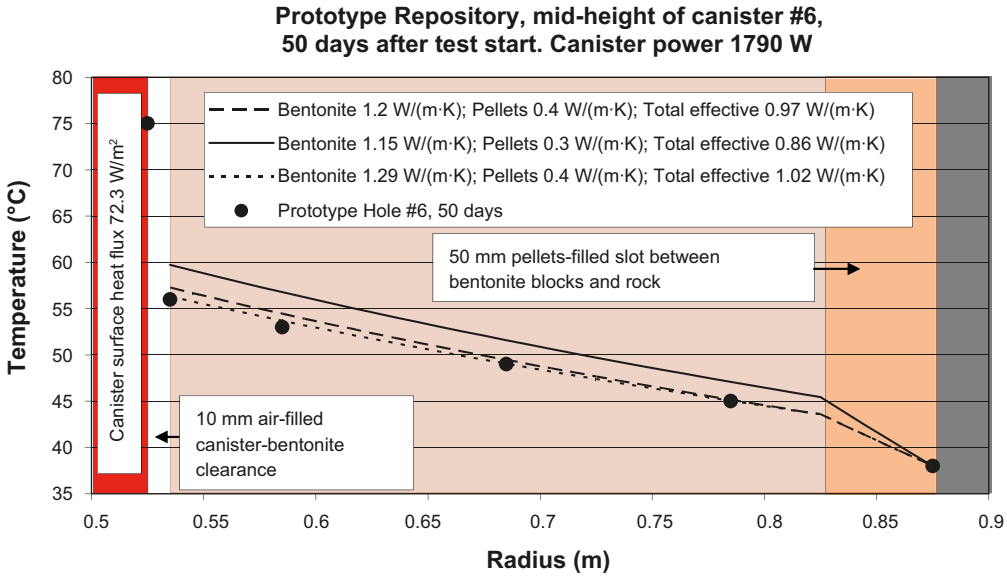

Figure 3-7. *Same as previous figure, but heat flux is only 74% of average surface heat flux. The best match is for the dotted line.*

For the best matches (dotted lines) the pellet/block conductivity ratio is about 0.33, irrespective of the flux assumption. This gives a pellet slot conductivity of just above 0.4 W/(m·K) assuming the block conductivity to be 1.25 W/(m·K). Similar comparisons made for the less systematically instrumented deposition hole #5, give slot conductivities of about 0.3 W/(m·K) /Kristensson and Hökmark 2007b/.

Setting λ_{block} to 1.25 W/(m·K) as suggested by results from lab-scale tests (cf. Figure 3-4) and then setting λ_{pellet} to 0.40 W/(m·K) as suggested by the slope ratio observations above gives $\lambda_{b(eff)}$ = 1.0 W/(m·K), cf. Figure 3-3. This value is proposed for use in Equation 3-3 for the reference evolution of the temperature drop across the bentonite buffer.

3.2.3 Reference evolution – summary

The model for calculation of the temperature drop across the buffer at canister mid-height is given by: (cf. Equations 3-3 and 3-4).

$$\Delta T_1(t) = \phi \frac{Q(t)}{A \cdot \lambda_{b(eff)}} \cdot R_0 \cdot \ln(R_2 / R_1) \qquad 3\text{-}7$$

For the data suggested above for the reference evolution this gives: (°C):

$$\Delta T_1(t) = 0.87 \cdot \frac{Q(t)}{17.66 \cdot 1.00} \cdot 0.525 \cdot \ln\left(0.875 / 0.535\right) = 0.01272 \cdot Q(t) \qquad 3\text{-}8$$

3.2.4 Estimate of uncertainty in buffer temperature drop

There are no experimental results from dry deposition holes with pellet fillings (other than hole #6 in the Prototype Repository) that could be used for verification and comparison. Assuming the block conductivity to be 1.15 W/(m·K) and the pellet filling conductivity to be 0.30 W/(m·K) gives $\lambda_{b(eff)}$ = 0.86 W/(m·K). Looking at Figure 3-8, this lower bound value would give a 3°C addition, approximately, to the temperature drop across the buffer compared to the reference evolution estimate of $\lambda_{b(eff)}$ (1.00 W/(m·K)) at the time of peak bentonite temperature some 10 years after deposition. For calculations related to the dimensioning problem, 3°C is therefore suggested to be a relevant estimate of the uncertainty in temperature drop across the bentonite buffer. However, variations in thermal properties of blocks and pellets will have an effect not only on the effective buffer conductivity but also on the flux redistribution (whereas the results in Figure 3-8 are based on the reference mid-height flux). The flux distribution will, in turn, have an influence on the effects of the open air-filled gap between the canister surface and the bentonite blocks (cf. next section). Therefore the effects of variations in thermal properties of rock and buffer are evaluated in a specific section at the end of this chapter.

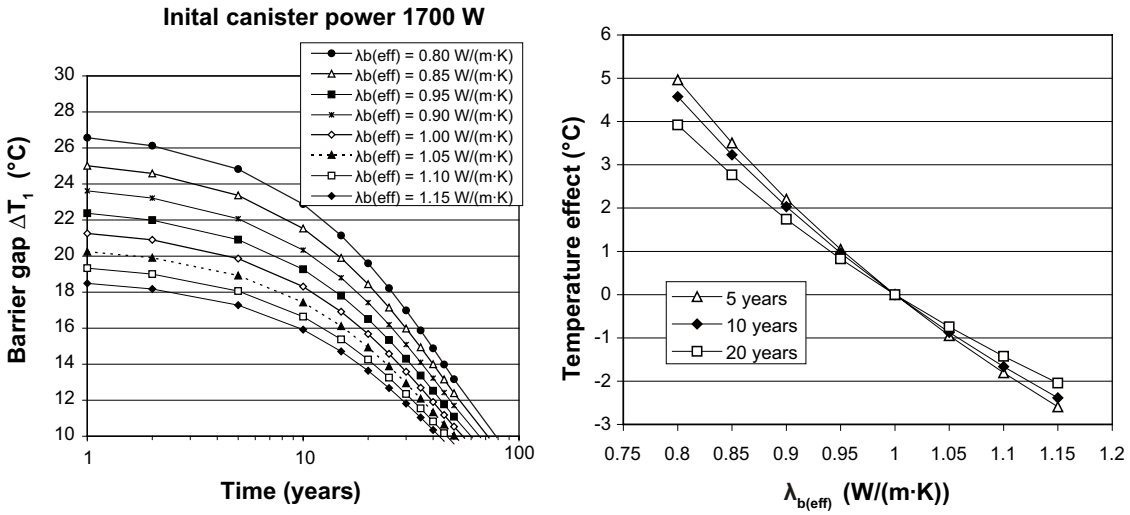

Figure 3-8. *Left: Temperature drop for different values of $\lambda_{b(eff)}$. Right: Relative temperature effect at different times after deposition. Setting $\lambda_{b(eff)}$ to 0.85 W/(m·K) rather than to 1.0 W/(m·K) would give an excess of about 3°C.*

3.3 Gap effect

3.3.1 Model

If the bentonite and the canister are in direct thermal contact at all points, the hottest bentonite will be found at canister mid-height, since this is the hottest part of the canister surface. If there is an insulating air-filled gap around the canister, the hottest bentonite will be found at the canister base/top (cf. Figure 1-2). The gap effect, i.e. the difference ΔT_2 between the bentonite temperature at canister mid-height and the maximum bentonite temperature, depends on the temperature difference ΔT_g across the air-filled gap and the difference ΔT_c between the copper surface temperature at mid-height and the temperature at the canister base/top.

For the dimensioning reference evolution, water uptake and moisture redistribution are ignored. This means that the geometry (e.g. the gap width) and the heat transport properties do not change over time and the gap effect $\Delta T_2(t)$ scales with the power output:

$$\Delta T_2(t) = \Delta T_2(0)\frac{Q(t)}{Q(0)} \qquad 3\text{-}9$$

3.3.2 Reference evolution – assessment of data

The issue is to find a relevant value of the initial gap effect $\Delta T_2(0)$. The deposition holes in the Prototype Repository have dimensions identical to the near-field reference design valid at the time of this report /SKB 2010d/. Properties established for blocks and pellets in the final design are likely to be identical or similar to those of the corresponding Prototype Repository buffer materials. Therefore, the data suggested for the dimensioning reference evolution are derived directly from measurements made in the dry Prototype Repository hole #6. Figure 3-6 and Figure 3-7 show that the temperature drop across the air-filled gap is 19°C at a power output of 1,790 W. The temperature difference $\Delta T_c(t)$ between mid-height and top/base is about 2°C, cf. Figure 3-9. Scaling the difference, 17°C, to the initial KBS-3 canister power, 1,700 W, gives 16°C. The reference evolution of the gap effect is therefore suggested to be given as:

$$\Delta T_2(t) = 16 \cdot \frac{Q(t)}{1700} = 0.00941 \cdot Q(t) \qquad (°C) \qquad 3\text{-}10$$

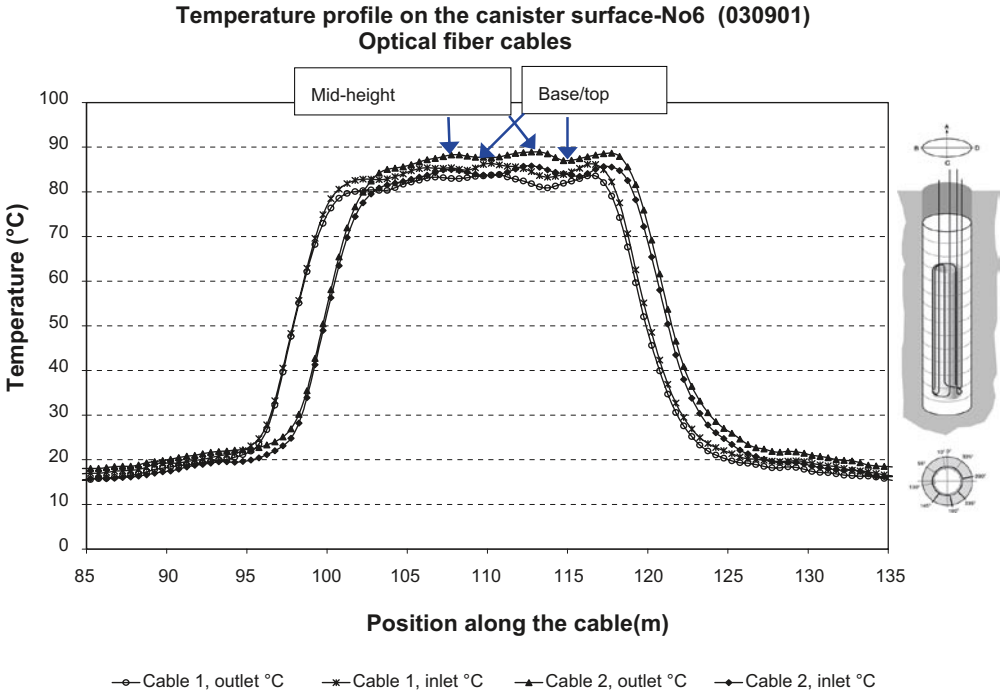

Figure 3-9. *Prototype Repository hole #6. Copper surface temperatures as measured by use of optic fibre cables. From /Goudarzi and Johannesson 2003/. The absolute values of the readings are probably disturbed by calibration and installation errors, but the variation along the length of the cables are judged to be correct. The same differences between mid-height and top/base readings are found for all Prototype Repository canisters being monitored by use of optic fibre cables.*

3.3.3 Gap effect reference evolution – relevance and validity

Using the Prototype Repository results as described above to assess and quantify the gap effect could be questioned:

- The results of the thermo-couple readings used to determine the surface temperature on canister #6 are not in agreement with the optic fibre readings. This is discussed and clarified in Appendix F.
- Even if the deposition hole used for the data assessment counted as dry at the time of buffer installation and the temperature data were collected soon after test start, there is no way to ensure that the canister-buffer gap had not started to close at some places, or that the gap was uniform from top to bottom around the Prototype Repository canister perimeter. Any disturbance of the gap geometry would tend to reduce the gap effect, meaning that the suggested reference evolution probably underestimates the worst case gap effect.
- The Prototype Repository canisters are heated by electrical heaters with a uniform heat load distribution, whereas KBS-3 fuel assemblies will have less power in the end-sections.

A numerical check of the gap effect with numerical one-canister Code_Bright models is made below. The models are described in detail in Appendix A.

Numerical check

A full description of the numerical one-canister Code_Bright models analyzed to get perspectives on the validity of the reference evolution is given in Appendix A. For the numerical check, the issue is to assign relevant heat transport parameters to the air-filled gap.

The temperature drop ΔT_g across the air-filled gap between canister and bentonite blocks is determined by the hot air conductivity (0.03 W(m·K), (cf. /Alvarez 1990/) and by conditions that control the efficiency of the radiant heat transfer across the gap.

If the emissivities e_c and e_b of the two opposite surfaces (copper and bentonite) are known, the effective gap conductivity can be estimated by /Hökmark and Fälth 2003/:

$$\lambda_{g(eff)} = \frac{e_c \cdot e_b}{e_c + e_b - e_c \cdot e_b} \sigma \cdot 4(T+273)^3 \cdot d + \lambda_{air} \qquad 3\text{-}11$$

Here σ is Stefan-Boltzmann's constant (5.66997E-8 W/(m²·K⁴)), T the average gap temperature, d the gap width and λ_{air} the hot air conductivity. The expression is valid only if the absolute temperature T+273 K is large compared with the temperature gap ΔT_g. Equation 3-11 is based on expressions given for the radiant heat transfer between two parallel, opposing surfaces of different temperature, cf. /Bird et al. 2002/. Figure 3-10 shows results for a set of assumptions regarding the average air gap temperature T. Different copper emissivity values given in the literature are indicated for comparison. Direct emissivity measurements performed on four copper surface samples picked from SKB's canister laboratory have given about 0.1 (mean value 0.0925, cf. Appendix C), meaning that the effective conductivity should be set at 0.04 W/(m·K).

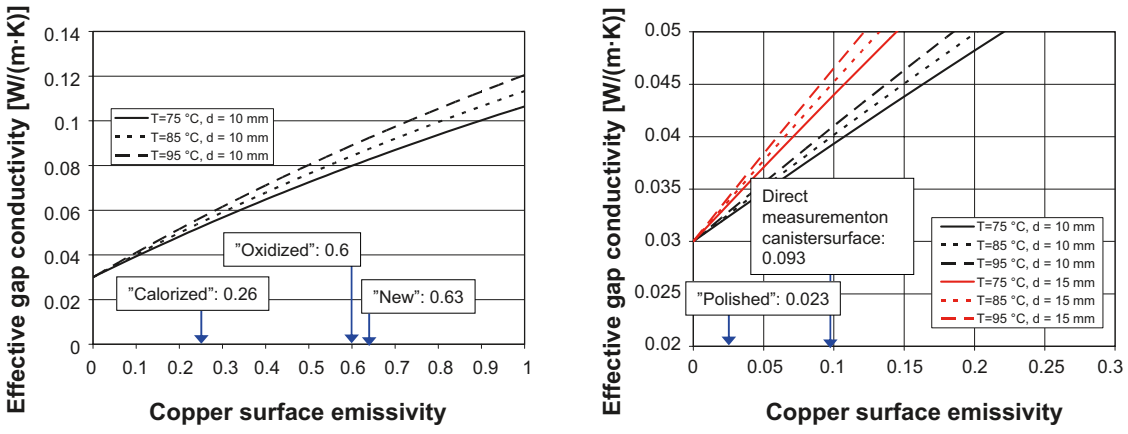

Figure 3-10. *Effective thermal conductivity of canister-bentonite gap as function of the copper emissivity for three assumptions regarding the average gap temperature.*

The results are much less sensitive to emissivity variations of the high-emissivity surface, i.e. that of the bentonite blocks /Hökmark and Fälth 2003/. The value used here (0.8) is on level with values usually associated with brick, rough steel, concrete etc.

Figure 3-11 shows results 10 years after deposition for three different rock conductivity assumptions. The gap effect ranges between 13.1 and 13.7°C. Figure 3-12 (left) shows the gap effect as a function of time for the three models. The right part illustrates basic features of the axisymmetric model. A full description is given in Appendix A.

The results in Figure 3-12 verify that the reference gap effect is a reasonable estimate of the effects of a 10 mm uniform gap with heat transport properties as described above, i.e. with a 0.1 copper surface emissivity.

One question, which will not be further addressed here, would be how the finish of the canister surface will change over time. If the surface finish tends to be more like "oxidized" (e = 0.6 /CRC 1973/) or "new" (e = 0.63 /Ageskog and Jansson 1999/) rather than between "polished" (e = 0.023 /Cheremissinoff 1986/) and "calorized" (e = 0.26 /CRC 1973/), after some years of exposure to the conditions in the deposition hole, this would increase the effective conductivity and reduce the temperature gap.

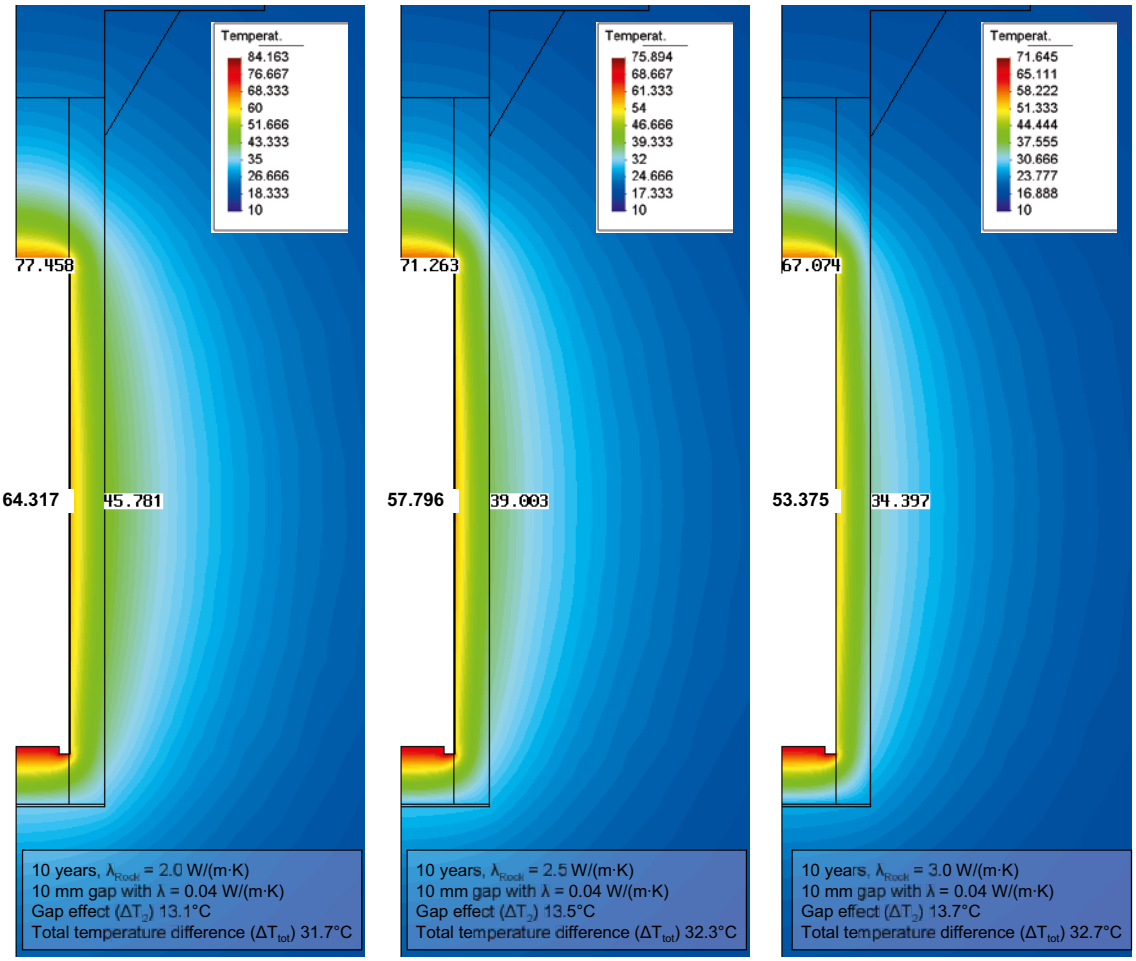

Figure 3-11. *Code_Bright temperature contours after 10 years of heating with one canister with power as described in Chapter 2.*

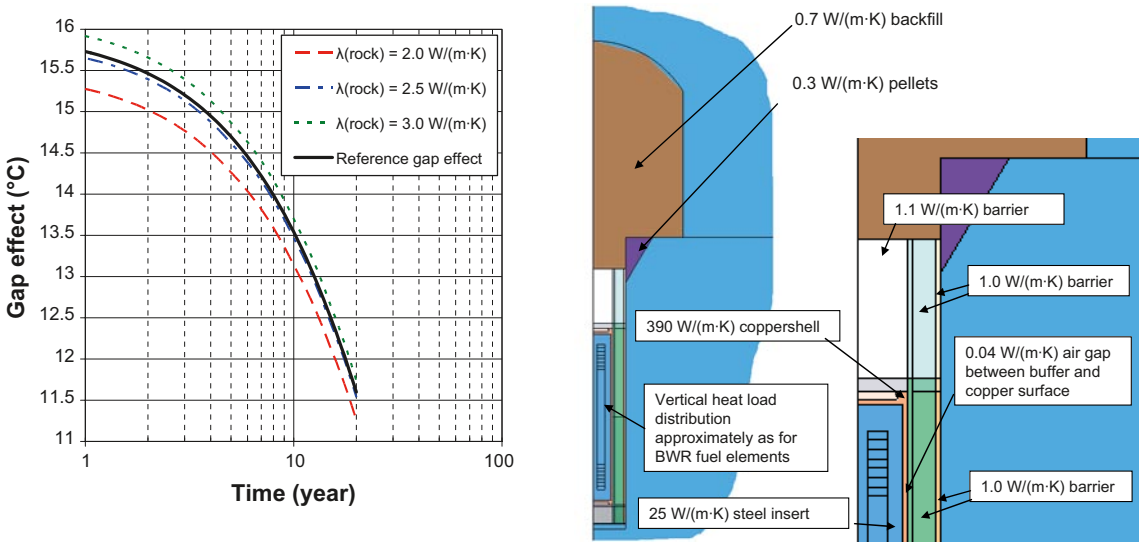

Figure 3-12. *Left: Numerically calculated gap effect for three different conductivity assumptions compared with reference evolution. Right: Details of the numerical model.*

3.4 Temperature difference between rock wall and bentonite – summary

3.4.1 Results

The temperature drop ΔT_1 across the bentonite buffer (cf. Section 3.2) and the effects of the air-filled canister-bentonite gap ΔT_2 (cf. Section 3.3) both scale with the decreasing canister power. Together they give the total difference $\Delta T_{tot}(t)$ between the canister mid-height rock wall temperature and the bentonite temperature at the top of the canister (cf. Figure 1-2). For the data selected for the reference evolution, the total difference is given by:

$$\Delta T_{tot}(t) = \Delta T_1(t) + \Delta T_2(t) = 0.02213 \cdot Q(t) \qquad 3\text{-}12$$

Figure 3-13 shows the reference evolution of $\Delta T_1(t)$, $\Delta T_2(t)$ and $\Delta T_{tot}(t)$. In the following section, the reference evolution is compared with results from different numerical one-canister models.

3.4.2 Reference evolution – comparison with numerical results

Effects of uncertainties in bentonite block and pellets conductivity are approximated to give about 3ºC at maximum in excess of the reference evolution established for the buffer temperature drop ΔT_1 at the time of peak temperature (cf. Section 3.2.4). The reference evolution of the gap effect ΔT_2 is based on an interpretation of one particular field experiment, i.e. without explicit use of parameter value estimates. The numerical check indicated that the reference evolution is a good upper bound estimate of the actual gap effect, provided that the gap width is 10 mm and that the copper surface emissivity does not drop below 0.1 (cf. Figure 3-12). The air-filled gap will provide the most efficient thermal insulation if it is uniform around the canister periphery from canister bottom to top, i.e. as in the numerical models. From that aspect, the numerical results represent worst case gap effects, meaning that the uncertainty, or rather the margin that would be needed to account for uncertainties, is small.

Below, numerically calculated total differences $\Delta T_{tot}(t)$ are compared with the reference evolution. A full description of the Code_Bright one-canister models used to generate the results is found in Appendix A. Figure 3-14 (left) shows $\Delta T_{tot}(t)$ for the cases previously pictured in Figure 3-12. These model all have a 10 mm gap with an effective conductivity of 0.04 W(m·K) and a mid-height buffer conductivity $\lambda_{b(eff)}$ of 1.0 W/(m·K). The differences are due to the different extents of heat flux redistribution: highly conductive rock will reduce these effects. Figure 3-14 (right) shows results from models where the bentonite blocks and the pellet slot have been modelled separately with conductivities that correspond to lower values of the effective mid-height conductivity $\lambda_{b(eff)}$. The temperature peak occurs some 5–15 years after deposition.

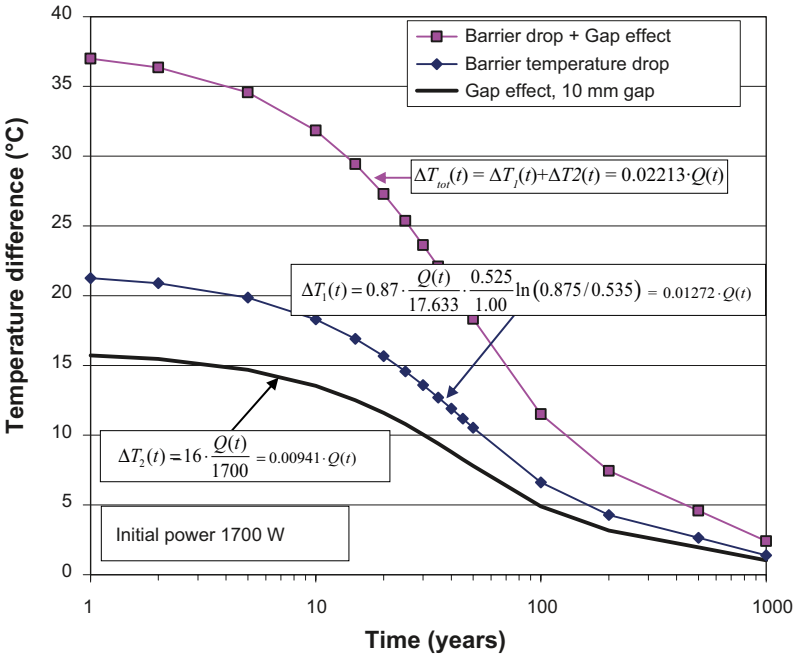

Figure 3-13. *Reference evolution of difference ΔT_{tot} with $\lambda_{b(eff)}$ = 1.00 W/(m·K) and with gap effect scaled to the Prototype hole #6 gap effect.*

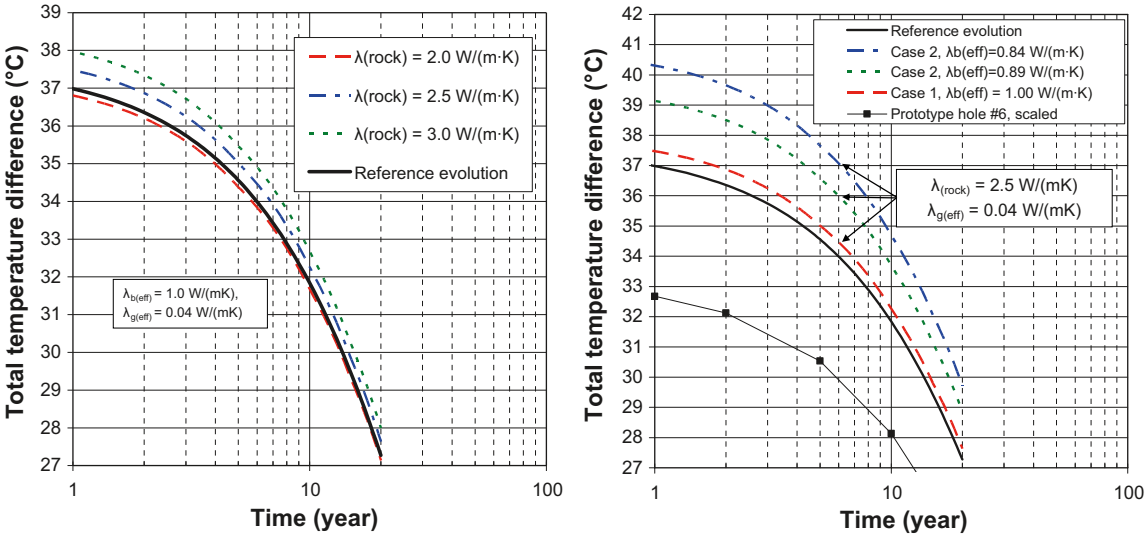

Figure 3-14. *Left: Influence of rock conductivity on difference between rock wall temperature and temperature at canister/bentonite interface on top of canister. Right: Influence of variations in buffer properties for one rock conductivity assumption.*

For low values of the rock conductivity the temperature peak occurs early while it occurs late for high values (cf. following chapters). The calculated difference does not exceed the reference evolution by more than 3°C during this time span for any of the cases presented in Figure 3-14.

The worst case would be high rock conductivity (less flux redistribution in interior of the deposition hole) combined with low buffer conductivity. This is illustrated in Figure 3-15 (left). The worst case combination gives about 3.3°C in excess of the reference evolution. In Figure 3-15 (right), the worst case evolution is also evaluated for the case that the canister is designed without flanges in lid and bottom, i.e. with a reduced height and surface area (cf. Figure 2-3).

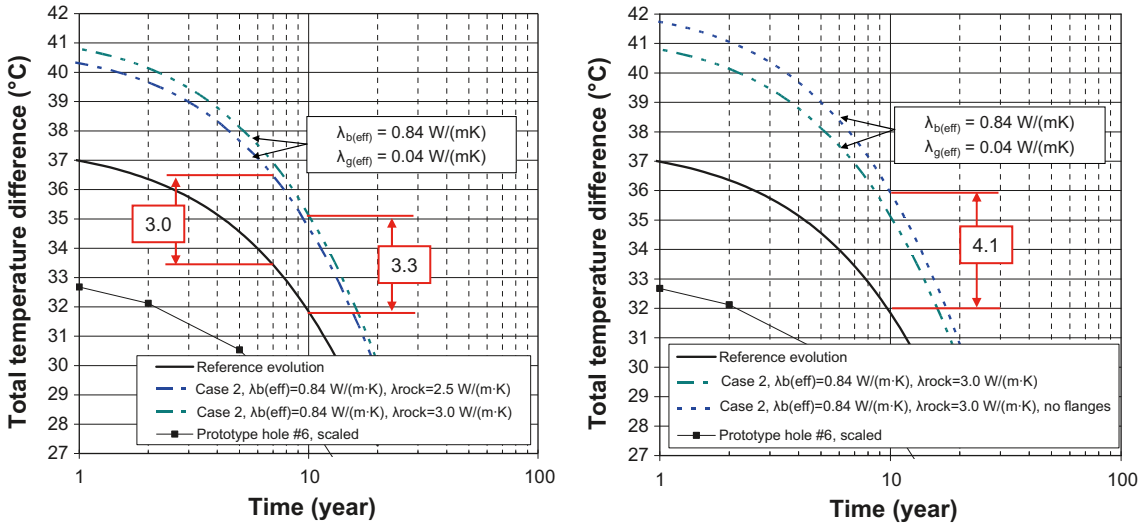

Figure 3-15. *Left: Lower bound values of buffer conductivity for two rock conductivity assumptions. The higher the rock conductivity, the later the peak temperature will occur. Right: Comparison between canister models with and without flanges.*

3.4.3 Uncertainties and need for margin in dimensioning calculations

Rock wall – canister top temperature difference ΔT_{tot}

The results shown in Figure 3-15 should be close to the largest possible difference ΔT_{tot} between the temperature at rock wall mid-height and the temperature at the copper/bentonite interface at the canister top, provided that the near-field design and the canister power are as assumed here and provided that there are no significant and systematic modifications of the buffer properties (density and initial saturation). Therefore these results can, in principle, be used to define a safe margin to add to the reference $\Delta T_{tot}(t)$ evolution when calculating buffer peak temperatures in layout simulations performed to establish the canister and tunnel spacing. There are, however, the following additional issues to consider:

- Thermally induced moisture redistribution. The thermal conductivity will be reduced in hot regions where vaporisation and vapour diffusion tend to reduce the saturation. The saturation and the conductivity will however increase in other regions, for instance in the pellets-filled slot. For conservative assumptions regarding the saturation-conductivity correlation the net effect is an increase of ΔT_{tot} of between 0.1 and 0.2°C (Appendix A).
- Distribution of heat generation along the canisters. The heat generation distribution assumed in the models pictured in Figure 3-14 and Figure 3-15 is based on burn-up models for BWR fuel assemblies. PWR fuel assemblies will have a slightly different burn-up distribution. This will give 0.1–0.2°C in excess of the model results shown in Figure 3-14 and Figure 3-15 (Appendix A).
- If the rock conductivity is unfortunately distributed along the height of the deposition hole, i.e. with low-conductivity rock systematically concentrated around the top and bottom parts of the canister, ΔT_{tot} will increase. Extreme cases may give about 0.5°C (Appendix A). 0.25°C is judged to be a realistic upper bound estimate of this effect.
- There is a possibility of thermally induced spalling in the walls of the deposition holes. The spalled zone must be assumed to have a lower conductivity than the surrounding intact rock. In unsupported holes, i.e. in holes without internal pressure, the scope and extent of the failure are likely to be similar to those observed in the open APSE hole /Andersson 2007/. The effect is estimated to be a canister temperature increase of 0.1°C (Appendix E).

To account for the points above, 0.75°C should be added to the results shown in Figure 3-14 and Figure 3-15. Figure 3-16 shows calculated and corrected (0.75°C addition) values of the excess temperature in relation to the reference evolution for different assumptions of the rock conductivity. Some of the values are interpolations. Note that these excess temperatures apply at the time of the temperature peak, which is approximated to occur about 7 years after deposition for rock conductivities in the range of 2.0–2.5 W/(m·K) and after about 10 years for rocks with conductivity of 3.0 W/(m·K). The time of the

peak is, however not a direct function of the rock conductivity, but rather of how the rock conductivity controls the canister spacing. For the purpose of defining margins in dimensioning calculations, the relations in pictured in Figure 3-16 are judged to be accurate enough. The following issues are ignored:

- The disturbance (reduction) of the heat flux across the buffer caused by nearby canisters. For the smallest allowed canister spacing (6 m) this disturbance is in the order of 1%, cf. Appendix A.
- Uncertainties in the conductivity of the tunnel backfill. Reducing the backfill conductivity from 0.7 W/(m·K) to 0.3 W/(m·K) would give an increase of 0.1°C (Appendix A).

Both effects described above are minor. In addition they tend to cancel out.

Rock wall temperature T_{wall}

The rock wall temperature cannot be obtained from the one-canister models described above. The rock wall temperature must be obtained from models that include numerous canisters and that take due account of the rock heat transport properties, including their spatial variability. This is how the numerical finite difference model described in Chapter 5 (which is used as the main tool for calculation of the rock wall temperature in the dimensioning calculations) is configured. In that large-scale model, the canisters are approximated by homogenous 30 W/(m·K) cylinders with uniform vertical heat load distribution. Code_Bright one-canister models, such as those described above, are analyzed to determine how that approximation impacts on the rock wall temperature, cf. Appendix A. Figure 3-17 shows result examples. The detailed models with real copper/steel properties, with a realistic vertical heat load distribution and with account of moisture redistribution are those used above to establish the ΔT_{tot} margin (cf. Figure 3-16). Compared to these models, the homogenized canister model overestimates the rock wall temperature by at least 0.7°C. This means that there will be a built-in overestimate in the finite difference model results that is on the order of 0.7°C, provided that the canisters are represented as described here, i.e. as homogeneous 30 W/(m·K) cylinders. Representing the canisters in more detail and with a more realistic (higher) value of the canister conductivity would reduce that overestimate. The canister approximation described in Chapter 5 is made for computational efficiency and may be subject to changes. The 0.7°C margin suggested in Chapter 6 to account for that approximation is therefore an example.

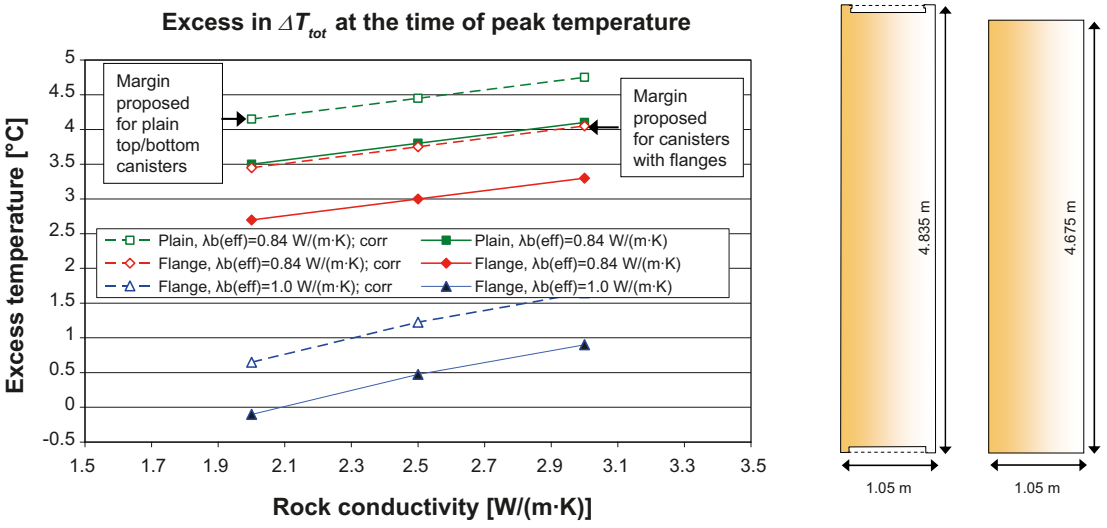

Figure 3-16. Left: Modelling results (excess temperature in relation to reference evolution) compiled to define ΔT_{tot} margin. Right: canister geometry with flanges and with plain top/bottom.

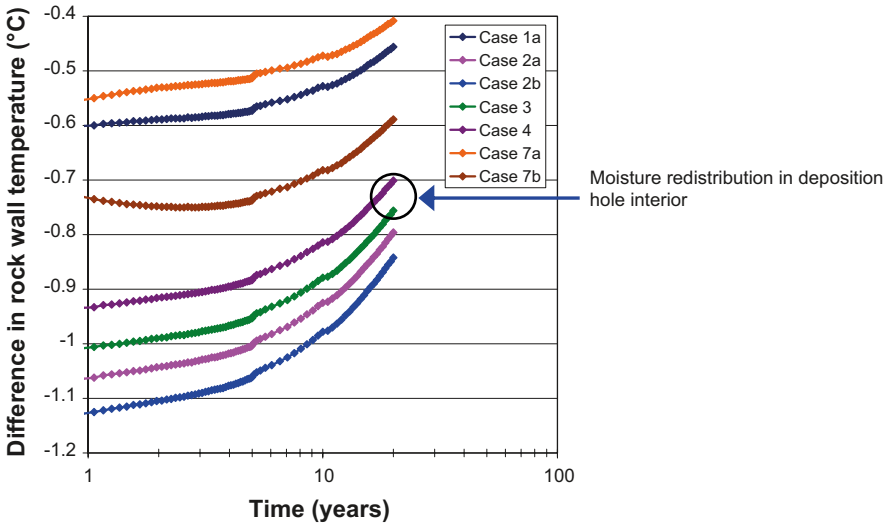

Figure 3-17. *Rock wall temperatures obtained from different detailed Code_Bright one-canister models compared with rock wall temperature from Code_Bright one-canister model with simplified and homogenized representation of canister, heat load and buffer (Case 11, cf. Appendix A). The detailed models with real copper/steel properties and with a realistic vertical heat load distribution give about 0.4–1.0°C lower rock wall temperatures than the simplified and homogenized Case 11 model. Compared with the models used to establish the* ΔT_{tot} *margin, the homogenized Case 11 model overestimates the rock wall temperature by at least 0.7°C.*

4 Peak temperature – Homogeneous rock properties

4.1 General

The temperature at the wall of the individual deposition contributes to determining the canister temperature and the maximum bentonite temperature within that particular deposition hole, as illustrated in Figure 1-2. Here an analytical solution for calculation of the rock wall temperature $T_{wall}(t)$ in a KBS-3 repository (or the temperature at any point within or outside the repository) is described. By adding the reference evolution $\Delta T_{tot}(t)$ of the difference between the rock wall temperature and the temperature at the canister top, estimates of the peak bentonite temperature can be obtained. The analytical solution captures the thermal evolution of the repository host rock at all scales in time and space and is a fast and useful tool for, for instance:

- Establishing the relative importance of the tunnel and canister spacing to the rock wall temperature.
- Exploring the importance of the deposition sequence to the rock wall temperature.
- Exploring how the rock wall temperature varies with position within the repository, e.g. rock wall temperatures in holes located close to tunnel ends compared to rock wall temperatures in central deposition holes.
- Exploring the effects of anisotropy.

The analytical solution cannot explicitly take account of the spatial variability of heat transport properties that is found in all rock domains investigated within the site investigation program. The rock heat transport properties must be assumed to be homogeneous. If the rock thermal properties are approximated by the rock domain mean values, the temperature at the walls of a large fraction of the deposition holes will be calculated with reasonable accuracy. The size of that fraction will, however, depend on the shape of the conductivity distribution. For deposition holes situated in low-conductive rock the solution will underestimate the rock wall temperature (and the peak buffer temperature) if the mean conductivity is used. For deposition holes situated in high conductive rocks the temperature will be overestimated.

To use the analytical solution to determine a trial value of the canister spacing that would fulfil the peak buffer temperature criterion (cf. Figure 1-3), a conductivity value must be picked from the low tail of the conductivity distribution established for the rock domain being considered. A very approximate way of doing this is presented in Appendix D.

4.2 Thermal analytical solution – description

In the KBS-3V concept, canisters are placed in vertical deposition holes beneath long parallel tunnels at depth *H* below the ground surface. The tunnels and deposition holes are separated by distances *py* and *px*, respectively. A schematic view of the repository layout is shown in Figure 4-1. Provided that

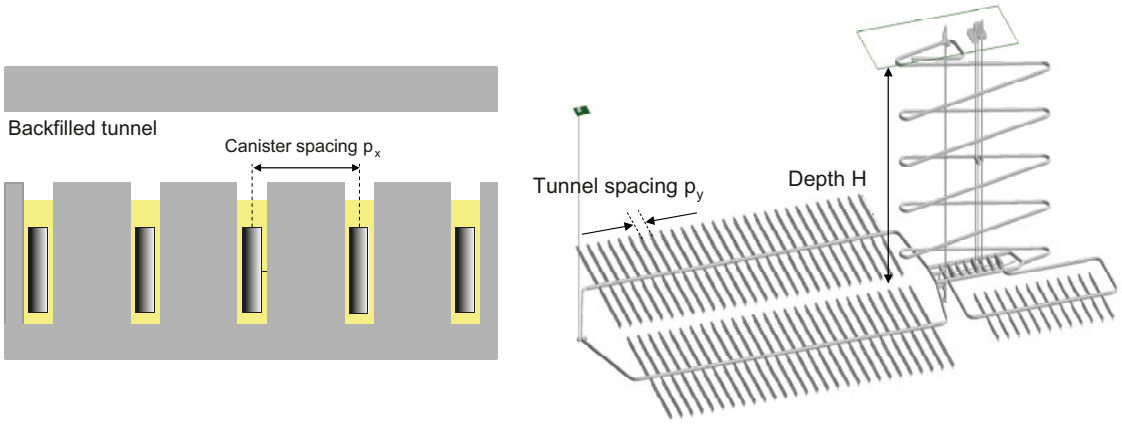

Figure 4-1. *Schematic view of the repository layout.*

the heat transport properties are uniformly and homogeneously distributed within the rock holding the repository, analytical calculation schemes, based on the principle of superposition, may be used to find the rock temperature increase at any point within the rock mass /Claesson and Probert 1996, Hökmark and Claesson 2005, Hökmark and Fälth 2003/. The analytical solution presented here is based on the approximation that the rock thermal conduction is linear. Geometric and thermal parameters can easily be varied in order to fit site specific data and investigate effects of different layout assumptions. A similar analytical solution scheme has been reported previously by /Hökmark and Fälth 2003/. The following is an extended and improved version that uses line sources and point sources to represent nearby canisters and combinations of rectangular heat sources to represent the rest of the repository.

4.2.1 Temperature at points outside panels

For the dimensioning of the repository, i.e. for determining canister and tunnel spacing, the thermal evolution above/below the repository and between deposition areas is not relevant. For repository components like plugs, borehole seals, shafts and ramps etc., which are located some distance away from the canisters, it will be required, however, that the thermal evolution can be described (also if there are no temperature limits) with reasonable accuracy. For points away from the heat-generating canisters the spatial variability in heat transport properties is much less important than for points at the walls of individual deposition holes, meaning that site mean values will be relevant and that the analytical solution is an expedient tool. A few examples are given for use as reference below.

A grid of canisters, such as the deposition areas (panels) shown in Figure 4-1 (right), can on a large scale be approximated as a rectangular heat source with power per unit area = $Q(t)/(px \cdot py)$, where $Q(t)$ is the time-dependent canister power /Claesson and Probert 1996/. For points at some distance from the panels (between one and two tunnel distances) the rectangular heat source is sufficient to calculate the temperature. Figure 4-2 (top) shows a schematic five-panel repository with 70 m between panels and with tunnel and canister spacing set at 40 and 6 m, respectively. There are 29 tunnels, each holding 41 canisters, in each panel. The repository is at 450 m depth and the canister power $Q(t)$ is as described in Chapter 2. Points A and B denote intersections with two arbitrarily selected vertical scan-lines. Figure 4-2 (centre) shows the temperature increase in a vertical section after 50 years resulting from the rectangular source representation of the panels. The vertical section is through the origin and across the panels. The bottom part shows corresponding results after 2000 years.

Figure 4-3 shows temperature increase as function of time at different points along the two scan-lines shown in the previous figure. Using the rectangular heat source solution, similar curves can easily be obtained for any point located at some distance from the canisters. Note that these results are all based on the assumption that all canisters are depositioned simultaneously. For each of the points the results apply with good accuracy for the local time-scale, i.e. with $t = 0$ at the time of deposition of the nearest canisters (cf. Section 4.4.4).

4.2.2 Temperature within panels

For points closer to the panels or within the panels, the details of the deposition geometry must be accounted for. Therefore, the panel temperature contribution inside a “window” positioned around the point of interest is subtracted and replaced with a more detailed representation of the individual canisters. Figure 4-4 illustrates this: The window has been dimensioned to hold three tunnel segments each containing 11 canisters. Inside the window, the local canister and its two nearest neighbours are represented by compound line sources /Hökmark and Fälth 2003/, see below. The second nearest neighbours are represented by ordinary line sources and the remaining canisters in the window by point sources.

4.2.3 Multi panel repository

Depending on the number of canisters and their position within the repository area, additional heat-generating panels can be added to the model. These may be placed anywhere within the rock mass and need not be of the same size or be deposited at the same time. Generally, for near-field analyses only canisters placed within a radius about 100 m of a given point will have any effect on the peak temperature at that point.

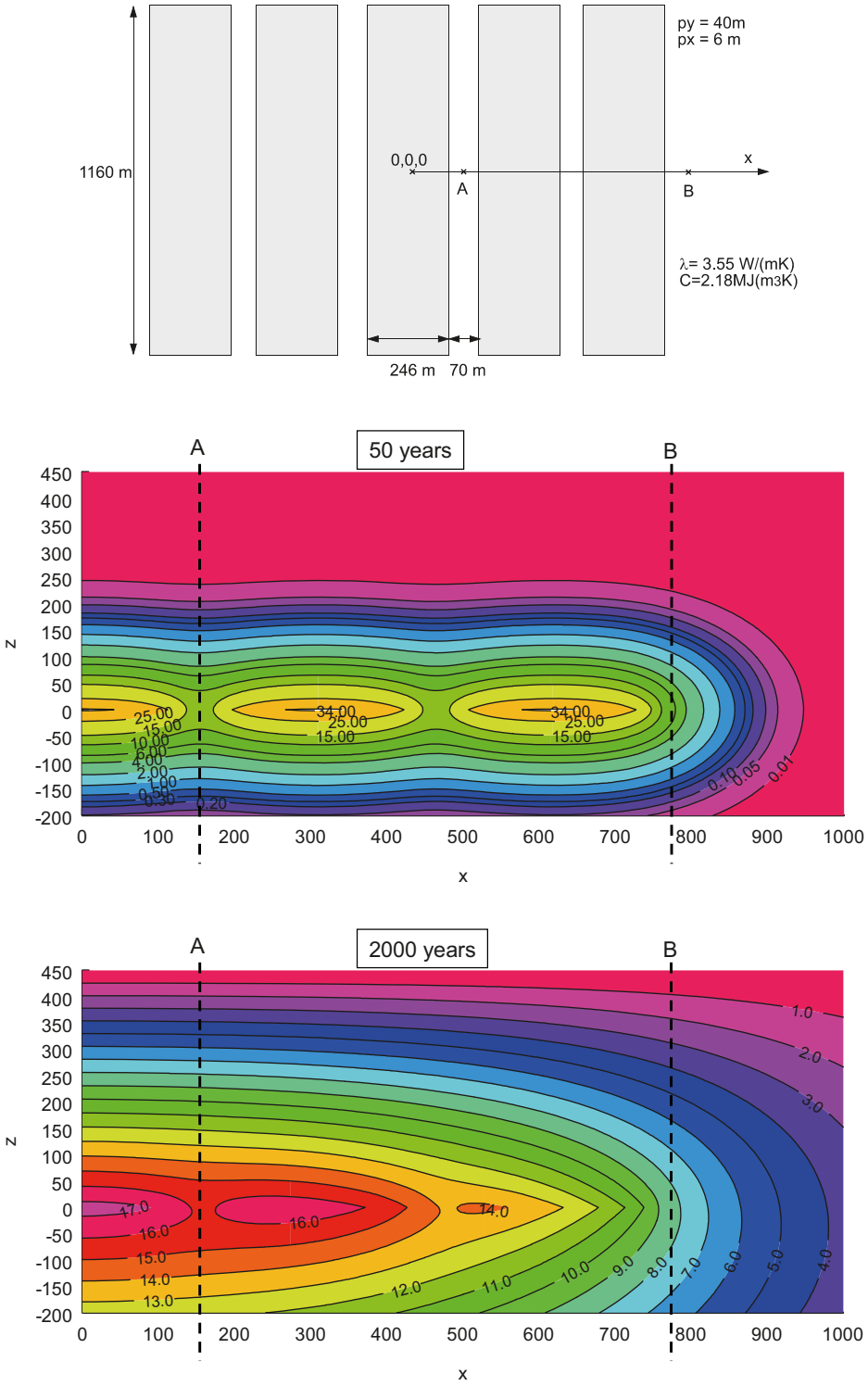

Figure 4-2. *Rock temperature increase calculated using rectangular heat sources. Values of the input parameters are shown in the top part.*

The governing equations for the analytical solutions in an isotropic medium are given in Section 4.3 (below). Corresponding expressions for the calculation of temperatures in anisotropic media, with different thermal conductivity in the coordinate directions, are presented in Appendix B.

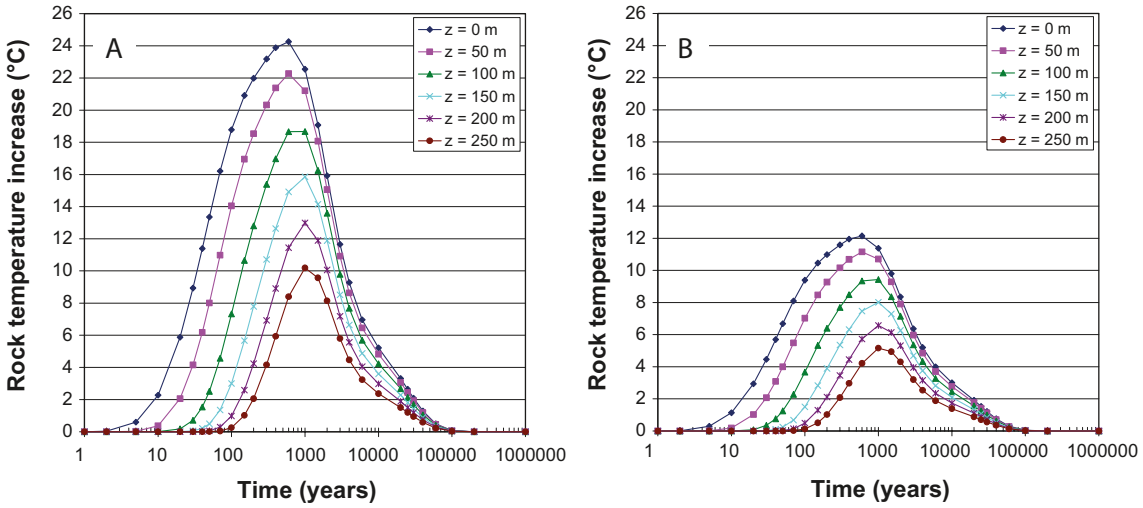

Figure 4-3. *Temperature increase at points on scan-lines A and B (cf. Figure 4-2). The legend gives the vertical distance to the repository.*

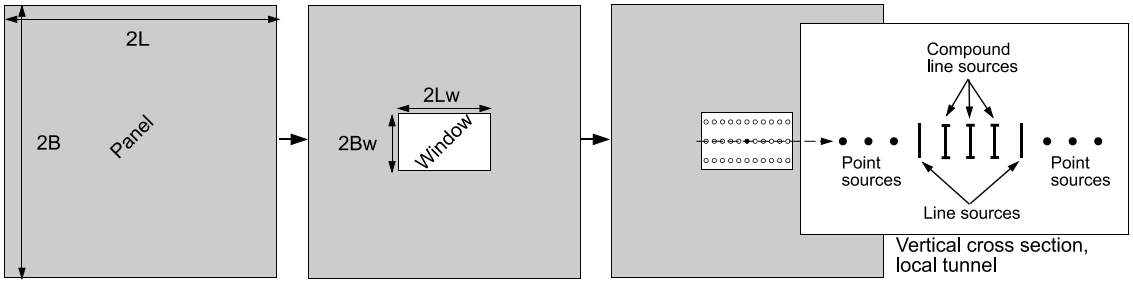

Figure 4-4. *Superposition of rectangular heat sources (panel, window) and line- and point sources.*

4.3 Analytical solution – governing equations

4.3.1 Point source

The temperature increase due to a point source with time-dependent power $Q(t)$ a radial distance r from its centre is given by /Carslaw and Jaeger 1959/:

$$T_p(r,t) = \frac{1}{\rho \cdot c \cdot \left(\sqrt{4\pi \cdot a}\right)^3} \int_0^t \frac{Q(t')}{(\sqrt{t-t'})^3} e^{-\frac{r^2}{4a(t-t')}} dt' \qquad 4\text{-}1$$

Here t is time, λ thermal conductivity, c specific heat capacity, ρ density and $a = \lambda/(\rho\, c)$ thermal diffusivity.

4.3.2 Line source

At short distances, the point source expression does not describe the temperature development from cylindrical heat sources well and should be replaced by line sources. The temperature increase due to a single line source, T_l, a radial distance r and vertical distance z from its mid-height is given by Equation 4-2. The solution is obtained from the expression for a point source (Equation 4-1) by integration over the entire height of the canister ($-H_c$, H_c), where $2H_c$ is the height of the canister.

$$T_l(r,z,t) = \frac{1}{\rho \cdot c \cdot 4\pi \cdot a} \int_0^t \frac{Q(t')}{2H_c(t-t')} e^{-\frac{r^2}{4a(t-t')}} \frac{1}{2}\left(\mathrm{erf}\left(\frac{H_c+z}{\sqrt{4a(t-t')}}\right) + \mathrm{erf}\left(\frac{H_c-z}{\sqrt{4a(t-t')}}\right)\right) dt' \qquad 4\text{-}2$$

4.3.3 Compound source

As seen in Figure 4-5 (left), the heat flux from a real cylindrical canister is not uniformly distributed along its length, instead it is larger at the canister top and base. Figure 4-6 shows that ordinary line source solutions overestimate the temperature at the rock wall by about 2°C. A more representative temperature distribution is given by the expression for a compound line source. A compound line source is given by the superposition of two ordinary line sources of different length and initial power /Hökmark and Fälth 2003/. The idea is schematically illustrated in Figure 4-5 (right).

The compound line source was calibrated to fit the thermal output, at canister mid-height, of a numeric FLAC model of a KBS-3V canister (cf. Figure 4-6) using the decay rate of 30-year-old fuel with initial power 1837 W/canister. It was found that a compound line source consisting of a superposition of two ordinary line sources with lengths as in Figure 4-5 (right) and power ratio $u_1/u_2 = 3.14$ (top/middle section) gave the best fit.

The compound source canister representation cannot be exactly correct for all cases. As noted in Chapter 3, the heat flux distribution around the canister depends on the existence of insulating gaps and on the distribution of burn-up within the fuel assemblies. The compound source described above is based on a no-gap deposition hole and on a uniformly distributed burn-up, which means that the rock wall temperature will be slightly overestimated.

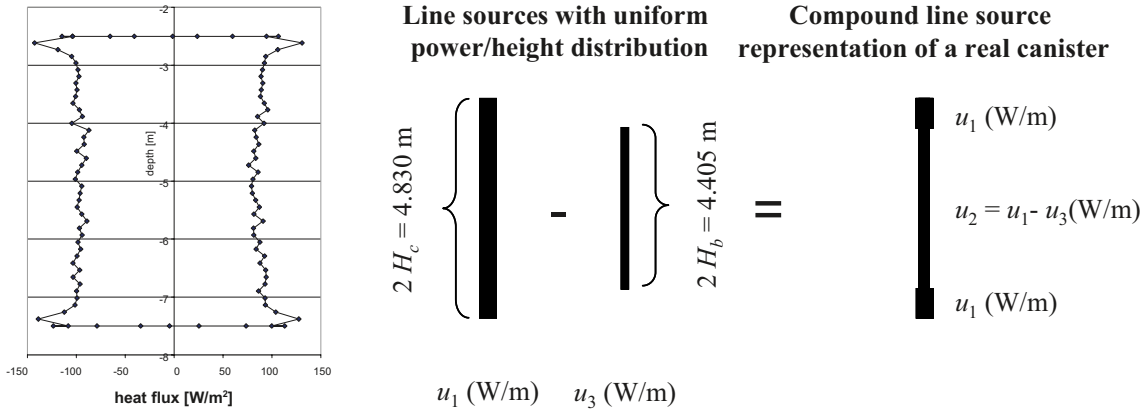

Figure 4-5. *Heat flux distribution from a real canister (left) from /Kristensson and Hökmark 2007a/. Compound line source representation of a real canister (right).*

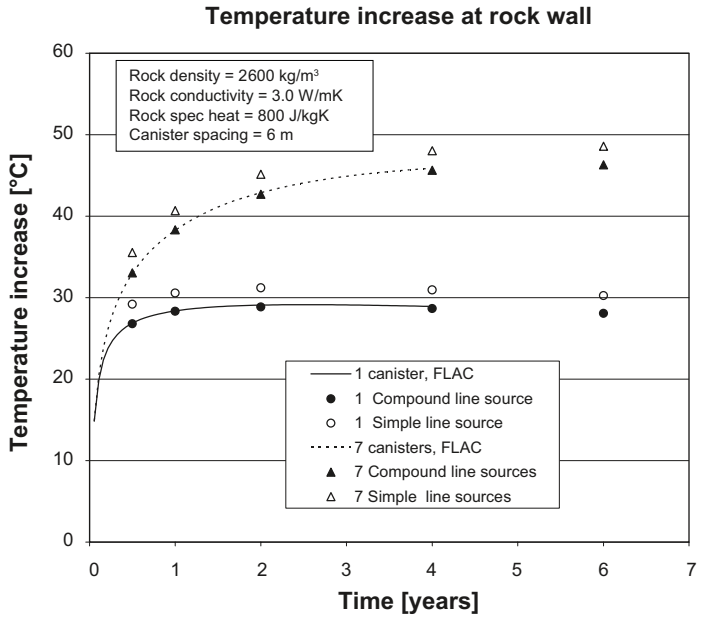

Figure 4-6. *Calibration of compound line sources, from /Hökmark and Fälth 2003/.*

4.3.4 Rectangular source

The expression for the increase in temperature due to a rectangular heat source /Claesson and Probert 1996/ with side lengths 2*L* (along tunnels) and 2*B* (across tunnels) and initial power per unit area, $Q(0)/(px \cdot py)$ is given by Equation 4-3. The parameters *px* and *py* are canister and tunnel spacing, respectively. The repository is located at $z = 0$ at depth *H* below the ground surface. *T(x,y,z,t)* is defined as the increase in temperature above initial conditions, which gives the boundary condition at the ground surface, $T(x, y, H, t) = 0$. This condition is achieved by adding a negative mirror heat source at $z = 2H$.

$$f = \frac{1}{\rho \cdot c\sqrt{4\pi \cdot a(t-t')}}\left(e^{-\frac{z^2}{4a(t-t')}} - e^{-\frac{(z-2H)^2}{4a(t-t')}} \right)$$

$$h = \frac{1}{4}\left(\mathrm{erf}\left(\frac{L+x}{\sqrt{4a(t-t')}} \right) + \mathrm{erf}\left(\frac{L-x}{\sqrt{4a(t-t')}} \right) \right)\left(\mathrm{erf}\left(\frac{B+y}{\sqrt{4a(t-t')}} \right) + \mathrm{erf}\left(\frac{B-y}{\sqrt{4a(t-t')}} \right) \right) \quad \text{4-3}$$

$$T(x, y, z, t) = \int_0^t \frac{Q(t')}{px \cdot py} f \cdot h \, dt'$$

4.4 Rock wall temperature – result examples

4.4.1 Canister in the central parts of a panel

The window is defined as a panel of dimensions $Lw = 11px/2$ and $Bw = 3py/2$ with negative power per area $= -Q(t)/(px\ py)$ symmetrically positioned around the canister (inside a larger panel) which is to be studied. The heat contribution inside the window is replaced with 3 tunnel segments, each containing 11 canisters, represented as shown in Figure 4-4.

For an arbitrary point within an N-panel repository (for instance a point at the wall of an arbitrarily selected deposition hole) the total rock temperature increase $T(x,y,z,t)$ is given by:

$$T(x, y, z, t) = T_{panel1} + \ldots + T_{panelN} + T_{window} \quad \text{4-4}$$

where T_{window} is calculated as described above, i.e. as the superposition of a negative rectangular source and a corresponding number of explicitly represented heat sources. Figure 4-7 shows an example. The panels holds 29 tunnels, each containing 41 canisters. The rock wall temperature at the specifically marked local canister varies with time as shown in the right part (full four panel repository).

As seen in Figure 4-7, during the first few years after deposition the local canister is the dominating source of the rock wall temperature at canister mid-height. More than 50% of the total temperature comes from the local canister. It takes many tens of years before panels other than the local one begin to influence. Putting additional deposition areas in the same plane as the local deposition area or even making the local deposition area "infinitely" large will not affect the maximum rock wall temperature.

4.4.2 Repository depth

Figure 4-8 shows the rock wall temperature increase at the same point as in the previous figure for the same layout and rock thermal property assumptions. Two additional depth assumptions are made. For the range considered here (300 m–10,000 m), the depth below ground surface does not impact until after 500 years. Since the peak temperature occurs long before that, this means that the repository depth is not important for the thermal dimensioning as far as the repository-driven temperature increase is concerned.

The repository depth will, however, impact on the initial temperature and consequently also on the total rock wall temperature according to the geothermal gradients established at the different sites.

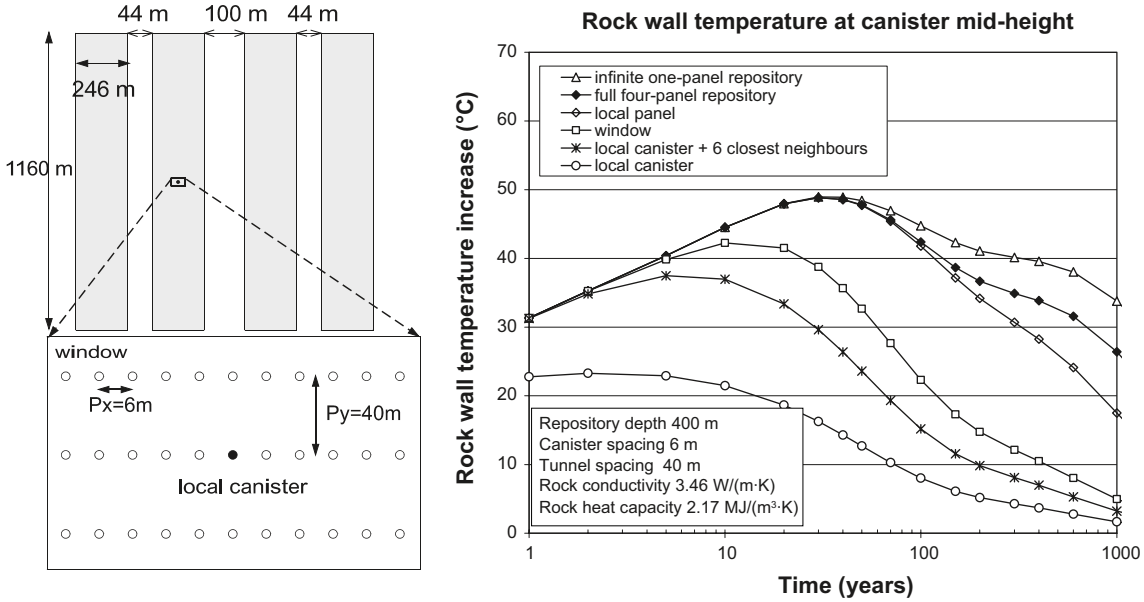

Figure 4-7. *Left: Schematics of four panel repository. Right: Rock wall temperature contributions from different parts of the repository.*

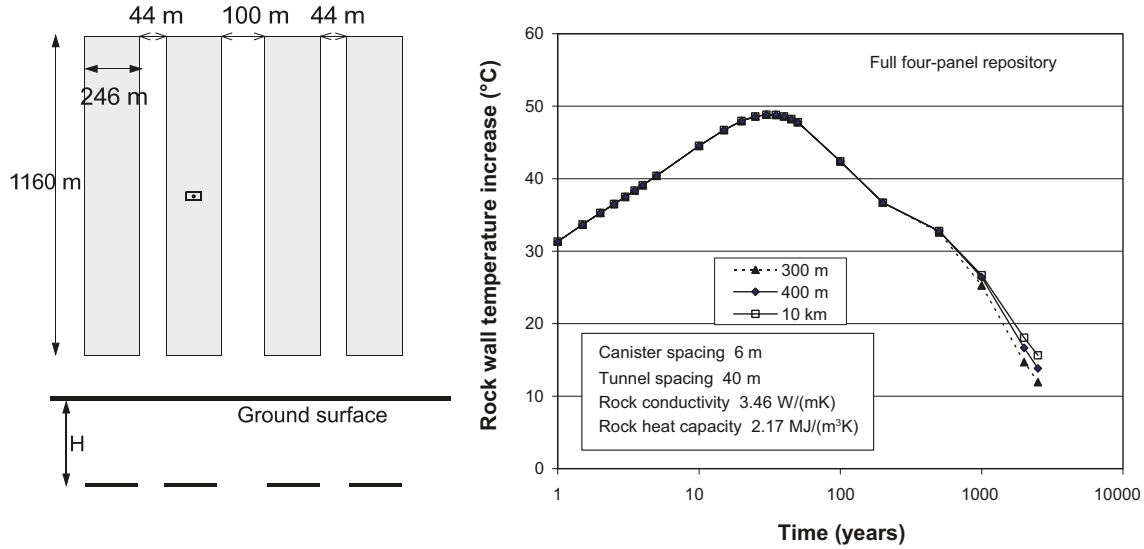

Figure 4-8. *Left: Horizonal and vertical sections through schematic four panel repoitory. Right: Rock wall temperature increase in the selected position for three different repository depth assumptions: H = 300 m, H = 400 m and H = 10,000 m.*

4.4.3 Canisters in panel edge regions

The rock wall temperature evolution shown in Figure 4-7 is valid for canisters in the central parts of the panels. Figure 4-9 and Figure 4-10 show corresponding results in a number of positions in the panel edge regions. The central canister results are included for comparison. The left part of Figure 4-9 shows the location of the canisters being analyzed and the way the window region was cut to obtain results at different distances from the edge. Positions 1 and 2 are at edges running across tunnels. Positions 3 and 4 are in corners. Position 5 is at an edge running along tunnels.

All results shown here regard the canister mid-height rock wall temperature which reaches a maximum some 25–40 years after deposition. The bentonite peak temperature, which is the design parameter of interest here, will be reached earlier: about 10 years after deposition. At the time of the peak bentonite

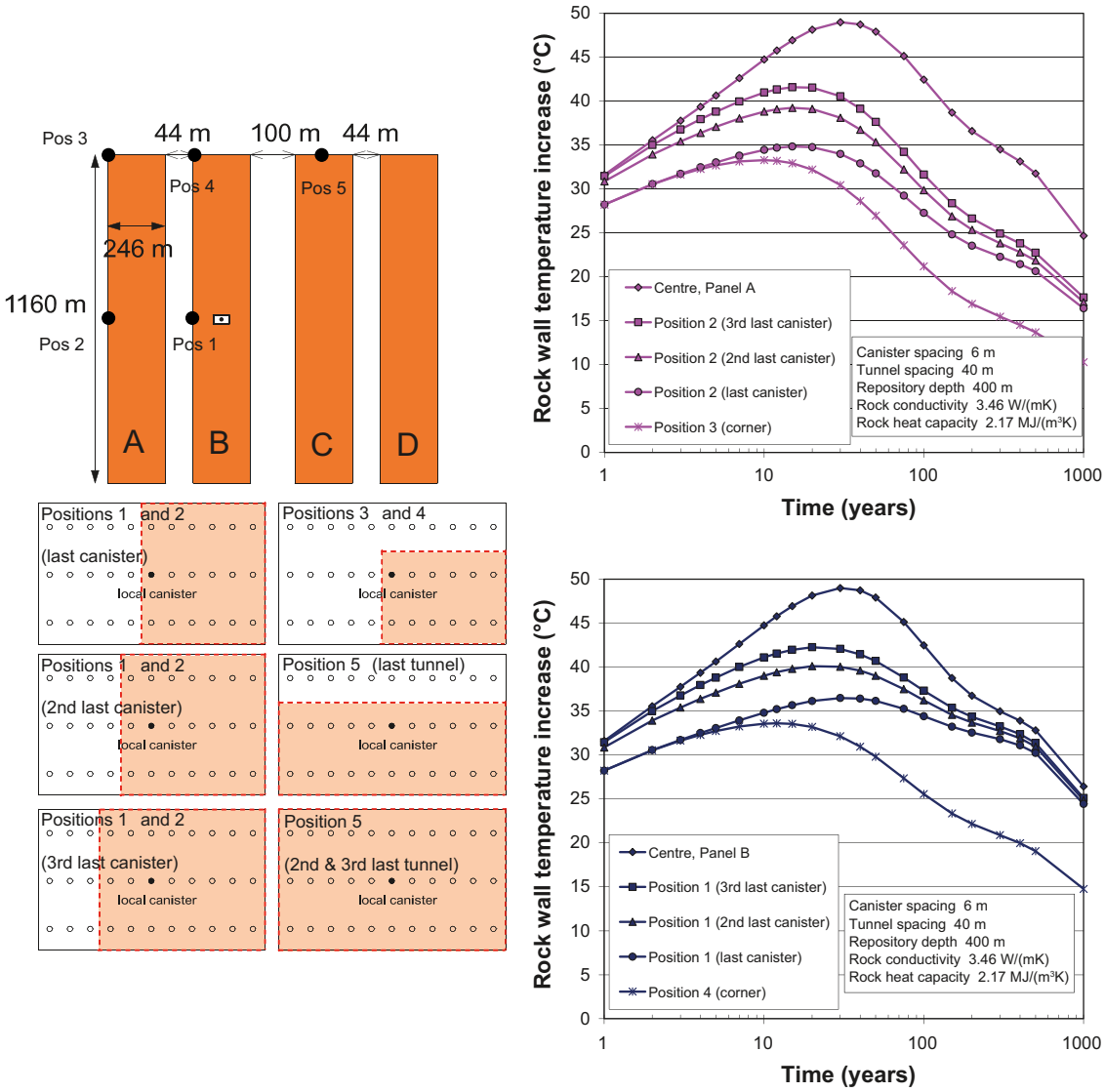

Figure 4-9. *Left: positions being analyzed. The lower part shows window geometry, i.e. regions with individually represented canisters. Upper right: rock wall temperature increase for different canisters in panel A. Lower right: Corresponding results for Panel B.*

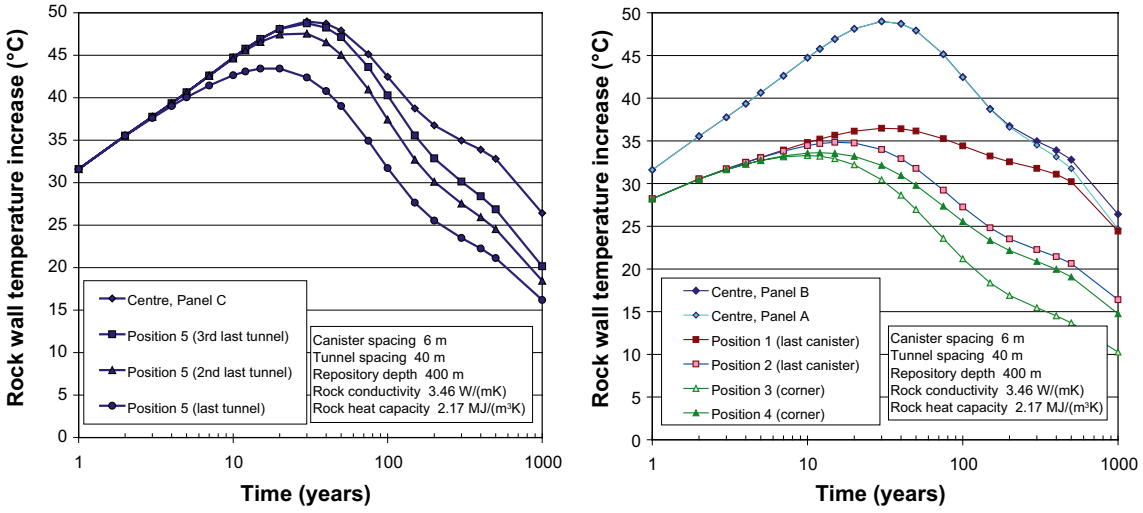

Figure 4-10. *Rock wall temperature increase in different positions. Left: Edge tunnel, 2nd and 3rd tunnel. Right: comparison between correspondingly located canisters in panel A and panel B.*

temperature, tunnel end canisters will be about 10 ºC colder than central canisters. Second and third canisters will be about 6ºC and 4 ºC colder, respectively (Figure 4-9, right). Fourth canisters will be one or two degrees colder (not shown here). The exact reductions will vary with heat transport properties and with canister spacing. Figure 4-10 (left) shows that there are temperature reductions in edge tunnels; about 2ºC after 10 years. Canisters in second and third tunnels will, however, have the same temperature as central canisters (after 10 years). Figure 4-10 (right) shows that there is very little difference between correspondingly located canisters in different panels after 10 years. At the time of the bentonite peak temperature it will be unimportant if a tunnel end faces the undisturbed rock outside the repository (such as canisters in position 2 in panel A) or the transport tunnel region between panels (such as canisters in position 1 in panel B). Assuming that there will be about 200 tunnels in the repository, these results imply that more than 1,000 canisters out of 6,000 will have significantly lower temperatures than the majority of the canisters.

4.4.4 Deposition sequence

The results above were obtained assuming all canisters to be deposited simultaneously whereas in reality the deposition will be distributed over a period of time. This means that the possibility that effects of heat generated by early canisters could reach positions of late canisters in time to raise the peak temperature is ignored. That effect would obviously be larger the longer the deposition is extended over time. Figure 4-11 shows the effect of extending over time for two canister positions and for two deposition rate assumptions: one canister every second day and one canister every fourth day.

The reference deposition order would be to start in the edge of one panel and then deposit systematically tunnel by tunnel and panel by panel as shown in Figure 4-11, top left and middle left. The bottom left part shows a “worst case” deposition order, starting in the centre of one panel and completing the deposition some 24 years later in a neighbour tunnel in the same panel. Here, the long time elapsed between deposition of the first canisters and the local one combined with the small distance (one tunnel spacing) between the first canisters and the local canister will give a significant preheating of the rock around the local canister.

The curves show the excess in canister mid-height rock wall temperature compared with simultaneous deposition. The local canister is deposited at time zero. For the systematic panel-by-panel deposition (upper right) there is very little consequence of ignoring the time aspect. This is in keeping with results reported earlier /Hökmark and Fälth 2003, Hökmark and Claesson 2005/. During the first 20 years, the effect is about 0.1°C for the slow deposition rate and much less for the fast one (2 days/canister). For the worst case deposition order, the effect is very significant (lower right).

4.5 Verification of analytical solution

The analytical solution has been verified and tested against the built-in thermal solution in the numerical code 3DEC /Fälth and Hökmark 2006/. In 3DEC, the heat generation is represented by grids of point sources. These can be stacked on top of each other to form line sources and compound line sources. The panels were positioned as in Figure 4-12. As seen in Figure 4-13 there is a very small discrepancy between the two solutions.

The 3DEC model used for the verification above contains compound sources, i.e. superposed vertical arrays of point sources. The strengths and lengths of the two arrays making up a 3DEC compound source were calibrated to match the heat flux redistribution around the analytical compound source, meaning that the two solutions are not fully independent. An additional, fully independent, verification is presented below. The contribution to the rock wall temperature from the local canister, i.e. from one individual compound source as shown in Figure 4-5, is calculated separately and compared with corresponding results from Code_Bright one-canister near-field models. The Code_Bright models were analyzed for two cases: with and without an air-filled gap between canister and bentonite (Figure 4-14). The agreement between the analytical solution and the no-gap Code_Bright results is very satisfactory. This should be expected: the analytical compound source solution was calibrated to match results from a no-gap FLAC model (cf. Figure 4-6). The Code_Bright results shown in Figure 4-14 (left) confirm the relevance of the FLAC calibration and point additionally to the effect of an air air-filled gap (increased redistribution of the canister surface heat flux, cf. following section).

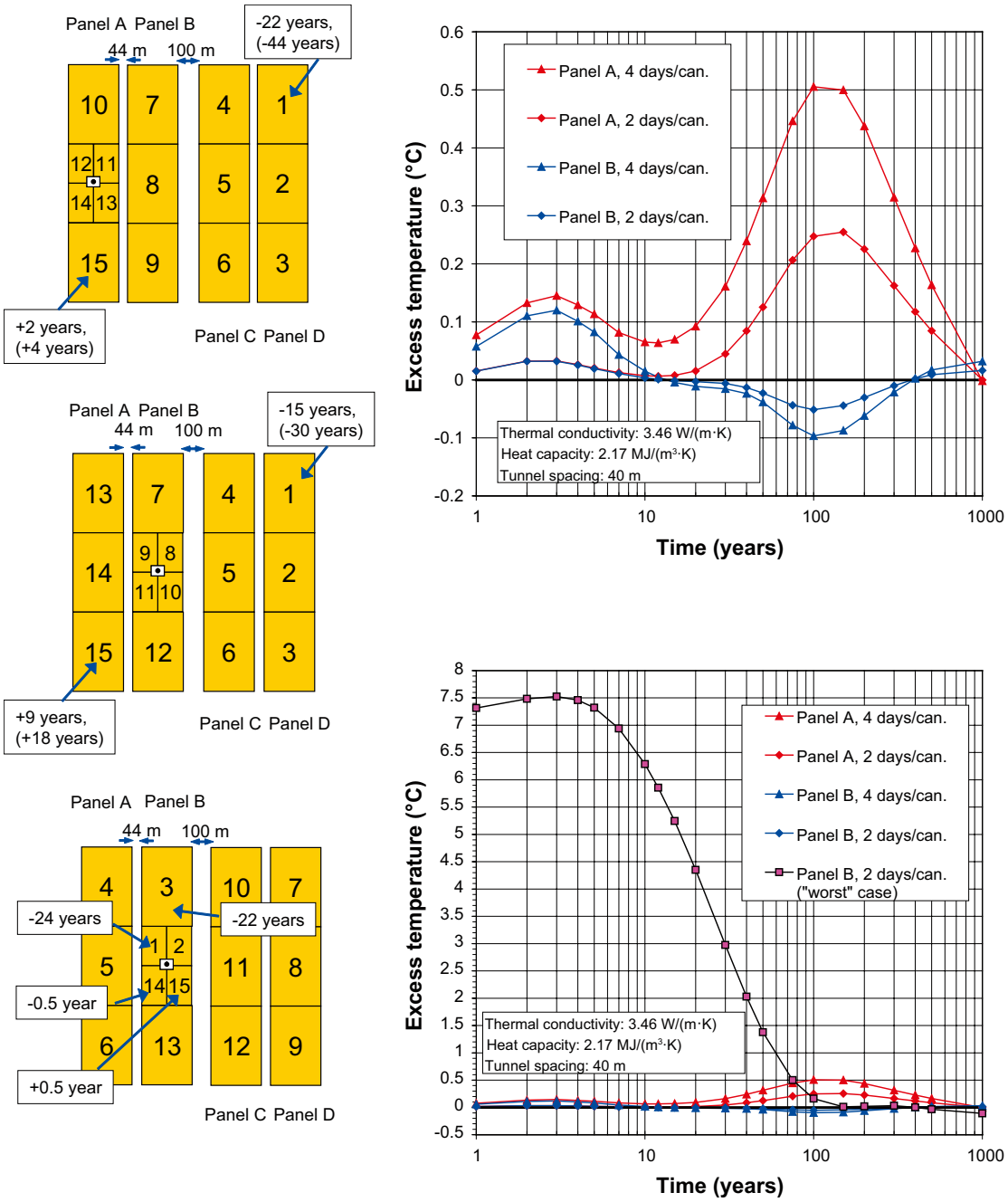

Figure 4-11. *Left: Subdivision of panels into smaller units with increased refinement of the time resolution around and in the window region. The canister being analyzed is located in the centre of panel A (upper left) or B (centre and lower left). Time zero is when the canister being analyzed is deposited. Deposition starts in sub-panel 1 and is finished in sub-panel 15 at the indicated instances of time. Times in parentheses regard the 4 days/canister deposition scheme. Right: Rock wall temperature excess (compared to simultaneous deposition).*

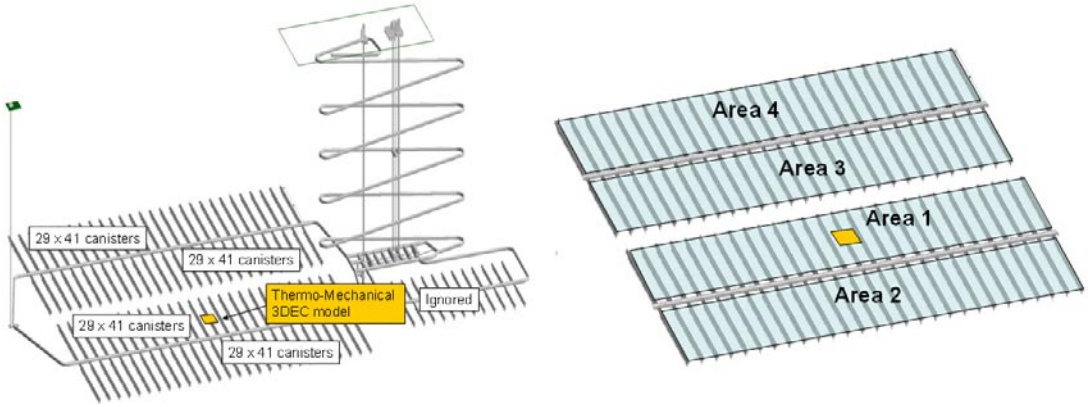

Figure 4-12. *Schematic figure of the general repository layout used in the comparison between 3DEC solution and analytical solution. The point of comparison is located at the wall of a deposition hole within the "Thermo-mechanical 3DEC model" volume.*

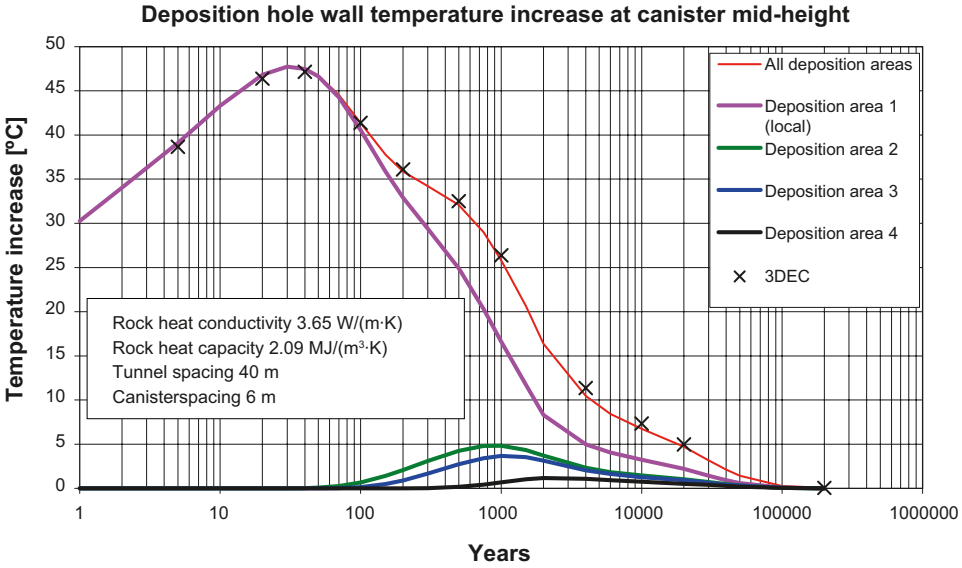

Figure 4-13. *Temperature increase at mid-height of the central deposition hole in the "Thermo-mechanical 3DEC model". The deposition area numbering is according to Figure 4-12 (right). The contributions from areas other than Area 1 are relatively unimportant and do not influence the local conditions until some 100–200 years after deposition. From /Fälth and Hökmark 2006/.*

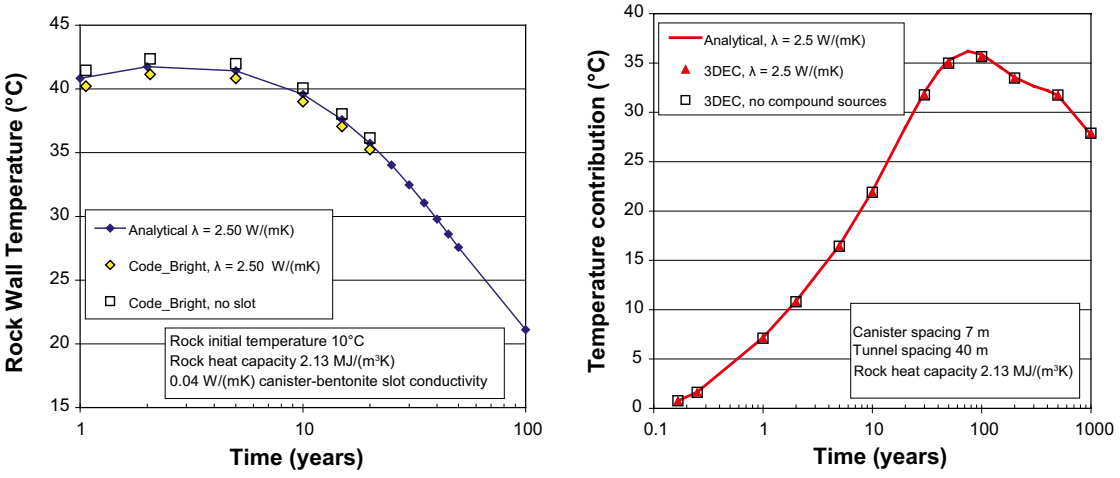

Figure 4-14. *Comparison of numerically and analytically calculated rock wall temperatures. Left: contribution from local canister. Right: contribution from all other canisters.*

Figure 4-14 (right) shows the contribution of all canisters except the local one to the rock wall temperature. There are two 3DEC model versions: nearest neighbours are modelled as compound sources or as simple line sources. Obviously, at least for a point at the wall of the deposition hole, canisters other than the closest (local) one do not need to be modelled as compound sources. This is in accordance with the results shown in Figure 4-6.

4.6 Analytically calculated peak buffer temperatures – result examples

The maximum bentonite temperature is obtained here as the sum of rock wall temperature $T_{wall}(t)$ and the reference evolution $\Delta T_{tot}(t)$ of the gap effect plus buffer temperature drop as follows (cf. Figure 1-2):

1. Calculation of the rock wall temperature. This temperature is approximated to be independent of the conditions in the interior of the deposition hole, except for the power and shape of the canister, but depends strongly on the heat transport properties of the rock and on the layout, i.e. the tunnel spacing and the canister spacing.
2. Calculation of the temperature difference $\Delta T_{tot}(t)$ between the rock wall and the canister/bentonite interface at the top of the canister, as described in Chapter 3.
3. Addition of the rock wall temperature and the temperature difference to get the bentonite temperature at the hottest point.

Figure 4-15 shows results for canisters deposited in the central parts of panels for two rock conductivity assumptions. Here the canister spacing has been set at 7.5 m and 6.0 m, respectively, to get the same peak buffer temperature in both cases.

4.7 Uncertainties and margins

4.7.1 General

There are built-in overestimates/underestimates as well as uncertainties in the analytical scheme. The effects of uncertainties and over/underestimates on ΔT_{tot} are the same as those described in Chapter 3.

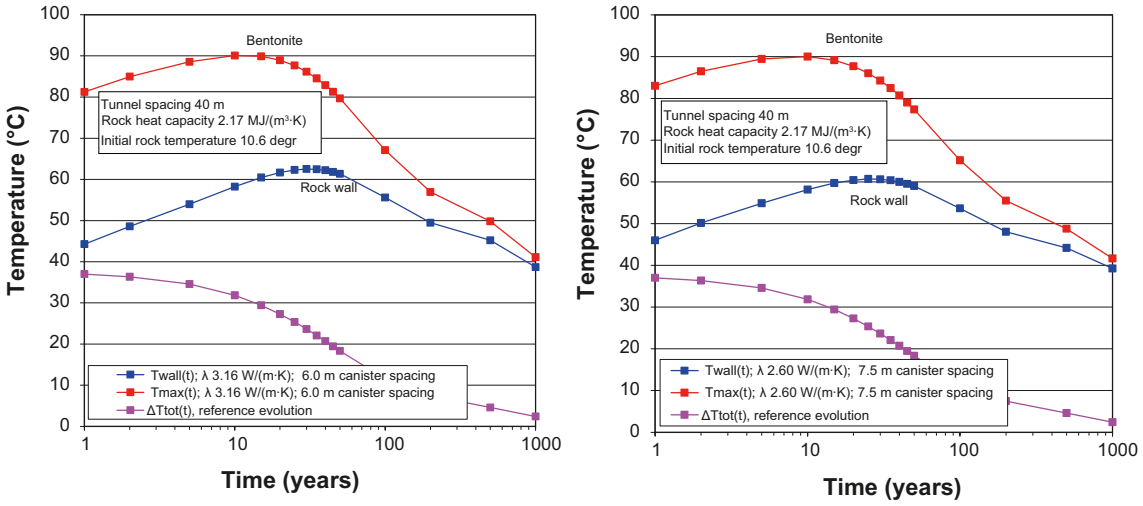

Figure 4-15. *Result examples. Peak buffer temperatures for two combinations of rock conductivity and canister spacing.*

Uncertainties in rock properties data and in the initial temperature are described in Chapter 6. There are two model simplifications of some importance that impact specifically on the analytically calculated values of T_{wall}:

- The heat flux redistribution. The compound source is not configured to account for gaps and for details in the burn-up distribution.
- The backfilled tunnel is ignored.

The effects of both these issues are discussed below. At least approximately they tend to cancel out. The margins required to cover effects on ΔT_{tot} as described in Chapter 3 (3–4°C) and the margins required to cover rock property data and initial temperature uncertainties described in Chapter 5 (1–2°C) will determine the total temperature margin that would be required if the canister spacing were to be based on the analytical solution. In the examples shown above in Figure 4-15, the margin to the 100°C threshold appears to be 10°C. The analytical solution presented in this chapter will however be used only to provide trial values of the layout parameters, whereas the final layout will based on results of the numerical finite difference model presented in the following chapter (cf. Figure 1-3). Therefore, it is not meaningful to establish the required analytical margin without too much rigor. In the nomographic charts presented in the following, the total margin is arbitrarily approximated to 8°C. The margins applied in the final layout work will be based on the description given in Chapter 6.

4.7.2 Heat flux distribution

The analytical solution (i.e. the compound source) does not take the additional heat flux redistribution that follows from open canister-bentonite gaps into account. Figure 4-16 shows that this overestimates the rock wall temperature (of dry deposition holes) by a little more than 1ºC. The compound source does not account for the burn-up distribution within the assemblies. This gives an underestimate of 0.1–0.2 ºC (Appendix A). These two simplifications together are estimated to produce an overestimate of the rock wall temperature of 1ºC.

4.7.3 Influence of the backfilled tunnel

The deposition tunnel and the top 1 m of the deposition holes will be filled with a backfill material with a lower thermal conductivity than the rock. This cannot be accounted for in the analytical solution, meaning that there will be small underestimates in the analytically determined rock wall temperature at canister mid-height 5 m below the tunnel floor. The Prototype Repository at the Äspö HRL has recently been modelled thermally in three dimensions and in great detail /Kristensson and Hökmark 2007a/. Figure 4-17 shows canister mid-height temperatures calculated for a number of backfill thermal conductivity assumptions, assuming the Prototype Repository rock mass conductivity to be 2.72 W/(m·K). Ignoring the tunnel backfill appears to generate an underestimate of about 0.6 ºC, provided that the

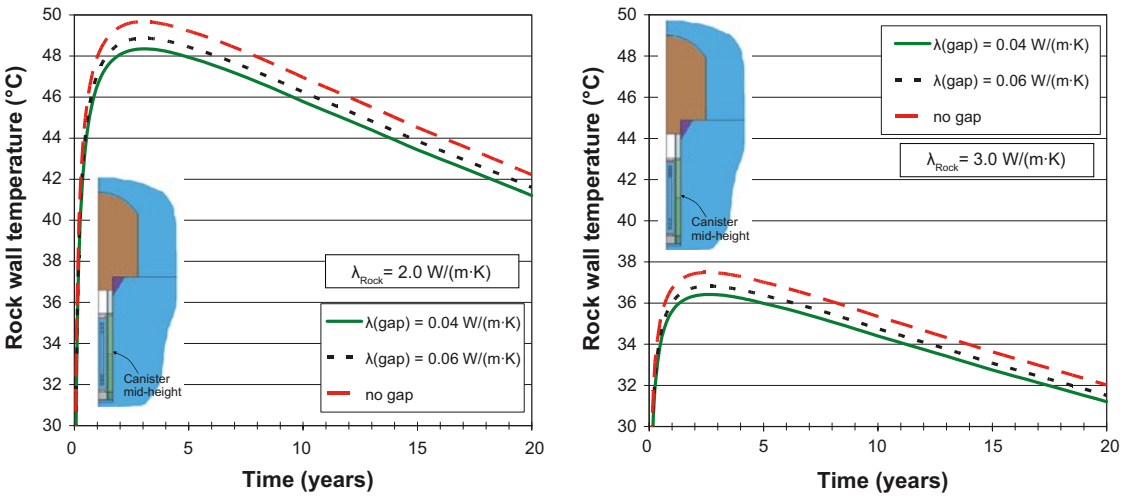

Figure 4-16. Code_Bright one-canister model results. Rock wall temperature at canister mid-height for different assumptions regarding the effective canister-bentonite gap thermal conductivity (See Appendix A).

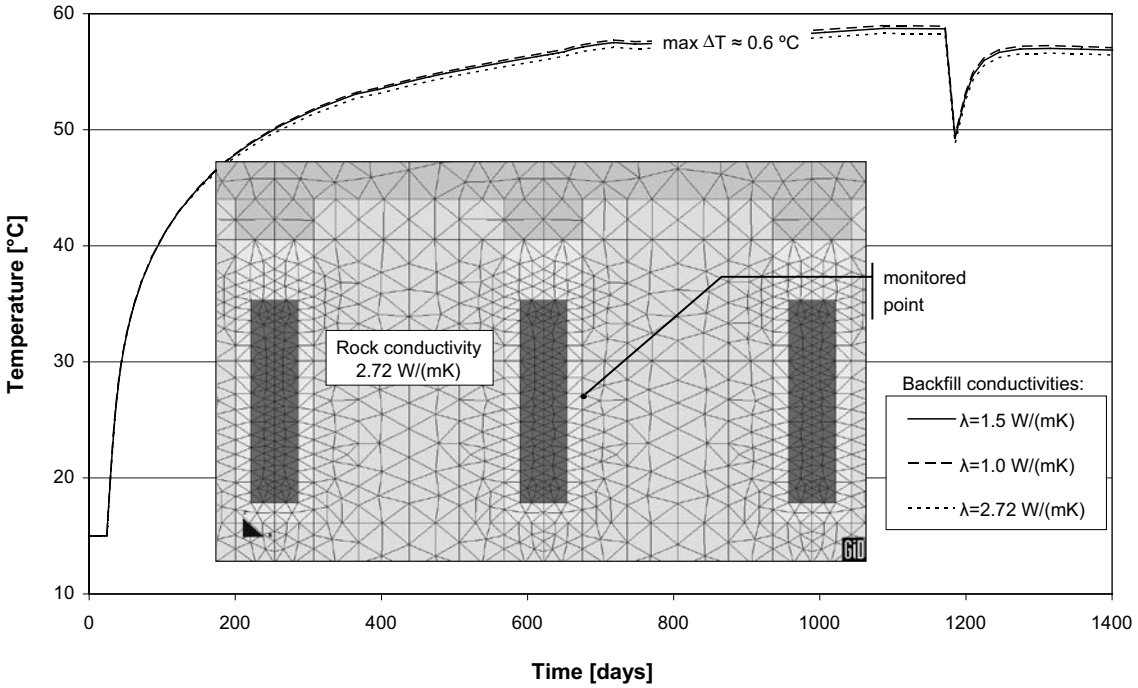

Figure 4-17. *Rock wall temperature at canister mid-height for different backfill conductivity assumptions. Results from /Kristensson and Hökmark 2007a/.*

backfill conductivity is as low as 1.0 W/(m·K). This is in agreement with previous work, cf. /Ageskog and Jansson 1999, Hökmark and Fälth 2003/. There is a possibility that the backfill conductivity is even lower, meaning that the underestimate in the analytical solution may be higher, perhaps around 1ºC.

4.8 Nomographic charts

Figure 4-18 shows peak buffer temperatures calculated as described above for a large number of conductivity and layout assumptions. Here the in-situ temperature is set at 0°C, meaning that some 10 or 15°C must be added, depending on the conditions at the site being considered. The heat capacity is set at 2.17 MJ/(m^{3}K). To use nomographic charts such as this for layout considerations, the heat capacity value will have to be set according to site data.

The analytical solution is fast enough that numerous calculations with different layout and heat transport property assumptions can be conducted in few minutes. The nomographic chart in Figure 4-18 is based on many hundreds of automated calculations of the peak buffer temperature. Each of the 546 plot symbols corresponds to one individual conductivity-spacing assumption. Each was analyzed in the number of 1-year steps necessary to reach and pass the peak value, starting one year after deposition. For the highest values of the canister spacing the peak occurs 3–5 years after deposition, for the lowest values after some 15 years. A fixed value was used for the heat capacity here. The automatic calculation scheme can easily be modified to take conductivity-capacity correlations into account.

The nomographic chart shows the peak temperature increase at the top of the canister. To arrive at the actual peak temperature, the initial undisturbed rock temperature must be added. The margin required to account for data and model uncertainties and for systematic over/underestimates has been set at 8°C. If the undisturbed rock temperature is 11°C, this means that the maximum allowed calculated increase would be 81°C. The intersections with the horizontal 81°C line give the spacing required to ensure that this condition is met for different rock thermal conductivities. This is illustrated for two conductivity cases: 2.8 and 2.4 W/(m·K) which appear to require a canister spacing of 6.6 and 8.0 m, respectively.

The nomographic chart in Figure 4-18 is based on the reference tunnel spacing, 40 m. If it is necessary to optimize the layout for volume (or area) rather than for total tunnel length, smaller distances between tunnels must be considered. Figure 4-19 shows two examples of tunnel/canister spacing charts produced

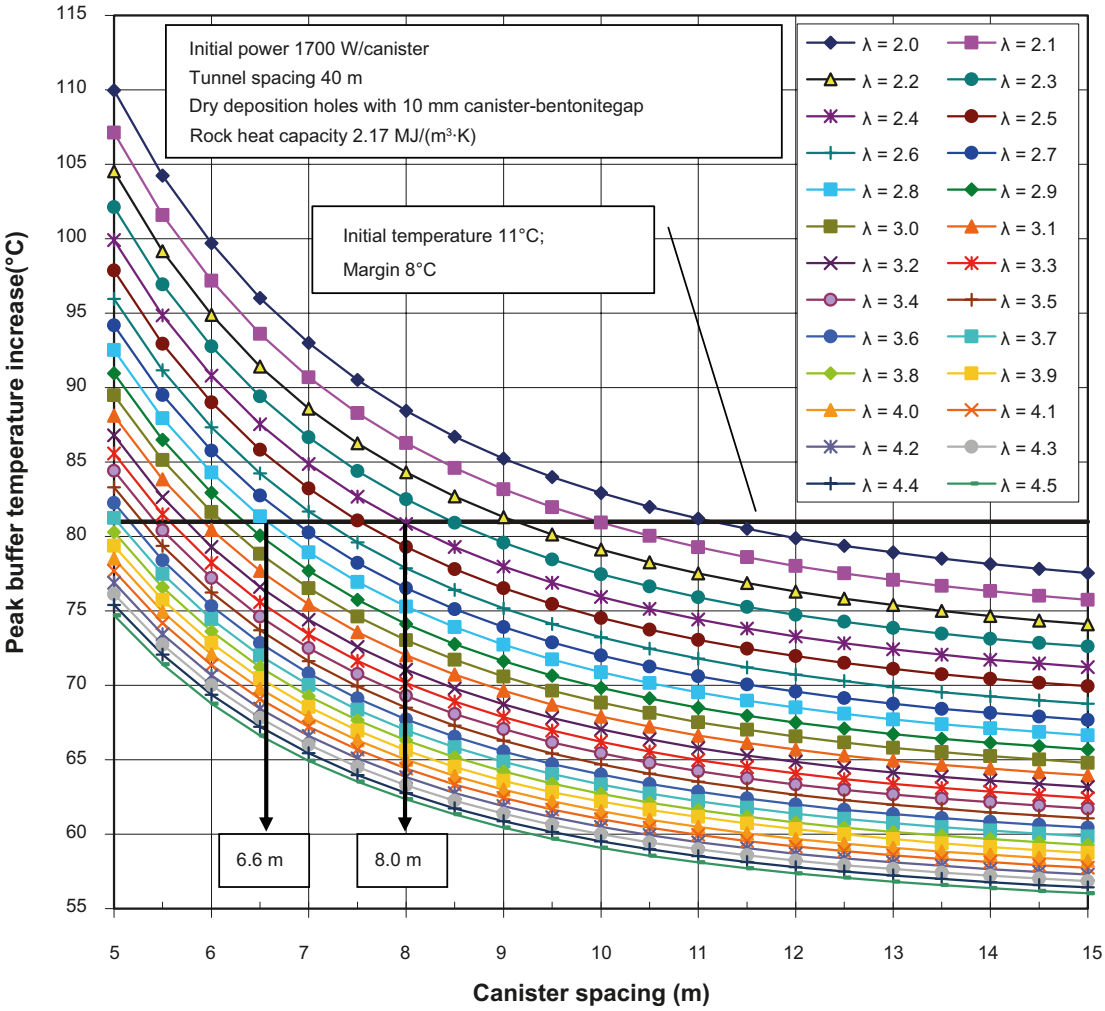

Figure 4-18. *Peak buffer temperature increase as function of canister spacing for a number of rock conductivity assumptions. To get the absolute value the in-situ temperature must be added. The margin is set to 8°C.*

by use of the analytical solution. Here, the initial undisturbed temperature has been set at 11.16°C and 14.8°C, respectively, and the model/data margin as earlier at 8°C, i.e. the 92°C isoline temperature includes the peak temperature increase as well as the initial temperature. Taking the 2.9 W/(m·K) curves as examples, the charts illustrate a way to reduce repository area at the expense of increasing total tunnel length. If the tunnel spacing is reduced from 40 m to 30 m, the canister spacing must be increased from 6.5 m to 7.5 m (upper example) and from 7.1 m to 8.15 m (lower example). This means an area reduction of about 15% for each canister, i.e. a significant reduction of the total rock volume required to accommodate the repository.

4.9 Account of spatial variations

The analytical solution cannot account for spatial variations. In order to use nomographic charts of the type shown in Figure 4-18 for estimation of the required minimum spacing, a relevant dimensioning value of the rock domain conductivity must be selected. The rock domain mean value would be approximately appropriate for a large fraction of the canisters, but would overestimate the heat dissipation for canisters in low-conductive parts, and consequently underestimate the temperature for these canisters. Therefore the rock domain mean conductivity value cannot be used to determine the domain spacing.

Reasonable estimates of the dimensioning conductivity can be obtained by recognizing that the increase of the temperature of any individual canister is determined not only by the local heat dissipation which is controlled by the properties of the nearest rock. The contribution from other canisters (which makes out

about 50% of the temperature increase at the time of the peak buffer temperature 5–15 years after deposition, cf. Figure 4-7) depends on heat transport properties averaged over larger rock volumes than those that control the local heat dissipation. An approximate way of establishing reasonable guess or trial values of the dimensioning conductivity in rock domains with different types of conductivity distributions is given in Appendix D. The scheme described in Appendix D takes the rock domain property distribution, but not the associated geology-based spatial correlation, into account.

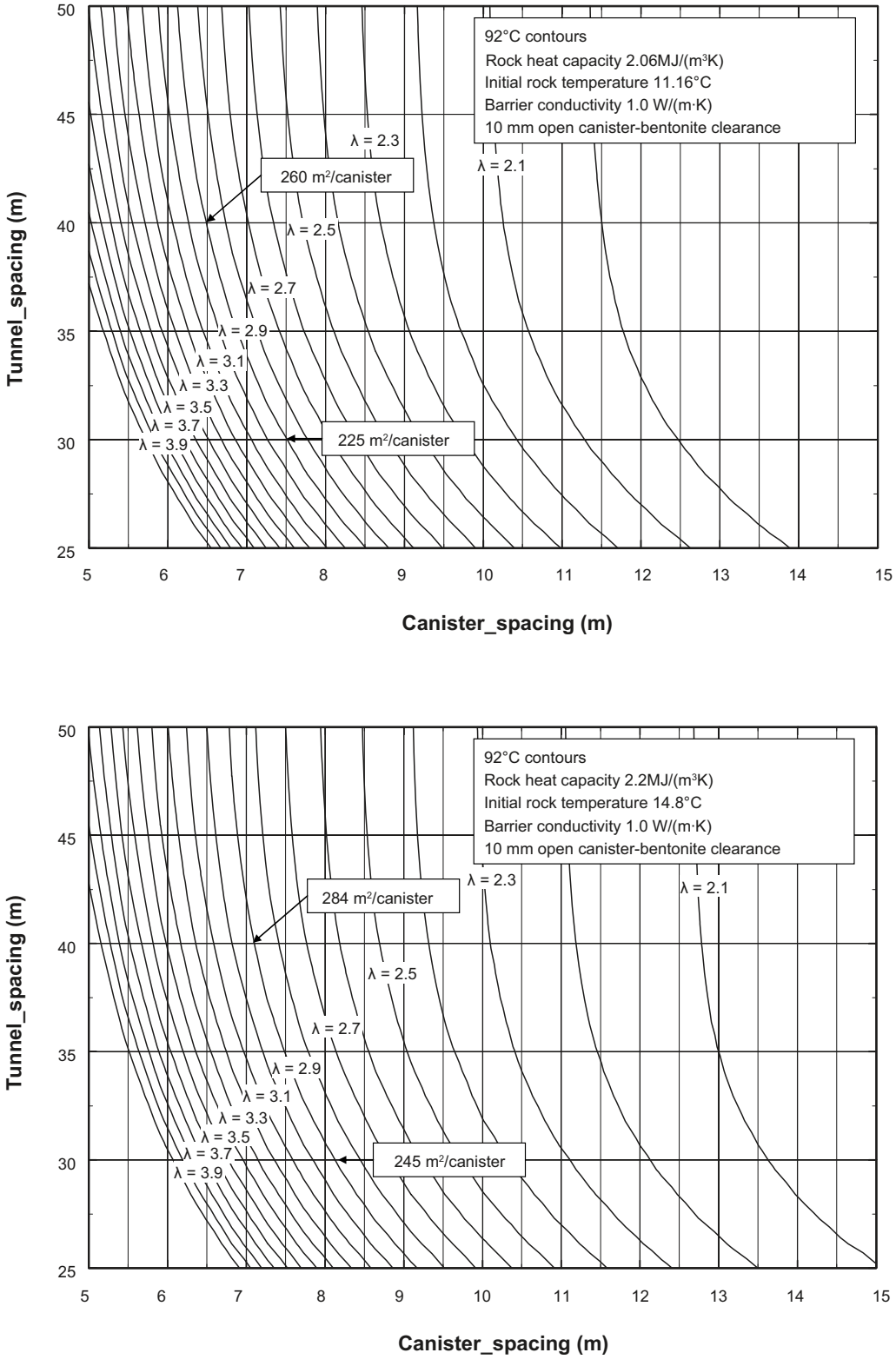

Figure 4-19. *92°C peak temperature isolines for two assumptions regarding initial temperature and the rock heat capacity.*

5 Assessment of buffer peak temperature – inclusion of spatial variabiltiy

5.1 General

The method for determining the peak buffer temperature described in the previous chapter is based on an analytical solution for calculating the rock wall temperature. A schematic expression (the "reference evolution", cf. Chapter 3) for the difference $\Delta T_{tot}(t)$ between the rock wall temperature and the bentonite temperature at the top of the canister is then added to find the peak buffer temperature.

Provided that mean values of the rock thermal properties are used, the analytically obtained peak temperatures will be approximately relevant for a large number of canisters. For canisters positioned in volumes with low conductive rocks the analytical method (with mean thermal properties) will underestimate the peak temperature, and consequently the canister spacing required to ensure that the peak temperature does not exceed the design threshold. For canisters in high conductive rocks the analytical method will overestimate the peak temperature, and consequently the required canister spacing.

Given the distribution of rock thermal properties of the rock domain being considered, it would be possible, at least theoretically, to establish values of the equivalent homogeneous properties that effectively would control the thermal evolution in worst case positions (cf. Section 4.9). However, establishing equivalent homogenous properties is not a well-defined problem with a well-defined problem scale. The relative importance of the rock immediately surrounding the individual canister and rock at different distances, for instance, will change over time. In addition, the temperature contributions from neighbouring and distant canisters are determined by properties averaged over much larger volumes than those that control the heat dissipation from the local canister.

In the present chapter a numerical approach is described that automatically respects the variation in scale and which also takes direct account of the rock domain distribution of the rock thermal properties and the spatial variability of these. The numerical finite difference scheme gives the rock wall temperature at canister mid-height. The peak buffer temperature is then obtained by addition of $\Delta T_{tot}(t)$ as described above for the analytical solution. In the strategy for thermal dimensioning of the repository the numerical approach is used to establish the minimum canister spacing required to ensure that the design criterion is met in all parts of the repository, i.e. also those dominated by rock types belonging to the low conductivity tail of the different rock domain distributions.

5.2 Overview of the numerical approach

In the thermal site descriptive models for Forsmark /Back et al. 2007, Sundberg et al. 2008a/ and Laxemar /Sundberg et al. 2008b/ stochastic modelling of the spatial thermal conductivity in the rock mass is performed according to the strategy developed in /Back and Sundberg 2007/. About 500–1,000 realisations are performed for each rock domain. Each realisation contains typically 125,000 cells at 1–8 m^3 (simulation cube with the side of 50–100 m). Each cell contains information of the thermal conductivity and the heat capacity. A code identifying the actual TRC (Thermal Rock Class /Back and Sundberg 2007/) is also connected to each cell. The realisations are used as input to a numerical calculation model with a deposition tunnel and 9 canisters. If necessary, the realisations are in a local coordinate system due to considerations made in the thermal modelling /e.g. Back et al. 2007/, in order to take into account the geological anisotropy.

In the numerical model, data is collected from each cell in the realisation and transformed into the coordinate system for the numerical model. In the numerical model, the origin is at the centre of the central canister with the x-axis parallel to the deposition tunnel. The deposition tunnel is orientated in the decided direction.

The heat flow and maximum temperature are simulated by the numerical model. In the model, the redistribution of the heat flow due to the gap effect (described in Chapter 3) is taken into account by using a reduced buffer thermal conductivity in the radial direction to the canister. In order to avoid a computer-time-consuming detailed description of the canister and to incorporate practical

experience (see Chapter 3), the maximum bentonite temperature is calculated backwards from the mid-height rock wall temperature. Numerical calculations are made for a number of realisations and the maximum buffer temperature is calculated. In a pre-processing step, the realisations are ranked in an expected order, from the realisation with the lowest thermal conductivity in a weighted volume around each canister, to the realisation with the highest thermal conductivity.

One of the benefits with the numerical approach is that it includes all scales of the thermal rock property distributions. Therefore, there is no need to try to find the right percentile of the rock domain conductivity distribution in a "relevant" scale that is dimensioning for the domain. However, having established the canister spacing it is possible to backwards evaluate the effectively dimensioning conductivity by examining the relevant nomographic chart (cf. Figure 4-18) and then compare with the rock domain distribution to find the percentile that actually turned out to determine the spacing. The percentiles may not necessarily be the same for different rock domains due to scale effects.

5.3 Input data to numerical model

Input to the numerical model is summarized in the following bullets:

- Realisations with the spatial thermal conductivity distribution from the thermal stochastic modelling in 1–2 m scale (based on the thermal site descriptive model).
- Related distribution of heat capacity.
- TRC code (in each cell in the realisations).
- Temperature coefficient for thermal conductivity and heat capacity, if needed.
- Initial temperature at repository level (and temperature gradient).
- Spacing between tunnels and canisters.
- Data on coordinate transformation (transform coordinates for data from realisation to numerical model).
- Orientation of deposition tunnel.

In addition, the following input is also needed:

- Values of heat production in canister and thermal properties for tunnel, bentonite and canister.
- Effective thermal conductivity between rock wall and canister.

5.3.1 Thermal rock properties

Input to the numerical model comes from the thermal site descriptive model. The main objective of the thermal modelling is to provide an adequate spatial statistical description of the rock mass thermal conductivity and its uncertainties for the needs of repository design and safety assessment. A new strategy for thermal modelling has been developed /Back and Sundberg 2007/. The previous methodology for thermal modelling did not take the spatial correlation fully into account during simulation. The result was that the variability of thermal conductivity in the rock mass was not sufficiently described. Experience from earlier thermal SDMs indicated that development of the methodology was required in order describe the spatial distribution of thermal conductivity in the rock mass in a sufficiently reliable way, taking both variability within and between rock types into account.

The new strategy for thermal modelling is summarized in Figure 5-1. It includes stochastic simulation of both the geology (the spatial distribution of different thermal rock classes, TRCs) and the spatial distribution of thermal conductivity in each TRC. Output from the simulations is a large number of realisations of the lithological rock domain properties. The geological and thermal realisations are merged together and realisations of the spatial distribution of thermal conductivity in 3D are produced.

The scale used in the simulations is decided at an early stage. Here, the simulation scale is defined as the size of a grid cell in the simulation. The simulation domain (or simulation volume) is defined as all the grid cells in a realisation. Due to practical restrictions, such as computer capacity and time limitations, the practical limit for the number of grid cells is currently in the order of 10^6 in a simulation domain.

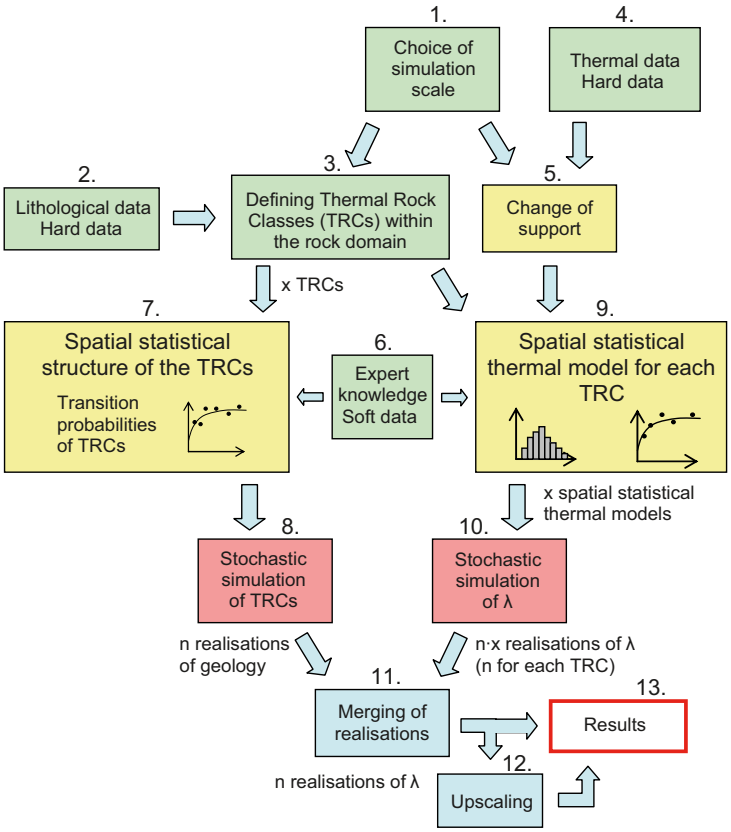

Figure 5-1. *Schematic description of the approach for thermal modelling of a rock domain (λ represents thermal conductivity) /Back and Sundberg 2007/.*

The following considerations are taken into account when choosing the simulation scale:

- The simulation scale must be sufficiently small to reflect small-scale variations in lithology and thermal properties that may be of importance. Typical lengths of the important rock types should be considered.
- For 3D simulations representing large rock volumes, the simulation scale must be sufficiently large so that the number of grid cells does not become too large.
- The data requirements in SKB's design work must be considered when the simulation scale is defined.

In the thermal site descriptive model at Forsmark /Back et al. 2007/, a 1 m simulation scale and simulation volume of 50·50·50 m was chosen. In Figure 5-2, examples of modelling results from Forsmark are presented. 1,000 realisations have been produced for Rock domain RFM029 /Back et al. 2007/ and 500 for Rock domain RFM045 /Sundberg et al. 2008a/.

In the realisation each cell contains information about:

– Thermal conductivity.

– Code for the TRC.

Also the heat capacity is needed in the modelling. In the site descriptive model in Forsmark, a relationship between thermal conductivity and heat capacity was found /Back et al. 2007/. The heat capacity (C) is calculated from thermal conductivity (λ) by a second order linear equation. It is also possible to add a random error to C, if desired. This error is based on the uncertainty in the prediction of C from λ using the regression equation. This is further described in /Sundberg et al. 2008a/. In the Laxemar area there is no obvious relation between thermal conductivity and heat capacity. In Laxemar the heat capacity is calculated randomly from a normal distribution from each TRC /Sundberg et al. 2008b/.

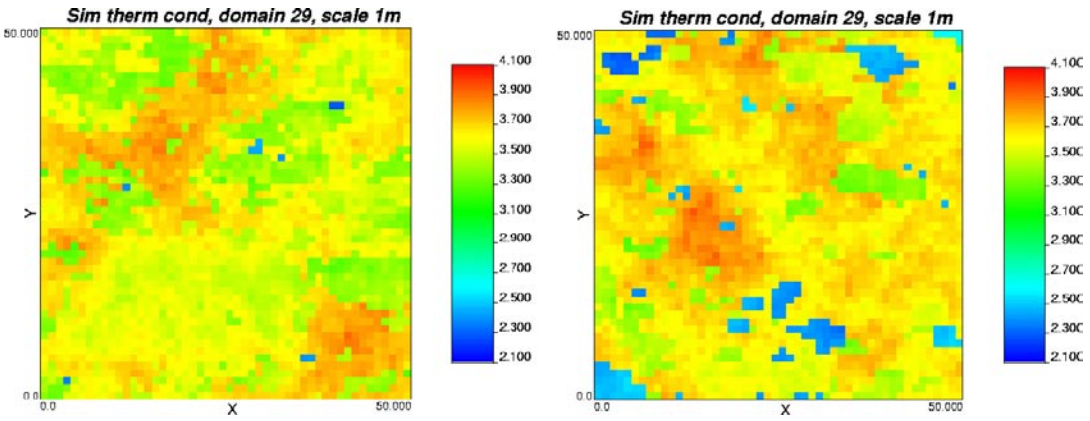

Figure 5-2. *Examples of modelling results of thermal conductivity from Rock domain RFM029 in Forsmark. 2D slices of the 3D realisations /Back et al. 2007/.*

In the geological simulation it is possible to take the anisotropy into account. A coordinate transformation in 3D is needed to take into account lineation and foliation of subordinate rock types. This results in rotated realisations. When using the realisations as input to the numerical model, the model is orientated in accordance to the foliation (if any) and proposed direction of deposition tunnels.

5.3.2 Thermal properties of canister, buffer and backfill

For simplification sake, the canister is described as a homogeneous cylinder in the numerical model. In reality, the canister consists of an inner core of cast iron with a protecting layer of copper at the outer surface. The vertical thermal conductivity used has an influence on the redistribution of heat flow and consequently on the mid-height rock wall temperature, which, in turn, is used for backwards calculation of the maximum bentonite temperature. However, the time step in the numerical calculation is heavily dependent on the magnitude of the thermal conductivity in the canister. In order to reduce the computer time needed for the simulation, a reduced thermal conductivity has been used in the simulations (30–50 W/(m·K) instead of approximately 100 W/(m·K). This simplification has only a small influence on the calculated maximum bentonite temperature and can be corrected for (see Appendix A and further discussion in Chapter 6).

The effective thermal conductivity of the bentonite between the canister and the rock wall (in radial direction) is reduced in order to include the thermal resistance of an air-filled gap (see Chapter 3). For example, if the effective thermal conductivity of a 10 mm gap is 0.04 W/(m·K) and the thermal conductivity of the bentonite buffer is 1 W/(m·K), the resulting thermal conductivity in the radial direction is calculated to 0.58 W/(m·K).

The heat capacities of canister, buffer and tunnel have little or no influence on the maximum buffer temperature.

The thermal properties of the materials involved in the thermal process are given in Table 5-1. In Chapter 6 uncertainties are further discussed.

Table 5-1. Example thermal properties of materials numerically modelled in the repository, see also discussion in text.

Thermal property	Value	
Thermal conductivity – gap (10 mm)	0.04	W/(m·K)
Thermal conductivity – bentonite (elsewhere)	1.0	W/(m·K)
Thermal conductivity – backfill tunnel, depending on water saturation and density	0.6–1.5	W/(m·K)
Volumetric heat capacity – canister	4.0	MJ/(m^3·K)
Volumetric heat capacity – bentonite	2.92	MJ/(m^3·K)
Volumetric heat capacity – backfill tunnel, depending on water saturation and density	3.07	MJ/(m^3·K)

5.4 Numerical modelling of the thermal process

5.4.1 Introduction

The main focus is to test the influence of heterogeneous thermal properties in the rock mass where the repository is located. The repository consists of the several parallel tunnels from which canisters are placed in deposition holes. The distance between adjacent tunnels and the spacing between adjacent deposition holes are assumed to be constant. The design criterion is a given maximum temperature of the bentonite surrounding the canister. The heterogeneity of the rock will result in a certain variation in the maximum bentonite temperature reached in different deposition holes. The aim of the simulation tool developed here is to be able to predict the maximum bentonite temperature of any deposition hole given a realistic variation of the rock mass and a set of design parameters such as tunnel spacing, deposition hole spacing and time-varying canister heat output.

The approach chosen is to simulate a segment of a tunnel in the repository. The studied region is assumed to be bounded in the horizontal direction by symmetry planes with no heat flow across the surfaces. The temperature at canister mid-height of the rock wall is simulated and a correlation from a detailed study of the thermal process in a deposition hole with canister for homogeneous rock is used to estimate the maximum buffer temperature.

5.4.2 Numerical method and model

The numerical simulation of the thermal process in the repository is performed using the explicit finite difference method (FDM). Governing equations for the 3D conductive heat transport and the details of the numerical method (FDM) are described in /Eftring 1990/. The repository and a certain part of the surrounding rock are described by dividing the region into grid of parallelepipedical sub volumes with different thermal properties. The subdivision is made with smaller cells around the canisters in order to describe details of construction and obtain a better resolution of large temperature gradients. The cell size expands outwards from the canisters. The simulated region consists of a segment including one tunnel with nine deposition holes in a row. This region is bounded by symmetry planes in the horizontal directions. In the vertical direction it extends to a distance beyond which thermal conditions have negligible influence on the maximum canister temperature. A simple manual has been produced for the numerical model (SKBdoc ID 1184267).

The numerical grid is a compromise between level of detail and reasonable execution time on the computer. Small cell sizes and a large number of cells result in long execution times. The chosen grid gives an execution time of about 4 hours on a PC with dual core processor. In order to estimate the error of the simulation, this grid was made finer by bisecting the cell width in each direction. The execution time then became roughly one week. The error can be estimated by combining the results of the two grids, see 5.5.3 and /Blomberg 1996/.

Validation of the numerical model is made in Section 5.5.

5.4.3 Assigning thermal rock properties to the numerical mesh

Realisations of thermal properties

The realisation of thermal properties, is described in an orthogonal mesh orientated in a transformed coordinate system (x''', y''', z''') obtained by rotation of the global coordinate system (x, y, z). This transformation is necessary to take into account the principal direction of anisotropy. The global coordinate system has its x, y, z-axes pointing in the easting, northing, and elevation directions, respectively. The transformation from system (x, y, z) to system (x''', y''', z''') is obtained through rotation in 3 steps and is described in Appendix D in /Sundberg et al. 2008a/.

The realisation describes the thermal properties of the rock in a grid of identical blocks. The grid has a number $N_x \cdot N_y \cdot N_z$ of cuboidal blocks (cubical if the side lengths are identical) orientated along the axes of the transformed coordinate system (x''', y''', z'''). This coordinate system is orientated in the principal direction of anisotropy, which is as a function of the mineral stretching and foliation planes. The side lengths of the blocks are D_x, D_y, and D_z. In the simulations made in Forsmark, the extent of the realization (simulation volume) is a cube-shaped volume with a side length of 50 m. This volume was divided into cubes with a side length of 1 m ($N_x=N_y=N_z=50$; $D_x=D_y=D_z=1.0$ m) where each cube has a unique rock type and thermal properties assigned in the stochastic modelling. The numerical model can use realisations with different size of simulation volume and blocks.

Numerical mesh for simulation of the thermal process

The numerical mesh used for the simulation of the early thermal evolution within the repository is given in an orthogonal grid (x_g, y_g, z_g) with the x_g-axis and y_g-axis in the horizontal plane and z_g-axis in the vertical direction. The origin of the coordinate system is chosen to coincide with the midpoint of the central canister in the simulated segment. The main axis of the tunnel is along the x_g-axis and points in a direction specified by an (clockwise) angle from the northing direction (y-axis). This implies that the grid (x_g, y_g, z_g) which is based on the orientation of the tunnel has a different orientation than the global system (x, y, z).

The calculation mesh is made up of a large number of parallelepipedical cells. Because of the misalignment of systems (x‴,y‴,z‴) and (x_g, y_g, z_g), the procedure to fill the cells of the numerical mesh with thermal properties from the blocks of a realisation must take into account that a cell may cut through several blocks. Each cell in the numerical mesh is therefore divided into $n_x \cdot n_y \cdot n_z$ identical parallelepipedical sub-cells, orientated along the axes of the orthogonal coordinate system (x_g, y_g, z_g). In the current version of the numerical model, the numbers n_x, n_y, and n_z may take values between 1 and 5, so that maximum number of sub-cells becomes $5 \cdot 5 \cdot 5 = 125$.

The next step is to find the thermal properties of the realisation at the mid-point of each sub-cell. The mid-point, expressed by the coordinates in the (x_g, y_g, z_g) system, is then transformed to the (x''', y''', z''') system of the realisation. This transformation is best explained as a two-step transformation. First, the coordinates in the system (x_g, y_g, z_g) are transformed to the system (x, y, z) (based on tunnel orientation). Secondly, the coordinates in (x, y, z) system are transformed to the (x''', y''', z''') system (based on the transformation of the realisation, e.g. /Sundberg et al. 2008a/). A search routine finds the corresponding block with its thermal properties ($\lambda_{i,j,k}$ and $C_{i,j,k}$) and these values are assigned to the sub-cells of the numerical grid cell. This procedure is repeated for each ($n_x \cdot n_y \cdot n_z$) sub-cells of the cell. The volumes of each sub-cells is denoted $v_{i,j,k}$ and they are all the same.

The thermal conductivity of the numerical grid cell is then calculated using the self-consistent approximation (SCA) for a 3-phase material /Sundberg 1988/:

$$\lambda_e = \frac{1}{3}\left(\sum_{i=1}^{n_x}\sum_{j=1}^{n_y}\sum_{k=1}^{n_z} \frac{v_{i,j,k}}{2\lambda_e + \lambda_{i,j,k}} \right)^{-1} \qquad 5\text{-}1$$

The equation is solved with an iterative procedure where the accuracy is set to 0.0001 W/(m·K) where the starting value for λ_e is taken as the geometric mean value:

$$\lambda_e = \prod_{\substack{i=1,n_x \\ j=1,n_y \\ k=1,n_z}} \lambda_{i,j,k}^{v_{i,j,k}} \qquad 5\text{-}2$$

The volumetric heat capacity C of the numerical grid cell simply becomes the average value of the volumetric heat capacity $C_{i,j,k}$ of the sub-cells:

$$C = \frac{1}{n_x n_y n_z} \sum_{i=1}^{n_x}\sum_{j=1}^{n_y}\sum_{k=1}^{n_z} C_{i,j,k} \qquad 5\text{-}3$$

If the search routine requests thermal properties for a point outside of the realisation region, the algorithm will duplicate the values from the closest boundary point. If the point is outside a side of the realisation volume, the value of the closest realisation cube will be used. If the point is outside an edge, the values of the closest edge cube and its two neighbour cells on the sides will be averaged. Finally, if the point is outside a corner, an average of the corner cube and the three neighbouring edge cubes will be used.

5.4.4 Temperature-dependent thermal properties in the rock

The thermal properties in the rock exhibit depend on the temperature. The relative change in properties caused by temperature changes of 100°C may be on the order of 10–20%. In the numerical programme it is possible to take this temperature dependency into account. It is assumed that the thermal conductivity λ and the volumetric heat capacity C have a linear dependence of the temperature:

$$\lambda = \lambda_0 \cdot (1 + \alpha_\lambda (T - T_0)) \qquad (\mathrm{W/(m \cdot K)}) \qquad 5\text{-}4$$

$$C = C_0 \cdot (1 + \alpha_C (T - T_0)) \qquad (\mathrm{J/(m^3 \cdot K)}) \qquad 5\text{-}5$$

The property values are λ_0 and C_0 at the reference temperature T_0. The linear coefficients α_λ and α_C are given for each rock type. In the numerical simulation, a volume average value of these coefficients is used for each grid cell. The reference values λ_0 and C_0 are assigned in the same way as described above (Section 5.4.3). The thermal properties are updated at a time interval of about one day in the simulation.

5.4.5 Numerical calculation of rock wall temperature

The numerical grid used in the finite difference model approximates the cylindrical shape of the canister and the deposition hole by number of rectangular cells. In order to obtain the rock wall temperature, an algorithm to calculate a representative rock wall temperature at a certain location is developed. The method is based on extrapolation of the radial temperature gradient from a point located on a circle in the rock just outside the deposition hole. An example showing the coarse grid is given in Figure 5-3. The fine grid is shown in Figure 5-4.

An average rock wall temperature is calculated by taking the mean value of the estimated temperature at 360 equally spaced points around the circle representing the rock wall. The temperature T_c at the evaluation point is calculated based on a bilinear interpolation of the heat flux components q_x and q_y in the cell. See Figure 5-5.

The heat flux vector is denoted:

$\overline{q} = (q_x, q_y, q_z)$ (W/m^2)

The unit vector in the radial direction is:

$\hat{r} = (\cos\theta, \sin\theta, 0)$

The radial heat flux then becomes:

$q_r = \overline{q} \cdot \hat{r} = q_x \cdot cos\theta + q_y \cdot sin\theta$ (W/m^2)

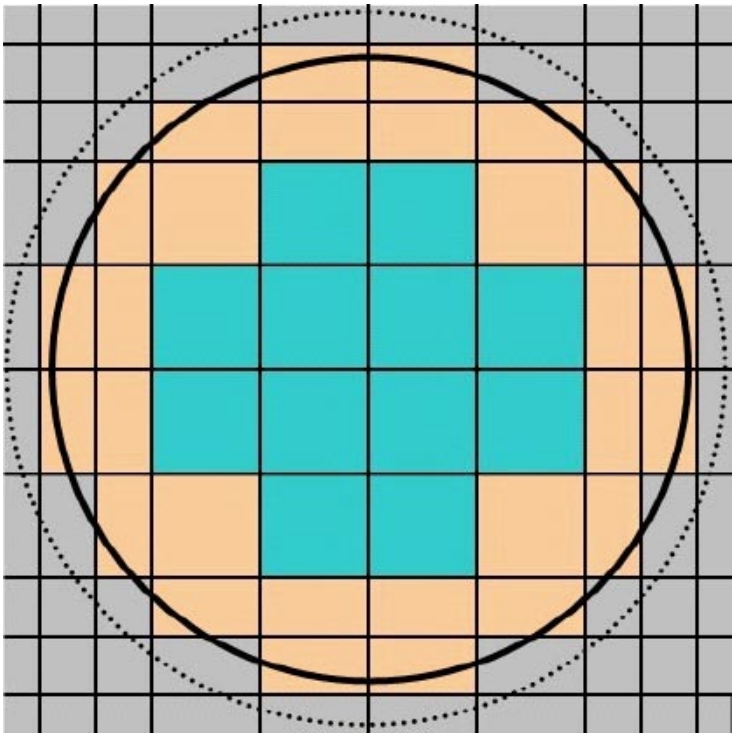

Figure 5-3. *Numerical grid (coarse grid) in a horizontal plane through the canister (blue), bentonite (pink) and rock (gray). The rock wall is indicated with a solid line. The rock wall temperature is estimated based on extrapolation from the outer circle (dashed line).*

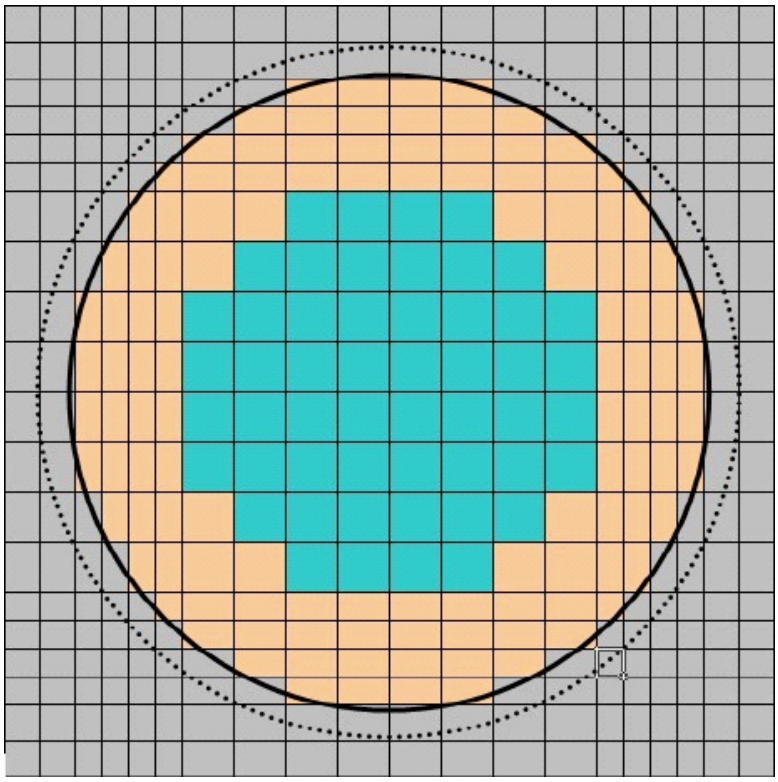

Figure 5-4. *Numerical grid (fine grid) in a horizontal plane through the canister (blue), bentonite (pink) and rock (gray). The rock wall is indicated with a solid line. The rock wall temperature is estimated based on extrapolation from the outer circle (dashed line).*

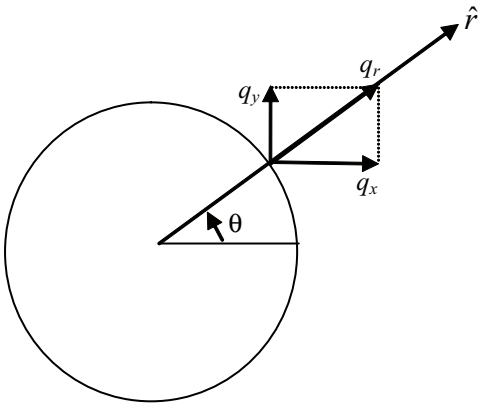

Figure 5-5. *The radial heat flux q_r obtained by vector addition of the heat flux components q_x and q_y at the evaluation point. The angle between the radial direction and the x-axis is denoted* θ.

The radial heat flow per vertical meter at the evaluation point radius r_c is then:

$$q' = q_r \cdot 2\pi \cdot r_c \text{ (W/m)} \qquad 5\text{-}6$$

The steady-state thermal resistance, which should be an especially good approximation at maximum temperature conditions, between the evaluation point at radius r_c and the deposition hole wall radius r_2 is defined by:

$$R = \frac{\ln(r_c / r_2)}{2\pi\lambda_{cell}} \quad \text{(K/(W/m))} \qquad 5\text{-}7$$

where λ_{cell} is the thermal conductivity of the cell containing the evaluation point.

The temperature difference between rock wall and the evaluation point now becomes:

$$\Delta T = q' \cdot R = q_r \cdot \frac{r_c \cdot \ln(r_c / r_2)}{\lambda_{cell}} \qquad 5\text{-}8$$

Finally, the rock wall temperature may be written:

$$T_{wall}(t) = T_c(t) + q_r(t) \cdot \frac{r_c \cdot \ln(r_c / r_2)}{\lambda_{cell}} \qquad 5\text{-}9$$

The radial distance of the evaluation point (radius of the evaluation circle) should be chosen so that the estimated rock wall temperature is fairly stable to small changes of this radial distance. At a smaller radius of the evaluation circle, the disturbance due to the jagged representation of the deposition hole perimeter is evident. Figure 5-6 gives an example from a case with uniform rock thermal conductivity (3.16 W/(m·K)) and deposition hole radius 0.85 m. Stable estimates are obtained at 0.95 m and 0.89 m for the coarse and fine grid respectively. The difference in absolute temperature is a general effect of the grid resolution where the coarser grid tends to give slightly higher values. Based on this example, it was decided to use an evaluation circle with a radius of 1.0 m when the deposition hole radius is 0.875 m.

Note that the rock wall temperature used to calculate the maximum bentonite temperature is the average of 360 equally spaced points along the deposition hole wall perimeter.

5.4.6 Local process

Detailed investigations of the thermal process in deposition hole with a canister have been performed in Chapter 3. Therefore, the time-dependent relation for difference between the maximum bentonite temperature and the wall temperature of the deposition hole has been adopted in the numerical solution for the local process. The temperature difference is evaluated in two steps. The first part gives the difference between the inner bentonite surface and the rock wall at an elevation corresponding to the mid-height of the canister (see also Equation 3-8):

$$\Delta T_1(t) = 0.87 \cdot (Q(t) / A) / \lambda_b \cdot r_0 \cdot \ln(r_2 / r_1) \qquad 5\text{-}10$$

where $Q(t)$ is the heat generation rate, A is the canister surface area, r_0 is the canister radius, r_1 the buffer inner radius and r_2 the deposition hole radius. The formula is given for a bentonite thermal conductivity, λ_b, set equal to 1.0 W/(m·K). The variation of rock wall temperature in different directions was found to be small.

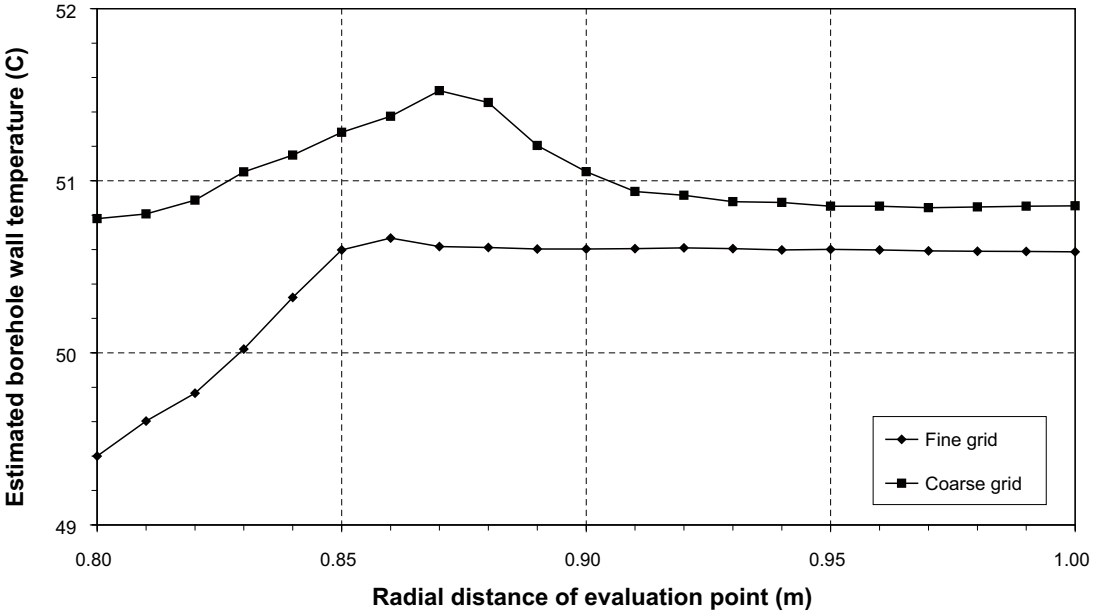

Figure 5-6. *Evaluated rock wall temperature at an example deposition hole wall radius of 0.85 m as a function of the radius of the evaluation circle.*

The second part gives the difference between the maximum bentonite temperature at the base of the canister and the temperature at the buffer (bentonite) inner surface at mid-height (including the thermal resistance of a 10 mm gap between the canister and buffer inner surface) (see also Equation 3-10):

$$\Delta T_2(t) = 16 \cdot Q(t) / Q(0) \qquad 5\text{-}11$$

With the initial heat generation rate, the canister and deposition hole dimensions assumed for this design, the total temperature difference between maximum bentonite temperature T_{max} and the rock wall temperature T_{wall} becomes (see also Equation 3-12):

$$T_{\max}(t) - T_{wall}(t) = \Delta T_1(t) + \Delta T_2(t) = 0.02213 \cdot Q(t) \qquad 5\text{-}12$$

The maximum buffer temperature is calculated for each time step by simply adding the temperature difference in Equation 5-12 to the mid-height deposition hole temperature, calculated numerically, see Equation 5-9.

5.4.7 Ranking realisation procedure

The most critical design issue regards the maximum temperature in the bentonite. For a given geometric setup (tunnel spacing, deposition hole spacing, etc), the worst case is determined by low thermal conductivities of the rock around the critical canister. As the numerical simulations are fairly time-consuming, it would be helpful if a certain number of potential worst cases could be found by a screening of the different rock thermal conductivity realisations in the repository. In order to achieve this objective, the geometric mean value of the rock thermal conductivity and the mean rock type distribution were calculated in four zones around each canister. The first zone extends from the rock wall to a distance of 2.5 m from the canister. The second, third and fourth zones lie in the 2.5–5 m, 5–10 m, 10–15 m intervals respectively. The zones are calculated as a cylinder (length: canister length +1 m (0.5 m above and below canister)) with a half sphere in each end. The volumes of the four zones are approximately 170, 800, 5,030 and 12,230 m^3. After screening there will be a large number of thermal realisations, these can be ranked according to thermal conductivity in the different zones.

A total weighted value for all zones was given based on the general heat flow equation (Fourier's law):

$$q = -\lambda \frac{\Delta T}{\Delta x} \text{ (W/m}^2\text{)}$$

Based on a simulation with uniform thermal conductivity λ, the heat flow q was evaluated at midpoints in the four zones (with intervals Δx). The temperature change ΔT in each interval is assumed to have dependence roughly expressed by:

$$\Delta T \approx -q \frac{\Delta x}{\lambda}$$

The weighting coefficients, for the total weighted value, are chosen to be 0.4, 0.25, 0.25, and 0.1 for the four zones, respectively (based on calculated heat flow). Based on experiences from calculations at the different sites, the weighting coefficients may be modified in the future.

Example results of the ranking procedure together with numerical calculation results are shown in Section 5.6.

5.5 Validation of numerical model

The simulation method has been validated for different test cases regarding the global thermal process, influence of boundary conditions, and the local thermal process. The model has previously been used in a study titled "Inverse modelling of thermal conductivity from temperature measurements at the prototype repository" /Sundberg and Hellström 2009/.

5.5.1 Global thermal process

The global thermal process of the simulation method has been tested against a commercial heat conduction model. These calculations were carried out using a PC-program for three-dimensional heat transfer, HEAT3 version 5.0, which has been developed at the Department of Building Physics, Lund University, and at the Building Technology Group, Massachusetts Institute of Technology. The program manual is available at http://www.buildingphysics.com. The calculation method is described by /Blomberg 1996/. HEAT3 5.0 is validated against and complies with European Standard EN ISO 10211-2.

The details of the repository were simplified in this comparison. Nine canisters are placed in a row with 6 m spacing. The ground region is a rectangular-shaped volume. In the horizontal direction of the tunnel, the ground region extends 60 m away from the first canister and 40 meters away from the ninth canister. The region is 40 m wide in the horizontal direction perpendicular to the tunnel. The vertical extension is 120 m with the bottom of the canister located at mid-height. The boundary conditions for ground region assume that there is no heat flow through the boundary. The canisters were assumed to have a quadratic cross-sectional area. Thermal properties are homogeneous throughout the region and there are no thermal contact resistances between the canisters and the surrounding rock. Thermal conductivity and volumetric heat capacity is 2.8 W/(m·K) and 2.2 MJ/(m^3·K) respectively. Initial temperature is 15.0°C. The temperature at the midpoint of the central canister and in a point 10 m from the central canister in a direction perpendicular to the row of canisters is given in Table 5-2.

The agreement between the simulation model and the HEAT3 program is very good, especially at the maximum canister temperature. The differences in temperature are due to the differences in the numerical grid sizes.

5.5.2 Boundary conditions

Neighbouring tunnel

The extension of the simulated ground region in the vertical direction is chosen so that the boundary conditions imposed do not influence the maximum canister temperature, which is supposed to be reached within 30 years. A vertical extension of 120 m was found to fulfil this condition. In order to have an influence, the heat wave created by the heat generation in the canisters must reach the outer boundary and be reflected back to the canisters within this time frame.

The repository is assumed to have a large number of parallel tunnels, so that the simulation around each tunnel can be assumed to be similar due to symmetry. With homogenous thermal properties, it is then assumed that these conditions can be modelled with a vertical symmetry plane inserted halfway between the tunnels. Since the purpose of the model is to account for heterogeneous thermal properties, the accuracy of this assumption has to be tested.

Table 5-2. Comparison between the simulation model and the heat transfer code HEAT3. See text for further details.

Time (years)	Temperature at canister midpoint		Temperature at a radial distance of 10 m	
	Model	HEAT3	Model	HEAT3
0.5	63.9	64.3	15.5	15.3
1	67.2	67.5	16.7	17.1
2	69.8	70.0	18.8	19.3
3	70.9	71.0	20.3	20.8
4	71.5	71.5	21.6	22.0
5	71.8	71.9	22.7	23.1
6	71.9	71.9	23.7	24.0
7	72.0	71.9	24.5	24.7
8	71.9	71.9	25.3	25.4
9	71.8	71.8	25.9	26.1
10	71.7	71.6	26.5	26.7

The test was performed with the HEAT3 model for two cases. The first case considers a repository with nine canisters and a tunnel assuming symmetric conditions such that the ground region is bounded by vertical symmetry planes halfway between the tunnels. The distance between the tunnels is 40 m. In this simulation, no symmetry is considered along the row of canisters and the ground region extends from the canisters so that the boundary conditions imposed have negligible influence. In the second case, the simulation also includes the neighbouring tunnel. The details of the repository are very close to the design case with different thermal properties of canister, deposition hole, bentonite, and tunnel backfill. The tunnel is assumed to be cylindrical. Thermal conductivity and volumetric heat capacity is 3.16 W/(m·K) and 2.17 MJ/(m^3·K) respectively. Initial temperature is 10.6°C. In the second case, the thermal conductivity of the second tunnel is assumed to be 10% higher, i.e. 3.48 W/(m·K). The situation is shown in Figure 5-7.

The average canister temperatures for the two cases are given in Table 5-3. The difference in maximum temperature between the single tunnel and tunnel 1 for the two tunnel case is 0.2°C. The maximum temperature is higher for the case with two tunnels where the neighbouring tunnel region has higher thermal conductivity. The reason is that the thermal disturbance from the neighbouring canisters is conducted faster through the high conductive material and reaches the tunnel region 1 before the heat wave for the case of a single tunnel is reflected in the symmetry plane.

The assumption of symmetry in the heterogeneous case is reasonable, but involves an uncertainty that, in this case, increased the maximum canister temperature with 0.2°C when the thermal conductivity of the neighbouring tunnel region was 10% higher. If an additional neighbouring tunnel with the same elevated thermal conductivity was modelled, the increase will be slightly higher. It is obvious that the influence will be less if the tunnel spacing is increased since the thermal disturbance will arrive later with lower amplitude.

Figure 5-8–Figure 5-10 show the computed temperature field after 10 years for a single tunnel. The temperature field for the case of two parallel tunnels is given in Figure 5-11.

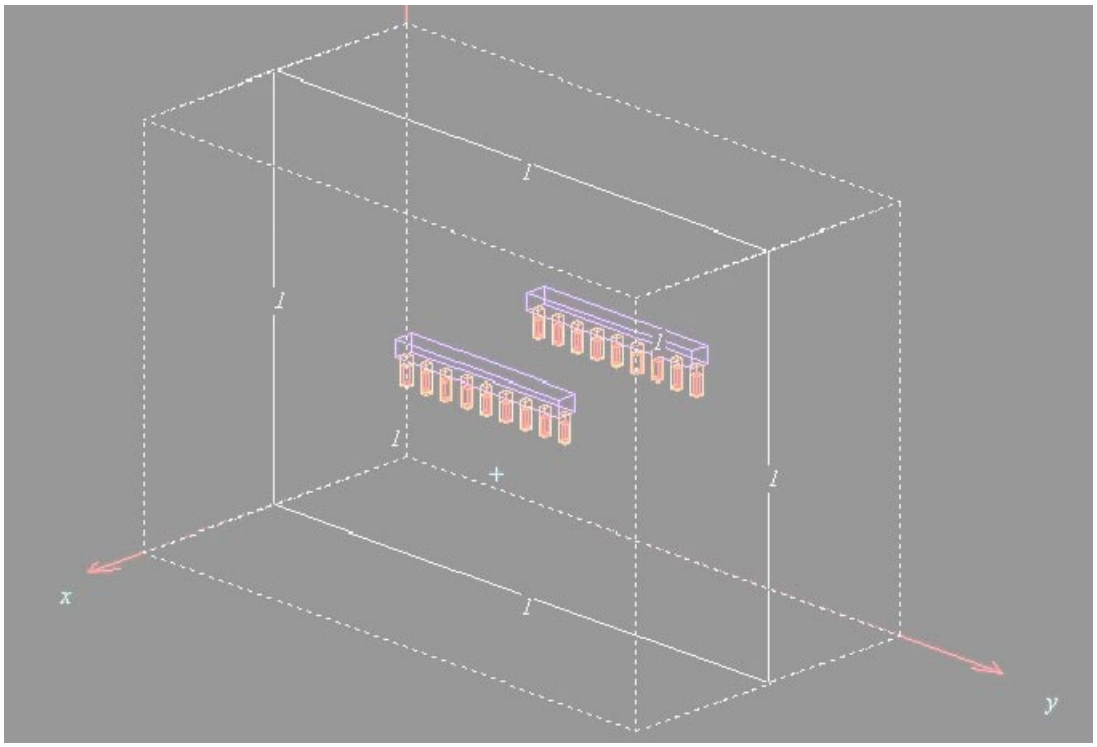

Figure 5-7. *Simulation of two parallel tunnels.*

Table 5-3. Average canister temperature computed with HEAT3 for a case with a single tunnel and a case with two tunnels where the second tunnel region has a thermal conductivity that is 10% higher.

Time (years)	Average canister temperature		
	Single tunnel	Two tunnels	
		Tunnel 1	Tunnel 2
	λ=3.16	λ=3.16	λ=3.48
0.5	79.0	79.1	77.4
1	83.8	83.9	81.7
2	87.8	87.9	85.3
3	89.5	89.5	86.7
4	90.3	90.5	87.4
5	90.5	90.9	87.7
6	90.6	91.0	87.8
7	90.8	90.9	87.7
8	90.6	90.7	87.4
9	90.3	90.4	87.1
10	89.9	90.0	86.7

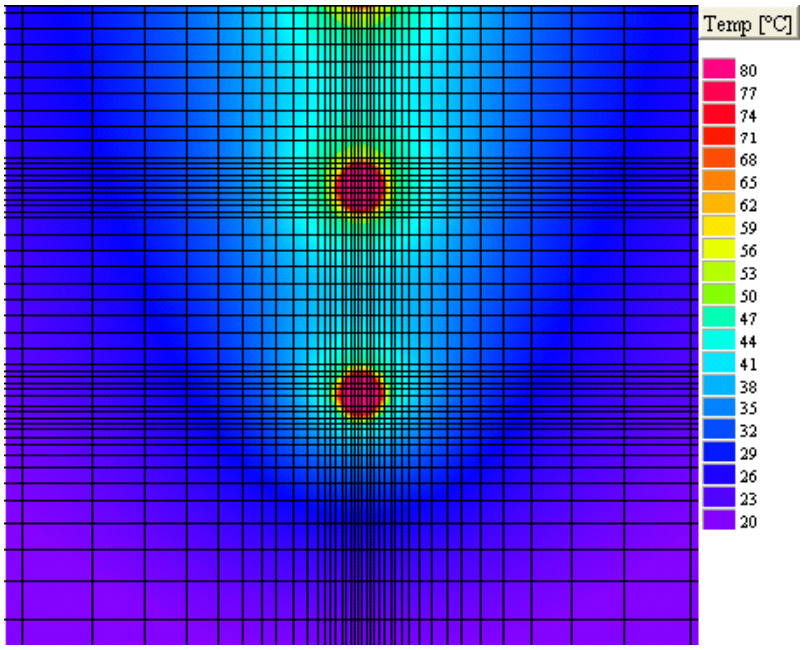

Figure 5-8. *Part of the computed temperature field in a horizontal plane at mid-height of the canisters after 10 years. The numerical grid sizes are indicated by the solid lines.*

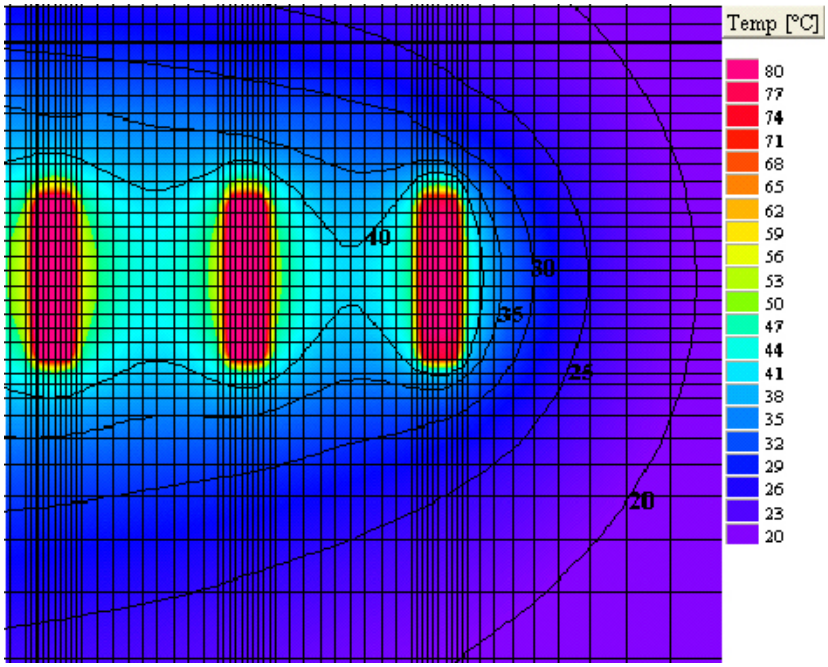

Figure 5-9. *Part of the computed temperature field in a vertical plane through the midpoint of the canisters after 10 years. The numerical grid sizes are indicated by the solid lines.*

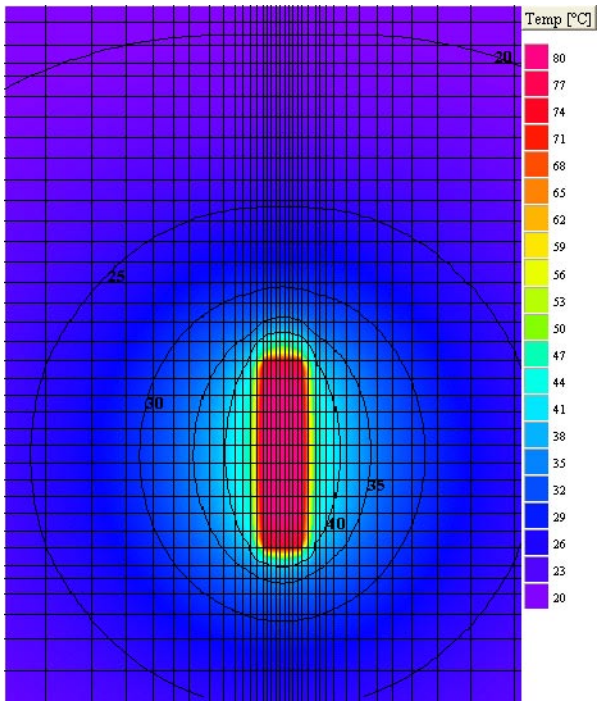

Figure 5-10. *Part of the computed temperature field in a vertical plane through the midpoint of the central canister and perpendicular to the tunnel direction after 10 years. The numerical grid sizes are indicated by the solid lines.*

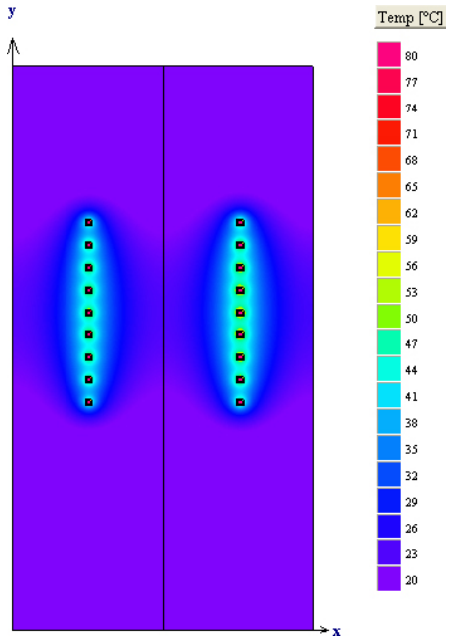

Figure 5-11. *Computed temperature field in a horizontal plane at mid-height of the canisters after 10 years for the case of two parallel tunnels.*

Finally, a calculation was made for the case of two tunnels assuming that vertical symmetry planes could also be inserted at a distance of half deposition hole spacing outside the first and ninth deposition hole. This would resemble the conditions in the central part of a tunnel with a long row of deposition holes. Figure 5-12 shows the temperature field. The average canister temperature is given in Table 5-4.

In the previous case, the maximum temperatures of the central canister in tunnel 1 and 2 were 91.0°C and 87.8°C. In the case with closed boundaries in the tunnel directions, the highest temperatures were 93.1°C and 89.8°C. The difference in maximum average canister temperature is the same for the two cases. The temperature level is about 2°C higher due to the closed boundary. The maximum also occurs later, at 10.5 years, for this case.

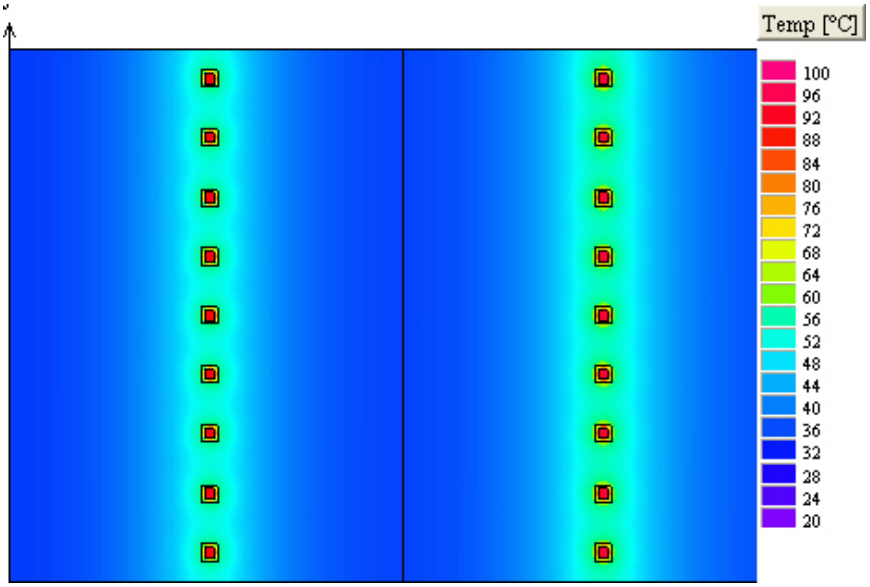

Figure 5-12. *Computed temperature field in a horizontal plane at mid-height of the canisters after 10 years for the case of two parallel tunnels. The ground region is bounded by vertical symmetry planes located at a distance of a half deposition hole spacing outside row of deposition holes.*

Table 5-4. Average canister temperature computed with HEAT3 for a case with a single tunnel and a case with two tunnels where the second tunnel region has a thermal conductivity that is 10% higher. The ground region is bounded by vertical symmetry planes located at a distance of a half deposition hole spacing outside row of deposition holes.

Time (years)	Average canister temperature	
	Tunnel 1	Tunnel 2
	λ=3.16	λ=3.48
0.5	79.2	77.5
1	84,0	81.8
2	88.0	85.4
3	89.9	87.1
4	91.0	88.0
5	91.8	88.7
6	92.3	89.1
7	92.7	89.5
8	92.9	89.7
9	93.0	89.8
10	93.1	89.8
11	93.1	89.8
12	93.1	89.8
13	93.0	89.7

Direction along the tunnel

There may be an influence of heterogeneous thermal properties in the direction along the tunnel. Here, we have chosen to include nine canisters in the simulation. The results from the outer two canisters in both directions are excluded in the final analysis due to expected significant influence from the region outside the symmetry plane. For example, if the first canister is surrounded by rock with unusually low conductivity, the symmetry plane doubles this volume and may create an irrelevant case with an exaggerated correlation length of low conductivity rock types.

In Figure 5-13, this situation is further analysed. One of the canisters 1 to 5 is surrounded with low conductive rock. In the figure, the resulting maximum temperature and the influence on the other canister are analysed. It is obvious that the largest influence occurs when the low conductive rock is close to the boundary, i.e. canister 1. The result is scale dependent but it seems to be a sufficient precaution to exclude canister 1–2 and 8–9 from the evaluation.

5.5.3 Numerical precision

Two different numerical grids were used to estimate the error of the calculation according to a procedure described in /Blomberg 1996/. The cell-sizes of the original grid were bisected to obtain a grid with finer resolution. The results from the two grids can be combined to find an asymptotic value for numerical grid with an infinite number of cells, which should then be the “exact” solution.

The two test cases, further described in Section 5.5.4, gave similar deviations for the two grids. The coarse grid over-predicted the temperature rise at the rock wall with 1.6% and 1.7% for the low and high conductivity case respectively. The fine grid overestimated the temperature increase with 0.4% for both test cases.

At maximum buffer temperature, the temperature rise at the rock wall is about 48°C. This means that the coarse grid over-predicts the maximum temperature with about 0.8°C, whereas the fine grid over-predicts with only 0.2°C.

5.5.4 Comparisons with analytical solution

Comparisons have been made between the numerical solution and the analytical solution described earlier in this report. Two cases have been considered with data in Table 5-5. Homogeneous conditions

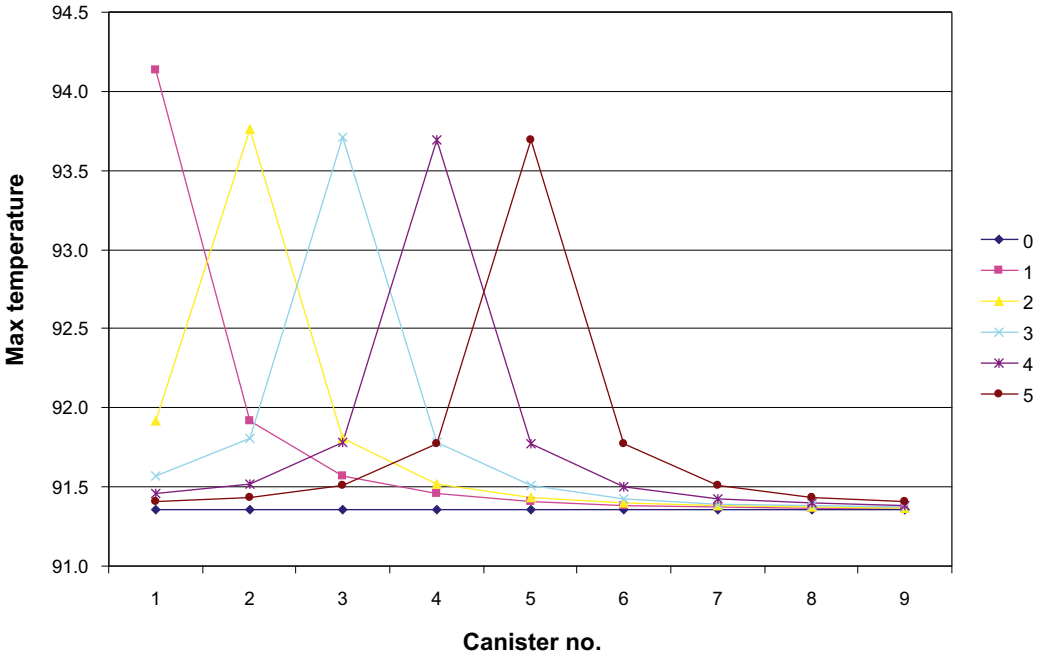

Figure 5-13. *Maximum temperature for a canister in low conductive rock and the resulting temperature for all canisters when a volume of low conductive rock is "moving" from canister 1 to canister 5. The model has nine canisters. Outside canisters 1 and 9 a symmetry planes are situated. The "low" conductive rock has 10% lower thermal conductivity compared to host rock (3.15 W/(m·K), cc 6 and 40 m).*

Table 5-5. Data used in comparison between analytical and numerical solution.

Parameter	Case 1	Case 2
Spacing between canister, m	6	7.5
Spacing between tunnels, m	40	40
Thermal conductivity, W/(m·K)	3.16	2.60
Heat capacity, MJ/(m^3·K)	2.17	2.17
Initial in-situ temperature, °C	10.6	10.6

in thermal properties have been assumed for both cases. The numerical calculation is made with both coarse and fine grids. The results from the comparisons are shown in Figure 5-14–Figure 5-16. In the figures, the numerical solution has been calculated with a normal (coarse) and a fine grid.

The differences between the analytical and numerical solutions are all due to differences in the calculation of the rock wall temperature (since the same reference evolution $\Delta T_{tot}(t)$ has been added to both to find the maximum bentonite temperature). The most relevant comparison is between the analytical solution and the fine-grid numerical one (Figure 5-14–Figure 5-16). Here, the agreement is very satisfactory with a difference of less than 0.5°C. Yet, the analytical solution ignores the tunnel backfill giving an underestimate of about 0.6°C. On the other hand, however, the analytical compound source (cf. Chapter 4) is not configured to account for the extra flux redistribution caused by the air-filled canister-bentonite gap, whereas the numerical solution is. This gives a balancing overestimate in the analytical solution which is of a similar magnitude.

Given the above results, the agreement between the results from the numerical and analytical solution is convincing enough to count as a verification of the basics of the numerical method.

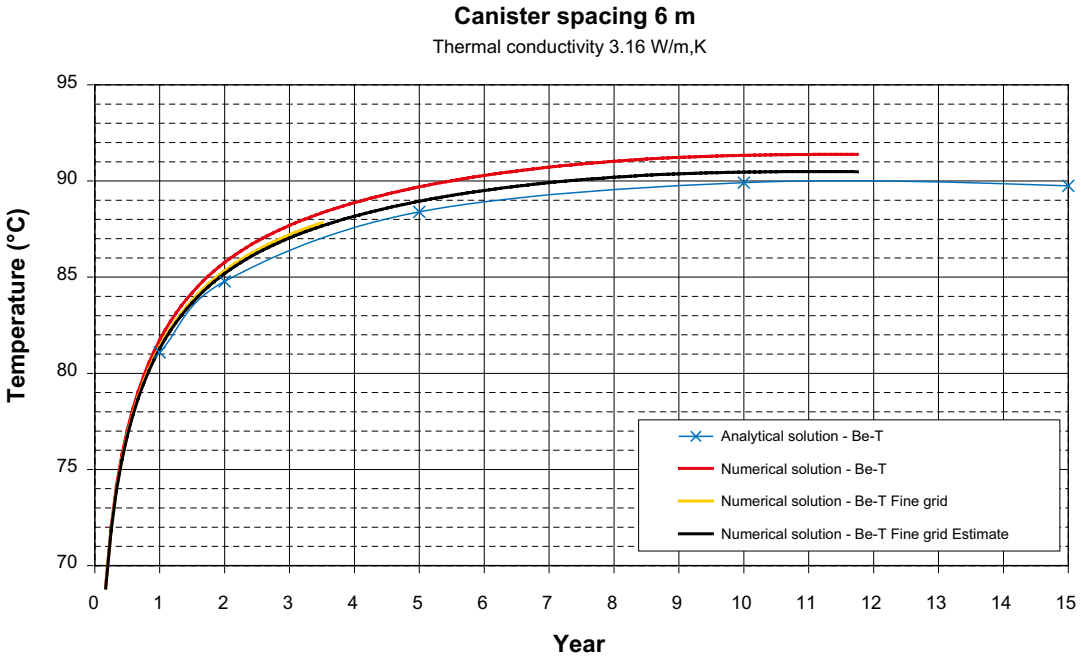

Figure 5-14. *Results of comparison between analytical and numerical solution with canister spacing 6 m and thermal conductivity 3.16 W/(m·K).*

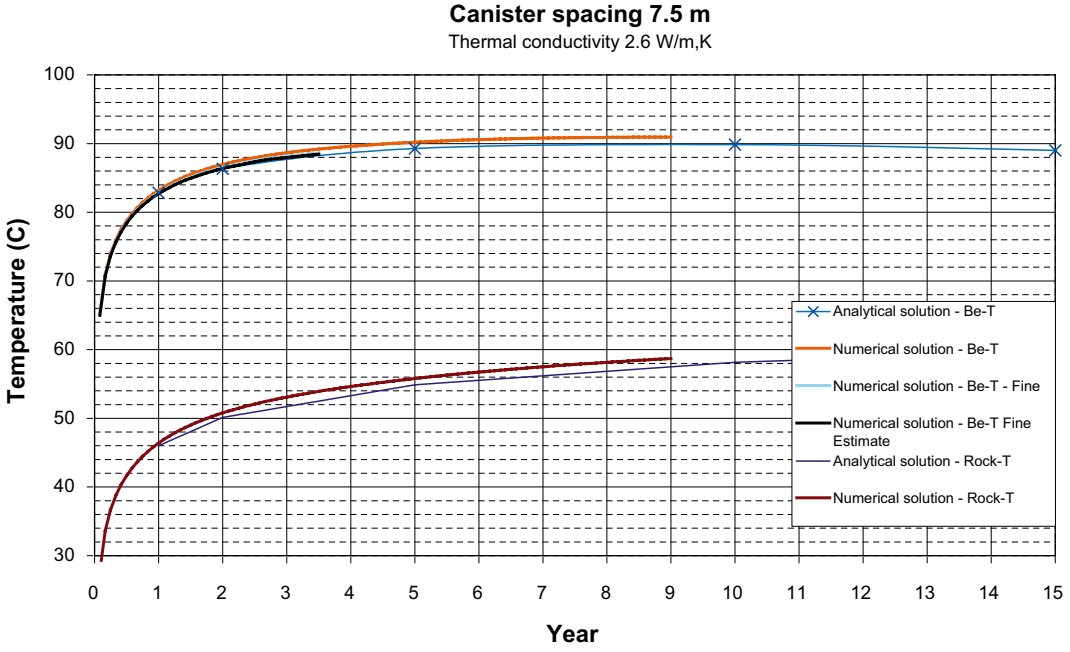

Figure 5-15. *Results of comparison between analytical and numerical solution with canister spacing 7.5 m and thermal conductivity 2.6 W/(m·K).*

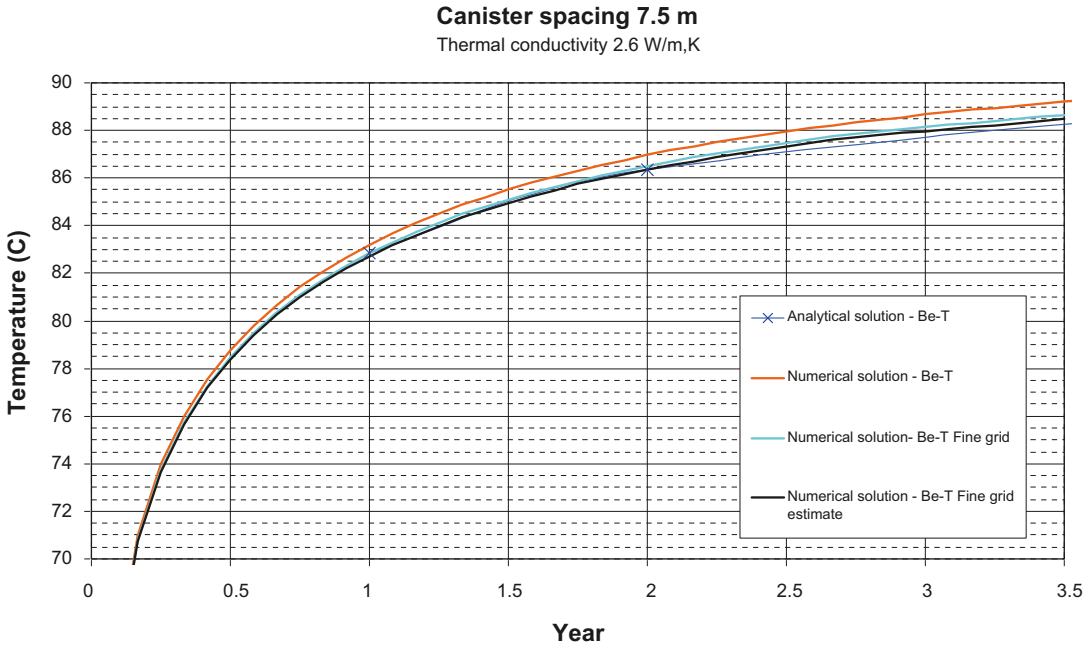

Figure 5-16. *Results of comparison between analytical and numerical solution with canister spacing 7.5 m and thermal conductivity 2.6 W/(m·K), details for 0–3.5 years.*

5.6 Example results

Example results from numerical simulations have been calculated for Rock domain RFM045 in Forsmark. Observe that that the calculations are based on thermal site descriptive modelling stage 2.2 /Back et al. 2007/. Rock domain RFM045 in Forsmark has been remodelled in stage 2.3 /Sundberg et al. 2008a/. Furthermore the maximum temperature criterion, i.e. the margin to the 100°C threshold, is not specified. Consequently, the example results shown in this section can only be used for illustration purposes.

5.6.1 Ranking results vs. calculated maximum buffer temperature

The ranking procedure calculates a weighted thermal conductivity, as described in Section 5.4.7, for each of the nine canisters in each realisation (approx 500–1,000) of the thermal rock properties. The realisations are sorted according to the lowest weighted thermal conductivity for any of the 5 central canisters in each realisation (canister 3–7). Thus, the first ranked realisation has the lowest weighted thermal conductivity and should consequently also have the highest calculated temperature if the ranking procedure picked the realisations in the right order. However, a perfect match between ranking based on weighted thermal conductivity and ranking based on calculated temperature cannot be expected. Selecting the first ten ranked realisations is a reasonable precaution to ensure that the realisation with the lowest thermal conductivity has been included in the temperature calculations and to ensure that the temperature criterion is met.

In Table 5-6 example results of the ranking procedure are shown, together with results on the calculated maximum temperature for a number of realisations. The first ranked realisation has the highest calculated temperature as well. Table 5-6 and Figure 5-17 illustrate that the ranking procedure, based on weighted thermal conductivity, reflects rather well a ranking based on temperature for this example. The results in Table 5-6 verify that the precaution of including the “worst” ten realisation for this example is sufficient (with some margin) to ensure that the temperature criterion is met.

Table 5-6 also illustrates that the tested canister spacing is satisfactory for all canisters if the actual temperature criterion is 95°C. If the temperature criterion is 94°C, one single canister does not meet the criterion. If the criterion is 93°C, none of the first ten ranked realisations meet the criterion.

Table 5-6. A number of realisations with the lowest thermal conductivity according to the ranking procedure for Rock domain RFM045 together with calculated peak tempearture. Canister spacing 6.5m, tunnel spacing 40 m, start temperature 11.1°C. Based on thermal site descriptive model stage 2.2 /Back et al. 2007/. The column with "TRC 17" is further explained in Section 5.6.3.

Ranking	Realisation No	Canister with highest temperature, no	Weighted thermal conductivity, W/(m·K)	Max temperature, °C	TRC 17,%
1	374	3	2.58	94.23	95
2	304	5	2.61	93.97	95
3	351	3	2.62	93.47	59
4	229	3	2.66	93.60	89
5	94	3	2.67	–	96
6	259	4	2.68	93.61	70
7	361	7	2.68	92.60	73
8	133	4	2.68	93.03	99
9	154	4	2.71	93.05	92
10	261	6	2.72	93.10	82
15	171	5	2.78	92.22	70
20	22	3	2.80	91.86	72
30	382	4	2.84	91.40	53

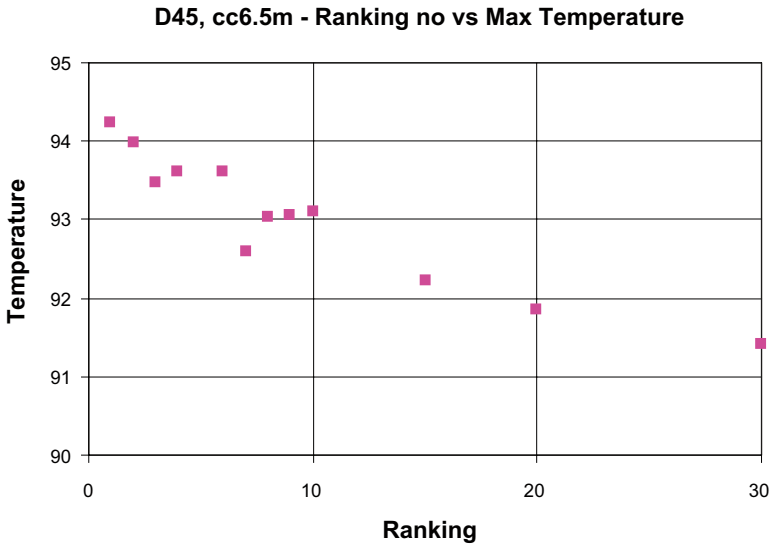

Figure 5-17. *Ranking vs. maximum buffer temperature. Example results from Rock domain RFM045 in Forsmark (canister spacing 6.5 m). Based on thermal site descriptive model stage 2.2 /Back et al. 2007/.*

5.6.2 Example results of numerical modelling

Figure 5-18 shows the temperature distribution along a tunnel where the various peak canister temperatures are visible. Figure 5-19 shows the temperature distribution in the xz-plane, illustrating the temperature difference in the canisters.

5.6.3 Example on possible optimization

There are different possibilities on optimization of the repository design since a large part of the rock mass has much more favourable thermal properties compared to the canister with lowest thermal conductivity. This is further discussed in Chapters 7.4 and 8.4. For example, in the ranking procedure the rock type composition is also calculated in the different volumes used for calculation of the weighted thermal conductivity around each canister. This can be used to examine if a special rock

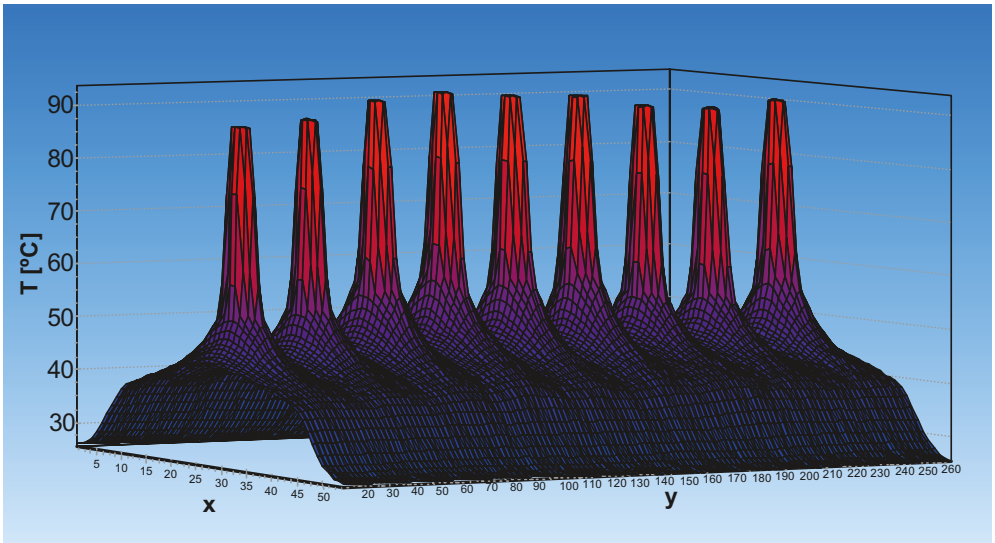

Figure 5-18. *Example results of simulated temperatures in the xy-plane for Rock domain RFM045 in Forsmark. Realisation no 382, canister spacing 6.5 m. Based on thermal site descriptive model stage 2.2 /Back et al. 2007/.*

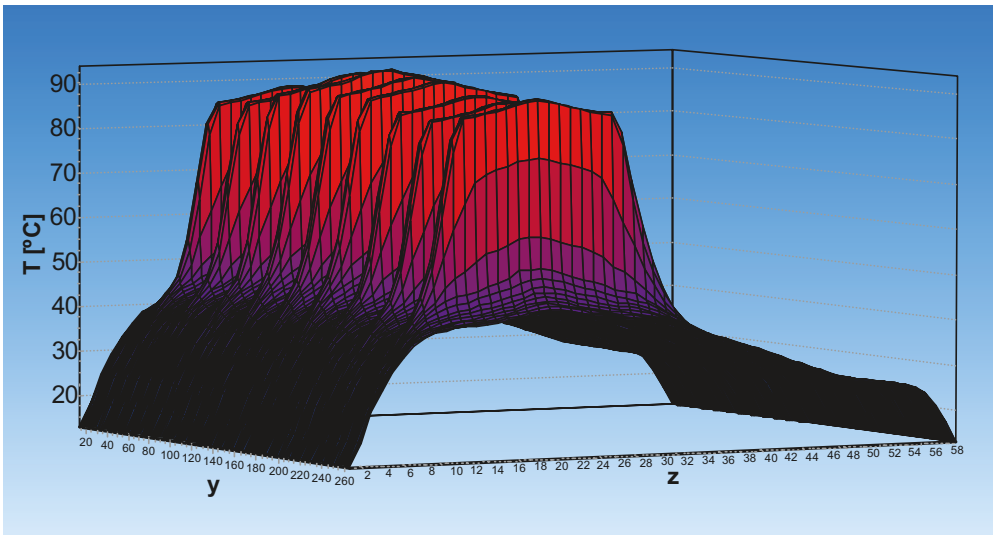

Figure 5-19. *Example results of simulated temperatures in the xz-plane for Rock domain RFM045 in Forsmark. Realisation no 382, canister spacing 6.5 m. Based on thermal site descriptive model stage 2.2 /Back et al. 2007/.*

type in, for example, the near-field of a canister, seems to have a large effect on the weighted thermal conductivity. If possible, this can be used to estimate a loss criterion based on the presence of a special rock type that can be identified in the tunnel.

This is illustrated in Table 5-6. The column with TRC 17 represents the proportion of the TRC with the lowest thermal conductivity (amphibolite) in a radius of 2.5 m from the canister (approximately the same dimension as deposition tunnel). Figure 5-20 shows that the peak buffer temperature is significantly reduced when the amphibolite proportion is reduced.

In future design work it will be possible to use conditional stochastic thermal simulations of a rock mass containing a few deposition tunnels as input to the numerical model. Conditional simulation takes into account the observations (known data points) made of both geology and thermal conductivity. This will make it possible to optimize the repository layout to a much higher degree.

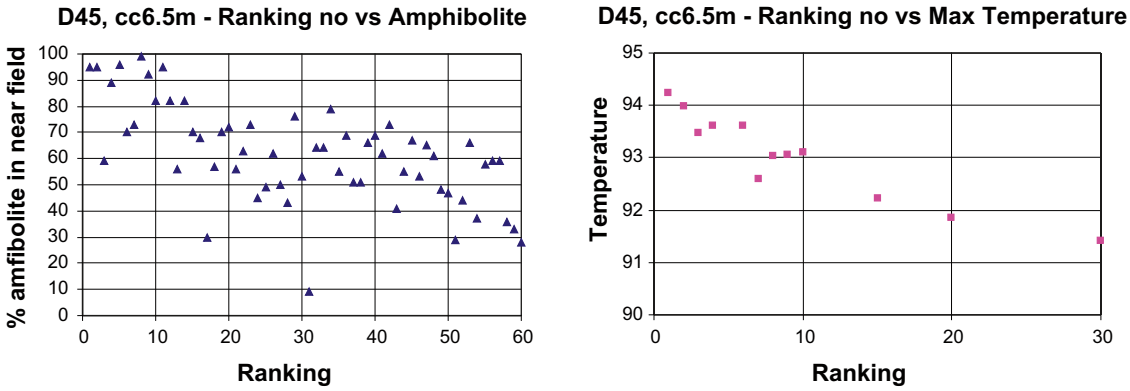

Figure 5-20. *Ranking vs. percentage of low conducting Amphibolite in a radius of 2.5 m from canister (left) and Ranking vs. Maximum Bentonite Temperature. Example results from Rock domain RFM045 in Forsmark canister spacing 6.5 m. Based on thermal site descriptive model stage 2.2 /Back et al. 2007/. Ranking no. 30 and 60 correspond only to approximately 0.5 and 1% respectively of the total number of canisters.*

5.7 Uncertainties

The studied region is assumed to be bounded in the horizontal direction by symmetry planes with no heat flow across the surfaces.

The influence of a neighbouring tunnel region with a 10% higher conductivity was found to yield 0.2°C higher canister temperature when the tunnel spacing was 40 m, cf. Section 5.5.2. This influence will increase with higher thermal conductivity differences and with closer tunnel spacing. If only one tunnel is included in the simulation, the possible influence constitutes an uncertainty. An alternative would be to include the two adjacent tunnel regions in the simulation, which would certainly be enough to eliminate any significant influence on maximum buffer temperature from surrounding tunnels.

There may also be an influence of heterogeneous thermal properties in the direction along the tunnel. Here, we have chosen to include nine canisters in the simulation. The results from the outer two canisters in both directions are excluded in the final analysis due to expected significant influence from the region outside the symmetry plane. This assumption has been analyzed and it seems to be a sufficient precaution. The error due to symmetry effects is small.

For a homogeneous rock, the maximum rock wall temperature should be attained close to the mid-height of the canister. In the heterogeneous case, this is not necessarily the case. Depending on the relative difference of rock thermal conductivities near the deposition hole, the rock wall temperature will vary in a more unpredictable way with the highest temperature likely to be found near large segments with low conductivity rock. This is further evaluated in Chapters 3 and 6.

The correction for a less detailed description of the canister is also further evaluated in Chapters 3 and 6. All uncertainties are summarized in Chapter 6.

6 Uncertainties and margins – summary

6.1 General

For the dimensioning of the repository such that the temperature criterion is met for all canisters, the maximum buffer temperature at the hottest canister must be calculated. The calculation scheme comprises the following steps (cf. Figure 1-2):

- Calculation of the temperature $T_{wall}(t)$ at the wall of the deposition hole. The deposition hole must be situated in the rock domain portion representing the most unfavourable geometrical arrangement of low conductivity rock elements that is reasonably possible (cf. Chapter 5).
- Calculation of the difference $\Delta T_{tot}(t)$ between the rock wall temperature at canister mid-height and the surface temperature at the top of a canister in a dry deposition hole (cf. Chapter 3).
- The maximum bentonite temperature $T_{max}(t)$ is then obtained as $T_{wall}(t) + \Delta T_{tot}(t)$.

There are uncertainties as well as systematic under- and overestimates in the calculation schemes. This means that the dimensioning of the repository, i.e. establishing canister and tunnel spacing for the different rock domains at a given site, must be made with a margin to the 100°C threshold. There are numerous aspects of the problem that are associated with only small uncertainties. Taken one by one, these have little effects on the calculated maximum bentonite temperature and would not require more than rough upper bound estimates to be relevantly accounted for. If too schematic upper bound estimates are made of each individual effect, they would, however, add up to a substantial total effect and result in an exaggerated total margin. This is the reason why fractions of degrees are considered in the assessment of the different effects in the following sections.

The numerical values and ranges suggested below are present-day best estimates and should be subject to revisions in the future in case of concept modifications or if new information should become available.

6.2 Uncertainties in the local buffer/canister solution

For the difference $\Delta T_{tot}(t)$, the reference evolution defined in Chapter 3, cf. Equation 3-12, is used in all examples presented here. The reference evolution is based on best-estimate values of buffer heat transport properties in dry deposition holes, on numerically assessed estimates of heat flux redistribution effects, and on open gap effects observed in a particularly dry Prototype Repository deposition hole. While the reference evolution is judged to be reasonably realistic for dry KBS-3 deposition holes it is probably not a worst case (cf. Section 3.4.2). The reference evolution is approximated to be independent of the surrounding rock, whereas the real evolution will be slightly different for different rock heat transport properties. The uncertainties described in Section 3.4.3 regard the heat transport properties in the buffer, effects of moisture redistribution, effects of the rock thermal conductivity distribution in the rock closest to the walls and effects of possible variations in the heat load distribution along the height of the canister. The margins required to cover these uncertainties are shown in Figure 3-16 and summarized below in Table 6-1. The canister geometry for the two cases (with and without flanges) is shown in Figure 2-3. The present-day reference design is that with flanges. The plain top/bottom option is included here for completeness and to provide perspectives on the importance of design details. All results discussed in the following are based on the reference flange design.

Table 6-1. Margin required to account for uncertainties and under/overestimates in the local buffer/canister solution.

	Rock conductivity 2.0 W/(m·K)	Rock conductivity 3.0 W/(m·K)
Canister with flanges	3.45°C	4.05°C
Canister with plain top/bottom	4.15°C	4.75°C

6.3 Uncertainty in the calculation of rock wall temperature

6.3.1 General

There are systematic under/overestimates as well as actual data and model uncertainties as described in previous sections. Since the numerical method described in the previous chapter will be used for the actual dimensioning calculations, whereas the analytical solution is used to get first trial values of the required spacing, the under/overestimates specifically associated with the analytical solution are unimportant from the strategy point of view. In addition, the agreement between analytically and numerically obtained results is sufficient to establish general confidence in the basic performance of both solutions (cf. Figure 5-14 to Figure 5-18). Here, the genuine uncertainties in input data and the under/overestimates associated with the numerical scheme described in the previous chapter are compiled.

6.3.2 Uncertainties in input data

Anisotropy within rock type

Anisotropy between different rock types (e.g. dykes) is taken into account in the thermal modelling of thermal rock properties in each rock domain. However, anisotropy within rock type (foliation, lineation) is not taken into account and must consequently be handled as an uncertainty.

If there is a systematic anisotropy such that the nominal rock conductivity is λ with different values of λ_x, λ_y and λ_z such that $\lambda^3 = \lambda_x \cdot \lambda_y \cdot \lambda_z$, the resulting buffer peak temperature may be higher (or lower) than in the isotropic case with $\lambda_x = \lambda_y = \lambda_z$. This means that a margin must be applied to account for anisotropy.

The analytical solution described in Chapter 4 can be used to estimate the importance of the anisotropy to the temperature contribution from the rest of the repository, i.e. from all canisters other than the local one, provided that the principal directions of the conductivity tensor are aligned with the deposition geometry (cf. Appendix B). The worst case is if the foliation planes strike along the tunnels and dip 90 degrees, since this would impact most on the horizontal heat transport away from the tunnels, which is particularly important during the first 10–20 years after deposition. For this case of foliation orientation, the temperature contribution from the rest of the repository will increase (in comparison to corresponding isotropic conditions) by between 0.2°C and 0.8°C for anisotropy factors ranging between 15 and 50% (Appendix B). For differently oriented foliation planes the effects will be smaller.

The analytical solution cannot account for the anisotropy effects on the heat dissipation from the local canister. The results obtained from the numerical one-canister models described in Appendix B indicate that the local canister contribution to the rock wall temperature could increase by 0.5°C to 1.5°C, provided that foliation dips 90 degrees. For other dip angles, the effects will be smaller.

It is suggested that the margin applied to cover effects of within-rock-type anisotropy be based on Table 6-2 below (cf. Appendix B). Note that the values below represent upper bound effects with worst case orientation of the foliation plane in relation to the direction of the deposition tunnels and with the same anisotropy in all rock volumes (i.e. in all TRCs). The anisotropy is a typical site-specific uncertainty and could, with favourable direction of the deposition tunnels, have a lowering effect on the peak buffer temperature.

Bias in thermal conductivity and heat capacity at room temperature

In the numerical model presented in Chapter 5, heat transport properties are assigned to 1 m cubes of rock. At this scale the standard deviation is typically about 0.1 W/(m·K) (0.08–0.13) for the dominating thermal rock classes at the two sites /Back et al. 2007, Sundberg et al. 2008b/. A systematic, global mis-prediction of the conductivity by 0.1 W/(m·K) would give an error of about 2.0°C in peak

Table 6-2. Underestimate of peak buffer temperature if foliation planes strike along tunnels and dip 90 degrees.

Anisotropy	Local canister	Rest of repository	Total
15%	–0.5°C	–0.2°C	–0.7°C
50%	–1.5°C	–0.8°C	–2.3°C

temperature in low-conductivity rocks (2.0 W/(m·K)) and of about 1.2°C for intermediate values (3.0 W/(m·K)), cf. Figure 6-1. The standard deviation given at the 1 m scale in the site reports is, however, not necessarily a relevant measure of the rock conductivity uncertainty in peak temperature calculations:

- The peak buffer temperature is determined by rock properties in volumes much larger than 1 m cubes.
- The rock domain realisations selected for numerical simulations (cf. Chapter 5) will be those with the lowest effective conductivity in the relevant model sections closest to the canisters, meaning that values are picked from the low conductivity sides of the TRC distribution and that, consequently, the actual range of variation on the low conductivity side of the mean is small.
- There is no indication of a bias that would cause an overestimation of the measured thermal conductivity. On the contrary, the main experimental method used in the site investigations, the Transient Plane Source (TPS) method, appears to underestimate the thermal conductivity compared to the divided bar method /Sundberg and Kukkonen 2003/.
- The accuracy of TPS measurement according to manufacture specifications is ±2%, resulting in approximately ±0.05 W/(m·K).

It is, therefore, suggested that the margin required to cover uncertainties in the rock conductivity should be one half of the values shown in Figure 6-1 (left), i.e. about 1.0°C for low conductivity rocks and 0.6° for intermediate and high conductivity rocks.

For the heat capacity the standard deviation given for the sample-scale data given in the site reports is typically about 0.1 MJ/(m^3·K) /Sundberg et al. 2008a, b/. For the rock wall temperature this corresponds to about 0.6°C (Figure 6-1, right). On the 1 m scale, the variability in capacity is likely to be even smaller, giving an insignificant variation in rock wall temperature. Since the methods used in the site modelling appear to give identical mean values, it is suggested that effects of capacity uncertainties are too minor to be taken into account.

In conclusion, the margin required to cover uncertainties in data given for the heat transport properties of the different TRC´s in the site models is suggested to range between 0.6°C and 1.0°C, depending on the rock conductivity, cf. summary in the end of this chapter.

Uncertainty in modelled heterogeneity in thermal site descriptive models

It is proposed here that the basic lithological data for each rock domain is regarded as representative and the Thermal Rock Class definitions as adequate. Whenever necessary, subdivisions into subdomains have been made in the thermal site descriptive models in order to reproduce the variability in rock type proportions and spatial correlation lengths /Back et al. 2007, Sundberg et al. 2008b/. There could still

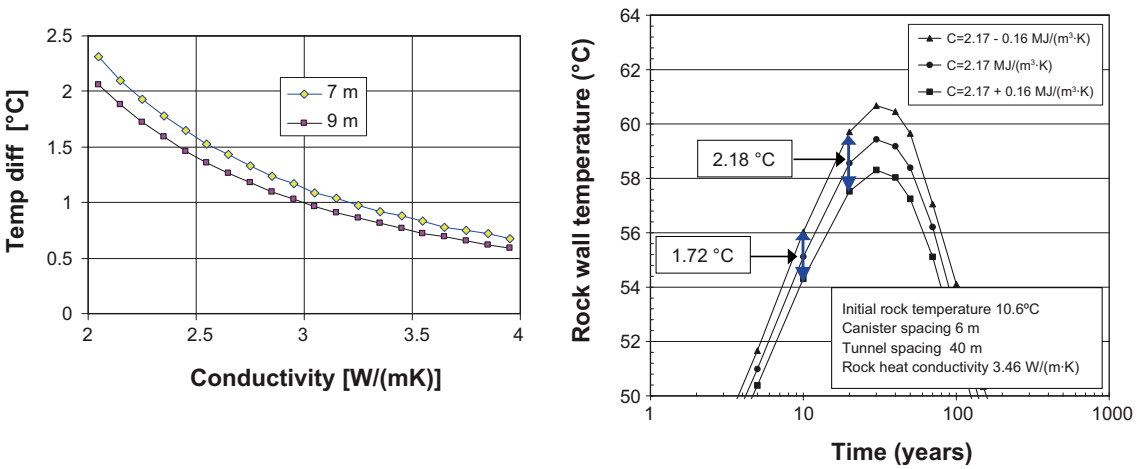

Figure 6-1. *Left: Effect on calculated peak buffer temperature of systematic, global 0.1 W/(m·K) conductivity mis-prediction. Right: Sensitivity of rock wall temperature to heat capacity variations. The typical 0.1 MJ/(m^3·K) standard deviation established for the dominating TRCs at the sites would correspond to a rock wall temperature variation of about 0.6°C.*

be uncertainties in the spatial variability, i.e. it is theoretically possible that none of the realisations of the geology produce large enough bodies of low-conductivity rocks to cover the worst possible cases. If a sufficiently large number of realisations of the site models are produced, the possible influence of the uncertainty on the buffer temperature is judged to be negligible or small, 0–0.5°C.

Uncertainty in the initial temperature

The variation between temperatures measured in different boreholes varies between the sites. Typically that variation is on the order of 0.1–0.4°C /Sundberg et al. 2008a, Sundberg et al. 2008b/. In addition there is possible bias in the measurements which is estimated to be in the order of 0.25°C. This gives an uncertainty in the range of 0.35–0.65°C.

The initial temperature relevant for the dimensioning problem may differ from the present-day rock temperature because of heat generated during tunnel excavation, drilling of deposition holes and other activities in the tunnel before deposition and closure. There will also be effects of ventilation. The effects of these disturbances will depend on the tunnel excavation method, the mechanical work expended on drilling, the duration of the ventilated phase, the temperature of the ventilation air, etc. At the time of this report it is not possible to estimate these effects or even to establish if the net effect will be a decreased or an increased effective background temperature.

Temperature dependence in thermal properties

The thermal conductivity usually decreases with temperature (typically by about 10% per 100ºC), whereas the heat capacity increases (typically by about 25%/100 ºC, cf. /Back and Sundberg 2007). For low conductivity rocks the temperature dependence is close to 0 or at least small enough that the conductivity and capacity dependencies cancel out /Sundberg et al. 2008a, b/. This seems to be valid for rock types like granite, granodiorite and quartzmonzodiorite. However, especially rock types like gabbro and amphibolite may deviate from this general behaviour.

In the numerical model, it is possible to explicitly include these dependencies, provided that they can be established qualitatively for the dominating rock types. If not, it is suggested that the margin required to cover the uncertainties associated with temperature dependence is set to:

- 0.5°C for low conductivity rocks (2.0–2.5 W/(m·K)).
- 1°C for high conductivity rocks (3.0–3.5 W/(m·K)), i.e. assuming that the near-field temperature has increased effectively by 30°C at the time of the peak (cf. Figure 6-2) such that the conductivity has decreased by about 3%, i.e. by about 0.1 W/(m·K). The effects of the increased capacity in the near-field are conservatively ignored.

Conductivity data is based on measurements performed at room temperature. At repository depth, the in-situ conductivities will be slightly higher because of the lower temperature. The effects of the lower in-situ temperature are, however, small and are suggested to be (conservatively) ignored.

Pressure dependence in thermal conductivity

All thermal conductivity data given in the site reports is based on measurements performed on stress-free samples. At repository depth the in-situ conductivities will be slightly higher because of the stresses, approximately 1–2% for water saturated samples (0.02–0.06 W/(m·K)) (eg. /Walsh and Decker 1966/), resulting in approximately –0.5°C for both low and high conductive rock according to the discussion of bias above. However, the stress dependence has not been addressed in the site investigations. It is, therefore, suggested that the margin mentioned above is lowered to –0.2°C if no site specific data is available.

Tunnel backfill

The backfill conductivity value assumed in the one-canister models described in Chapter 3 is 0.7 W/(m·K). This value is based on the assumption that the backfill consist of a mixture of bentonite blocks and pellets and that are both dry. At the time of this report there is no detailed information on the actual block-pellets proportions or on the initial saturation and void ratio of the backfill material to be used in KBS-3 deposition tunnels. The sensitivity of the rock wall temperature to backfill conductivity variations

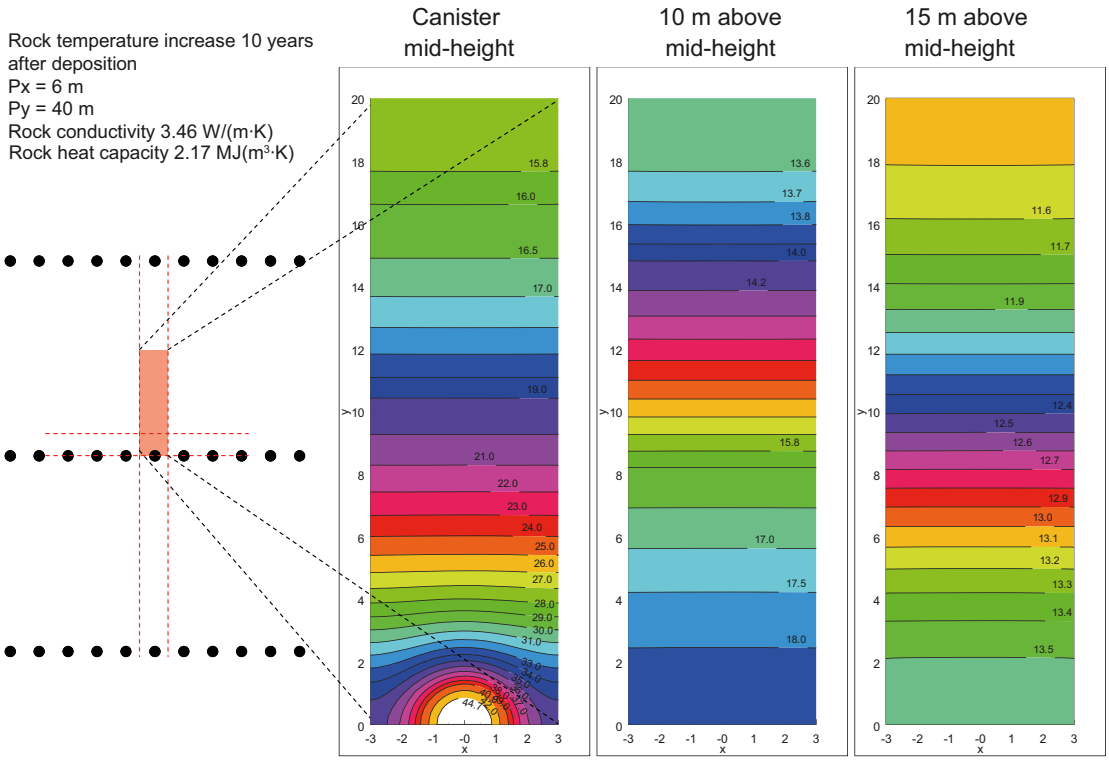

Figure 6-2. *Contours of unit cell temperature increase at three different levels, calculated by use of the analytical solution described in Chapter 4.*

is however small as noted by /Hökmark and Fälth 2003/ and directly demonstrated in /Kristensson and Hökmark 2007a/. For the axis-symmetric one-canister models described Chapter 3, a backfill conductivity reduction from 0.7 W/(m·K) to 0.3 W/(m·K) would give a rock wall mid-height temperature increase of about 0.05°C (Appendix A). On condition that a reasonably correct value (e.g. 0.7 W/(m·K)) is used in the numerical model described in Chapter 5, there is no need to account for any uncertainties in the backfill conductivity in the dimensioning analyses. It could be noted, too, that the actual tunnel cross section area is slightly overestimated in the numerical model since optimization of the tunnel area has been made recently, cf. /SKB 2010d/. The effect of overestimating the tunnel cross section area is small but on the conservative side.

Uncertainties in the chosen strategy for thermal dimensioning

The strategy implies sampling with five canister positions in a large number of thermal property realisations of each rock domain. The total number of sampled canister positions in each domain is in the same order of magnitude as the planned total number of canisters in the whole repository (the number of realisations, and consequently the number of sampling, in small domains may be lower).

Although the numbers are quite large, there are, of course, uncertainties associated with the identification of the most unfavourable canister positions. Because the sampling is not infinite, there will always be a possibility, at least theoretically, that canister positions exist that are even more unfavourable than the worst case that have been identified during the sampling. It is estimated that less than 1 ‰ of the rock mass will have even lower thermal conductivity. The number of sampled positions is so large that the estimated maximum temperatures are believed to be reasonable estimates of the worst conditions at the real repository (approximately 6,000 canisters). In other words, it has been assessed that the used statistical approach in a realistic way emulates the conditions for the real repository.

6.3.3 Numerical model uncertainties and under/overestimates

In this section under/overestimates resulting from simplifications made in the numerical modelling (cf. Chapter 5) are summarized, e.g. effects of the boundary conditions, the grid resolution and the schematic representation of canister and buffer.

Boundary conditions

The model geometry used for the actual simulations includes a length section of one tunnel with nine canisters in the central parts of a deposition area. The vertical boundaries of the numerical model are adiabatic symmetry planes between tunnels and canisters, see Figure 5-12. This means that the thermal properties of the rock surrounding neighbouring tunnels and heat sources (outside the model volume) are automatically assumed to be identical to the properties of the modelled volume. For the low conductive domain realisations picked for temperature calculations, this is not likely to be the case. Instead neighbouring rock will typically have a higher conductivity, meaning that geometrical symmetry planes are not truly adiabatic. This appears to give an underestimate of the peak buffer temperature in the low-conductive tunnel sections that are actually analyzed. The underestimate is typically around 0.2°C (cf. Section 5.7) if the rock surrounding one of the adjacent tunnels has 10% higher thermal conductivity (3.48 compared to 3.16 W/(m·K)). This underestimation will be larger with increased difference between the mean rock thermal conductivity and the low conductivity rocks that dominate the numerically modelled volume and the figure is thus site specific. However, it is reasonable to believe that the underestimation will be lower at an overall lower thermal conductivity (compared to the example above) since the peak of the bentonite temperature occurs earlier and the temperature wave from the adjacent tunnel will move slower.

The typical difference between the mean thermal conductivity in a rock domain and the typical thermal conductivity between a canister and the boundary to adjacent tunnel (in low conductive rock) is estimated to be 5–15%. It is suggested that a typical margin of between 0.2° and 0.5°C (2·0.1°C and 2·0.25°C) is used (two adjacent tunnels and 40 m distance between tunnels) to avoid underestimation of the temperature due to boundary conditions (if the distance between tunnels is smaller, the influence of boundaries increases). However, this margin should be evaluated site specifically.

There may also be an influence of heterogeneous thermal properties in the direction along the tunnel. However, the error due to such symmetry effects seems to be small when only the 5 central canisters (of totally 9) are considered (cf. Section 5.7).

Representation of canister and buffer

The numerical model cannot represent the details of the deposition hole interior. The finite difference scheme gives small time steps and long execution times if the models include materials with large differences in transport properties. Therefore, the canister is modelled as one homogeneous body with slightly reduced conductivity rather than as a compound steel/copper cylinder. No account is made of any axial distribution of the heat generation such as described in Chapter 3 for the local canister/buffer solution. All this will impact on the heat flux distribution in the deposition hole interior and give a rock wall temperature overestimate which will depend on the conductivity value selected for the homogeneous canister. Setting the canister conductivity to 30 W/(m·K) will give an overestimate of about 0.7°C (cf. Chapter 3).

Numerical precision

For computational efficiency, it is expedient to analyze models with reasonably refined calculation grids. The course grid option described in Section 5.5.3 overestimates the maximum temperature by about 0.8°C compared to ideally refined grid. Depending on the grid resolution selected for the dimensioning analyses, a corresponding correction must be made to the margin.

6.4 Margins

6.4.1 Summary of uncertainties and model simplifications

The uncertainties and the effects of model simplification are summarized here to assess the margin that should be applied in dimensioning calculations. Note that the margin does not need to be identical for all sites and for all rock domains. The magnitudes of some of the effects depend on the rock conductivity. There are also the effects of anisotropy which must be evaluated differently in different rock domains (i.e. if it turns out to be important to keep margins at a minimum).

Table 6-3 summarizes effects of uncertainties related to the local solution, Table 6-4 the uncertainties related to the rock wall temperature and Table 6-5 the total margin estimated to cover both. The margin is slightly different for the analytical and the numerical approach. The analytical solution does not account for e.g. deposition tunnel and flux redistribution due to gap effect and the numerical model have e.g. reduced thermal conductivity in order to optimize calculation time. The margin is optimized for the numerical approach. However, the margin for the analytical solution is of the same magnitude. Since the analytical solution is used for guess values of canister spacing only, the same margin as for the numerical approach is used.

Table 6-3. Local solution.

ΔT_{tot}, difference between rock wall temperature and maximum bentonite temperature		Rock conductivity 2.0 W/(m·K)		Rock conductivity 3.0 W/(m·K)
Uncertainties related to:				
U1	Geometry of air-filled canister/bentonite gap and variations in buffer conductivity	2.7°C		3.3°C
U2	Moisture redistribution in buffer		0.2°C	
U3	Spalling		0.1°C	
U4	Vertical variation of rock conductivity along deposition hole		0.25°C	
U5	Vertical distribution of heat generation in the canisters		0.2°C	
Sum ΔT_{tot}		3.45°C		4.05

Table 6-4. Numerically calculated rock wall temperature.

T_{wall}, Rock wall temperature at canister mid-height at the time of buffer temperature peak		Rock conductivity 2.0 W/(m·K)		Rock conductivity 3.0 W/(m·K)
Uncertainties related to:				
U6	Anisotropy (maximum set for an assumed factor of 1.15 and worst case orientation of foliation plane) depending on tunnel orientation		0–0.7°C (1	
U7	Bias in thermal properties	1.0°C		0.6°C
U8	Heterogeneity, site models (in the lower tail)		0–0.5°C (1	
U9	Initial temperature		0.35–0.65°C (1	
U10	Temperature dependence (if these dependencies are not accounted for in the calculations)	0.5°C		1°C
U11	Pressure dependence		–0.2°C	
U12	Tunnel backfill		0°C	
U13	Strategy uncertainties		–	
Sum (uncertainties)			1.65–3.15°C	1.75–3.25°C
Over/underestimate because of numerical model simplifications				
S1	Representation of canister		–0.7°C	
S2	Numerical precision		–0.8°C	
S3	Boundary conditions		0.2–0.5°C (1	
Sum (under/overestimates)			–0.85–0.55°C	
Total T_{wall}			0.35–2.15°C	0.45–2.25°C

(1 This will be site dependent.

Table 6-5. Total margin (values in parenthesis: if temperature dependence is accounted for in numerical calculation).

	Rock conductivity 2.0 W/(m·K)	Rock conductivity 3.0 W/(m·K)
Local solution	3.45°C	4.05
Total T_{wall}	0.35–2.15°C	0.45–2.25°C
Total margin	3.8–5.6°C	4.5–6.3°C
	(3.3–5.1°C)	(3.5–5.3°C)

6.4.2 Margin definition

The margins required to cover the different uncertainties appear to depend on the rock domain and the site being considered. Defining the margin for a given rock domain will be a matter of judgement, and of navigating and interpolating in the tables above. An example is given below.

Margin example

Assume that the dimensioning rock conductivity is in the range 2.0–2.5 W/(m·K) and that the anisotropy factor is on the order of 10% at average with foliation planes dipping about 45 degrees and striking about 45 degrees in relation to the tunnel direction. Canisters are assumed to have flanges (cf. Figure 3-16). Relevant values of U1, U6, U7, U8, U9, U10, and S3 need to be estimated, while the other effects would be as in the tables above.

A relevant estimate of U1 would be 2.9°C giving a margin for ΔT_{tot} of 3.65°C (cf. bottom row in Table 6-3).

- Relevant estimates of U6 and U7 would be 0.3°C (anisotropy), 0.8°C (property bias), respectively.
- Assume that the uncertainty in the heterogeneity effect (U8) can be estimated to 0.1°C.
- Assume that the in-situ temperature results from the investigation boreholes vary within 0.2°C. This gives U9 = 0.25+0.2°C = 0.45°C, cf. 6.3.2 (uncertainty in initial temperature).
- U10 should be set at 0.5°C (temperature dependence in low conductivity rocks).
- S3 (boundary condition) is evaluated site specific and set at 0.2°C.

This gives a T_{wall} margin of 0.65°C (cf. bottom row of Table 6-4).

The margin to apply in dimensioning calculations would be 3.65°C + 0.65°C = 4.3°C.

6.4.3 Margin and application of the temperature criterion

It should be noted here that the scheme established above for definition of margins is based on strict application of the temperature criterion, i.e. the bentonite temperature must not exceed 100°C anywhere in any deposition hole. The hottest canisters will be found in dry deposition holes and the hottest bentonite on the top of these canisters, whereas all bentonite in the 0.35 m space between canister and rock wall, including the bentonite closest to the vertical canister surfaces, will be significantly cooler. The bentonite regions in which the temperature will approach the design limit are restricted to very small volumes just above the top surface. Five centimetres above that surface, the temperature will be at least 2°C lower, cf. Figure 6-3 below. Note that the temperatures shown in this figure do not include contributions from other canisters than the local one. The temperature differences between the different points are, however, independent of all other canisters and of the layout.

It may be worthwhile to consider applying the criterion to the bentonite at some distance from the top surface, rather than at that very surface where (in the reference case of canister design, i.e. with flanges) the buffer does not contribute much to the isolation or the mechanical protection of the canister. A possibility would be to apply the criterion to the bentonite 5 cm above the top surface, which would cut at least 2°C off the margin.

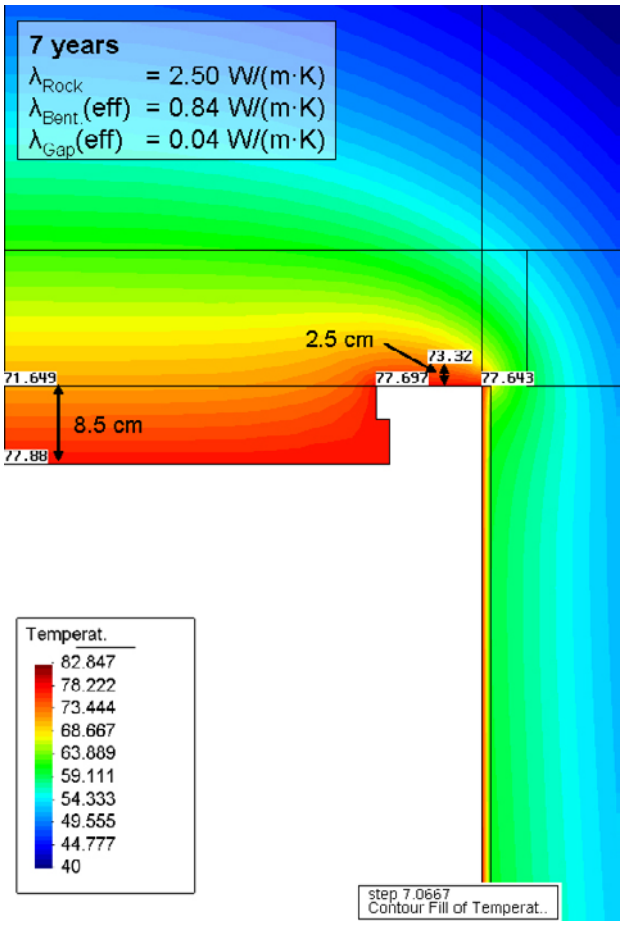

Figure 6-3. *Bentonite temperature around top of the canister (Appendix A).*

7 Strategy

7.1 General

This report is primarily intended to be used as a basis for the thermal dimensioning of Layout Step D2 presented in the Site Engineering Reports for the Forsmark and Laxemar sites. Future layout work will be based on more detailed information on site properties, less schematic assumptions on the power distribution among the canisters and possibly improved near-field design solutions and installation procedures. All this will allow for optimization measures. The focus here is on layout D2.

7.2 Layout D2

For layout D2 the following applies:

- All canisters should be assumed to have an initial power of 1,700 W and decay characteristics as described for mixtures of BWR and PWR fuel of different burn-up and different age (cf. Chapter 2).
- The tunnels spacing is fixed at 40 m.
- The peak buffer temperature must not exceed 100°C for any canister. This means that:
  - all canister positions should count as dry with air-filled gaps between canister and buffer,
  - model and data uncertainties in the temperature calculations must be translated into a reliable temperature margin. That margin could differ slightly between sites and rock domains, depending, for instance, on whether there is anisotropy in heat transport properties.
- The canister spacing must not be smaller than 6 m, even if calculations show that the temperature criterion would be fulfilled with a smaller spacing.
- The canister spacing should be set at one value for each of the rock domains identified at the two sites. The spacing should be based on the layout conditions in the central parts of the deposition areas. The spacing should be sufficient, but not larger than necessary (except for when the 6 m rule applies), to meet the temperature criterion.
- No optimization should be made. No attempts should be made to modify the spacing, e.g. in peripheral parts of the deposition areas, or to take advantage of the lower peak temperatures that will be found for the majority of the canisters.

7.3 Implementing the strategy – D2

The issue is to set the canister spacing for the different rock domains. The following steps should be taken, (cf. Figure 1-3):

- The margin to the threshold temperature is determined (i.e. it is established that the calculated peak buffer temperature should be less than e.g. 95°C). Determining the margin is a question of navigating and interpolating in the tables presented in Chapter 6 (steps 2 and 3 in outline flowchart, Figure 1-3).
- A nomographic chart, as shown in Figure 4-18, is established for the rock domain by use of the analytical solution. The chart should be generated using the rock domain mean value of the heat capacity. Once the chart is established, it can be used for any assumptions regarding the initial temperature and choice of temperature margin (step 4 in outline flowchart).
- Based on the thermal conductivity distribution suggested for the rock domain on the 5 m scale, a best guess value of the dimensioning domain conductivity is made. Experience shows that the value should be picked in the 0.1–2% range of the low conductivity tail (cf. Appendix D). Note that this is uncertain and depends on the shape of the low conductivity tail of the rock domain conductivity distribution and on the spatial autocorrelation.

- A trial spacing corresponding to the best guess dimensioning conductivity is obtained from the nomographic chart (step 5 continued).
- A sufficient number of stochastic realisations of the spatial distribution of the thermal properties are produced to describe the variability in the whole rock domain. A number of 500–1,000 realisations are judged to be enough. The number depends on the rock domain size, i.e. the number of canisters to be deposited (step 6 in outline flowchart).
- A finite difference model of a central tunnel in a deposition area located in the rock domain being considered is generated as described in Chapter 5. The spacing is set at the trial value (step 7 in outline flowchart).
- A number of simulations of up to the first 20 years of heat generation are made. The simulations stop when the peak buffer temperature has been reached. The simulations are based on a selection of the thermal rock domain realisations. The selection is based on an automated ranking system that picks the potential worst case models, i.e. the rock domain model realisations that would maximize the concentration of low-conductivity cells around the central canisters in the finite difference model (step 7 continued).
- If the numerical modelling verifies the trial spacing statistically, i.e. if it appears that the maximum peak temperature found among the selected worst case models matches the criterion (with account of the margin determined for the rock domain), this spacing can be established as the spacing for that rock domain. If not, and if the difference is large, the simulations may have to be repeated with a correspondingly modified spacing. If the difference is small, it will be sufficient to correct the spacing using the slope of the temperature- spacing curves in corresponding part of the nomographic chart (step 8 in outline flowchart).

Having established the rock domain spacing, the nomographic chart can be revisited to find the corresponding effective conductivity, i.e. the percentile of the conductivity distribution that actually determined the spacing. This would, however, not have any significance other than giving feedback to the process of trial spacing determination.

7.4 Optimizing the layout – following layout versions

The following possibilities for optimization should be recognized.

- If it turns out that the available rock volume could be insufficient, it may be necessary to consider reducing the tunnel spacing at the expense of increasing the total tunnel length and the construction costs. Canister-tunnel spacing charts (cf. Figure 4-19) can easily be generated for this purpose as needed, and used to quantify and optimize the volume saving. In the current version of the numerical model, it is possible to handle tunnel cc-distances in the interval 30–40 m.
- There may be other reasons to consider reducing the tunnel spacing. If, at some instance of time, it appears that the bentonite peak temperatures will be systematically lower than now expected for all canisters or for a substantial fraction of the canisters (for instance, if it turns out that the near-field design can be improved by reducing the canister-bentonite gap width from 10 to 5 mm), it may not be possible to take full advantage of this if the canister spacing is close to the allowed minimum (6 meters) in the initial layout. If the repository layout is not fully optimized for total tunnel length initially, the possibilities will be better.
- Since there will be many hundreds of canister positions (in tunnel ends; cf. Section 4.4.3) that can accommodate canisters with significantly higher initial power than the target 1,700 W, it will be worthwhile to plan the canister production carefully and coordinate it with the layout work. At some point of time in the canister production process, it will no longer be possible to find and combine fuel assemblies that add up exactly to the initial target power, meaning that following canisters will have to be under- or over-powered. The tools for establishing the number and the excess power distribution of overpowered canisters that can be deposited in tunnel ends are given in this report.

- An additional possibility to optimize the repository is to identify well-conducting parts of the rock mass and use it to accommodate canister with closer spacing (however still ≥6 m) or canisters with higher power.
- It may also be possible to identify volumes with low-conductivity rock, avoid these volumes ("loss of deposition hole positions"), modify the conductivity distribution to apply only for the remainder of the rock domain and then proceed with the dimensioning in that remainder according to that updated, i.e. improved, distribution.

When underground, it is possible to optimize the layout for smaller rock volumes compared to repository scale, e.g. the rock mass containing a few deposition tunnels. Conditional simulations that take into account observations of both geology and thermal conductivity is a possible tool to produce data to numerical simulations, in combination with measurements in a relevant scale and other observations.

Another possibility that may be considered in the future is that the temperature criterion or the margin is changed for some reason. This would not be a genuine layout optimization but would have influence on the distance between canisters. A possible revision of the way of applying the temperature criterion was indicated as an example in Section 6.4.3.

8 Conclusions and discussion

This report has described a strategy for dimensioning the KBS-3 repository such that the bentonite buffer temperature will not exceed 100°C for any canister deposited at any of the two sites considered for the repository. For both sites, Forsmark and Laxemar, thermal site descriptions exist /Back et al. 2007, Sundberg 2008a, b/. The strategy presented in this report can be applied directly to the sites using the thermal data found in the thermal site reports.

The strategy is focussed on layout step D2 for which a set of design premises has been specified, e.g. the spacing between tunnels is fixed at 40 m and the initial canister power is set at 1,700 W for all canisters. In addition, there should not be any optimization of the layout, i.e. the canister spacing should be set to the same value in each rock domain such that the temperature criterion is met for each canister. The methods described here to calculate the key parameter, the peak buffer temperature, and the uncertainties associated with it, are however general enough that they can be modified to be applied to the dimensioning problem for less specific cases as well.

The hottest canisters will be those deposited in dry deposition holes in low-conductivity rock in central parts of the deposition areas. The dimensioning parameter is, therefore, the peak buffer temperature in such deposition holes. The problem of calculating the peak buffer temperature in any deposition hole can be resolved into two, largely independent, problems:

1. Calculating the difference between temperature at the wall of the deposition hole and the temperature at the hottest point of the buffer.
2. Calculating the rock wall temperature.

The peak buffer temperature is then found by adding these two together. In all results examples shown here, as well as in previous similar work on the thermal evolution of the KBS-3 repository, the peak buffer temperature will occur 5–15 years after deposition.

There are model- and data uncertainties as well as over- and underestimates associated with both calculations above, meaning that a margin to the design threshold must be established. Establishing a safe, yet not overly conservative, margin is an important issue.

8.1 Local buffer/canister solution

For the strategy given here, the temperature difference between the rock wall and the hottest buffer point, the reference evolution, cf. Equation 3-12, is estimated using laboratory-scale data of MX-80 bentonite thermal conductivities combined with recordings from a well instrumented and dry deposition hole in the Prototype Repository at Äspö HRL. The following is concluded:

- Approximately 50% of the temperature difference is due to effects of still-open gaps between canister and buffer, cf. Figure 3-13.
- If the heat transport properties in the dry Prototype Repository hole #6, as found 50 days after test start with insignificant effects, if any, of wetting, drying and moisture redistribution, were representative of a dry KBS-3 deposition hole, then the reference evolution will over-predict the peak buffer temperature by 4°C, cf. Figure 3-14 (right).
- The margin suggested for the local solution would cover the following assumptions:
  - The canister-bentonite gap is and remains perfectly uniform from top to bottom around the canister periphery, giving maximal thermal insulation of the canister.
  - The emissivity of the copper surface remains for about 10 years at the value found for canister surface samples obtained from the canister laboratory.
  - The initial effective buffer conductivity at canister mid-height is as low as 0.85 W/(m·K).
  - Effects of spalling and unfortunate distribution of conductivity in the rock immediately surrounding the walls of the deposition hole.
  - Moisture redistribution in the deposition hole.
  - Variations in the vertical heat generation distribution.

All of the above assumptions appear to be conservative. The question whether the margin specified for the local solution in Table 6-3 (cf. also Figure 3-16) is sufficient is a matter of judgement. Compared to the results from the dry Prototype Repository hole#6, for instance, the margin is effectively 7°C as inferred from Figure 3-14 (right).

8.2 Rock wall temperature and peak buffer temperature

There are two independent methods of rock wall temperature calculation: An analytical and a numerical one. In both methods, the rock wall temperature depends on the layout, i.e. on the canister spacing and on the rock thermal properties, whereas the details of the conditions in the interior of the deposition holes are unimportant. Values of the peak buffer temperature are found in the same way regardless of the method used to find the rock wall temperature, i.e. by addition of the local canister/buffer solution. The following general conclusions are made:

- For identical layout and property assumptions, the two methods give results in a very good agreement, cf. Figure 5-14 and Figure 5-15.
- The analytical and numerical rock wall temperature solutions have been extensively tested and verified by comparison with results obtained from other independent codes. This (and the agreement between the two) means that both methods should count as verified.
- The analytical solution captures the thermal evolution of the repository on all scales in time and space. It can be used for fast and efficient investigations of the effects of distributing the deposition over time, of varying the deposition sequence and to explore the importance of the conditions around the edges of the repository or close to end/beginnings of deposition tunnels.
- The analytical solution cannot take the spatial variation of the rock thermal properties into account. To use the nomographic charts produced here by use of the analytical method for spacing decisions, a method to determine the effective conductivity in the low-conductive parts of the rock domain under consideration is required. While such methods have been developed and tried, they cannot provide more than reasonable approximations (cf. Appendix D).
- The numerical method takes the spatial variation and the spatial autocorrelation in both thermal conductivity and heat capacity, as described in rock domain thermal models, directly into account. It also simulates the heat flux redistribution caused by gap effects and temperature influences from the backfilled tunnel. In addition, it is possible to account directly for the temperature dependence in thermal properties. To decide if a given canister spacing will be sufficient, i.e. give peak buffer temperature below the threshold, heat generation simulations must be performed with numerous realisations of the thermal rock domain model.
- The most important and critical uncertainty is that of the local buffer/canister solution. The uncertainty margin associated with the local solution is about 3.5–4°C, depending on the rock heat transport properties (cf. Figure 3-16). Looking at the nomographic chart shown in Figure 4-18, this corresponds to a systematic and global underestimate of the rock thermal conductivity of 0.2 –0.3 W/(m·K).

8.3 Strategy – layout step D2

The strategy proposed here, i.e. to use a relevant nomographic chart and the rock domain conductivity distribution to find a trial value of the spacing, and then use the numerical method to target in on a safe minimum, has the following advantages.

- It minimizes the need for extensive numerical work. Each rock domain will require finite difference simulations with one or two spacing values. The nomographic chart used as point of departure can be produced within minutes.
- The uncertainties specifically associated with the analytical method (effects of ignoring the impact of the backfilled tunnel, cancelling out temperature dependencies of conductivity and capacity, ignoring extra heat flux redistribution caused by the open canister-bentonite gap) become unimportant.

It should be noted that there is no generally valid percentile of the conductivity distribution that automatically would correspond to the effective conductivity that controls the spacing, i.e. it is not possible to calibrate the process of selecting a trial value, for instance by use of the nomographic chart. The shape of the distribution, and in particular of the low conductivity part, will determine the effective dimensioning conductivity.

8.4 Optimization

The D2 strategy, as described here, sets the domain canister spacing at the same value in the entire domain such that the 100°C criterion will be met for a central canister with an initial power of 1,700 W deposited in completely dry, worst-case low-conductivity rock.

The majority of the canister positions will be deposited in volumes of rock that dissipates heat much better than the low-conductivity rock that controls the layout decisions. There are also many hundreds of positions near the tunnel ends that would get buffer temperatures lower than the threshold regardless of the local heat transport conditions. This means that there is significant room for layout optimizations. Note, however, that the canister spacing must not be smaller than 6 m.

For the Forsmark site, with high rock conductivities (and minimum spacing probably not much larger than 6 m), the simplest way to prepare for taking advantage of this would be to reduce the tunnel spacing, increase the dimensioning minimum canister spacing correspondingly (cf. Figure 4-19), and then modify that spacing as the construction progresses and detailed information on the local conditions is obtained.

For the Laxemar site, with low rock conductivities (and minimum canister spacing significantly larger than 6 m), it should be possible to modify the canister spacing without reducing the tunnel spacing.

There may be a possibility that the near-field design will be improved in the future, for instance by reducing the width of the canister-bentonite gap. It can easily be shown that this would reduce the dimensioning peak buffer temperature by about 5°C. If this appears to be likely, the simplest way to prepare taking advantage of it would be to reduce the tunnel spacing.

In addition to spacing modifications, there will be a possibility to control and plan the canister production, i.e. the power distribution, to take advantage of high conductivity positions, tunnel-end effects and near-field design improvements.

9 References

Ageskog L, Jansson P, 1999. Heat propagation in and around the deep repository. Thermal calculations applied to three hypothetical sites: Aberg, Beberg and Ceberg. SKB TR-99-02, Svensk Kärnbränslehantering AB.

Alvarez H, 1990. Energiteknik. Studentlitteratur, Lund.

Andersson C J, 2007. Äspö Hard Rock Laboratory. Äspö Pillar Stability Experiment, Final report. Rock mass response to coupled mechanical thermal loading. SKB TR-07-01, Svensk Kärnbränslehantering AB.

Back P-E, Sundberg J, 2007. Thermal Site Descriptive Model. A Strategy for the Model Development during Site Investigations. Version 2.0. SKB R-07-42, Svensk Kärnbränslehantering AB.

Back P-E, Wrafter J, Sundberg J, Rosén L, 2007. Thermal properties. Site descriptive modelling Forsmark – stage 2.2. SKB R-07-47, Svensk Kärnbränslehantering AB.

Bird R B, Stewart E-W, Lightfoot E, 2002. Transport Phenomena. John Wiley and sons, NY.

Blomberg T, 1996. Computer modelling of Building Physics applications. Department of Building Physics, Lund University. P.O. Box 118, S-221 00 Lund, Sweden. Report TVBH-1008. ISRN LUTVDG/TVBH–96/1008–SE/1-188. ISBN 91-88722-05-8.

Brantberger M, Zetterqvist A, Arnbjerg-Nielsen T, Olsson T, Outters N, Syrjänen P, 2006. Final repository for spent nuclear fuel. Underground design Forsmark, Layout D1. SKB R-06-34, Svensk kärnbränslehantering AB.

Börgesson L, Fredriksson A, Johannesson L-E, 1994. Heat conductivity of buffer materials. SKB TR-94-29, Svensk Kärnbränslehantering AB.

Carslaw H S, Jaeger J C, 1959. Conduction of Heat in Solids, 2nd ed. Oxford University Press.

Cheremisinoff N P, 1986. Fundamentals of Momentum and Heat Transfer. In: Handbook of Heat and Mass Transfer, Vol 1: Heat Transfer Options. Gulf Publishing Company, Houston, Texas.

Claesson J, Probert T, 1996. Temperature field due to time-dependent heat sources in a large rectangular grid. Derivation of analytical solution. SKB TR-96-12, Svensk Kärnbränslehantering AB.

CRC, 1973. Handbook of Chemistry and Physics. The Chemical Rubber CO, Cleveland, Ohio.

Eftring B, 1990. Numerisk beräkning av temperaturförlopp. Ett fysikaliskt betraktelsesätt. (Numerical Calculation of Thermal Processes. A Physical Approach, in Swedish). Ph.D. thesis, Dept. of Building Science, Lund University.

Fälth B, Hökmark H, 2006. Mechanical and thermo-mechanical discrete fracture near-field analyses based on preliminary data from the Forsmark, Simpevarp and Laxemar sites. SKB R-06-89, Svensk Kärnbränslehantering AB.

Goudarzi R, Johannesson L-E, 2003. Äspö Hard Rock Laboratory. Prototype Repository. Sensors data report (Period 010917–030901) Report No:7. SKB IPR-03-46, Svensk Kärnbränslehantering AB.

Goudarzi R, Johannesson L-E, 2006. Äspö Hard Rock Laboratory. Prototype Repository. Sensors data report (Period 010917–051201) Report No:14. SKB IPR-06-08, Svensk Kärnbränslehantering AB.

Hartley L, Hoch A, Jackson P, Joyce S, McCharty R, Rodwell W, Swift B, Marsic N, 2006. Groundwater flow and transport modelling during the temperate period for the SR-Can assessment. Forsmark area – version 1.2. SKB R-06-98, Svensk Kärnbränslehantering AB.

Håkansson R, 2000. Beräkning av nuklidinnehåll, resteffekt, aktivitet samt doshastighet för utbränt kärnbränsle. SKB R-99-74, Svensk Kärnbränslehantering AB.

Hökmark H, Fälth B, 2003. Thermal dimensioning of the deep repository. SKB TR-03-09, Svensk Kärnbränslehantering AB.

Hökmark H, Claesson J, 2005. Use of an analytical solution for calculating temperatures in repository host rock. Engineering Geology (81), pp. 353–364.

Kristensson O, Hökmark H, 2007a. Prototype Repository. Thermal 3D modelling of Prototype Repository. SKB IPR-07-01, Svensk Kärnbränslehantering AB.

Kristensson O, Hökmark H, 2007b. Prototype Repository. THM modelling of the bentonite buffer. Canister mid-height 1-D radial models, holes #1 and #3. SKB IPR-07-22, Svensk Kärnbränslehantering AB.

SKB, 1999. Deep repository for spent nuclear fuel. SR-97 – Post closure safety. Main Report Volume 1. SKB TR-99-06, Svensk Kärnbränslehantering AB.

SKB, 2006. Long-term safety for KBS-3 repositories at Forsmark and Laxemar – a first evaluation. Main Report of the SR-Can project. SKB-TR-06-09, Svensk Kärnbränslehantering AB.

SKB, 2009. Design premises for a KBS-3V repository based on results from the safety assessment SR-Can and some subsequent analyses. SKB TR-09-22, Svensk Kärnbränslehantering AB.

SKB, 2010a. Design, production and initial state of the buffer for the safety assessment SR-Site. SKB TR-10-15, Svensk Kärnbränslehantering AB.

SKB, 2010b. Design, production and initial state of the canister for the safety assessment SR-Site. SKB-TR-10-14, Svensk Kärnbränslehantering AB.

SKB, 2010c. Spent nuclear fuel for disposal in the KBS-3 repository. SKB TR-10-13, Svensk Kärnbränslehantering AB.

SKB, 2010d. Design, construction and initial state of the underground openings for the safety assessment SR-Site. SKB-TR-10-18, Svensk Kärnbränslehantering AB.

Sugita Y, Chijimatsu M, Suzuki H, 2003. Fundamental properties of bentonite pellets for Prototype Repository Project. In: Alonso and Ledesma (Eds.): Advances in understanding engineered clay barriers. Proceedings of the international symposium on large scale field test in granite. Sitges, Barcelona Spain, 12th–14th November, 2003. Balkema Publishers.

Sundberg J, 1988. Thermal Properties of Soils and Rocks. Publ. A 57, Dissertation. Geologiska institutionen, Chalmers University of Technology, and University of Göteborg.

Sundberg J, Kukkonen I, 2003. Comparison of thermal properties measured by different methods. SKB R-03-18, Svensk Kärnbränslehantering AB.

Sundberg J, Hellström G, 2009. Inverse modelling of thermal conductivity from temperature measurements at the prototype repository, Äspö HRL. International Journal of Rock Mechanics and Mining Sciences, Vol. 46, Issue 6, pp. 1029–1041.

Sundberg J, Wrafter J, Ländell M, Back P E, Rosén L, 2008a. Thermal properties Forsmark Modelling stage 2.3: Complementary analysis and verification of the thermal bedrock model, stage 2.3. SKB R-08-65, Svensk Kärnbränslehantering AB.

Sundberg J, Wrafter J, Back P-E, Rosén L, 2008b. Thermal properties Laxemar. Site descriptive modelling SDM Site Laxemar. SKB R-08-61, Svensk Kärnbränslehantering AB.

Thunvik R, Braester C, 1991. Heat propagation from a radioactive waste repository. SKB TR-91-61, Svensk Kärnbränslehantering AB.

Walsh J B, Decker E R, 1966. Effect of Pressure and Saturating Fluid on the Thermal Conductivity of Compact Rock. J. Geophys. Res., Vol. 71, No. 12, pp. 3053–3061.

Appendix A

Code_Bright one-canister models

A1 Introduction

In the KBS-3 concept, the safety criterion on temperatures states that the maximum bentonite temperature must not exceed 100°C anywhere in the repository. The main text of this report relates to finding a strategy to thermally design the repository such that the temperature criterion is always met.

The maximum bentonite temperature in a particular hole is determined by first calculating the rock wall temperature at canister mid-height, $T_{wall}(t)$, with due account of the deposition geometry (tunnel spacing and canister spacing) and the domain specific thermal model (initial temperature, distribution and spatial variability of thermal properties), see main text. Secondly, the total temperature difference $\Delta T_{tot}(t)$ between the rock wall at canister mid-height and the bentonite at the canister top is added to the rock wall temperature. ΔT_{tot} (Equation A-1) is a quantity for which a reference evolution has been established (see main text):

$$\Delta T_{tot}(t) = \Delta T_1(t) + \Delta T_2(t) = 0.02213 \cdot Q(t) \qquad \text{A-1}$$

Here, $Q(t)$ is the canister power, $\Delta T_1(t)$ the temperature drop across the buffer and $\Delta T_2(t)$ the additional effect of open (air-filled) gaps.

The purpose of this study is to investigate the influence on the rock wall temperature and on ΔT_{tot} of different assumptions regarding buffer properties, heat load distribution within the canister etc, in order to get perspectives on uncertainties in the reference evolution. The following is considered:

- Distribution of power along the fuel rods.
- Representation of the canister interior.
- The rock thermal conductivity.
- The thermal properties of the gap between the canister surface and the surrounding bentonite blocks.
- The thermal properties of the buffer.
- The thermal properties of the tunnel backfill.

All results are based on 2-D axisymmetric Code_Bright analyses of one individual canister. Code_Bright /CIMNE 2004/ is a Finite Element program specifically developed to analyse coupled THM processes in saturated and unsaturated porous media. Temperature contributions from canisters other than the local, i.e. explicitly modelled one, are ignored. For the purpose of this investigation, i.e. comparing temperatures at different points within the interior of a deposition hole, this is adequate. The net heat flux disturbances from the neighbouring canisters are small in the direction normal to the tunnel and cancel out in the tunnel direction, cf. Section A3.1.1.

In the present study, only the thermal logic of the program is used, thereby ignoring effects of the mechanical and hydraulic evolution. Effects of changes in the hydraulic conditions are evaluated from results obtained from coupled TH analyses reported by /Åkesson et al. 2010/, cf. Section A3.6.3.

A2 Model description

The geometry of the model at three different scales is shown in Figure A-1. The model is 2D-axisymmetric, with its symmetry axis on the vertical centre axis of the deposition hole.

The reference design of deposition holes includes a cut off wedge at the side of the deposition hole /SKB 2010d/. In the current modelling work, the wedge is represented as a hollow cone with the correct depth but with its radius adjusted such that the volume matches that of the reference design.

The outer dimensions of the copper canister are given by /SKB 2010b/ assuming that the minimum copper thickness is 50 mm everywhere.

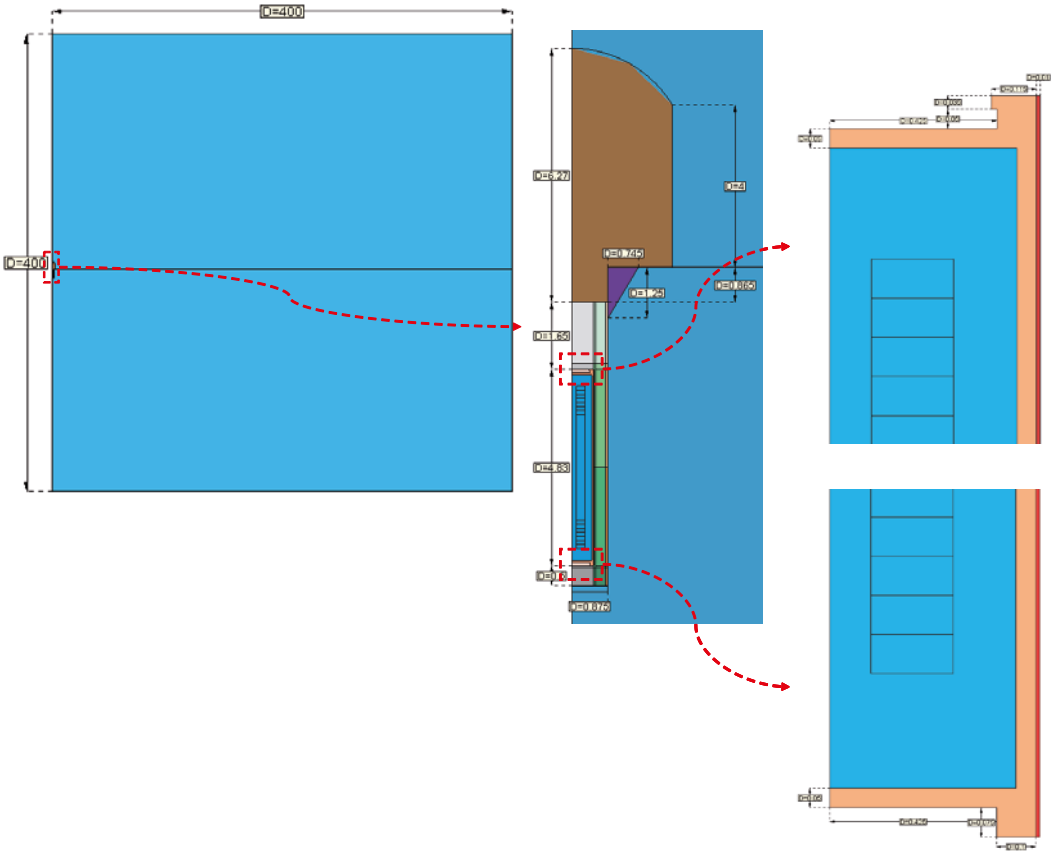

Figure A-1. *Model geometry at three scales. Dimensions are in metres.*

A cross-sectional view of the cast iron inserts containing the nuclear waste from BWR reactors is shown in Figure A-2 (left). In the models, the heat sources are represented as two 4 m long concentric cylinders with radii of 0.105 m and 0.315 m, respectively. The power is imposed uniformly along the circumference of each cylinder with 1/3 of the total power on the inner cylinder and 2/3 on the outer cylinder, representing 4 and 8 fuel elements, respectively. The vertical lines where the power is imposed within the cast iron insert are shown alongside the vertical power distribution in Figure A-3 (right).

In the models, the initial canister power, P(0), is 1,700 W. The relative burn-up is greater near the centre of the fuel rods, cf. Figure A-3 (left). It can be shown that the burn-up scales with the canister power /Håkansson 2000/. The initial power distribution along the fuel rods is presented in Figure A-3 (right).

Linear heat conduction has been used in the model. The boundary conditions are adiabatic at all model boundaries and the initial temperature is 10°C in the whole model.

The canister power decay can be expressed as:

$$P(t) = P(0)\sum_{i=1}^{7} a_i \exp(-t/t_i) \qquad \text{A-2}$$

The decay function coefficients, shown in Figure A-4, are obtained by fitting the exponential expression to power data, see main text. In the graph, the adopted piecewise linear function used as input to the model is indicated. The simulations have been run up to 20 years after deposition of the canister.

The material positions and their base case properties (density, specific heat, thermal conductivity and porosity) are presented in Figure A-5 and Table A-1, respectively. The geometry of the bentonite blocks, the pellet slot and the air-filled gap between the copper surface and the blocks is based on /SKB 2010a/, whereas the geometry of the deposition hole and the bottom plate is based on /SKB 2010d/.

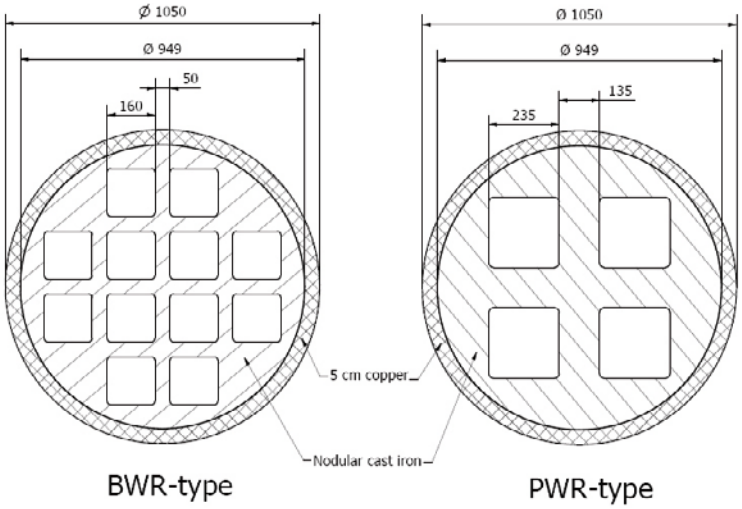

Figure A-2. *Cross-sectional view of cast-iron inserts for Boiling Water Reactors (left) and Pressurized Water Reactors (right). From /SKB 2010b/.*

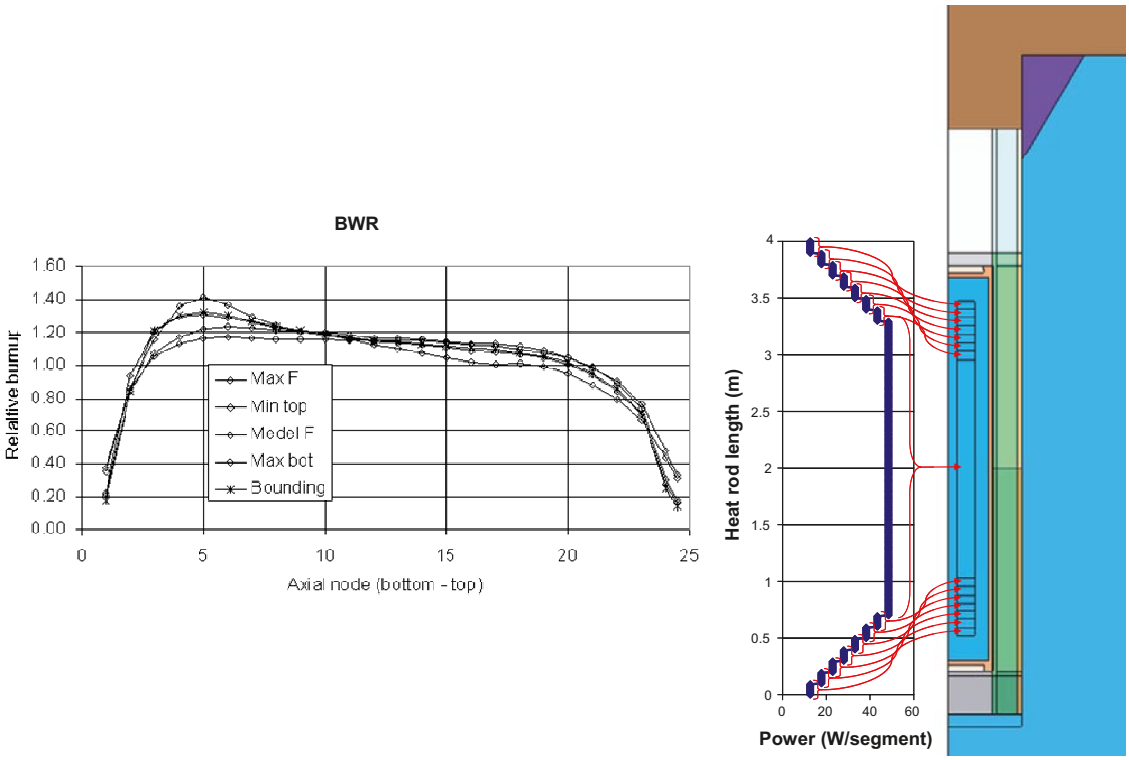

Figure A-3. *Left: Relative burn-up (for BWR-type fuel) along fuel rods. From P Grahn, SKB, e-mail communication 2010, cf. "Criticality calculations of disposal canisters" SKBdoc 1193244. Right: Modelled power distribution along fuel rods.*

i	t_i (years)	a_i
1	20	0.060
2	50	0.705
3	200	–0.055
4	500	0.250
5	2,000	0.025
6	5,000	–0.009
7	20,000	0.024

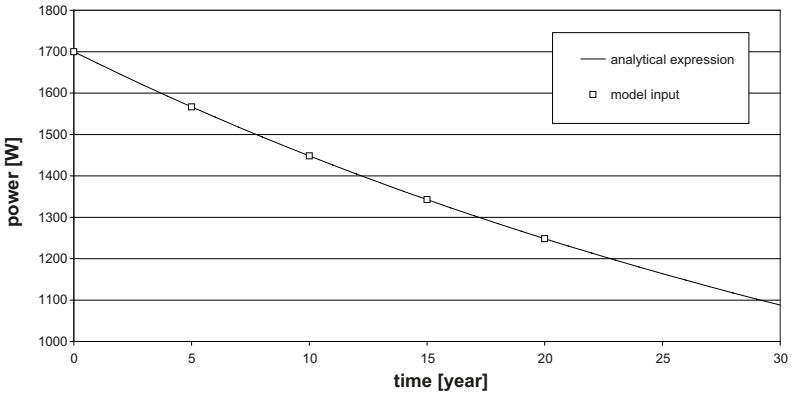

Figure A-4. *Decay function coefficients and the corresponding canister power graph.*

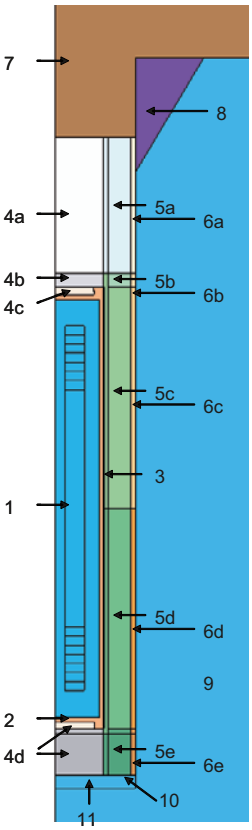

No	Material
1	Cast iron
2	Copper
3	Annular gap
4a-d	Bentonite, central parts
5a-e	Bentonite, peripheral parts
6a-e	Pellets in outer slot
7	Backfill
8	Wedge (Reference)
9	Rock
10	Copper plate
11	Concrete pedestal

Figure A-5. *Material positions.*

Table A-1. Base case material properties.

Material	Density (kg/m³)	Heat capacity (J/(kg·K))	Th. conductivity (W/(m·K))	Porosity (–)
1 Cast iron[1)]	7,200	500	25	0
2 Copper	8,930	390	390	0
3 Annular gap	1.3	1,000	0.04	0
4a-d Bentonite, central parts	2,780	800	1.1	0.355
5a-e Bentonite, peripheral parts	2,780	800	1.0	0.355
6a-e Pellets in outer slot	2,780	800	1.0	0.602
7 Backfill	2,500	780	0.7	0.5
8 Wedge	2,780	800	0.3	0
9 Rock	2,770	770	2.5	0
10 Copper plate[2)]	8,930	390	390	0
11 Concrete pedestal[3)]	2,770	770	2.5	0

1) The thermal conductivity is reduced to compensate for the cavities in the material.

2) Same properties as the copper canister.

3) The same material as the surrounding rock mass is used to model the concrete.

A model map with a description of all cases studied is given in Table A-2. In the deposition hole, heat transport is quasi stationary after a few days /Hökmark and Fälth 2003/. This means that values given for density, specific heat and porosity (other than those of the rock) are unimportant to the problem of the peak buffer temperature.

Table A-2. Model map. Description of conditions differing from those in Figure A-5 and Table A-1.

Model Code	Description
Case 1a	Properties according to Table A-1. Two versions: Base case (with copper plate beneath bentonite buffer). Alternative version (without copper plate, cf. Section A3.2.3).
Case 1b	λ_{Rock} = 2.0 W/(m·K).
Case 1c	λ_{Rock} = 3.0 W/(m·K).
Case 2a	Alternative buffer properties, cf. Table A-6.
Case 2b	Alternative buffer properties, cf. Table A-6.
Case 2c	Alternative buffer properties, cf. Table A-6; λ_{Rock} = 3.0 W/(m·K).
Case 3	Buffer properties corresponding to redistribution of moisture, cf. Table A-7.
Case 4	Buffer properties corresponding to redistribution of moisture, cf. Table A-7.
Case 5	Volumes of rock with reduced thermal conductivity around deposition hole, cf. Section A3.4.
Case 6a	Air-filled gap on top of canister, cf. Section A3.5.2.
Case 6b	Air-filled gap on top of canister and inner canister lid surface, cf. Section A3.5.2.
Case 7a	$\lambda_{Backfill}$ = 0.3 W/(m·K), cf. Section A3.6.1.
Case 7b	$\lambda_{Backfill}$ = 2.5 W/(m·K), cf. Section A3.6.1.
Case 8	Power distribution according to PWR-type fuel, cf. Section A3.3.2.
Case 9	Alternative canister design. Alternative buffer properties, cf. Figure A-10; λ_{Rock} = 3.0 W/(m·K).
Case 10a	No wedge. $\lambda_{Backfill}$ = 1.5 W/(m·K), $\lambda_{Cast\ iron}$ = 40 W/(m·K). Uniform power distribution, cf. Section A3.3.1.
Case 10b	No wedge. $\lambda_{Backfill}$ = 1.5 W/(m·K), $\lambda_{Cast\ iron}$ = 40 W/(m·K), cf. Section A3.3.1.
(Case 11)	Additional model with specific homogenized properties, cf. Section A3.2.1.

A3 Results

A3.1 General

A3.1.1 Flux contributions from other canisters

In the present report, all results are based on 2-D axisymmetric Code_Bright analyses of one individual canister. Temperature contributions from canisters other than the local, i.e. explicitly modelled one, are ignored. Assuming linear heat conduction, estimates of the error introduced by this simplification can be found by examining the distribution of horizontal heat flux from a single canister.

Figure A-6 shows the horizontal heat flux along a radial scan-line at canister mid-height together with estimates of the error in flux due to other canisters. The error in horizontal mid-height flux is calculated as the difference in flux contributions on either side of a canister at a given canister spacing, i.e. assuming an equal but opposite flux contribution from a canister on the other side. Here, only the nearest neighbours on either side are assumed to give a flux contribution. The contributions from all other canisters are assumed negligible. The redistribution of flux around deposition holes because of low-conductivity bentonite is also ignored.

The underestimate in canister flux decreases rapidly with the canister spacing. In this example (Case 2b), the heat flux at canister mid-height is underestimated by at most 1–2% (canister cc 6 m). In reality, the required canister spacing in rock with thermal conductivity as low as 2.5 W/(m·K) is considerably greater than 6 m, resulting in an underestimate of the mid-height flux of the order 0.5%.

A3.1.2 Temperature maxima

The maximum canister surface temperature, $T_{c\,max}$, occurs at canister mid-height and the minimum surface temperature on the edges, cf. Figure A-7. Assuming that there is a 10 mm air-filled annular gap between the canister and the buffer, the maximum bentonite surface temperature, $T_{b\,max}$, will occur at the centre of the canister top where the bentonite is in direct contact with the canister surface.

The expression, $T_{b\,max} = \Delta T_{tot} + T_r$, can be used to find the maximum bentonite temperature, cf. main text. Here, ΔT_{tot} is the total temperature difference between the bentonite temperature at the top of the canister and the rock wall temperature at canister mid-height. T_r is the rock wall temperature at canister mid-height.

In all models the initial temperature, T_i, is fixed at 10°C.

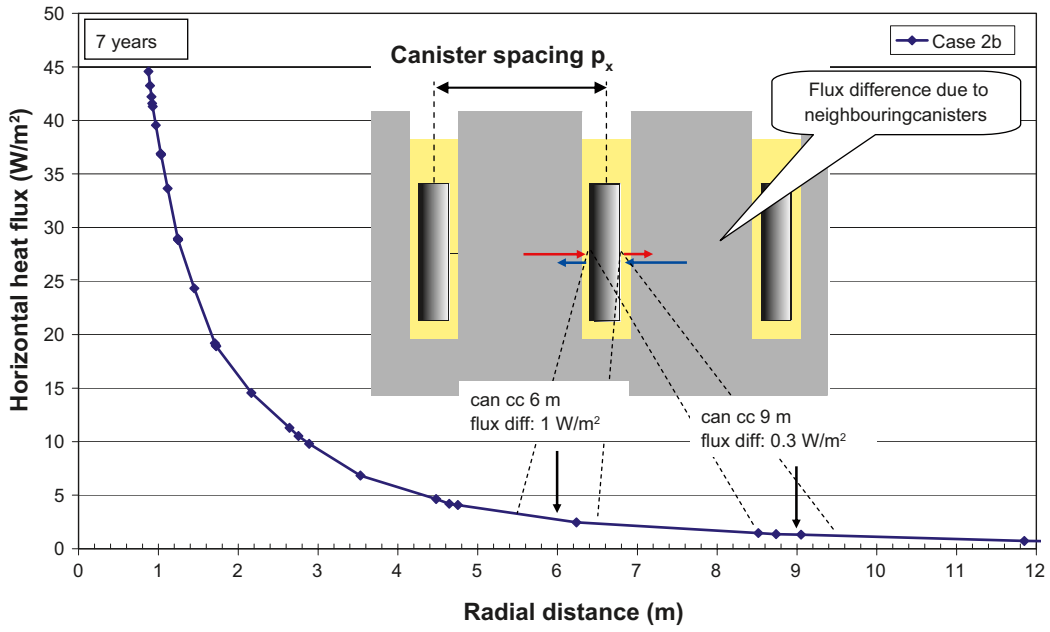

Figure A-6. *Horizontal heat flux after 7 years as a function of radial distance from the canister. The flux contribution to the surface heat flux from other canisters at a given canister spacing is calculated as the difference in flux contributions on either side of a canister at a given canister spacing, i.e. assuming there to be an equal but opposite flux contribution from a canister on the other side.*

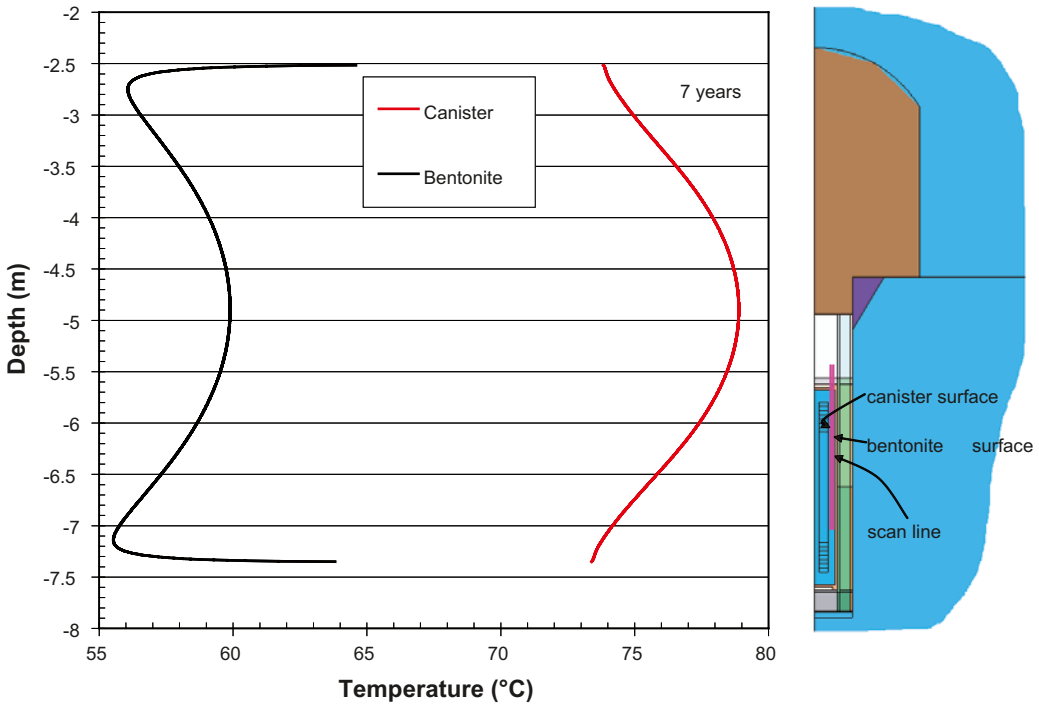

Figure A-7. *Canister and bentonite surface temperatures of Case 1a along a vertical scan-line after 7 years.*

A3.2 Influence of canister representation

A3.2.1 Homogenization

In previous modelling work, the canister has been assumed to be perfectly cylindrical and its power uniformly distributed along the fuel rods, see e.g. /Hökmark and Fälth 2003/. The present canister model is more detailed. In the current section, the more detailed model ('Reference model' Case 1a and 1b) is compared with a much simpler representation of the canister and the near-field geometry ('Homogenized' Case 11), cf. Figure A-8. The homogenized canister representation is used in the numerical work to obtain the dimensioning canister spacing at each site, cf. main text.

The following alterations have been made to the models (Reference → Homogenized):

- Canister: 4.835 m → 4.8 m.
- Fuel rods: 4.0 m → 4.4 m.
- Heat load: BWR-type distribution (Figure A-3, right) → Uniform.
- Canister thermal conductivity (Cu/Cast iron): 390/25 W/(m·K) → 30/30 W/(m·K).
- Deposition hole geometry: Wedge removed from the side of the hole /SKB 2010d/ → Cylindrical hole.
- In the reference model, the canister has been moved up 16.75 cm to accommodate for a copper plate and concrete pedestal at the bottom of the deposition hole.

Figure A-9 (left) shows the rock wall temperature at canister mid-height for both canister models. The temperature difference between the homogenized model and the reference model is presented in Figure A-9 (right).

A3.2.2 Canister design

The effects of the flanges of the canister are investigated by use of an alternative cylindrical canister design (Case 9), cf. Figure A-10. The removal of the flanges results in a canister that is 16 cm shorter than the reference case. As seen in Figure A-11, removing the flanges increases both the rock wall temperature and the total temperature difference.

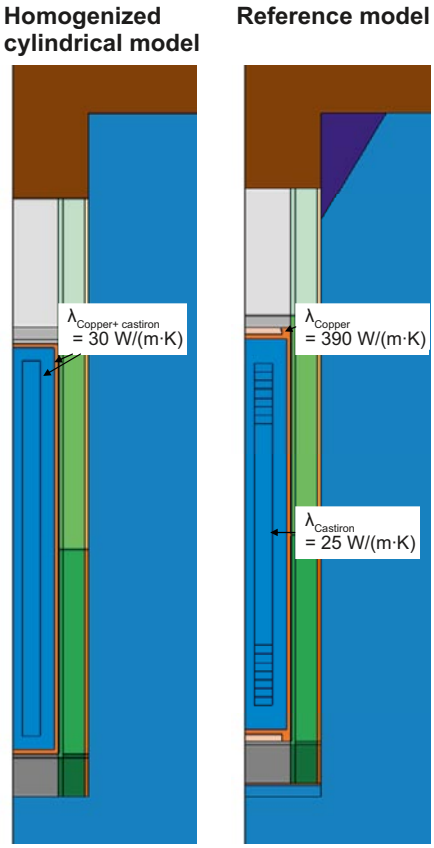

Material	λ (W/(m·K))	
Cast iron	25 (Reference)	30 (Homogenized)
Copper	390 (Reference)	30 (Homogenized)
Annular gap	0.04	
Bentonite, central parts	1.1	
Bentonite, peripheral parts	1.0	
Pellets in outer slot	1.0	
Backfill	0.7	
Wedge	0.3	
Rock	2.5 (Case 1a)	2.0 (Case 1b)

Figure A-8. *Left: Comparison between model geometries. Right: Summary of material properties.*

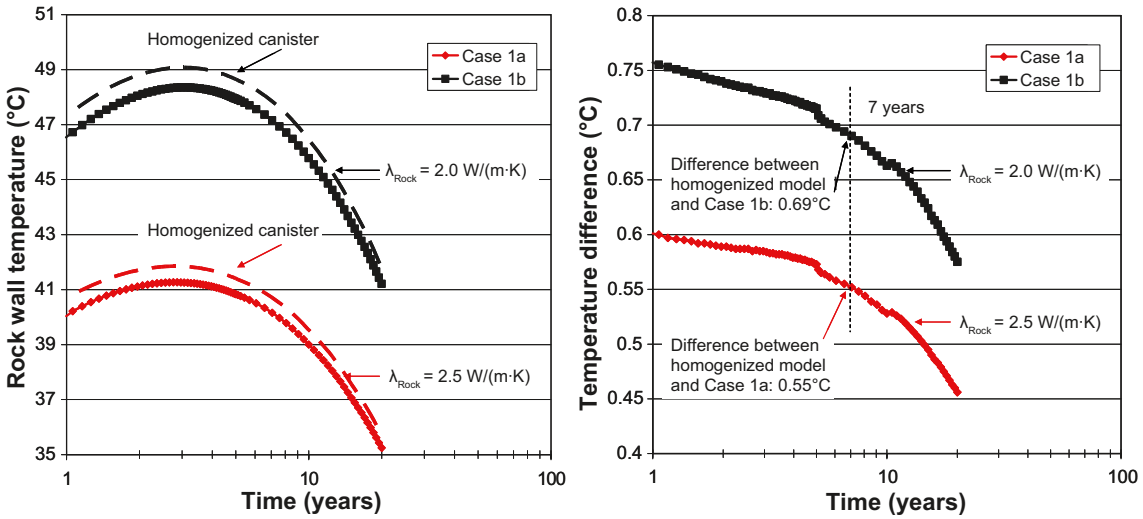

Figure A-9. *Left: Rock wall temperatures at canister mid-height. Dashed lines represent corresponding results from homogenized, cylindrical canister models. Right: Rock wall temperature difference at canister mid-height between homogenized canister model (Case 11) and Case 1a and 1b.*

Reference model Without flanges

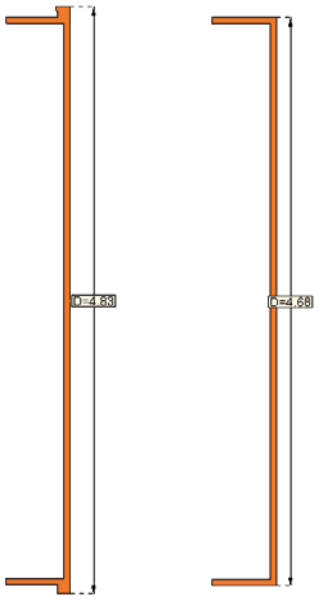

Material	λ (W/(m·K))
Annular gap	0.04
Bentonite, central parts	1.21
Bentonite, peripheral parts	1.21
Pellets in outer slot	0.26
Backfill	0.7
Wedge	0.3
Rock	3.0

Figure A-10. *Left: Comparison between model geometries. Right: Summary of material properties.*

A3.2.3 Influence of copper plate

Figure A-12 shows a comparison between the temperature distributions around the lower part of the deposition hole in Case 1a (left) and a corresponding version where the thin copper plate beneath the bentonite buffer is not included (i.e. the thermal conductivity is the same as the surrounding rock). As seen in the figure, the bentonite temperature beneath the canister is increased by about 0.2°C after 10 years when the copper plate is not included. The peak buffer temperature at the top of the canister and the rock wall temperature at canister mid-height are not affected by the presence of a thin copper plate.

A3.3 Power distribution along fuel rods

A3.3.1 Uniform power distribution

In previous modelling work, the canister's power has been assumed to be uniformly distributed along the fuel rods, see e.g. /Hökmark and Fälth 2003/. In reality, the relative burn-up is higher in the central parts of the fuel rods, cf. Figure A-3 (left).

In this section, the influence of the wedge in the deposition hole is not considered, i.e. the material is the same as the surrounding rock. Variations in the thermal conductivity of the backfill material in the tunnel, which has a considerably larger volume than the wedge, have only a marginal influence on the near-field temperatures, cf. Section A3.6.1. Therefore, it can be concluded that the wedge has very little influence on the temperatures in the canister's near-field. Here, no compensation is made for the cavities in the cast iron insert, i.e. the thermal conductivity is set to that of the solid material (40 W/(m·K)). The thermal conductivity of the backfill material in the tunnel is set to 1.5 W/(m·K).

Figure A-13 shows a comparison between the horizontal heat flux along the canister surface for either a BWR fuel-type distribution of canister power (cf. Figure A-3, right) or uniformly distributed canister power.

Figure A-14 shows the rock wall temperature at canister mid-height (top) together with the total temperature difference between the bentonite at the top of the canister and the rock wall temperature (bottom). As seen in the figure, the increase in horizontal mid-height flux results in slightly elevated rock wall temperatures. This is, however, compensated by a lower total temperature difference.

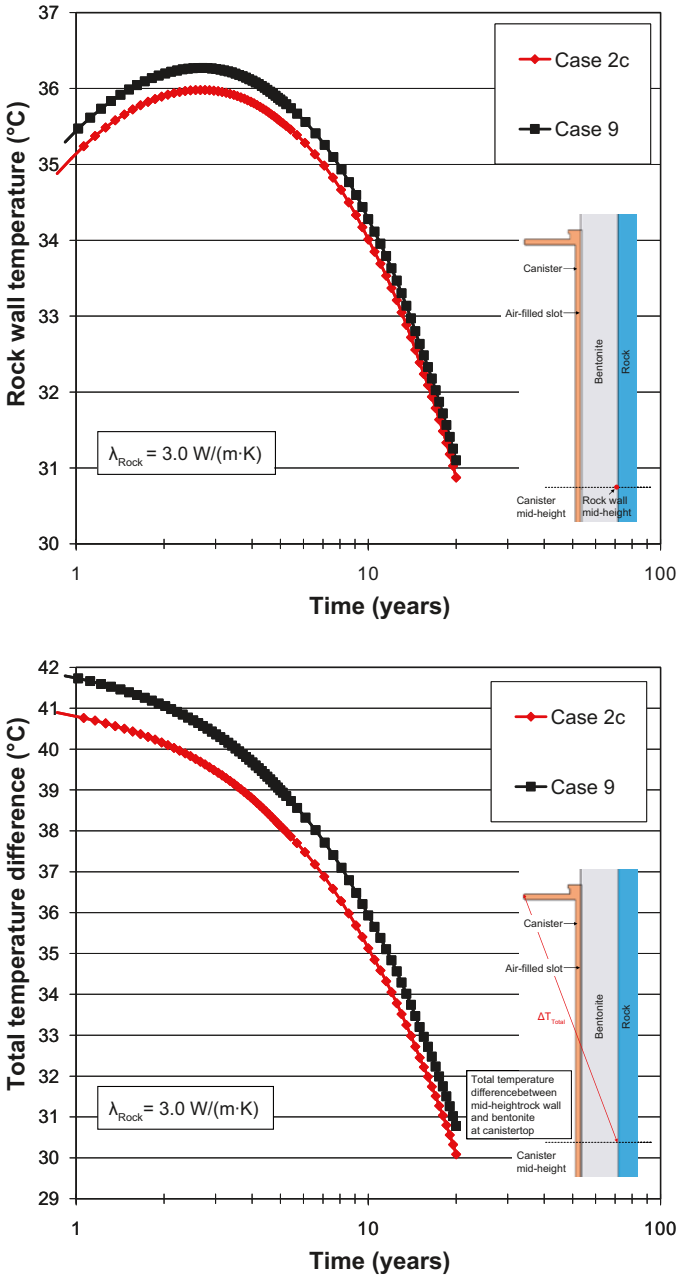

Figure A-11. *Top: Rock wall temperature at canister mid-height. Bottom: Total temperature difference between mid-height rock and bentonite at the canister top (ΔT_{tot}).*

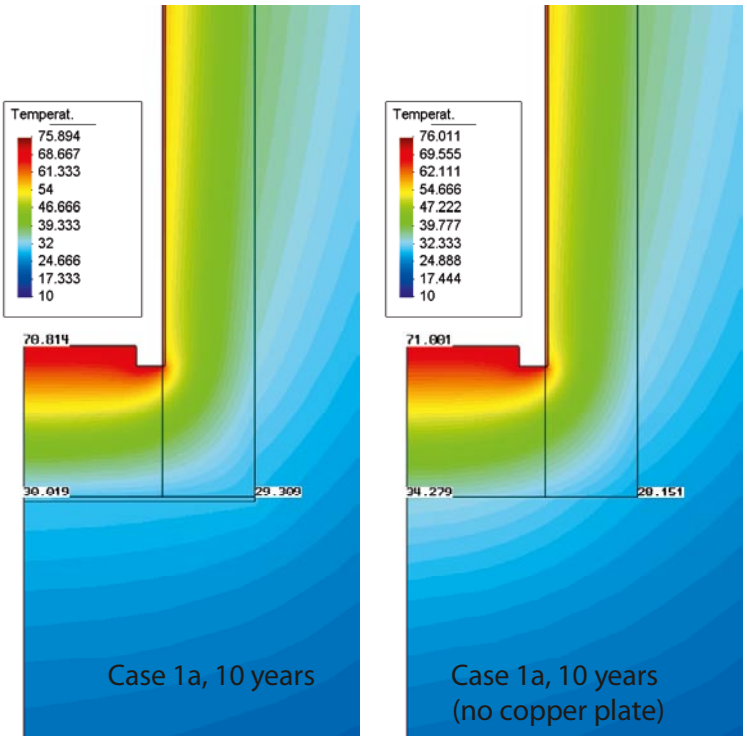

Figure A-12. *Temperature distribution after 10 years for Case 1a around the lower part of the deposition hole (left) compared with a corresponding case where the copper plate is not included (right).*

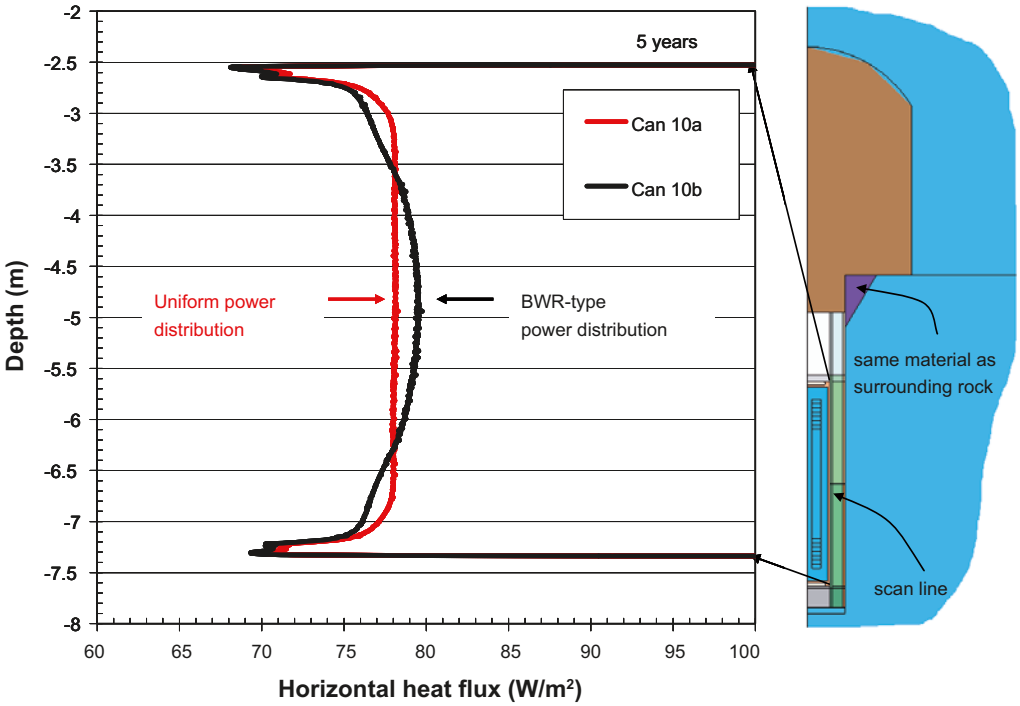

Figure A-13. *Horizontal heat flux profile after 5 years for vertical power distributions corresponding to BWR-type fuel and homogeneously distributed power along the fuel rods.*

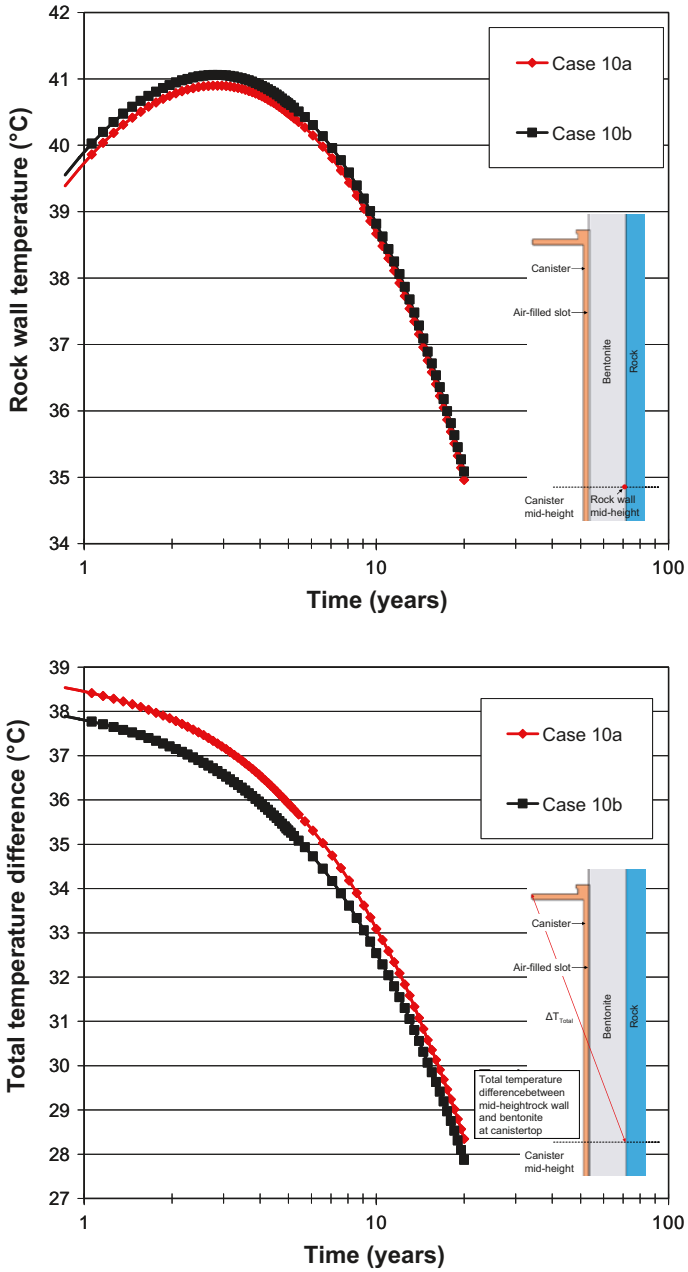

Figure A-14. *Top: Rock wall temperature at canister mid-height. Bottom: Total temperature difference between mid-height rock and bentonite at the canister top (ΔT_{tot}).*

A3.3.2 Fuel types

The majority of the fuel used in Swedish nuclear power plants is BWR-type /SKB 2010c/. The remaining part is mainly of PWR-type. Figure A-15 (right) shows the initial power distribution along the fuel rods for the two types of fuel.

Figure A-16 shows the horizontal heat flux profile after 5 years for the two types of nuclear fuel.

Figure A-17 (top) shows the rock wall temperature at canister mid-height. The corresponding total temperature difference between the bentonite at the top of the canister and the rock wall at canister mid-height is presented in Figure A-17 (bottom).

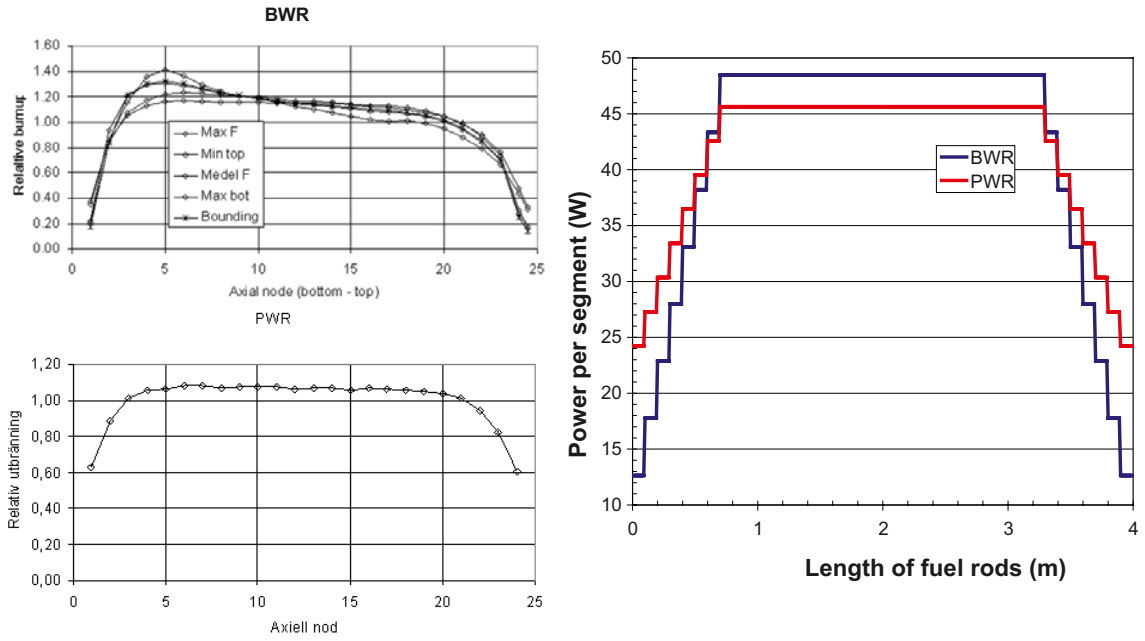

Figure A-15. *Left: Relative burn-up distributions for BWR and PWR-type nuclear fuel, from P Grahn, SKB, e-mail communication 2010. cf. "Criticality calculations of disposal canisters" SKBdoc 1193244. Right: Approximate initial power distributions along fuel rods.*

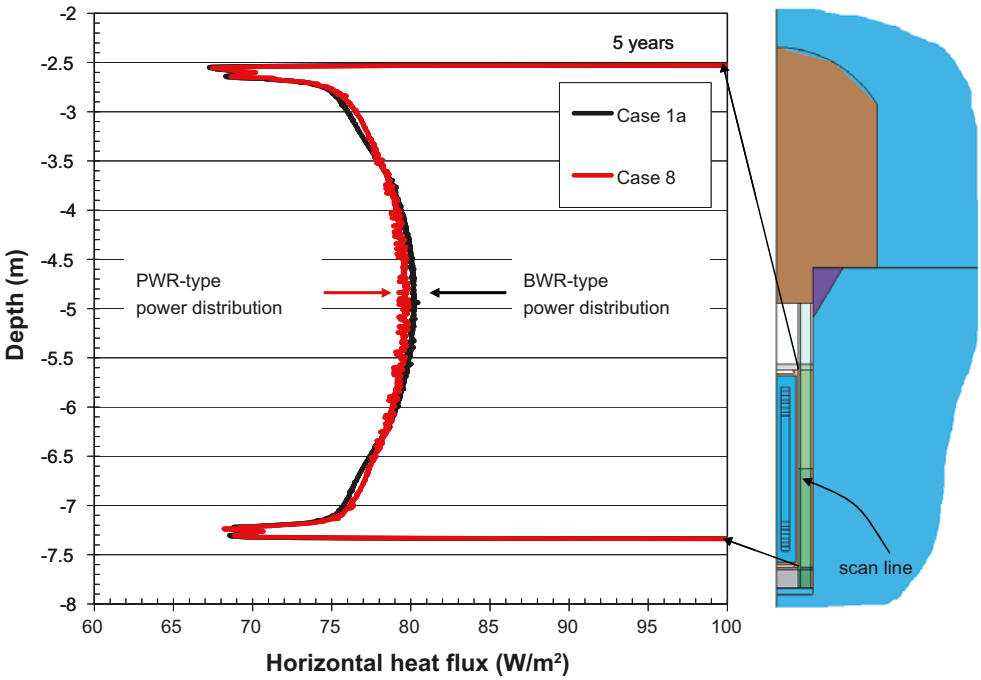

Figure A-16. *Horizontal heat flux profile after 5 years for vertical power distributions corresponding to BWR and PWR-type fuel.*

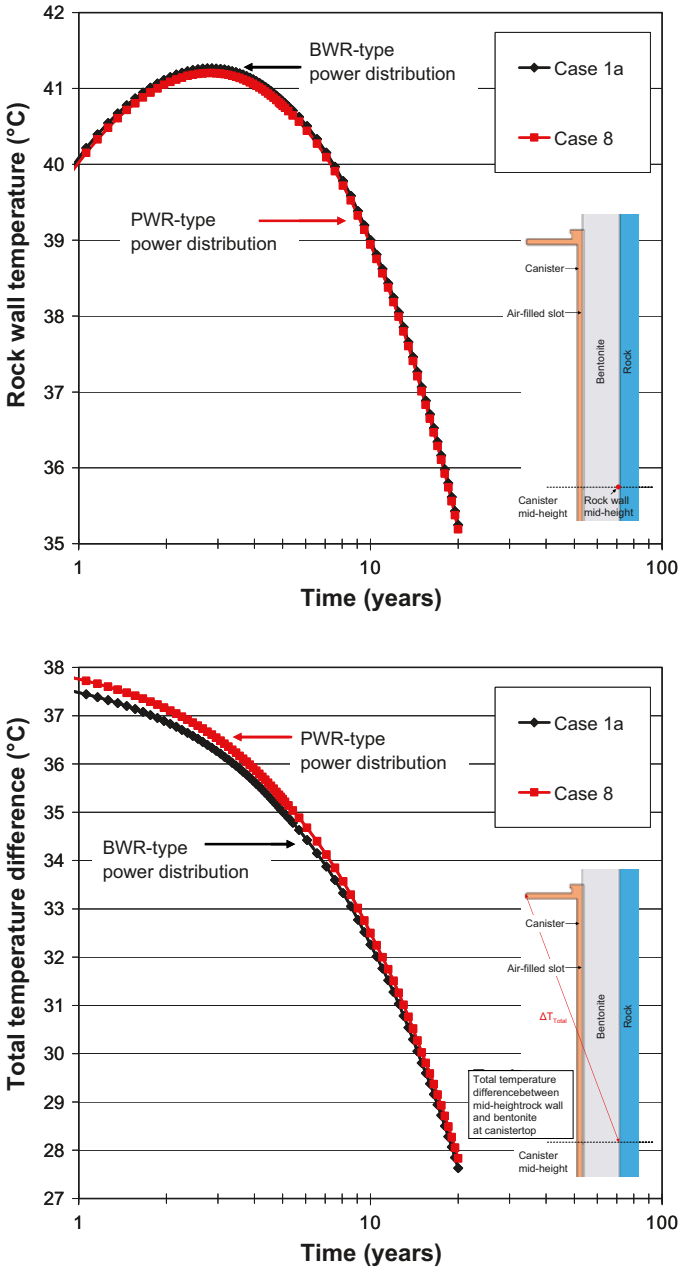

Figure A-17. *Top: Rock wall temperature at canister mid-height. Bottom: Total temperature difference between mid-height rock and bentonite at the canister top (ΔT_{tot}).*

A3.4 Variations in rock thermal conductivity

The thermal properties of the rock at the proposed repository sites are not homogeneously distributed within the rock mass /Back et al. 2007, Sundberg et al. 2008a, b/. Figure A-18 (right) shows examples of geometries with either homogeneous rock heat conduction (Case 1a and 1b) or volumes of low heat conduction surrounding the deposition hole (Case 5).

Figure A-18 (top left) shows the rock wall temperature at canister mid-height. The corresponding total temperature difference between the bentonite at the top of the canister and the rock wall at canister mid-height is presented in Figure A-18 (bottom left).

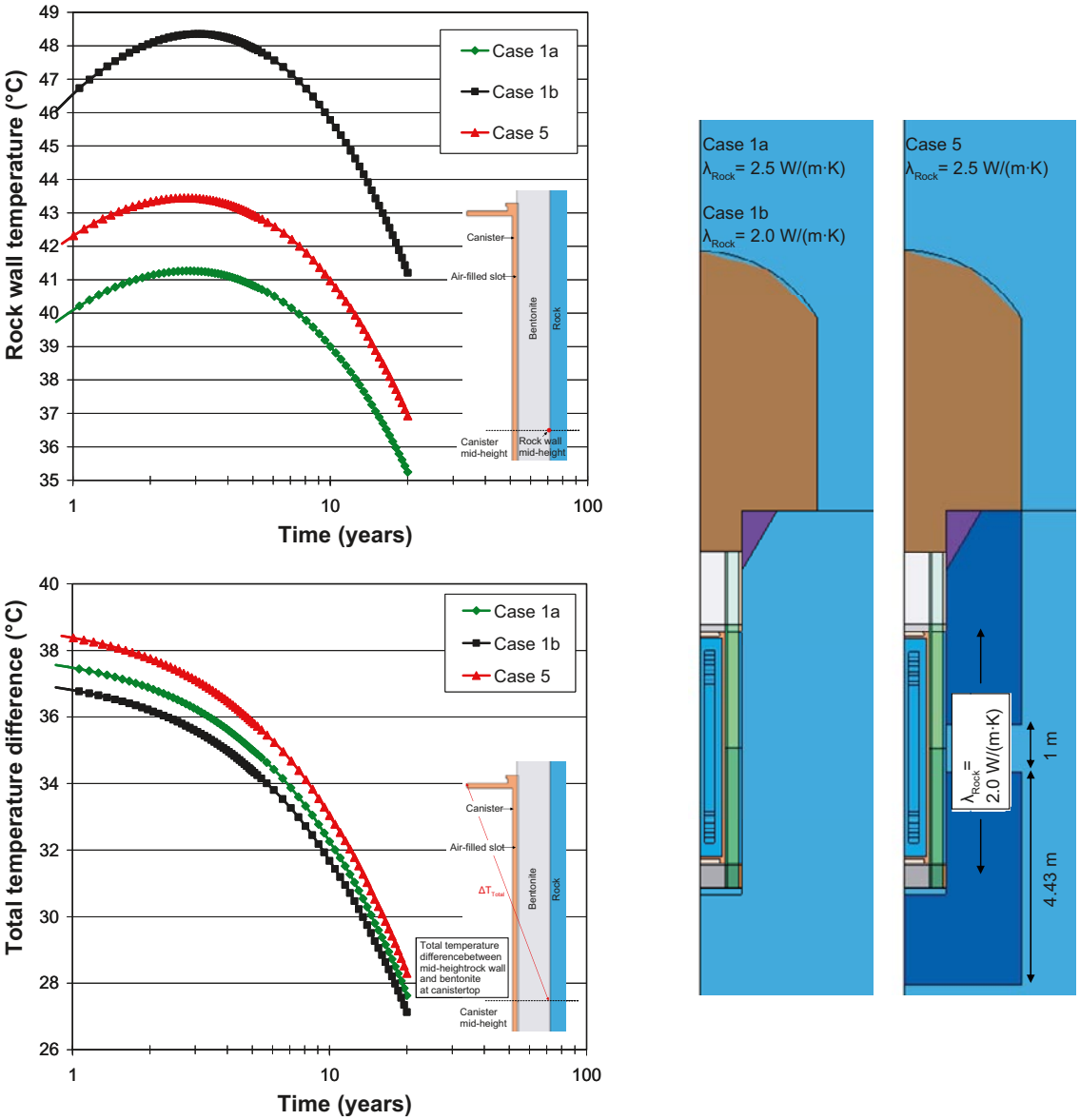

Figure A-18. *Top: Rock wall temperature at canister mid-height. Bottom: Total temperature difference between mid-height rock and bentonite at the canister top (ΔT_{tot}).*

A3.5 Variations in effective gap conductivity

A3.5.1 Annular gap around canister

The analytical expression for the temperature drop across the buffer, ΔT_1, is evaluated using the mean heat flux at canister mid-height. It is therefore of interest to evaluate how the flux, q, is affected by altering the gap conditions.

In addition to the base case effective gap conductivity, λ_{Gap} = 0.04 W/(m·K), two alternative assumptions regarding gap properties have also been tested in order to investigate the sensitivity to this parameter: λ_{Gap} = 0.06 W/(m·K) or no gap. In the model with no gap, the gap material is the same as the surrounding bentonite rings.

The influence of the gap material properties is studied for three different values of the rock conductivity: λ_{Rock} = 2.0, 2.5 and 3.0 W/(m·K). The material properties used in this investigation are presented in Table A-3.

Table A-3. Summary of rock and gap thermal conductivities used in the study.

Model code	Rock thermal conductivity (W/(m·K))	Gap thermal conductivity (W/(m·K))
Case 1a	2.5	0.04
		0.06
		no gap, *i.e.* 1.0 (same as bentonite)
Case 1b	2.0	0.04
		0.06
		no gap, *i.e.* 1.0 (same as bentonite)
Case 1c	3.0	0.04
		0.06
		no gap, *i.e.* 1.0 (same as bentonite)

Figure A-19 shows the total temperature difference between the bentonite on top of the canister and the rock wall temperature at canister mid-height for all nine cases in Table A-3. Figure A-20 shows the corresponding profile of the horizontal canister heat fluxes after 5 years.

The mid-height canister flux, q, is usually estimated from the mean value heat flux, i.e. ratio of the total canister power, Q, and the total canister surface area, A, multiplied with a reduction factor, ϕ, such that $\phi = q/(Q/A)$. The reduction factor ϕ, in each of the cases considered in this study, is presented in Table A-4.

A3.5.2 Gaps around flanges

In addition to the 10 mm annular gap between the canister surface and inner bentonite surface, two models with an increasing level of insulation around the copper lid have been analysed, cf. Figure A-21.

Figure A-22 shows the resulting temperatures after 7 years around the top of the canister for the three cases with either no gap (left), an open 10 mm gap above the flanges on top of the canister (middle) or an additional gap on the inner surface of canister's lid (right). In the models with gaps on or around the canister's flanges (Case 6a and 6b), there is some redistribution of the heat towards the centre of the lid – 1.9–2.2°C compared with the model where there is direct contact between the bentonite and canister surface. However, 85 mm into the bentonite at the centre of the canister, the difference between the models is only about 0.2–0.6°C.

Figure A-23 (top) shows the rock wall at canister mid-height for the three assumptions regarding gap geometry. The corresponding total temperature difference between the bentonite at the top of the canister and the rock wall at canister mid-height is presented in Figure A-23 (bottom). Note that very specific requirements regarding the geometry of the insulating gaps are needed to achieve this increase in rock wall temperature and total temperature difference (ΔT_{Tot}) compared with the reference case (Case 1a). This and the fact that the difference in bentonite temperature a few centimetres above the centre of the lid is small (cf. Figure A-22) suggest that cases with air-filled gaps around the flanges need not be further investigated.

Table A-4. Ratio mid-height/average heat flux after 5 years (%). Values in brackets represent ratio 2 m above/below canister mid-height, respectively.

Model code	λ_{Rock} (W/(m·K))	λ_{Gap} = 0.04 W/(m·K)	λ_{Gap} = 0.06 W/(m·K)	no gap
Case 1a	2.5	89.4 (87.7/87.7)	91.6 (90.2/90.3)	95.0 (95.6/95.9)
Case 1b	2.0	88.2 (87.6/87.7)	90.2 (90.2/90.4)	93.1 (95.9/96.3)
Case 1c	3.0	90.3 (87.8/87.7)	92.6 (90.2/90.2)	96.5 (95.3/95.6)

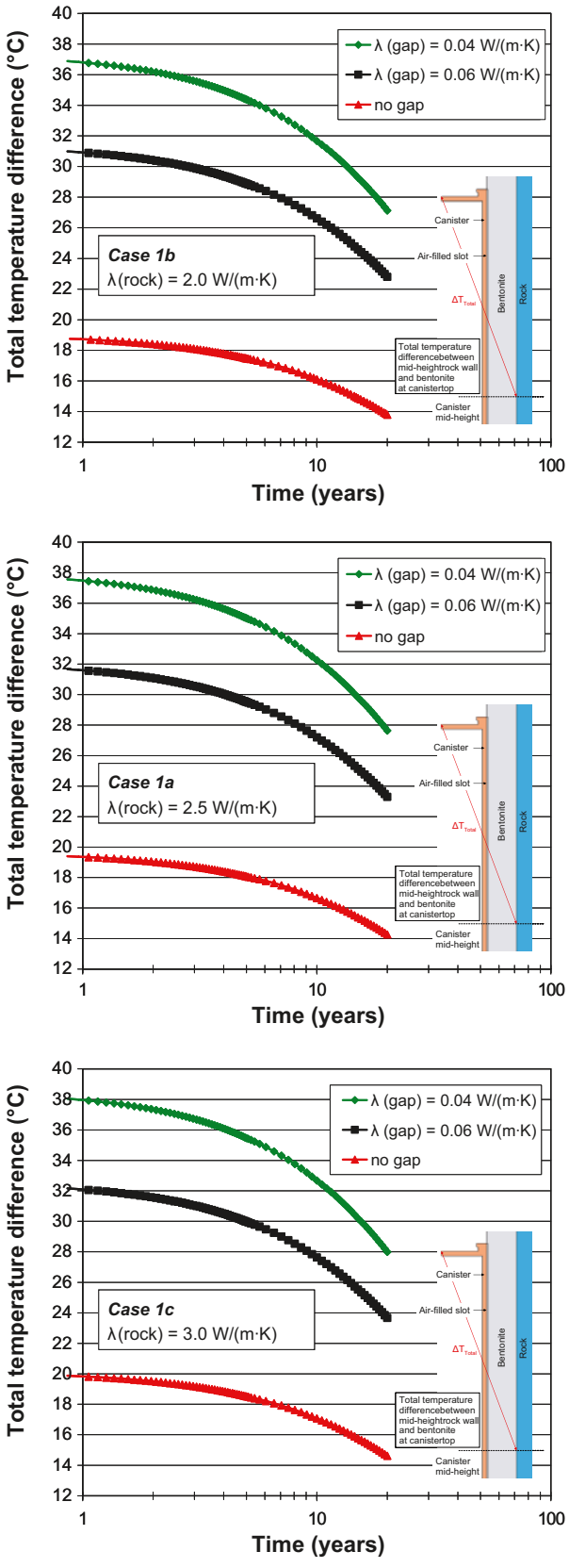

Figure A-19. *Temporal development of the total temperature difference (ΔT_{Tot}) over bentonite for a rock conductivity of 2.0 W/(m·K) (upper), 2.5 W/(m·K) (middle) and 3.0 W/(m·K) (lower).*

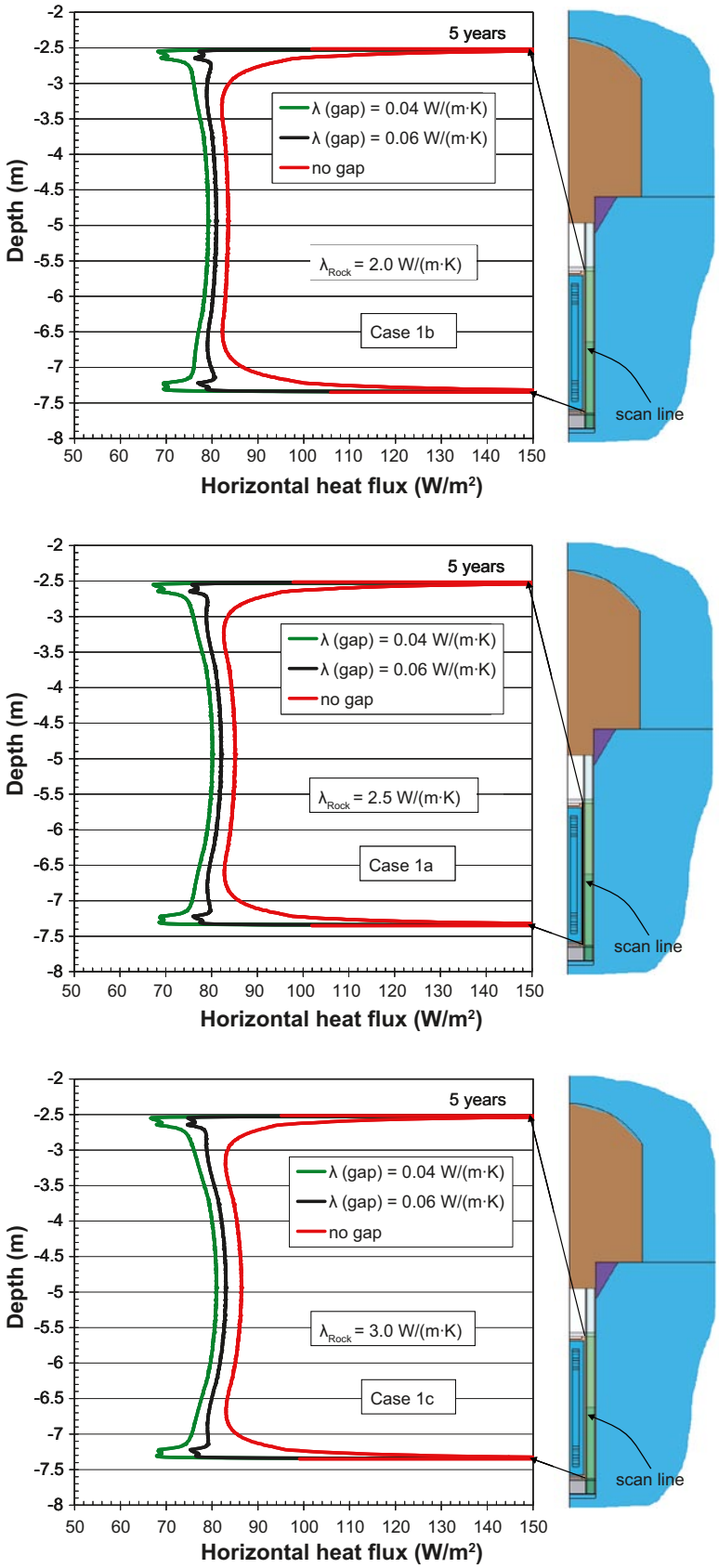

Figure A-20. *Horizontal canister heat flux profile after five years for a rock conductivity of 2.0 W/(m·K) (upper), 2.5 W/(m·K) (middle) and 3.0 W/(m·K) (lower).*

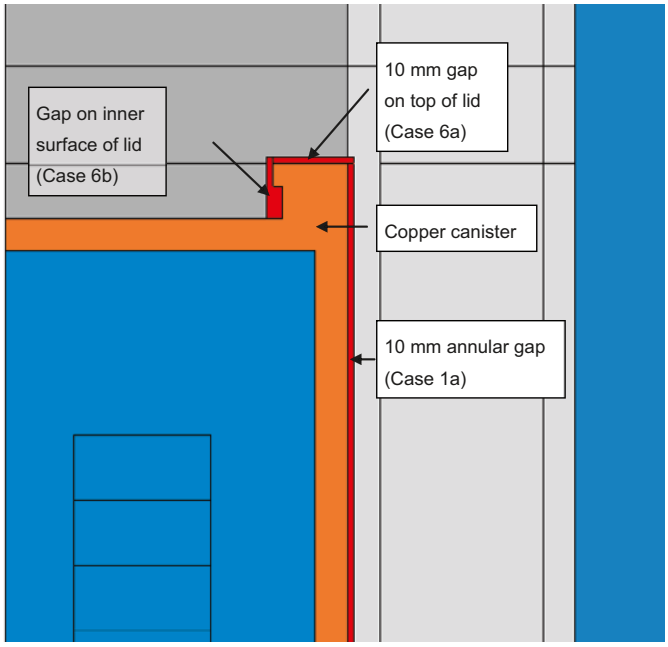

Figure A-21. *Representation of copper canister with an open 10 mm air-filled gap along the canister surface.*

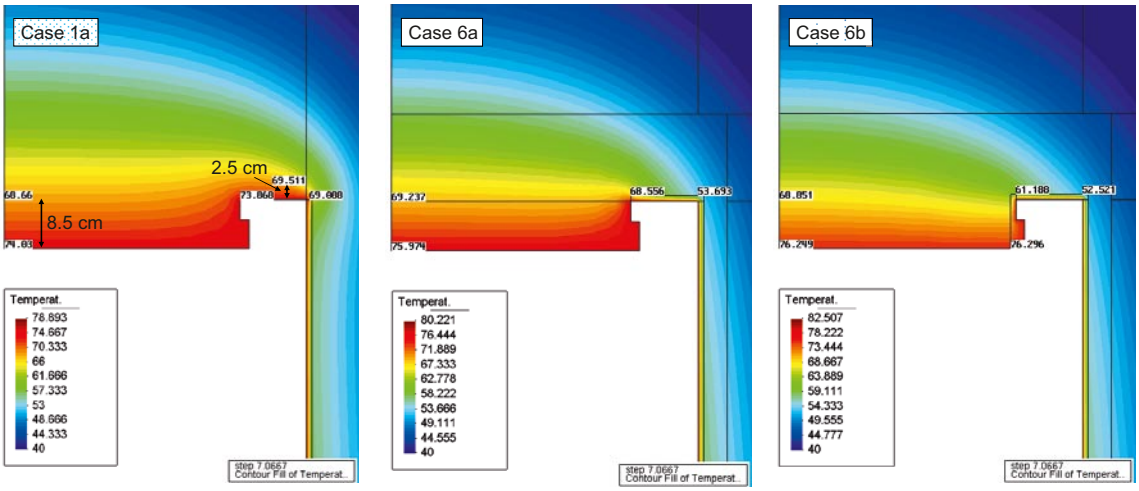

Figure A-22. *Bentonite temperatures around the canister lid after 7 years. Left: No gap between bentonite and copper surface on top of the canister. Middle: 10 mm air-filled gap between canister top and bentonite. Right: Air-filled gap between canister surface on the inner surface of the lid and bentonite. The copper canister and cast iron insert are hidden from view.*

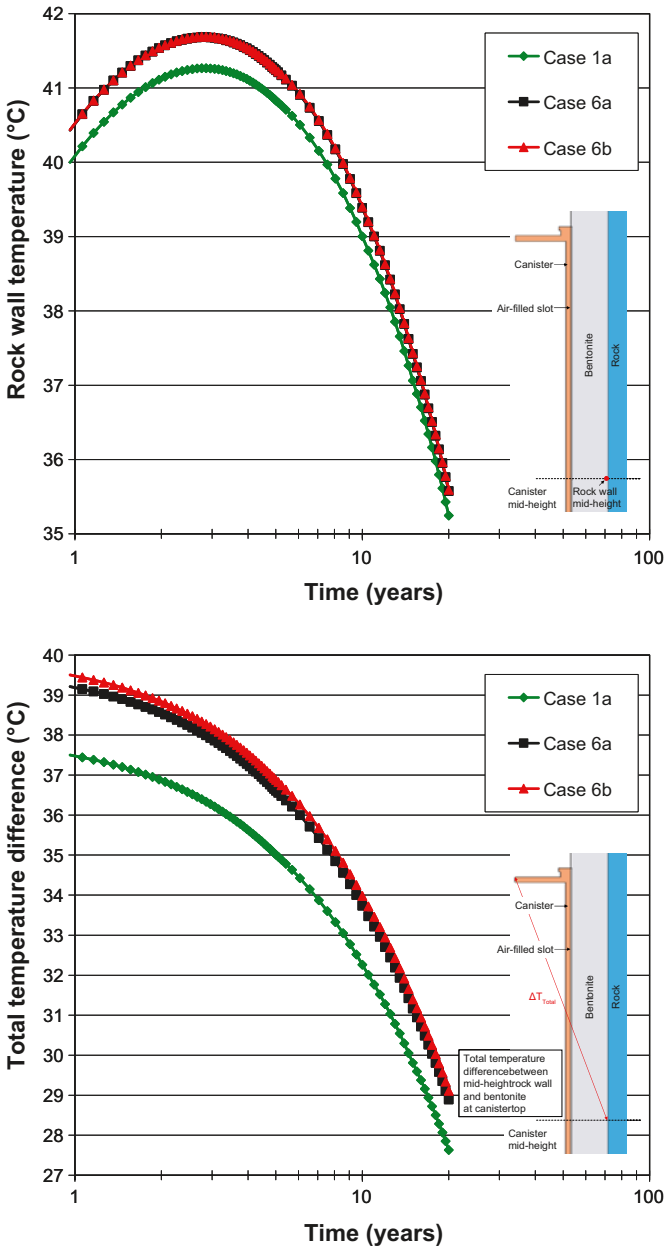

Figure A-23. *Top: Rock wall temperature at canister mid-height. Bottom: Total temperature difference between mid-height rock and bentonite at the canister top (ΔT_{tot}).*

A3.6 Variations in bentonite thermal properties

A3.6.1 Backfill properties

As the numerical models are axisymmetric around the vertical central axis of the deposition hole, the volume of the backfill material in the deposition tunnel is underestimated.

The effects on the rock wall temperature and the total temperature difference of varying the thermal conductivity of the backfill material are presented in Figure A-24. A summary of the material properties is presented in Table A-5.

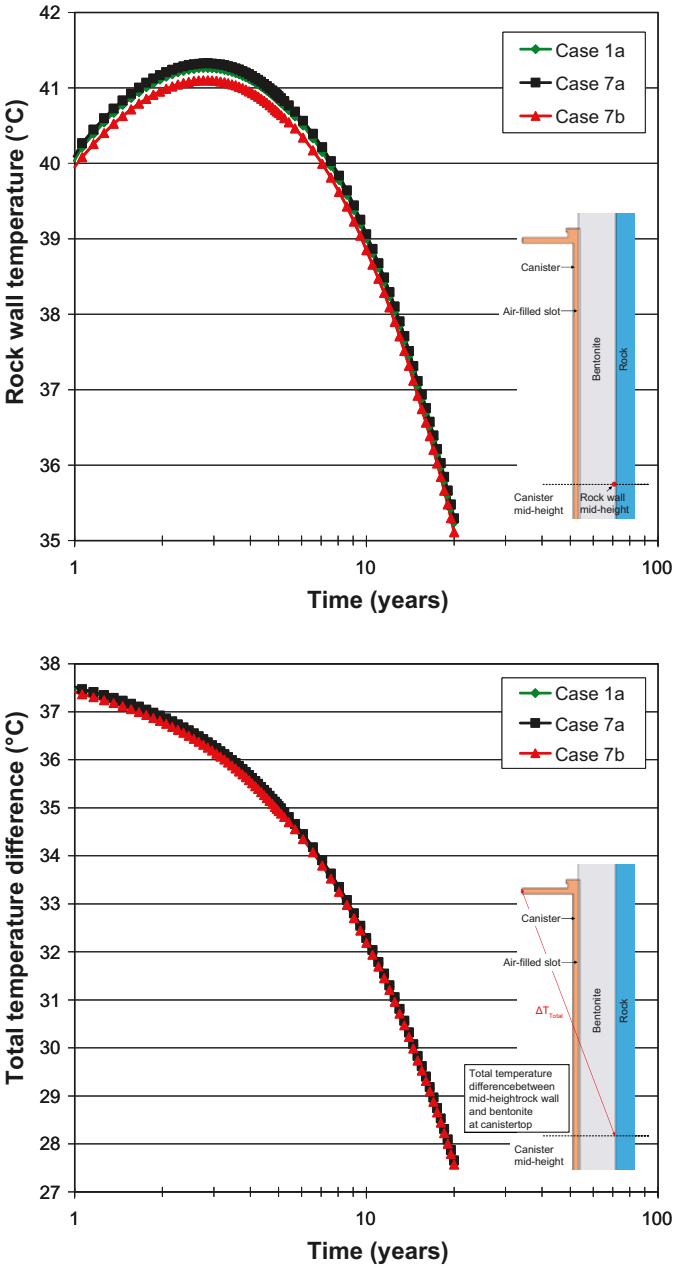

Figure A-24. *Top: Rock wall temperature at canister mid-height. Bottom: Total temperature difference between mid-height rock and bentonite at the canister top (ΔT_{tot}).*

Table A-5. Thermal conductivities of the backfill material.

Model code	$\lambda_{Backfill}$ (W/(m·K))
Case 1a	0.7
Case 7a	0.3
Case 7b	2.5 (same as rock thermal conductivity)

A3.6.2 Alternative buffer properties

Alternative sets of initial bentonite thermal conductivity values, with an explicitly modelled pellet slot (Case 2a, 2b and 2c), are presented in Table A-6. Here, the effective barrier conductivity at canister mid-height is reduced to 0.89 W/(m·K) (Case 2a) and 0.84 W/(m·K) (Case 2b and 2c). The reduced effective barrier thermal conductivity results in decreased horizontal heat flux at canister mid-height, cf. Figure A-25.

Figure A-26 and Figure A-27 show the rock wall temperature at canister mid-height alongside the total temperature difference for values of the rock thermal conductivity of λ_{Rock} = 2.5 W/(m·K) and λ_{Rock} = 3.0 W/(m·K), respectively.

A3.6.3 Moisture redistribution

In a fully coupled model, the exact temperature distribution due to all canisters in the repository needs to be captured. This is not possible in a 2D-axisymmetric model. An approximate temperature distribution can, however, be obtained by truncating the model a suitably chosen radial distance R from the symmetry axis and applying adiabatic conditions to the boundary. Results from TH-modelling /Åkesson et al. 2010/ show that as the bentonite buffer is heated there will be some redistribution of moisture and consequently the thermal properties will change, see Figure A-28. The saturation values can subsequently be translated into thermal conductivities /Börgesson et al. 1994/, cf. Figure A-29.

The resulting bentonite thermal conductivities based on the 15-year-results from the TH-models are presented in Table A-7. Case 2b is the initial state. Case 3 (less conservative) and Case 4 (more conservative) relate to different ways of translating saturation, which is the output from the numerical models, into thermal conductivity of bentonite materials, cf. Figure A-29.

Figure A-30 shows horizontal heat flux profiles after 5 years along the canister surface for each of the two moisture distribution cases (Case 3 and 4) compared with the initial case (Case 2b). The corresponding heat fluxes at canister mid-height are presented in Table A-8 as percentages of the mean value heat flux.

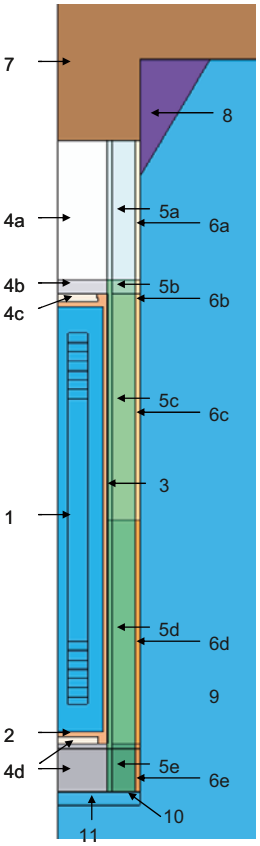

Table A-6. Buffer and backfill properties.

	Thermal conductivity (W/(m·K))				
Material ID	**Case 1a**	**Case 1c**	**Case 2a**	**Case 2b**	**Case 2c**
4a-d (c)	1.1 (1.1)	1.1 (1.1)	1.21 (1.0)	1.21 (1.0)	1.21 (1.0)
5a-e	1.0	1.0	1.21	1.21	1.21
6a-e	1.0	1.0	0.3	0.26	0.26
7	0.7	0.7	0.7	0.7	0.7
8	0.3	0.3	0.3	0.3	0.3
9	2.5	3.0	2.5	2.5	3.0
Effective thermal conductivity across barrier	**1.0**	**1.0**	**0.89**	**0.84**	**0.84**

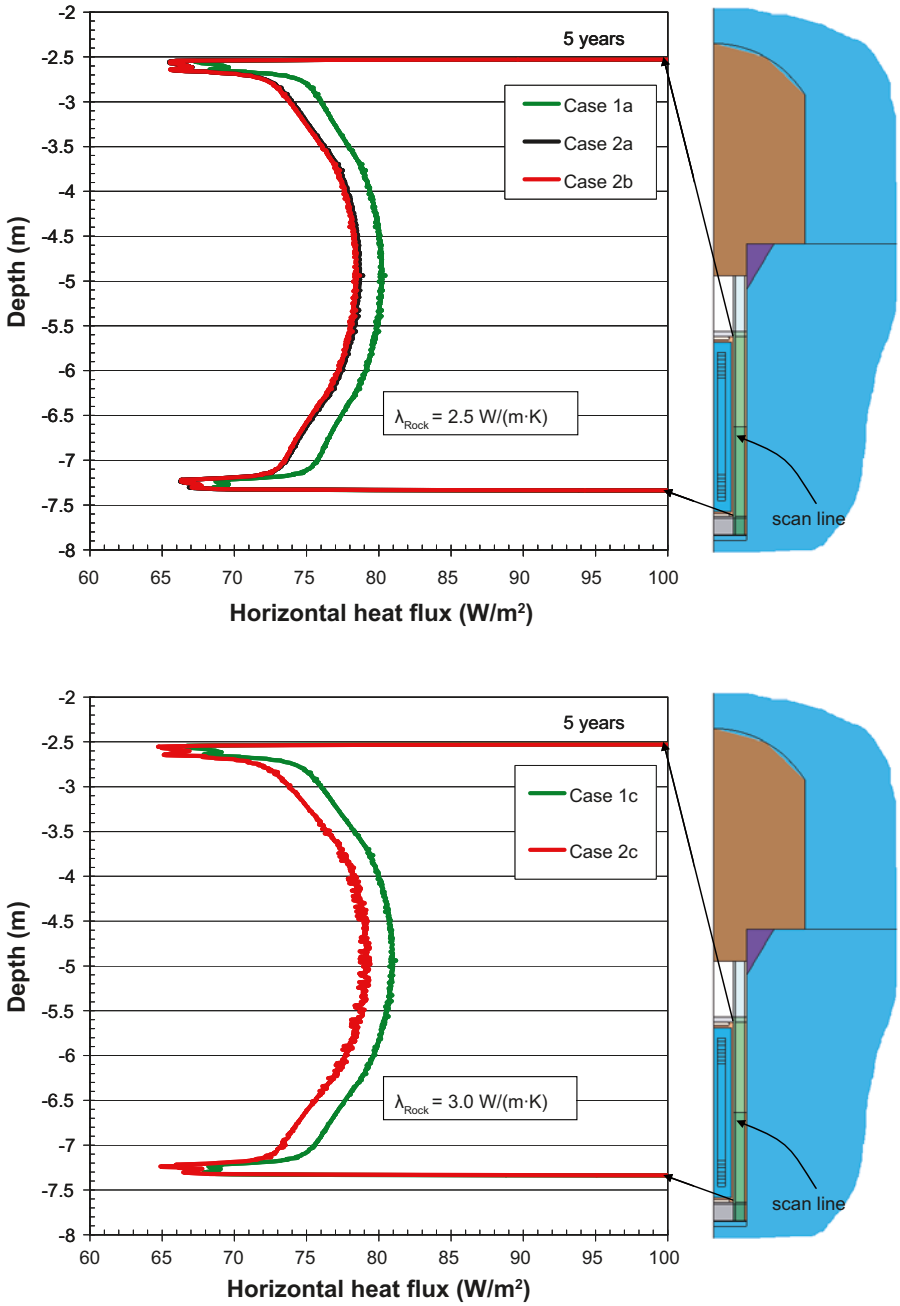

Figure A-25. *Horizontal heat flux profiles along the canister surface after 5 years.*

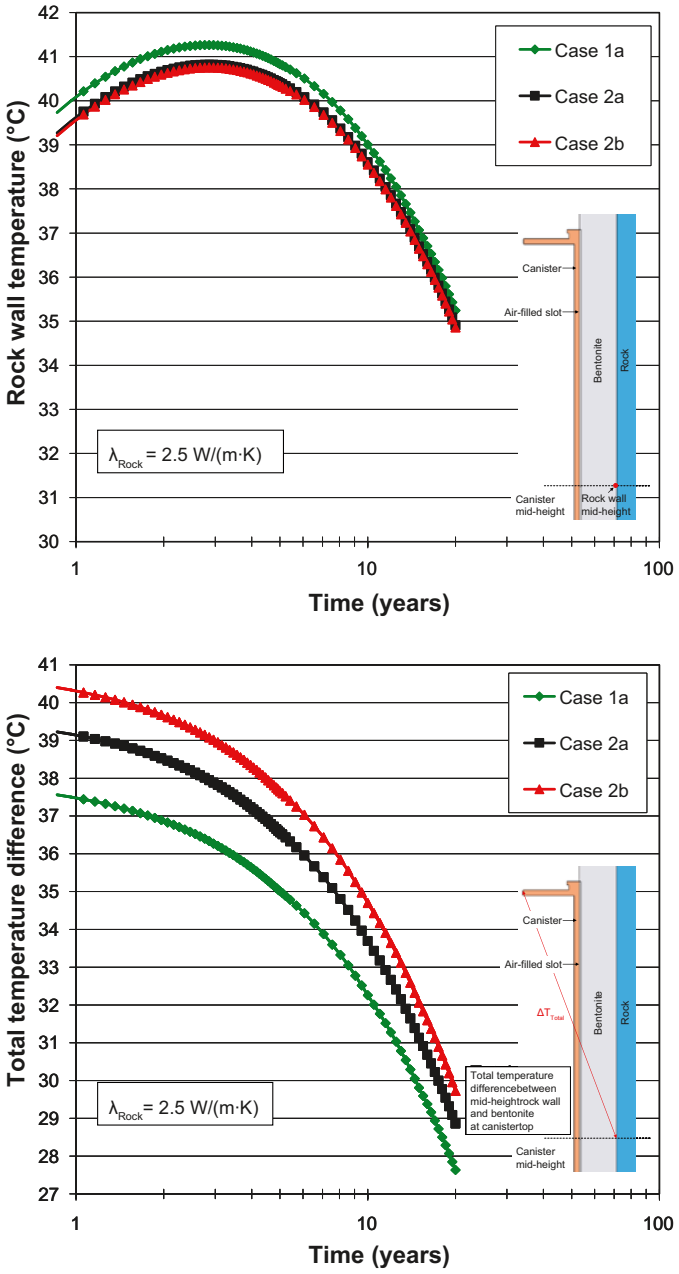

Figure A-26. *Top: Rock wall temperature at canister mid-height. Bottom: Total temperature difference between mid-height rock and bentonite at the canister top (ΔT_{tot}).*

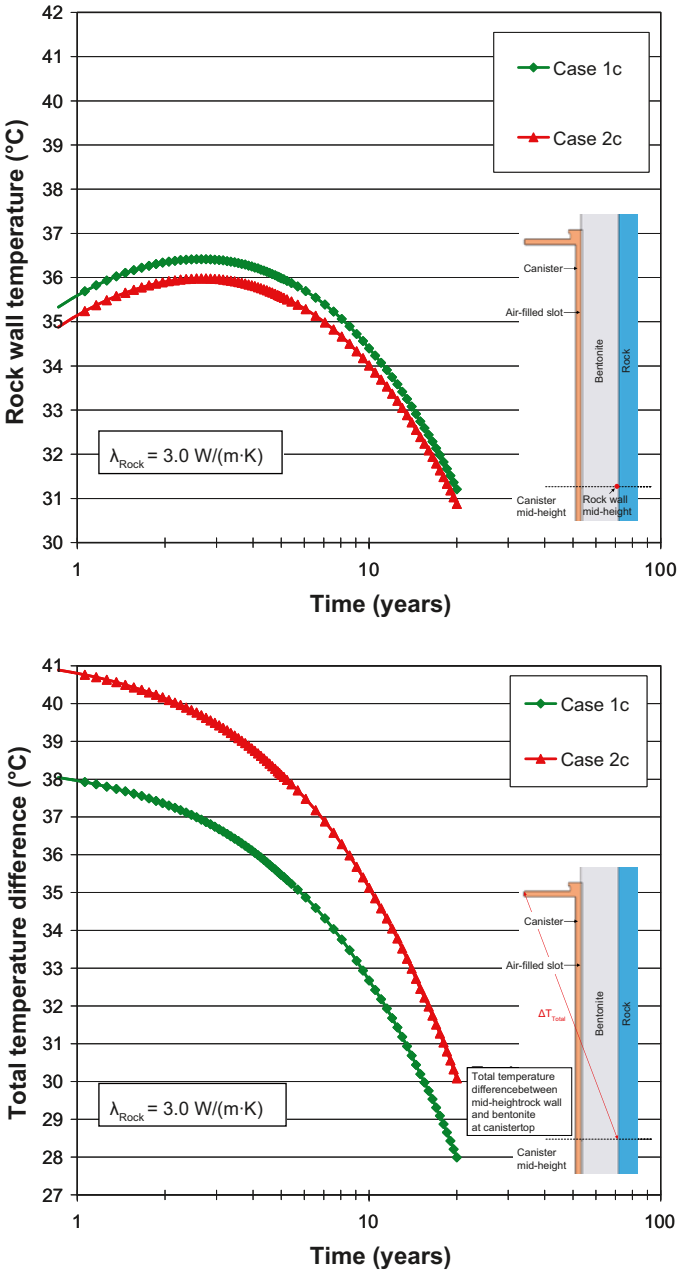

Figure A-27. *Top: Rock wall temperature at canister mid-height. Bottom: Total temperature difference between mid-height rock and bentonite at the canister top (ΔT_{tot}).*

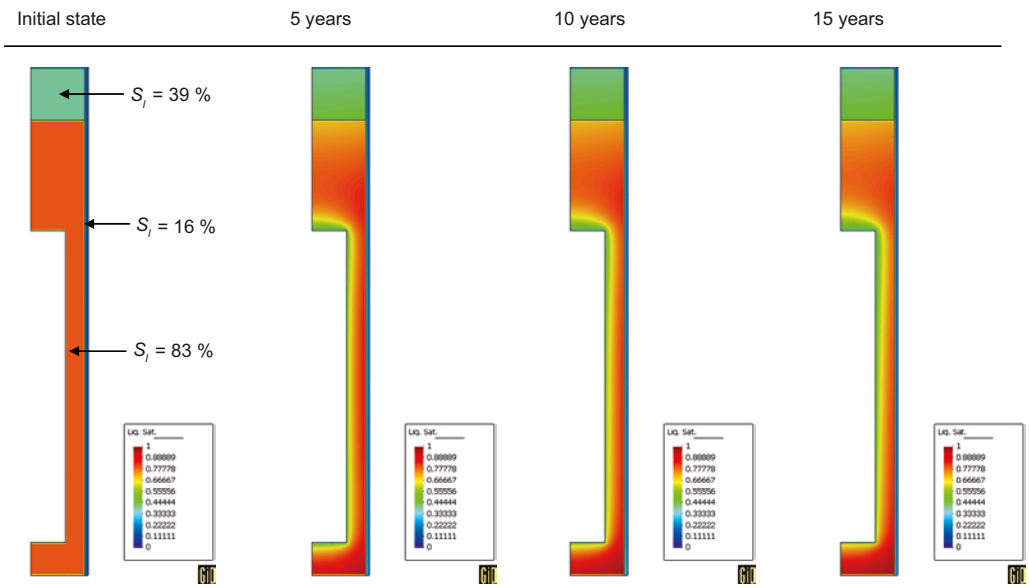

Figure A-28. *Liquid saturation in the bentonite materials initially and after 5, 10 and 15 years. From /Åkesson et al. 2010/.*

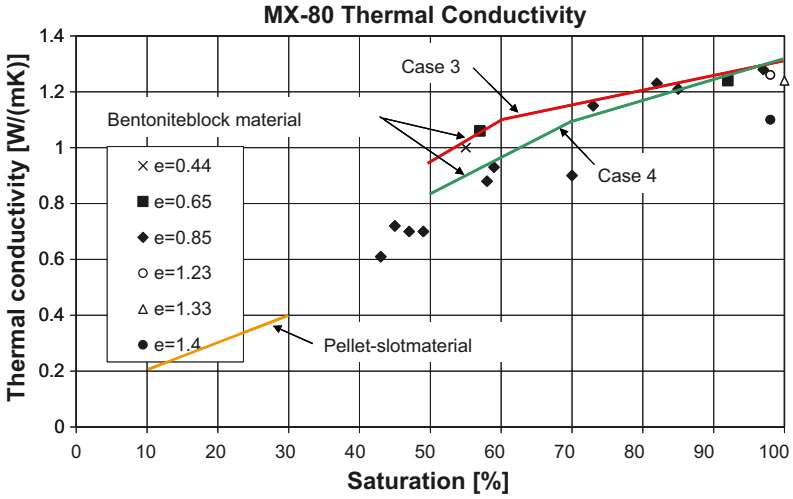

Figure A-29. *Thermal conductivity of MX-80 bentonite blocks as functions of saturation for different void ratios e. Modified from /Börgesson et al. 1994/.*

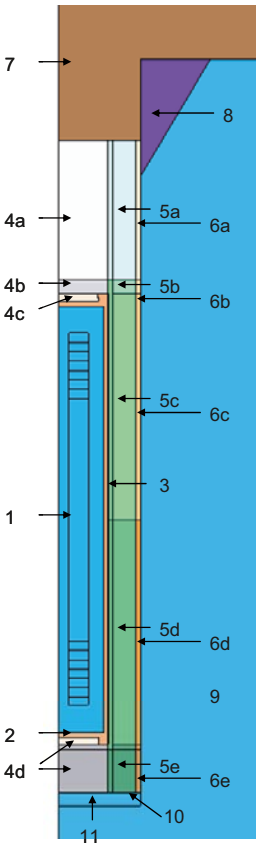

Table A-7. Buffer and backfill properties. From /Åkesson et al. 2010/.

	Thermal conductivity (W/(m·K))		
Material ID	**Case 2b**	**Case 3**	**Case 4**
4a	1.21	1.19	1.15
4b	1.21	1.03	0.92
4c	1.0	1.03	0.92
4d	1.21	1.21	1.18
5a	1.21	1.20	1.17
5b	1.21	1.17	1.13
5c	1.21	1.14	1.08
5d	1.21	1.17	1.13
5e	1.21	1.26	1.25
6a	0.26	0.31	0.31
6b	0.26	0.32	0.32
6c	0.26	0.32	0.32
6d	0.26	0.34	0.34
6e	0.26	0.39	0.39
7	0.7	0.75	0.75
8	0.3	0.3	0.3

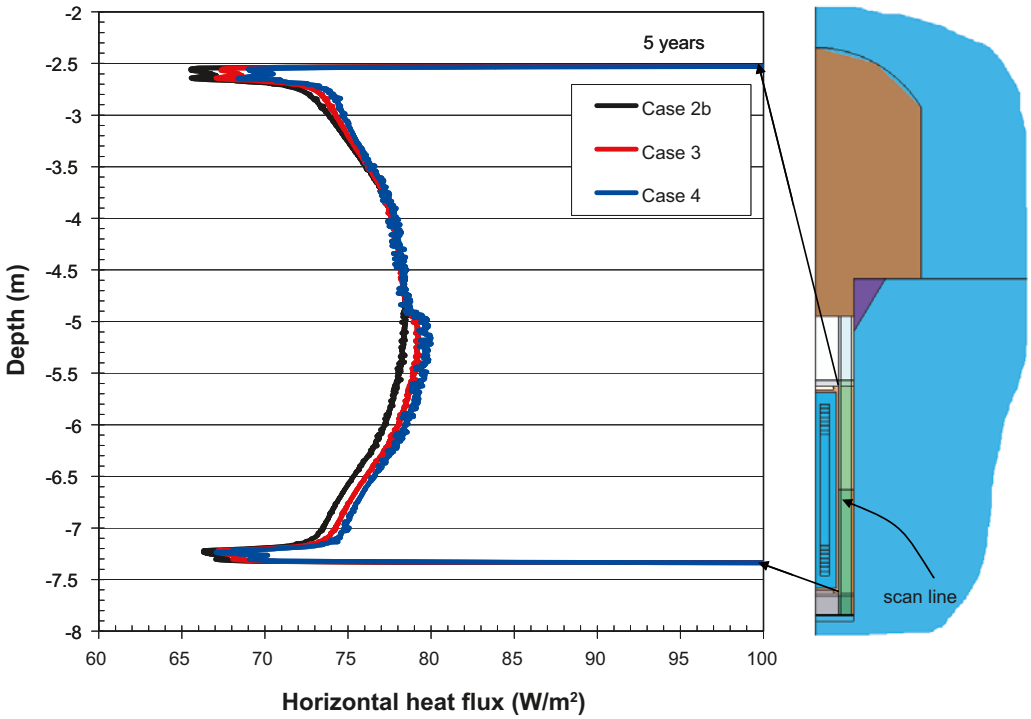

Figure A-30. *Horizontal heat flux profiles along the canister surface after 5 years.*

Table A-8. Percent of mean value heat flux at canister mid-height after 5 years. Values in brackets represent ratio 2 m above/below canister mid-height, respectively.

Model code	Percent of average canister surface flux
Case 2b	87.3 (85.3/84.9)
Case 3	87.7 (85.5/85.7)
Case 4	88.0 (85.8/86.2)

Figure A-31 shows the rock wall temperature (top) and the total temperature difference between the bentonite temperature at the top of the canister and the rock wall temperature at canister mid-height (bottom).

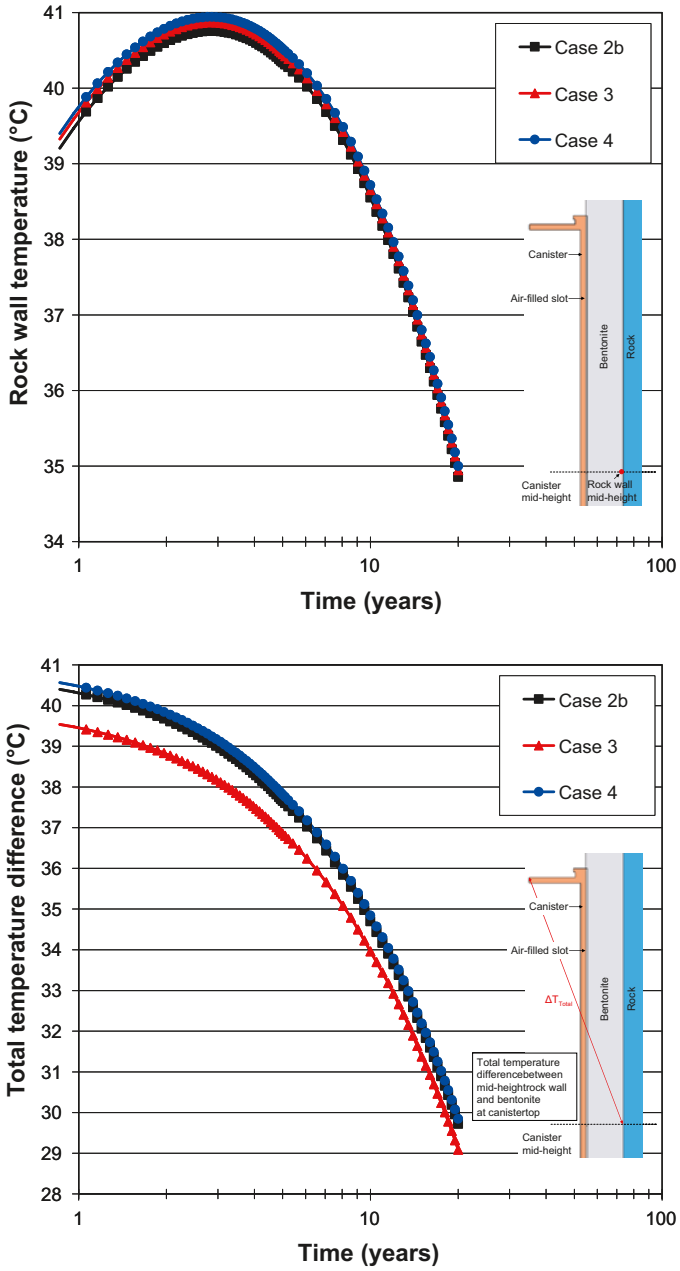

Figure A-31. *Top: Rock wall temperature at canister mid-height. Bottom: Total temperature difference between mid-height rock and bentonite at the canister top (ΔT_{tot}).*

A4 Conclusions and discussion

The temperature criterion states that the bentonite temperature must not exceed 100°C at any point within the repository. Therefore, the repository must be designed such that the criterion is always fulfilled, i.e. suitable tunnel and canister spacing must be determined.

The maximum bentonite temperature is found by calculating the rock wall temperature at canister mid-height, by use of a simple canister representation, and adding the reference evolution of ΔT_{tot} (Equation A-3).

$$\Delta T_{tot}(t) = \frac{Q(t)}{A}\frac{0.87}{\lambda_{b(eff)}} R_0 \cdot \ln(R_2/R_1) + 16 \cdot \frac{Q(t)}{Q(0)} \qquad \text{A-3}$$

where R_0 = canister radius
R_1 = buffer inner radius
R_2 = deposition hole radius
A = canister surface area
Q(t) = total canister surface heat flux at time t
$\lambda_{b(eff)}$ = effective barrier conductivity (blocks and pellets) = 1.0 W/(m·K)

The difference in rock wall temperature between the detailed reference canister models and the more schematic homogenized model (Case 11) is presented for various assumptions regarding distribution of heat load along the fuel rods, near-field distribution of thermal properties of the rock mass and the thermal properties of the bentonite buffer and backfill is presented in the figures below. In addition, the numerically calculated temperature difference between the bentonite at the top of the canister and the rock wall at canister mid-height is compared with the reference evolution of ΔT_{tot}.

For the cases investigated in this study, the following observations are made:

- For values of the rock thermal conductivity between 2.0–2.5 W/(m·K), a homogenized canister model overestimates the rock wall temperature at canister mid-height seven years after deposition by about 0.6–0.7°C, cf. Figure A-9.
- For uniformly distributed thermal properties, the total temperature difference grows with increasing thermal conductivity. The most unfavourable distribution of thermal properties (Case 5), i.e. rock with low thermal conductivity surrounding only the upper and lower parts of the deposition hole, will result in an increased total temperature difference, cf. Figure A-32.
- Reducing the length of the copper canister (Case 9), i.e. removing the flanges at the top and bottom, increases the rock wall temperature by 0.3°C assuming a uniformly distributed rock thermal conductivity of 3.0 W/(m·K). The corresponding increase in total temperature difference is about 1°C, cf. Figure A-11.
- The fuel from BWR-reactors (Case 1a) and PWR-reactors (Case 8) has different power distributions along the fuel rods. The two power distributions result, however, in only marginal temperature differences, cf. Figure A-33.
- One important effect of an open annular canister-bentonite gap is the redirection of the heat output such that the surface heat flux at canister mid-height is reduced from 93–96.5% (no gap) of the average surface heat flux to 88–90.5% (10 mm gap with effective conductivity 0.04 W/(m·K)), cf. Table A-4.
- Due to the axisymmetric representation of the models, the volume of the backfill materials in the tunnel is underestimated. Varying the thermal conductivity of the backfill material (Cases 1a, 7a and 7b) results in moderate changes in the rock wall temperature and very minor effects on the total temperature difference, cf. Figure A-34.
- Reducing the effective thermal conductivity over the bentonite buffer (Cases 2a and 2b) results in a redistribution of heat such that the rock wall temperature is reduced and the total temperature difference increases, cf. Figure A-34.
- Redistribution of moisture in the buffer materials (Cases 3 and 4) increases the radial mid-height canister flux compared with the initial state (Case 2b), cf. Table A-8. This results in a difference of about 0.2°C in the rock wall temperature and 1°C in the total temperature difference, cf. Figure A-34.

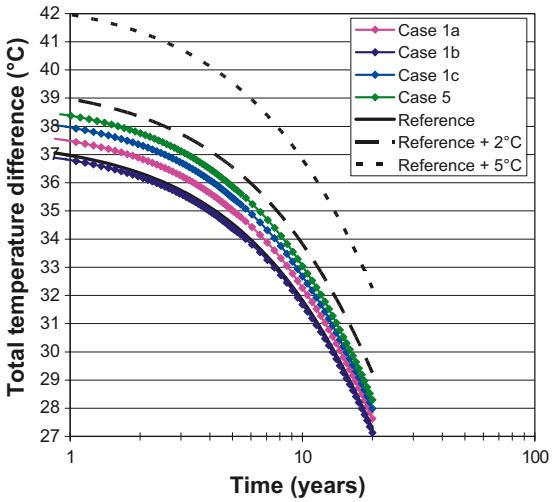

Figure A-32. *Total temperature difference for different assumptions regarding rock thermal conductivity and its distribution around the deposition hole.*

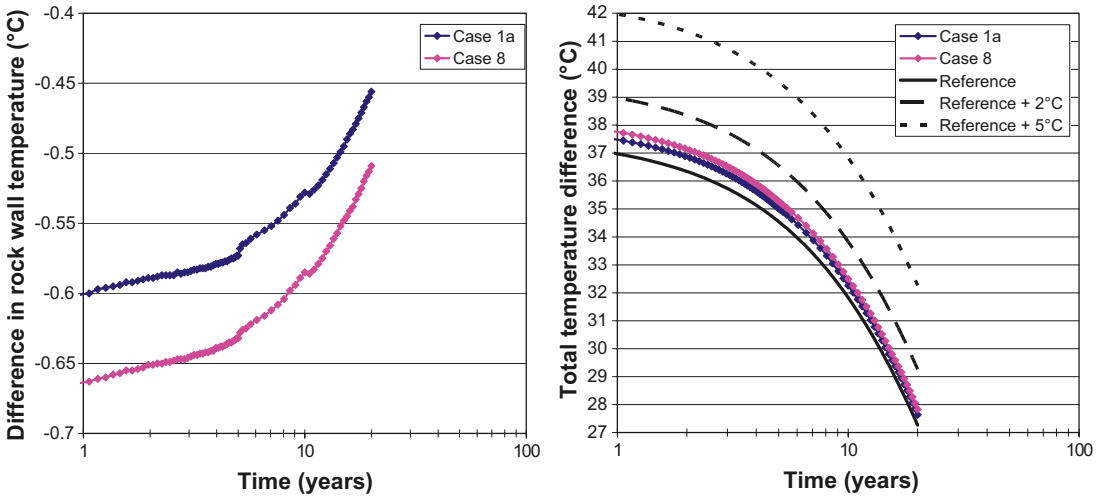

Figure A-33. *Left: Difference in rock wall temperature between the reference models and homogenized model (Case 11) for different assumptions regarding vertical power distribution along the fuel rods. Right: Corresponding total temperature difference compared with the reference evolution.*

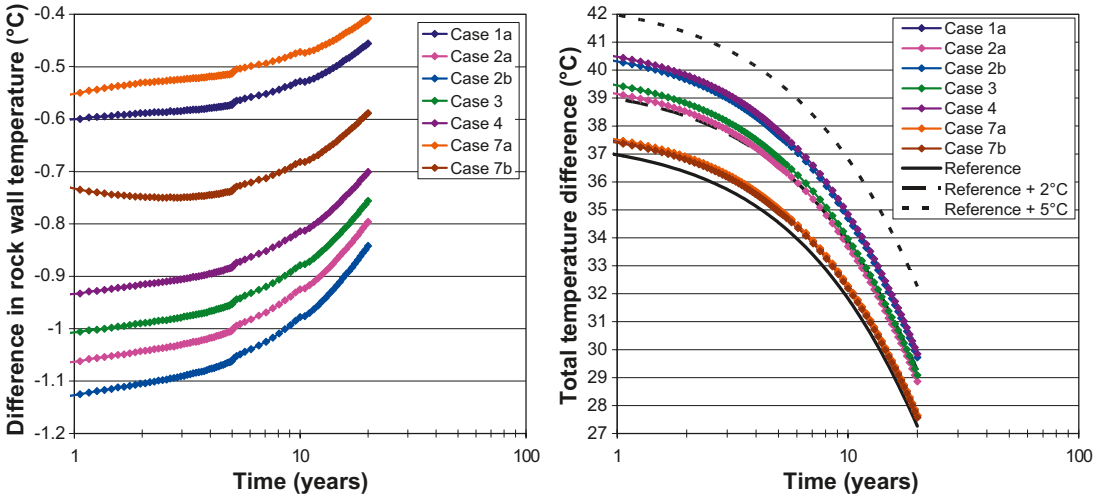

Figure A-34. *Left: Difference in rock wall temperature between the reference models and homogenized model (Case 11) for different assumptions regarding thermal properties of the bentonite materials. Right: Corresponding total temperature difference compared with the reference evolution.*

The thermal evolution of the nearfield was analyzed using axisymmetric models. For the purpose of the study, i.e. to compare the reference evolution suggested in the main text for the temperature difference $\Delta T_{tot}(t)$ between the wall of the deposition hole and the hottest buffer point with results from numerical models that take gaps, property variations (buffer, rock tunnel backfill), moisture redistribution and burn-up distributions into account, this is judged to be an adequate approach. The following, less important, aspects of the thermal near-field evolution would require a full 3D analysis:

- The details of the reference design of tunnels and deposition holes as given in /SKB 2010d/, e.g. the asymmetric excavation geometry with deposition holes not centred in the tunnel floor.
- A more detailed representation of the canister interior:
  - Geometry and heat conduction of the cast iron insert.
  - Positions and geometry of the fuel rods and their power distributions.
- Possibility of asymmetrical position of the canister in the deposition hole.
- Contributions from other canisters to the buffer heat flux. Note that this effect has shown to be very small here, at least for canisters with neighbours on both sides, cf. Section A3.1.1.

A5 References

Back P-E, Wrafter J, Sundberg J, Rosén L, 2007. Thermal properties. Site descriptive modelling Forsmark – stage 2.2. SKB R-07-47, Svensk Kärnbränslehantering AB.

Börgesson L, Fredriksson A, Johannesson L-E, 1994. Heat conductivity of buffer materials. SKB TR-94-29, Svensk Kärnbränslehantering AB.

CIMNE, 2004. Code_Bright. Version 2.2 users guide. Departemento de Ingenieria del Terreno, Cartográfica y Geofísica. Universidad Politécnica de Cataluña, Spain.

Håkansson R, 2000. Beräkning av nuklidinnehåll, resteffekt, aktivitet samt doshastighet för utbränt kärnbränsle. SKB R-99-74, Svensk Kärnbränslehantering AB.

Hökmark H, Fälth B, 2003. Thermal dimensioning of the deep repository. SKB TR-03-09, Svensk Kärnbränslehantering AB.

SKB, 2010a. Design, production and initial state of the buffer for the safety assessment SR-Site. SKB TR-10-15, Svensk Kärnbränslehantering AB.

SKB, 2010b. Design, production and initial state of the canister for the safety assessment SR-Site. SKB-TR-10-14, Svensk Kärnbränslehantering AB.

SKB, 2010c. Spent nuclear fuel for disposal in the KBS-3 repository. SKB TR-10-13, Svensk Kärnbränslehantering AB.

SKB, 2010d. Design, construction and initial state of the underground openings for the safety assessment SR-Site. SKB-TR-10-18, Svensk Kärnbränslehantering AB.

Sundberg J, Wrafter J, Ländell M, Back P-E, Rosén L, 2008a. Thermal properties Forsmark. Modelling stage 2.3. Complementary analysis and verification of the thermal bedrock model, stage 2.2. SKB R-08-65, Svensk Kärnbränslehantering AB.

Sundberg J, Wrafter J, Back P-E, Rosén L, 2008b. Thermal properties Laxemar. Site descriptive modelling. SDM-Site Laxemar. SKB R-08-61, Svensk Kärnbränslehantering AB.

Åkesson M, Kristensson O, Börgesson L, Dueck A, Hernelind J, 2010. THM modelling of buffer, backfill and other system components. SKB TR-10-11, Svensk Kärnbränslehantering AB.

Appendix B

Anisotropic conditions

B1 Governing equations

The analytical calculation scheme described in the main text for determining rock temperatures can be extended to anisotropic media where the directions of the principal heat conductivities coincide with the repository geometry.

The temperature increase due to a point source in an anisotropic medium with time-dependent power $Q(t)$ a distance (x, y, z) from its centre is given by /Carslaw and Jaeger 1959/:

$$T_p(x,y,z,t) = \frac{1}{\rho \cdot c \cdot \sqrt{4\pi \cdot a_x}\sqrt{4\pi \cdot a_y}\sqrt{4\pi \cdot a_z}} \int_0^t \frac{Q(t')}{(\sqrt{t-t'})^3} e^{-\frac{x^2}{4a_x(t-t')}} e^{-\frac{y^2}{4a_y(t-t')}} e^{-\frac{z^2}{4a_z(t-t')}} dt' \quad \text{B-1}$$

Here $a_x = \lambda_x/(\rho\, c)$, a_y and a_z are the thermal diffusivities in the three coordinate directions.

As for isotropic conditions (cf. main text), line source solutions are found by integrating the equation for a point source (B-1) along its entire length $(-H_c, H_c)$, where H_c is the canister half-height.

$$T_l(r,z,t) = \frac{1}{\rho \cdot c \cdot 4\pi\sqrt{a_x \cdot a_y}} \int_0^t \frac{Q(t')}{2H_c(t-t')} e^{-\frac{x^2}{4a_x(t-t')}} e^{-\frac{y^2}{4a_y(t-t')}} \frac{1}{2}\left(\operatorname{erf}\left(\frac{H_c+z}{\sqrt{4a_z(t-t')}}\right) + \operatorname{erf}\left(\frac{H_c-z}{\sqrt{4a_z(t-t')}}\right)\right) dt' \quad \text{B-2}$$

The expressions for the compound line sources are obtained from Equation B-2 by the same scale in height and power as described in the main text for isotropic conditions.

The panel solution with time-dependent power $Q(t)/(px{\cdot}py)$ is then obtained by integration over the rectangle $-L < x < L$ and $-B < y < B$. As with the corresponding expression for isotropic conditions, Equation B-3 gives the temperature increase above initial conditions:

$$T(x,y,z,t) = \int_0^{\sqrt{t/t_0}} \frac{Q(t - t_0 \cdot s^2)}{px \cdot py} f \cdot h \, ds$$

$$\text{where } f = \sqrt{\frac{t_0}{\rho \cdot c \cdot \pi \cdot \lambda_z}} \left(e^{-\frac{z^2}{4a_z t_0 s^2}} - e^{-\frac{(z-2H)^2}{4a_z t_0 s^2}} \right) \quad \text{B-3}$$

and

$$h = \frac{1}{4}\left(\operatorname{erf}\left(\frac{L+x}{s\sqrt{4a_x \cdot t_0}}\right) + \operatorname{erf}\left(\frac{L-x}{s\sqrt{4a_x \cdot t_0}}\right)\right)\left(\operatorname{erf}\left(\frac{B+y}{s\sqrt{4a_y \cdot t_0}}\right) + \operatorname{erf}\left(\frac{B-y}{s\sqrt{4a_y \cdot t_0}}\right)\right)$$

The solution accounts for the ground surface at $z = H$, such that $T(x, y, H, t) = 0$. The parameter t_0 may be arbitrarily chosen, but must be positive. By using the substitution, $t' = t - t_0 s^2$, Equation B-3 can be transformed into a time integral (such as in the panel solution for isotropic materials in main text).

B2 Demonstration examples

The principles of the analytical solution for anisotropic conditions are demonstrated in Figure B-1 for two points: one between two canisters (left) and one between two tunnels (right). For each of the points there are four cases:

- Medium is isotropic with heat conductivity λ = 3.55 W/(m·K) in all directions.
- Heat transport is short-circuited in the tunnel direction (λ_x = 100 W/(m·K)).
- Heat transport is short-circuited across tunnels (λ_y = 100 W/(m·K)).
- Heat transport is short-circuited in both horizontal directions ($\lambda_x = \lambda_y$ = 100 W/(m·K)).

For comparison, there is also a curve showing the corresponding panel solution, i.e. the temperature development that would be found at any point within the interior of a deposition area with perfectly, idealized smeared-out heat generation without account of the actual heat source positions. Here, the panel solution relates to the isotropic case with λ = 3.55 W/(m·K) in all directions. Comparing for completeness the two isotropic solutions (panel solution and discrete heat source solution) gives as expected the following:

- The tunnel point between canisters (*a)* is hotter than the panel average, meaning that the panel solution underestimates the temperature at all times.
- The point between tunnels (*b)* is cooler than the panel average, meaning that the panel solution overestimates the temperature at all times.

Anisotropy (short-circuiting in the two horizontal directions) has the following effects:

- Short-circuiting in tunnel direction (*x*): Both points get hotter. This is logical: point *a* gets hotter as a direct result of the efficient heat transfer from the efficiently cooled neighbouring canisters. Point *b* gets slightly hotter because the vertical heat transfer from the cooled canisters is reduced, i.e. the heat stays longer in the horizontal plane of the canisters.
- Short-circuiting across tunnels (*y*): Point *a* gets considerably cooler, whereas point *b* gets considerably hotter. This, too, is logical: The increased across-tunnel conductivity cools the tunnels and heats the rock between the tunnels.
- Short-circuiting in both horizontal directions. As expected, the temperatures at both points tend to the panel average.

For the KBS-3 type geometry, with the canister spacing being much smaller than the tunnel spacing, the sensitivity to changes in conductivity along tunnels is much less than changes in conductivity across tunnels.

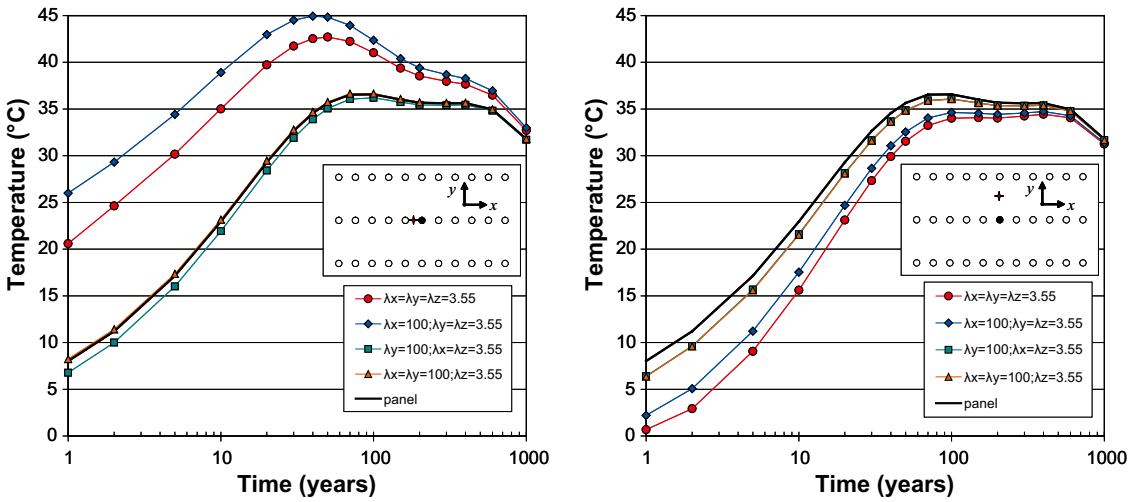

Point *a*: between two neighbouring canisters Point *b*: between two neighbouring tunnels

Figure B-1. *Demonstration of anisotropic solution by short-circuiting the heat conductivity in the horizontal directions at a point between two canister positions (left) and between two tunnels (right). Two isotropic cases are included for comparison: discrete heat sources and smeared-out heat generation (panel).*

B3 Verification of solution

The examples above demonstrates that the anisotropic solution gives results that are logical and qualitatively consistent with the input assumptions. A quantitative verification using the 2D finite difference code FLAC /Itasca 2005/ is made below.

Two FLAC models are analysed:

1. 2D model: horizontal cross section of one individual canister.
2. Quasi 3D model: Vertical axisymmetric section of one individual canister.

Table B-1 shows the different cases considered.

All cases are defined such that the geometric mean conductivity is 3.55 W/(m·K). The 2D model is used to check the anisotropic solution in the horizontal plane without regard to the axial, out-of-plane conductivity. The quasi 3D model is used to check the solution in vertical sections, assuming the conductivity to be isotropic in the horizontal plane. The analytical solution is not tested here for cases where the thermal conductivity takes on different values for all three principal directions simultaneously. For the purpose of verification this is not necessary.

The heat generation is specified in Table B-2. Note that the canister power data used in these examples is that applied in earlier assessments of the thermal evolution /Hökmark and Fälth 2003/ and does not agree exactly with the updated power data specified in the main text. The initial power, for instance, is 1,837 W instead of 1,700 W. This is however simply a scale factor and does not influence the conclusions.

The canister is 5 m in height, which gives 367.4 W per metre of canister length. In the horizontal 2D-model, the canister is infinitely long, which will give overestimated temperatures. For the purpose of verification this is not important.

The analytical solution used for the comparison is the line source solution (infinite for the 2D model and 5 m compound source for the axisymmetric model).

It should be noted that the anisotropic analytical solution cannot take the isotropic conditions in the interior of deposition hole into account. The medium is implicitly assumed to be homogeneously anisotropic everywhere. Therefore, it is not meaningful to verify (or use) the anisotropic analytical solution for points at very small distances from the wall of the deposition hole.

Table B-1. Heat conductivities for isotropic and anisotropic conditions.

	Horizontal cross section	Vertical cross section
Isotropic conditions	$\lambda_x=\lambda_z$= 3.55 W/(m·K)	$\lambda_r=\lambda_z$=3.55 W/(m·K)
15% anisotropy	λ_x= 3.719 W/(m·K)	λ_r= 3.468 W/(m·K)
	λ_y= 3.234 W/(m·K)	λ_z= 3.719 W/(m·K)
50% anisotropy	λ_x= 4.064 W/(m·K)	λ_r= 3.318 W/(m·K)
	λ_y= 2.709 W/(m·K)	λ_z= 4.064 W/(m·K)

Table B-2. FLAC model canister power as function of time after deposition.

Power expression	I	t_i [years]	a_i
Canister power $Q(t)$:	1	20	0.070477
$Q(t) = 1837 \cdot \sum_{i=1}^{7} a_i \exp(-t/t_i)$ (W)	2	50	0.712803
	3	200	–0.05102
	4	500	0.231494
	5	2,000	0.023651
	6	5,000	–0.00862
	7	20,000	0.021642

Figure B-2, Figure B-3 and Figure B-4 show that the analytical solution, at distances larger than about 3 m away from a deposition hole, is in very good agreement with the FLAC results. The two solutions agree within about two tenths of a degree at all points. Note that the horizontal 2D models, FLAC as well the analytical solution (Figure B-2), overestimate all temperatures.

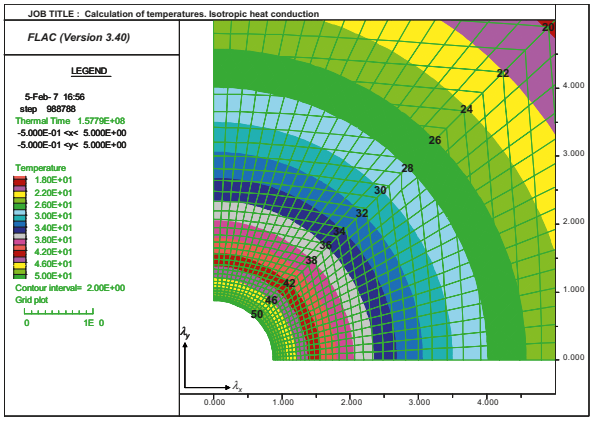

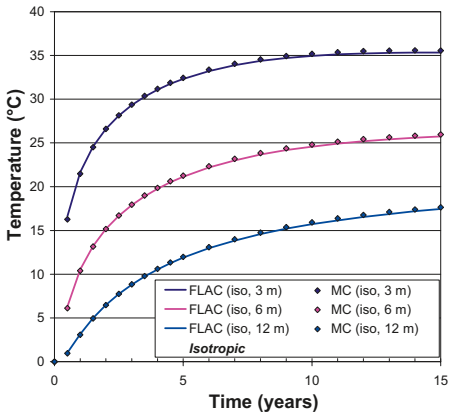

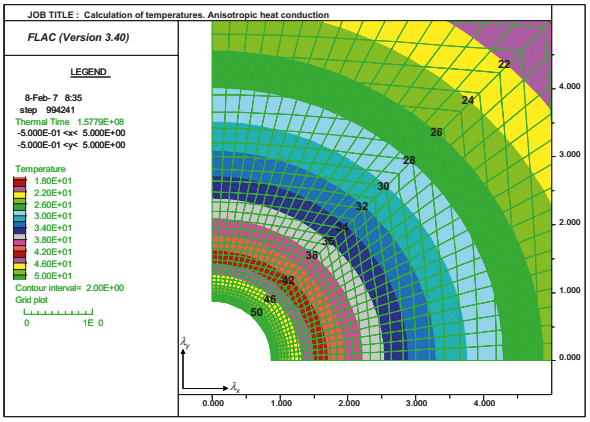

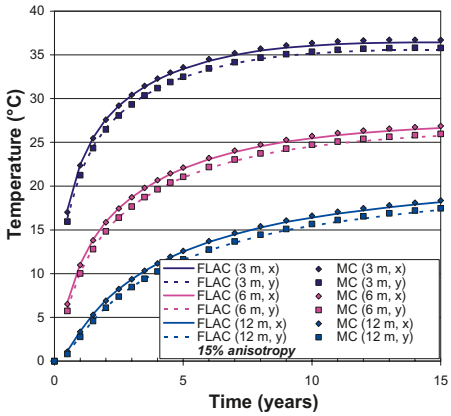

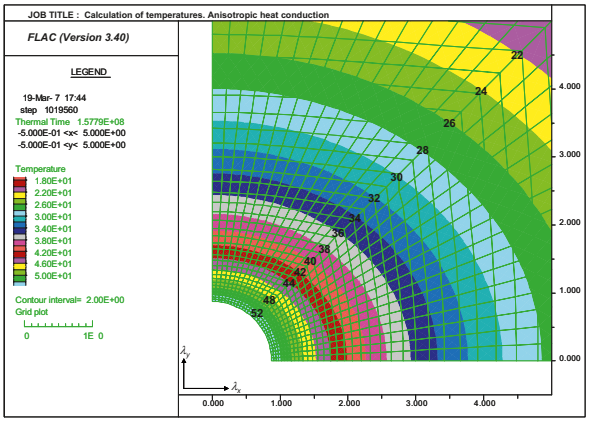

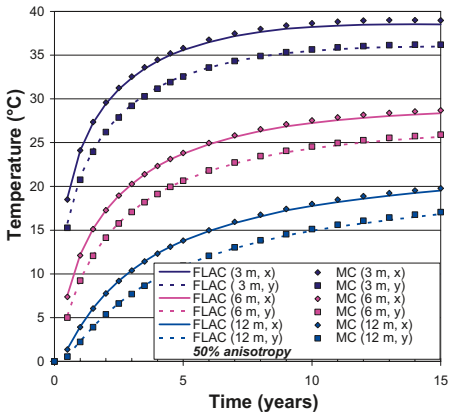

Top: Isotropic heat conduction, λ=3.55 W/(m·K)

Middle: 15% anisotropy with λ_x=3.72 and λ_y=3.23 W/(m·K)

Bottom: 50% anisotropy withλ_x=4.06 and λ_y=2.71 W/(m·K)

Top: isotropic conditions

Middle: 15% anisotropy

Bottom: 50% anisotropy

Figure B-2. *Left: Rock temperature increase (FLAC) after 5 years in a horizontal cross-section through an infinitely long canister. Right: Development (FLAC and analytical) of the rock wall temperature increase at different distances from the canister axis. For the anisotropic cases comparisons are made along both coordinate axes.*

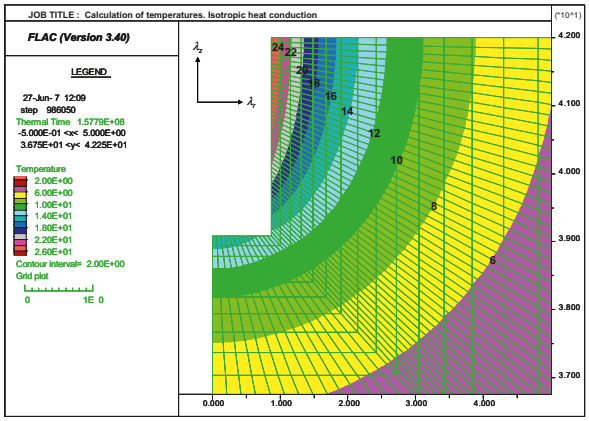

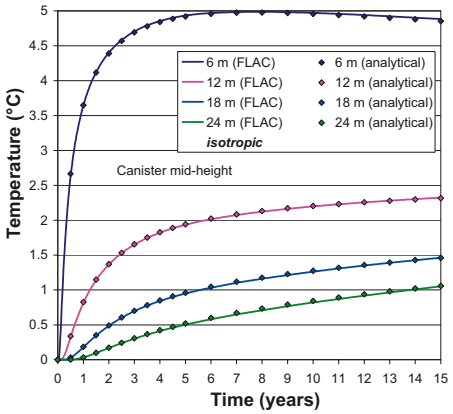

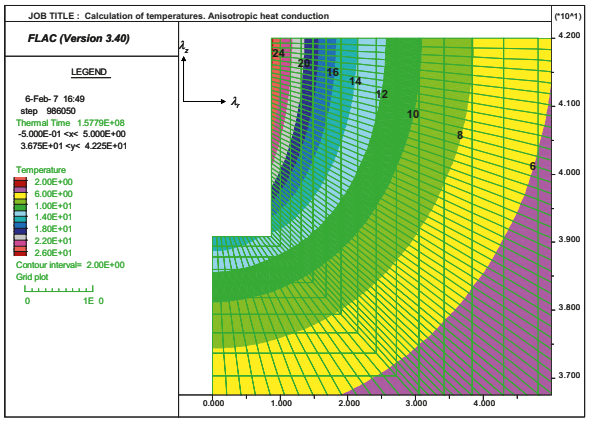

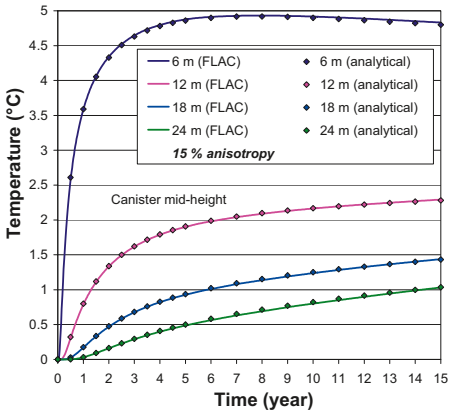

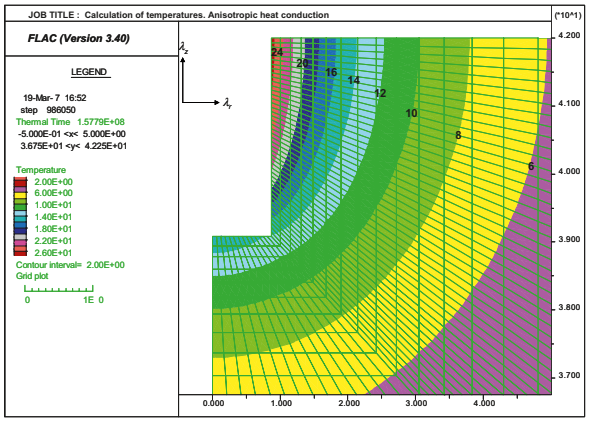

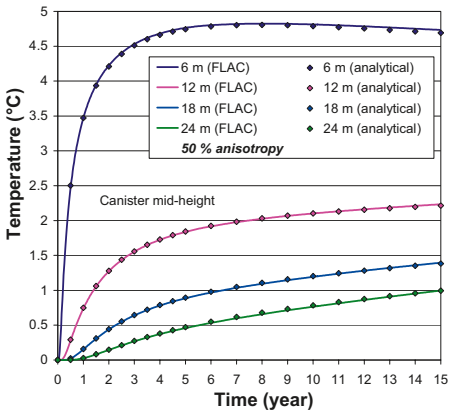

Top: Isotropic heat conduction, λ=3.55 W/(m·K)

Middle: 15% anisotropy with λ_r=3.47 and λ_z=3.72 W/(m·K)

Bottom: 50% anisotropy with λ_r=3.32 and λ_z=4.06 W/(m·K)

Top: Isotropic conditions

Middle: 15% anisotropy

Bottom: 50% anisotropy

Figure B-3. *Left: Rock temperature increase (FLAC) after 5 years in a vertical cross-section through a 5 m high canister. Right: Development (FLAC and analytical) of the rock temperature increase at different distances from canister axis.*

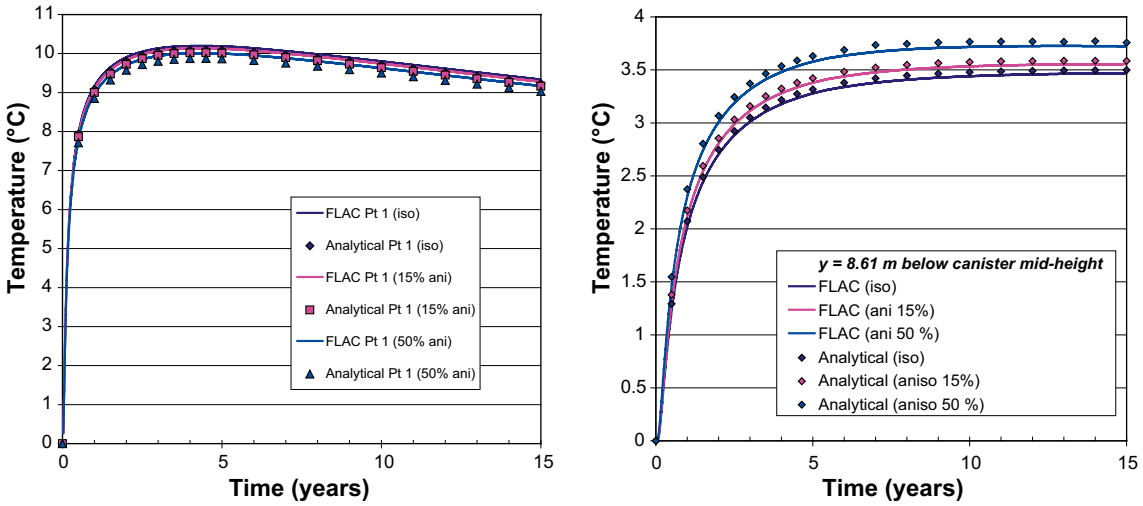

Figure B-4. *Rock temperature increase in the axisymmetric model. Left: point at mid-height at 3 m distance from canister axis. Right: Point 8.6 m below canister center.*

In addition to verifying the anisotropic version of the analytical solution, Figure B-2, Figure B-3 and Figure B-4 show that the modest anisotropy assumed here (15%–50%) does not influence the temperature field generated by one individual canister much. The temperature difference does not exceed two degrees at any of the examined points (note that all temperatures in Figure B-2 are overestimates).

B4 Effects of anisotropy on maximum bentonite temperature

Due to the isotropic conditions in the deposition hole interior, i.e. the space taken upp by the buffer, the anisotropic analytical solution cannot be used to find the contribution of the local canister to the local rock wall temperature. The contribution from all other canisters to that specific temperature is, however, very accurately calculated as demonstrated in the previous section. To find a relevant estimate of the effects of anisotropy on the rock wall temperature, the two contributions (that from the local canister and that from the rest of repository) are treated separately below.

The contribution from the local canister, or the effects of anisotropy to that contribution, can be estimated from the FLAC models. Figure B-5 shows comparisons between the maximum rock wall temperature for isotropic and anisotropic conditions. The difference is in the range 0.5–1.5°C for the anisotropy range considered here (15%–50%).

Figure B-6 shows the analytically obtained contribution to the local rock wall temperature from the rest of the repository, i.e. from the entire repository excluding the local canister, for the same assumptions regarding thermal conductivity. Here, the fuel is assumed to have the standard decay-rate of SKB reference fuel and initial power 1,700 W/canister (see main text). For the first 20 years after deposition the analytical solution for isotropic media will underestimate the total temperature contribution from the entire repository. Thereafter the temperature contribution will be overestimated. However, at the time of maximum bentonite temperature (approximately 10 years after deposition), the temperature contribution for 15% anisotropy is underestimated by only 0.2°C. The corresponding underestimate in temperature contribution is 0.8°C if the heat conductivities in the vertical direction and along tunnels were 50% higher than the heat conductivity in the direction along tunnels.

B5 Handling anisotropy

The effects of anisotropy in the 15%–50% range appear to be small on the local scale as well as on the repository scale. Table B-3 shows the effect (i.e. the underestimate) of ignoring anisotropy when calculating the maximum bentonite temperature.

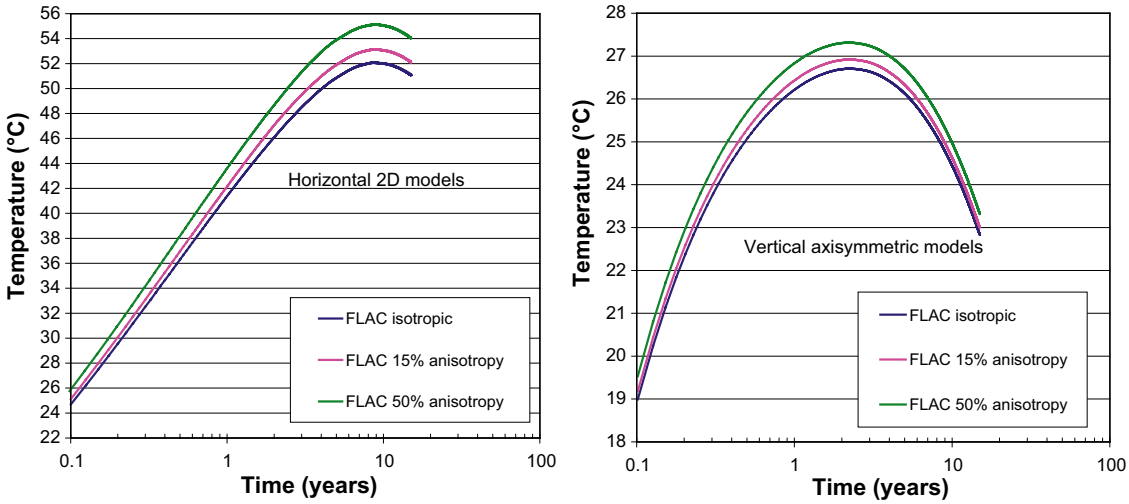

Figure B-5. *Maximum rock wall temperature in 2D-horizontal model (left) and quasi 3D axisymmetric model (right). Because the canister is infinitely long in the 2D model, all 2D temperatures are about twice as high as those of the axisymmetric quasi-3D model. This means that the 15% anisotropy case gives a rock wall temperature about 0.5°C above the isotropic ones and the 50% anisotropy about 1.5°C. Here, the fuel has initial power 1,837 W and decay-rate according to Table B-2.*

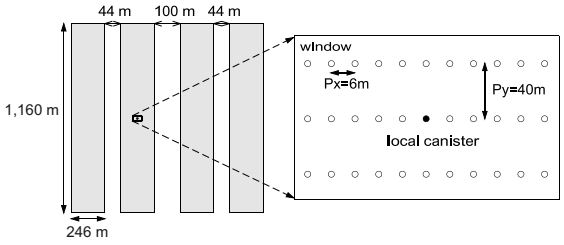

Depth below ground surface:	400 m
Canister spacing:	6 m
Tunnel spacing:	40 m
Density:	2,700 kg/m^3
Specific heat:	803.7 J/(kg·K)

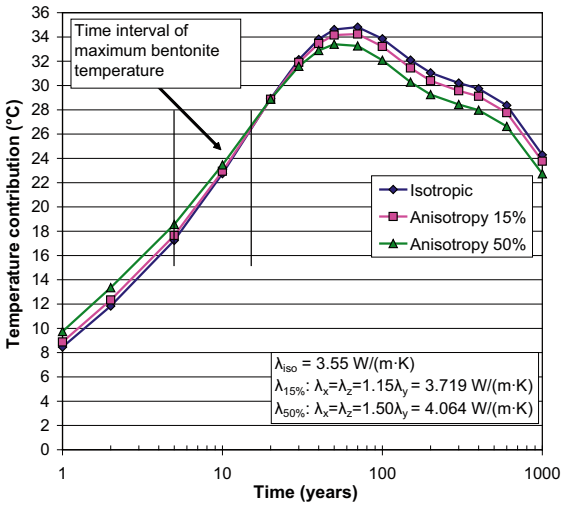

Figure B-6. *Temperature contribution from the repository (excluding the local canister) at the local canister position for two anisotropic cases compared with an isotropic case.*

Table B-3. Underestimate in maximum bentonite temperature.

Anisotropy	Local canister (from FLAC model)	Rest of repository (from analytical solution)	Total
15%	0.5ºC	0.2 ºC	0.7 ºC
50%	1.5 ºC	0.8 ºC	2.3 ºC

For the Forsmark site the anisotropy in thermal conductivity can be assumed to be about 15% /Back et al. 2007/. The smallest conductivity is found (approximately) in the direction across tunnels (i.e. as assumed here), provided that the tunnels are oriented NW-SE, i.e. in the direction of the major principal stress. Any other tunnel direction would result in smaller effects. Note that the horizontal heat transport between tunnels and the vertical heat transport dominate heat dissipation from the individual canisters, whereas heat transport along tunnels is relatively unimportant.

Considering all of the above, it is suggested that the maximum bentonite temperature should be calculated without regard to anisotropy and that effects of anisotropy should be accounted for in the repository layout by including an extra 0.7–2.3ºC margin in the total uncertainty margin, depending on the degree of anisotropy established for the rock domain being considered.

For Laxemar the anisotropy in thermal conductivity due to foliation is estimated to about 15% /Sundberg et al. 2008/. However, the magnitude and orientation of the anisotropy will vary within the Laxemar area due to variations in the degree of development and orientation of the foliation /Sundberg et al. 2008/.

B6 References

Back P-E, Wrafter J, Sundberg J, Rosén L, 2007. Thermal properties. Site descriptive modelling. Forsmark – stage 2.2. SKB R-07-47, Svensk Kärnbränslehantering AB.

Carslaw H S, Jaeger J C, 1959. Conduction of Heat in Solids, 2nd ed. Oxford University Press.

Hökmark H, Fälth B, 2003. Thermal dimensioning of the deep repository. SKB TR-03-09, Svensk Kärnbränslehantering AB.

Itasca, 2005. FLAC – Fast Lagrangian Analysis of Continua, User's guide. Itasca Consulting Group, Inc. Minneapolis.

Sundberg J, Wrafter J, Back P-E, Rosén L, 2008. Thermal properties Laxemar. Site descriptive modelling SDM Site Laxemar. SKB R-08-61, Svensk Kärnbränslehantering AB.

Emissivity of copper from electron beam welds

UPPSALA
UNIVERSITET

Lars Werme
Svensk Kärnbränslehantering AB
Box 5864
102 40 Stockholm

October 2003

Re.: The emissivity of copper from electron beam welds.

We have received four samples from electron beam welded copper canisters from SKB's canister laboratory for measuring of emissivity of copper. Two of the samples were marked TL18 and the other two were marked TL40, showing that the samples came from Tube Lids number 18 and 40. In order to separate from each other the the two sample from each lid, we relabelled them TL18a, TL18b, TL40a, and TL40b, respectively.

The copper samples were discoloured by a covering oxide layer and had to the eye a dull, non-shiny, appearance. We measured the emissivity in the infrared spectral region with a Bomem Michelson 110 FTIR spectrometer using a gold coated integrating sphere. As a reference, we used highly polished copper, which we assumed had an emissivity of 0.02. The resulting room temperature emissivities for the canister lid samples are listed in the table. The reflectance outside the measured interval was extrapolated and assumed to be constant and equal to the last measured value.

TL18a	0.11
TL18b	0.06
TL40a	0.09
TL40b	0.11

Arne Roos

Prof. Arne Roos
Dept of Engineering Sciences
Box 534, S-751 21, Uppsala, Sweden
Telephone +46 18 4713130
Telefax +46 18 500131
e-mail arne.roos@angstrom.uu.se

Appendix D

Analytical solution – approximate account of spatial variability

D1 General

In the analytical temperature calculations (see main text), each canister is assumed to be situated in an infinite volume of rock with uniform thermal conductivity. If that was the actual case at the repository sites, the nomographic charts produced by use of the analytical solution could be utilized directly to establish the minimum canister spacing required (everywhere) to satisfy the 100°C criterion, provided that relevant values (one conductivity value and one capacity value) of the heat transport properties are known. All canisters (except those at the tunnel ends/beginnings) would have the same peak buffer temperature.

In reality there will be spatial variations in rock thermal properties. Figure D-1 shows 5-m scale thermal conductivity distribution examples from two Forsmark rock domains (RFM029 and RFM045) /Back et al. 2007/. Basing the canister spacing on the rock domain mean value would mean that the 100°C criterion would be met for the majority of the canisters, but not for canisters deposited in low-conductivity portions of the domain.

The problem is to establish the minimum spacing that ensures that the criterion is met for all canisters. Dimensioning for the lowest conductivity found in the rock domain distribution would obviously be sufficient. Because of the small volume fraction occupied by low-conductivity rocks, this is likely to give a peak temperature much below the threshold even for the hottest canisters. Figure D-2 shows, using Rock domain RFM045 in Forsmark as an example, the spacing corresponding to the mean value, the mean value minus two and three units of standard deviation, and the spacing corresponding to the lowest value found in the distribution. Dimensioning for the lowest value (2.3 W/(m·K) would require a spacing of 8.5 m, whereas the mean would require only 5.3 m.

D2 Approximate approach

The heat transport in the interior of the deposition holes is practically independent of the layout and of the rock heat transport properties. The temperatures depend, however, on the boundary conditions, i.e. on the rock temperature at the wall of the deposition hole. The temperature increase at the deposition hole wall can be decomposed into two contributions

1. That from the local canister.
2. That from the rest of the repository.

The local contribution is determined mainly by how well the nearest rock surrounding the deposition hole dissipates the locally generated heat, whereas the contribution from the rest of the repository depends on properties averaged over much larger volumes. At the time of the temperature peak (about 10 years after deposition), the local contribution is about 45% (Figure D-3, left). This means that 55% of the rock

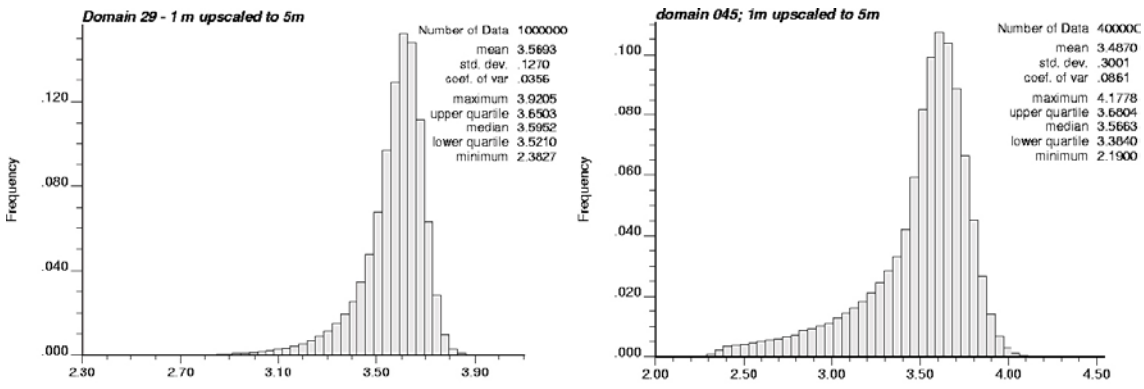

Figure D-1. *Distribution of thermal conductivity for Rock domains RFM029 and RFM045 at Forsmark. From /Back et al. 2007/.*

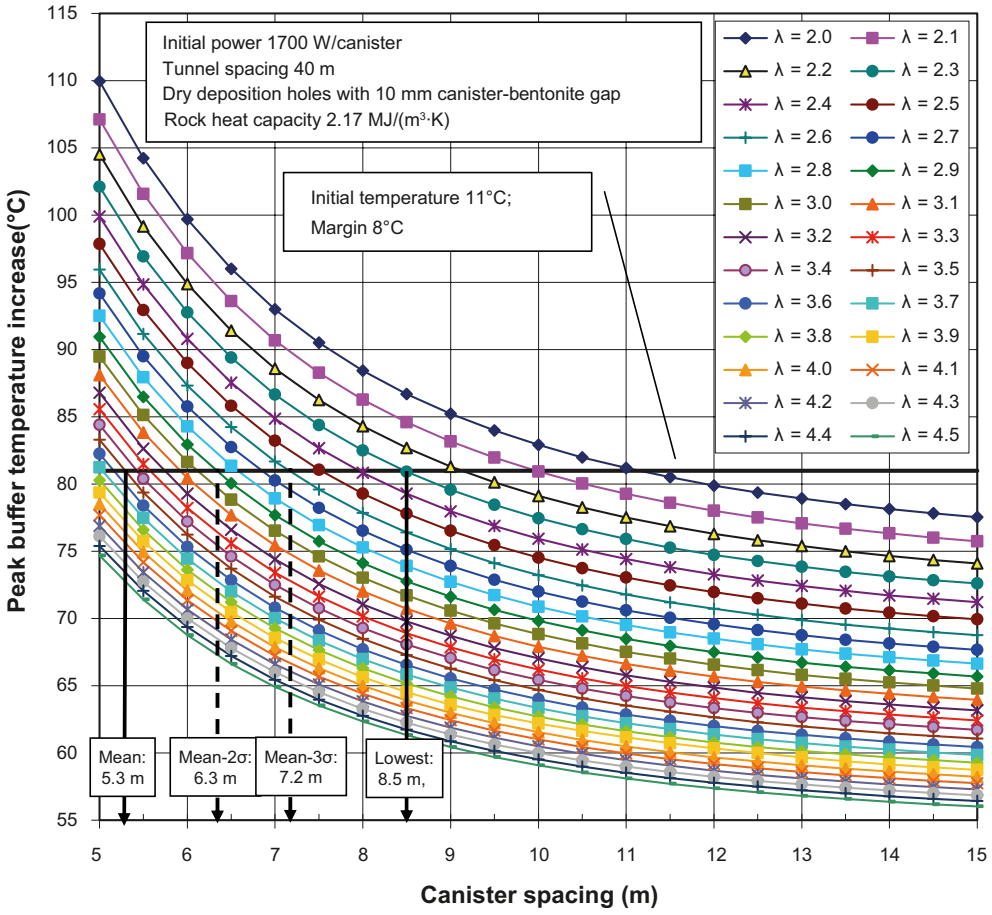

Figure D-2. *Spacing required in Rock domain RFM045 for different choices of the dimensioning conductivity assuming the initial temperature to be 11°C and the margin required to cover uncertainties and model simplifications to be 8°C.*

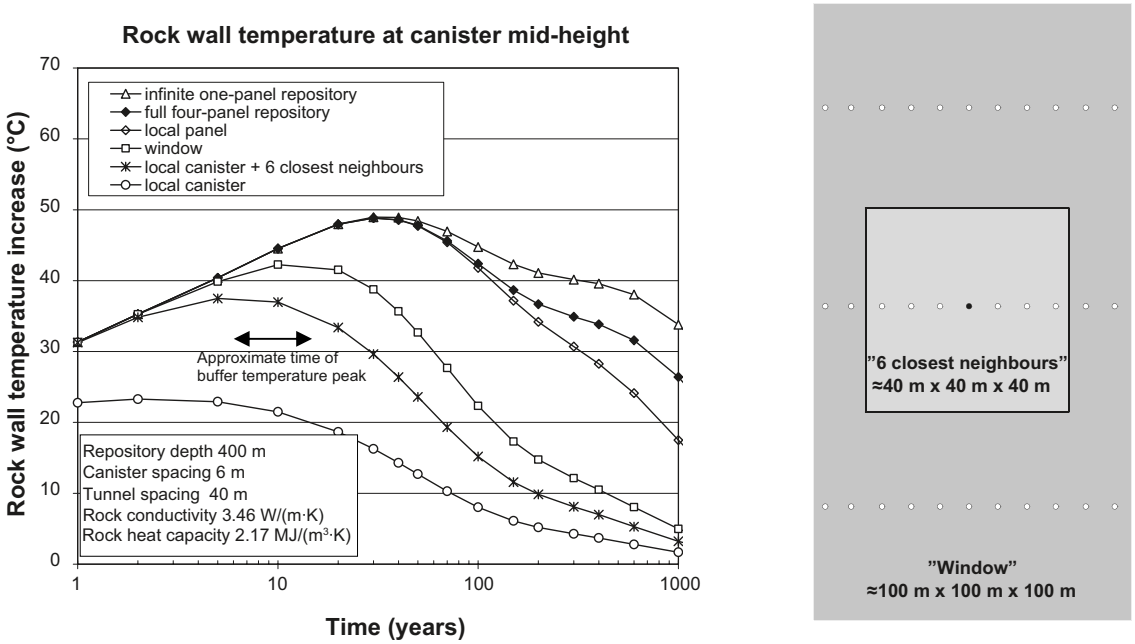

Figure D-3. *Left: rock wall temperature evolution (analytical results, cf. main text). At the time of the buffer temperature peak some 10 years after deposition, about 45% of the increase is due to the local canister. The majority of the remaining 55% is due to the 6 closest neighbors. Right: regions around local canister.*

wall temperature increase at that time is practically independent of the properties of the local rock embedment. The majority of the 55% contribution is due to the six closest neighbour canisters, meaning that the relevant volume for averaging should be at least about 40 m · 40 m · 40 m (cf. Figure D-3, right).

The site models give distributions on the 5 m scale and smaller, but not on the 40 m scale or larger. Up-scaling from 5 m to 40 m would cut the low tail part of the distribution, meaning that (taking Rock domain RFM045, cf. Figure D-1, right, as an example) the effective worst-case conductivity would increase from 2.3 W/(m·K) to a larger or much larger value. Assuming that the worst case conductivity on the 40 m scale corresponds to the mean value minus 1–3 units of standard deviation gives a conductivity range of 2.6–3.2 W/(m·K). Figure D-4 shows analytically calculated peak buffer temperatures as functions of the canister spacing for two cases of homogenous conditions: λ = 3.5 W/(m·K) and λ = 2.3 W/(m·K). These values correspond (approximately) to the mean value and to the minimum value (5 m-scale, cf. Figure D-1, right). The three mixed conductivity curves are additions of the local canister contribution, calculated for λ = 2.3 W/(m·K), to the contribution of all remaining canisters, calculated for three different values of λ. Note that theses curves are approximations based on mixed solutions, not regular calculation results: addition of the two solutions (the-one-canister solution and the rest-of-the-repository solution) is not a proper superposition. Note also that the mixed solutions approach the regular homogeneous solution when the canister spacing increases. This is because the contribution from canisters other than the local one (at the time of the peak temperature) decreases with spacing.

Assuming the effective conductivity of the worst case 40 m · 40 m · 40 m volume to be between 2.6 and 3.2 W/(m·K), i.e. between three and one units of standard deviation below the mean, it appears that the analytical homogenous solution overestimates the peak buffer temperature of a canister deposited in worst-case low-conductivity rock by at least 3-4°C (cf. Figure D-4, left).

There is a built-in overestimate in the mixed solution. The local canister contribution (cf. Figure D-4, upper right) of that solution must be modified to account for the finite extension of the low-conductivity rock surrounding the local canister. Figure D-5 shows results from numerical calculations (using the 2D finite difference program FLAC /Itasca 2005/) of the temperature distribution around a single canister, either embedded in rock with uniform thermal conductivity (2.3 W/(m·K)) or in rock where the volume closest to the canister (1,400 m^3) has a thermal conductivity of 2.3 W/(m·K) and the remaining rock a higher value. Accounting for the higher conductivity outside the 1,400 m^3 nearest surrounding reduces the rock wall temperature by about 1–1.5°C. Here it is again assumed that the outside conductivity ranges between 2.6 W/(m·K) and 3.2 W/(m·K), i.e. between three and one units of standard deviation below the mean.

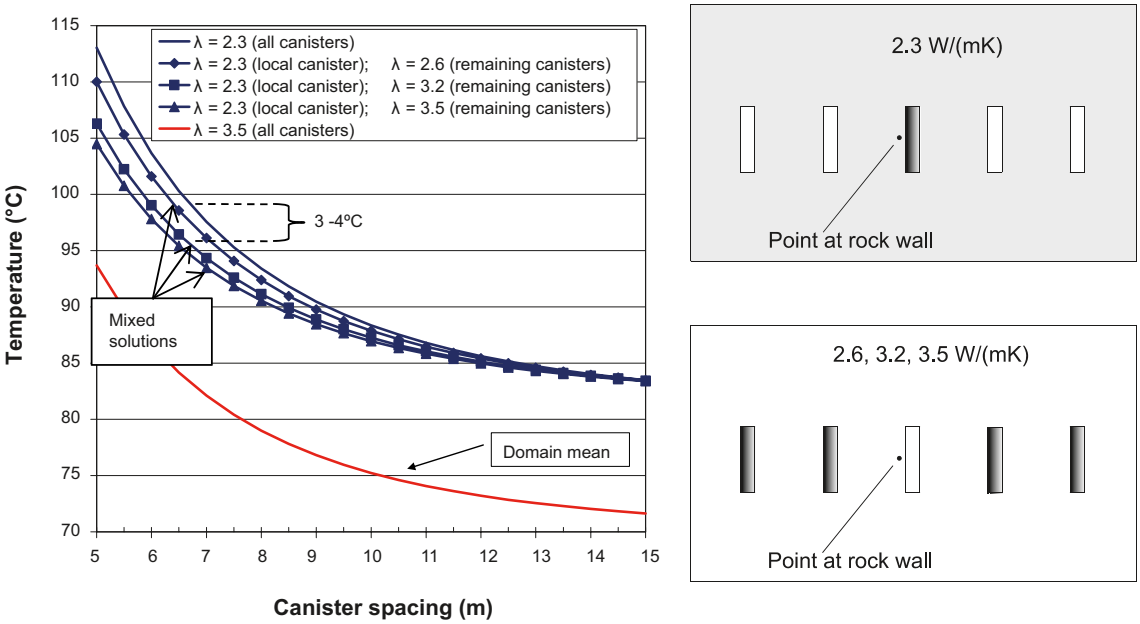

Figure D-4. *Left: Mixed solution estimates of the peak bentonite temperature. Right: schematics of solutions being mixed.*

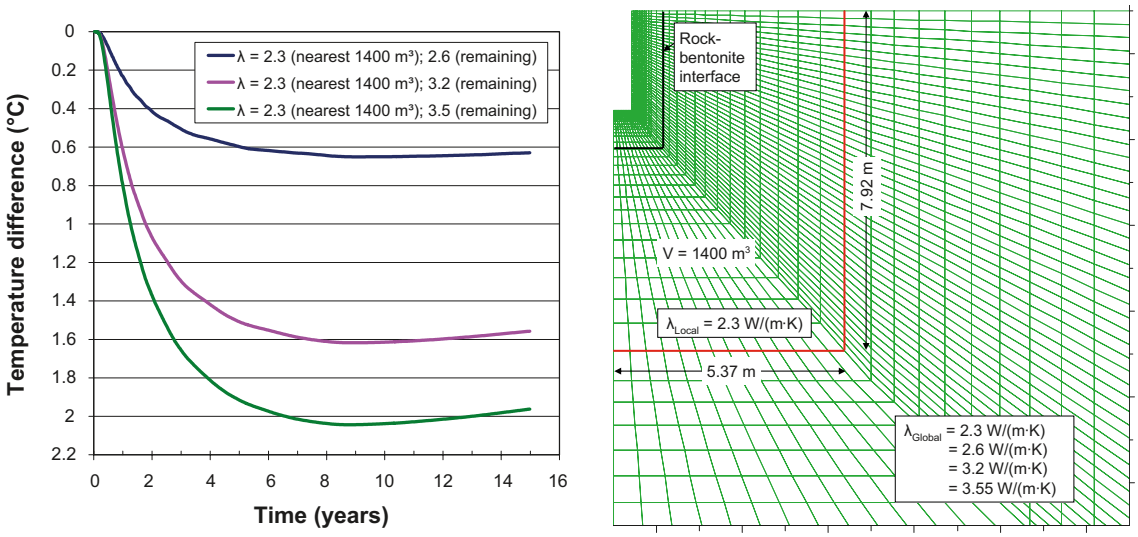

Figure D-5. *Temperature difference on the deposition hole wall between the case of uniform (low) thermal conductivity everywhere and low thermal conductivity in the volume nearest to the canister and a higher global value elsewhere (left). The higher conductivity in the enclosing volume reduces the rock wall temperature by 0.5–2°C for the cases pictured here. Schematic view of the numerical FLAC model (right).*

This gives a total temperature reduction of at least about 4.5°C for a canister deposited in rock belonging to the low-conductivity tail of the distribution. The analytically calculated peak bentonite temperatures with uniform thermal conductivity can now be scaled such that the temperatures are reduced by 4.5°C for a thermal conductivity of 2.3 W/(m·K) and correspondingly increased/reduced for other values of the local conductivity.

A model for temperature correction to be applied on the peak buffer temperature is suggested in Equation D-1, where λ is the thermal conductivity and $f(\lambda)$ is the corresponding cumulative frequency of the thermal conductivity in a given rock domain.

$$T_{corr}(\lambda) = 6.7 \cdot \left(\text{abs}\left(\frac{\lambda - \lambda_{mean}}{2.0 - \lambda_{mean}} \right) \cdot \left(\left(\frac{100 - f(\lambda)}{100} \right)^{0.3} - \left(\frac{f(\lambda)}{100} \right)^{0.3} \right) \right) \qquad \text{D-1}$$

By construction, the correction is zero for the mean conductivity and very small for conductivities near the mean. Here, the parameters are calibrated to give a 4.5°C reduction for the lowest conductivity reported for the 5-m scale at Forsmark. Examples are shown in Figure D-6 (lower). Lines with filled symbols represent uncorrected peak temperature distributions derived from the analytical solution, i.e. the small fraction of canisters deposited in rock with a conductivity of 2.3 W/(m·K) will have peak temperatures as if the they were part of a uniform 2.3 W/(m·K) repository. Similarly, the fraction of canisters deposited in, for instance, 4.0 W/(m·K) rock will have peak temperatures as if they were part of a uniform 4.0 W/(m·K) repository. The effect of the correction is to cut the tails and account for the mixed conductivity effects as described above (lines with unfilled symbols). The distributions used to generate the curves are shown in the top part. These are derived from /Back et al. 2007/, cf. Figure D-1.

D3 Result examples – Forsmark

The resulting temperature distributions are presented in Figure D-7, Figure D-8, Figure D-9 and Figure D-10. No distribution of canisters between the two rock domains has been done, i.e. all results are presented for 6,000 canisters.

The peak buffer temperature distribution with and without account of temperature corrections are shown in Figure D-7 and Figure D-8, respectively (Rock domain RFM029, Forsmark). To get less than one canister (out of 6,000) with peak temperature above the threshold, the canister spacing must be between 6 and 6.5 m (Figure D-8), say 6.25 m.

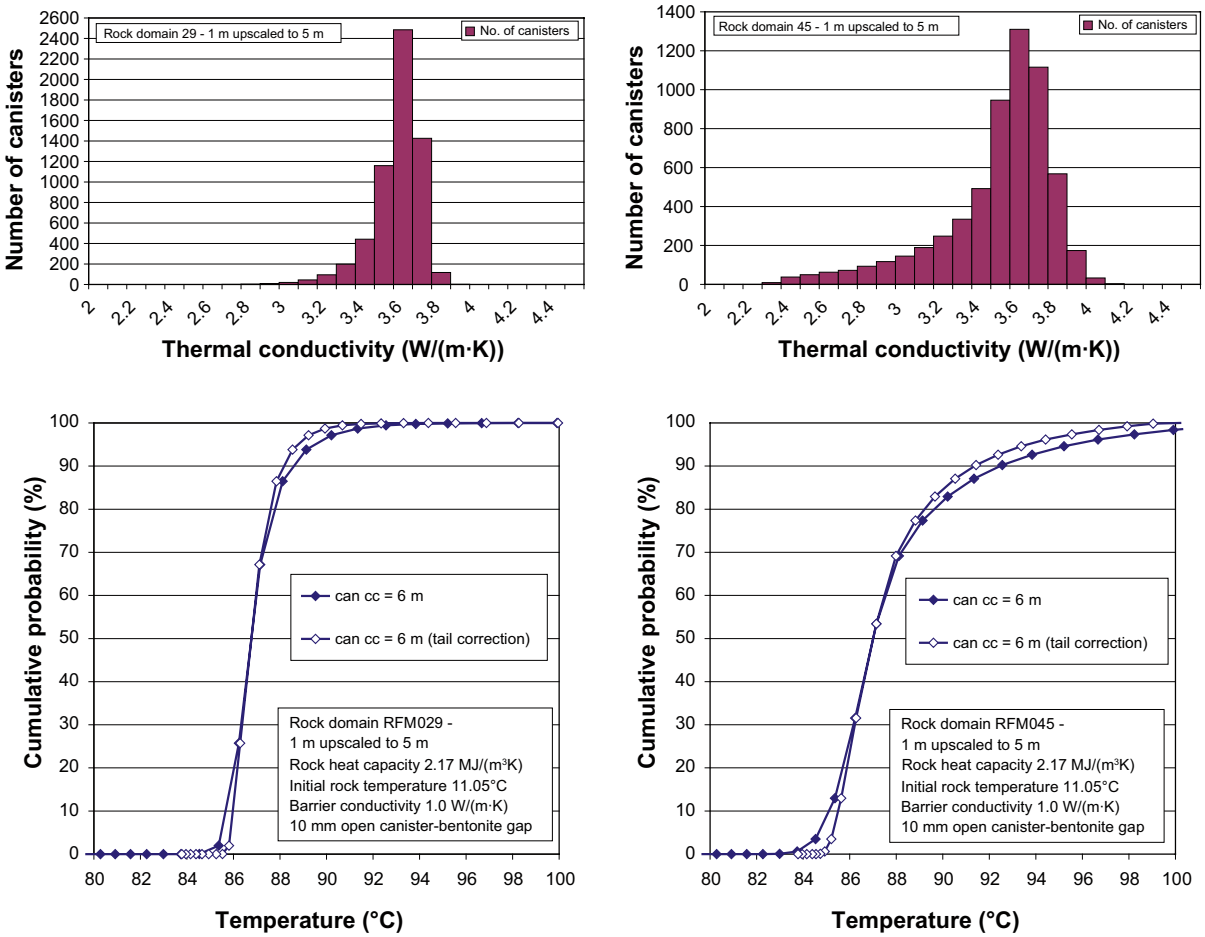

Figure D-6. *Top: Distribution of thermal conductivity in Rock domain RFM029 (left) and Rock domain RFM045 (right), modified from /Back et al. 2007/. Bottom: Corresponding effects on temperature distribution of a weighted frequency and deviation from domain mean in Rock domain RFM029 (left) and Rock domain RFM045 (right).*

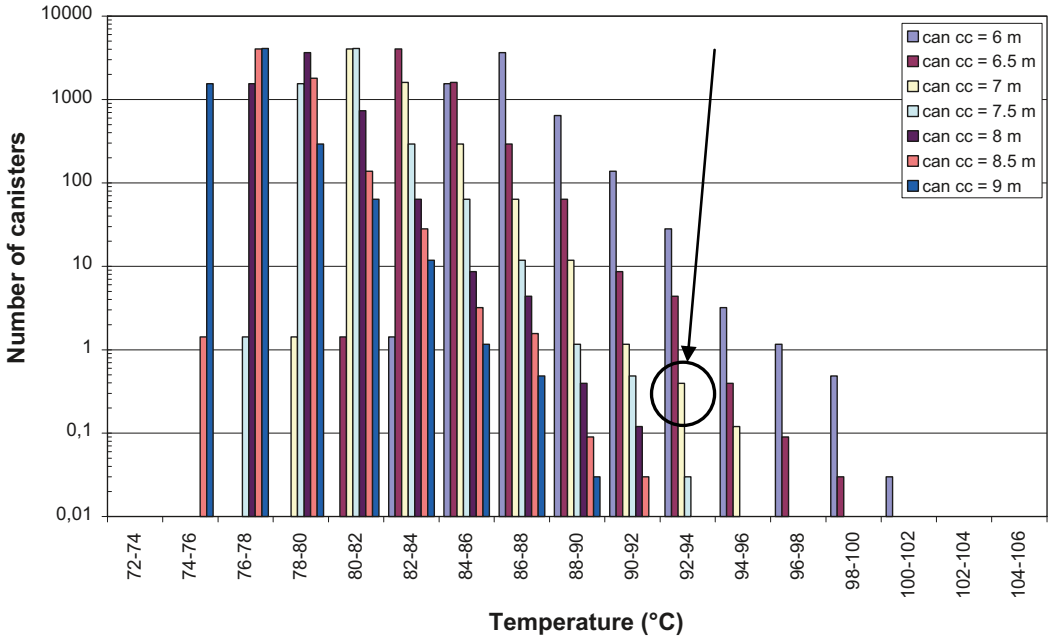

Figure D-7. *Rock domain RFM029: Initial power (all 6,000 canisters) = 1,700 W. In situ temperature (450 m) = 11.05°C. No corrections. To bring the number of canisters with peak temperatures above the 92°C threshold below one, the spacing must be about 7 m (circled).*

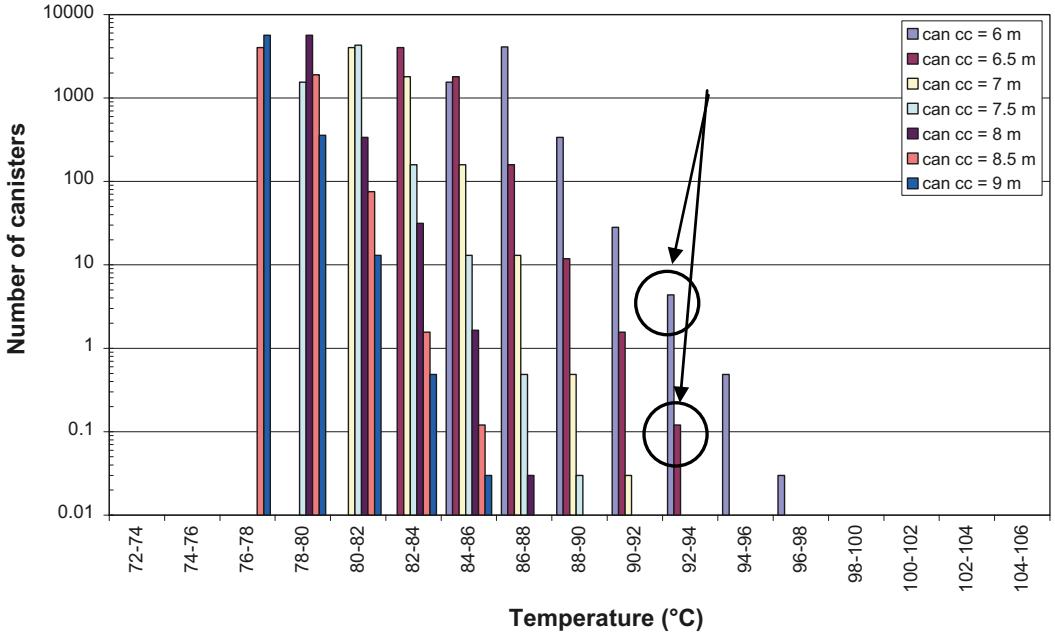

Figure D-8. *Rock domain RFM029: Initial power (all 6,000 canisters) = 1,700 W. In situ temperature (450 m) = 11.05°C. Correction for tail-effects. To bring the number of canisters with peak temperatures above the 92°C threshold below one, the spacing must be between 6 and 6.5 m (circled).*

Figure D-9 and Figure D-10 show corresponding results for Rock domain RFM045. To get less than one canister (out of 6,000) with peak temperature above the threshold, the canister spacing must be between 7 and 7.5 m (Figure D-10), say 7.25 m. Having established a preliminary spacing, the corresponding conductivity, a "guess" dimensioning conductivity, can be obtained from the nomographic chart.

Table D-1 summarizes the results found here for Forsmark. Note that these results are approximate examples.

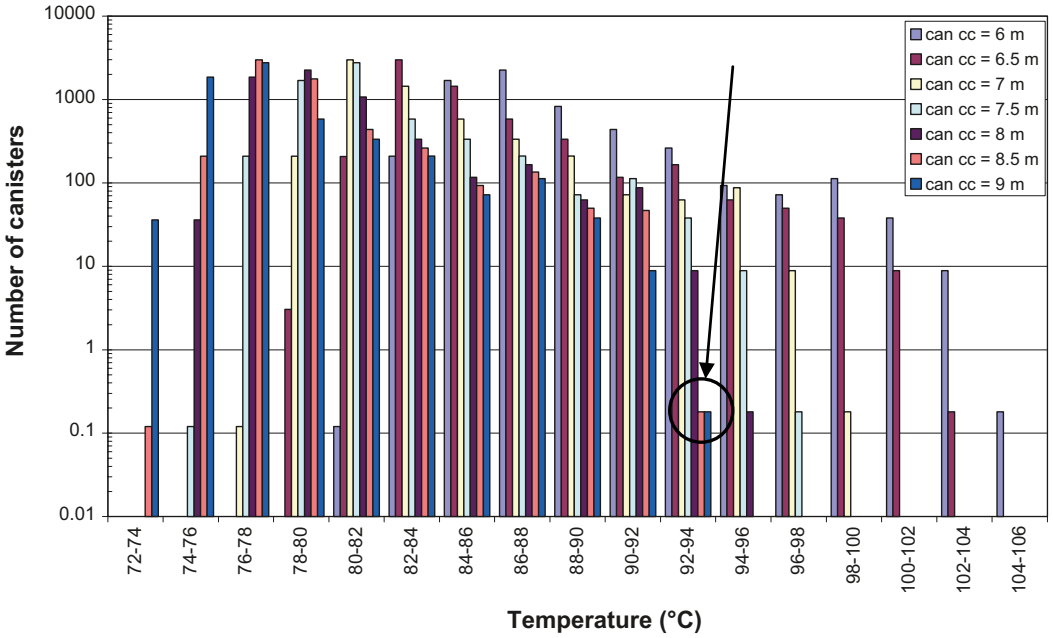

Figure D-9. *Rock domain RFM045: Initial power (all 6,000 canisters) = 1,700 W. In situ temperature (450 m) = 11.05°C. No corrections. To bring the number of canisters with peak temperatures above the 92°C threshold below one, the spacing must be at least 8.5 m (circled).*

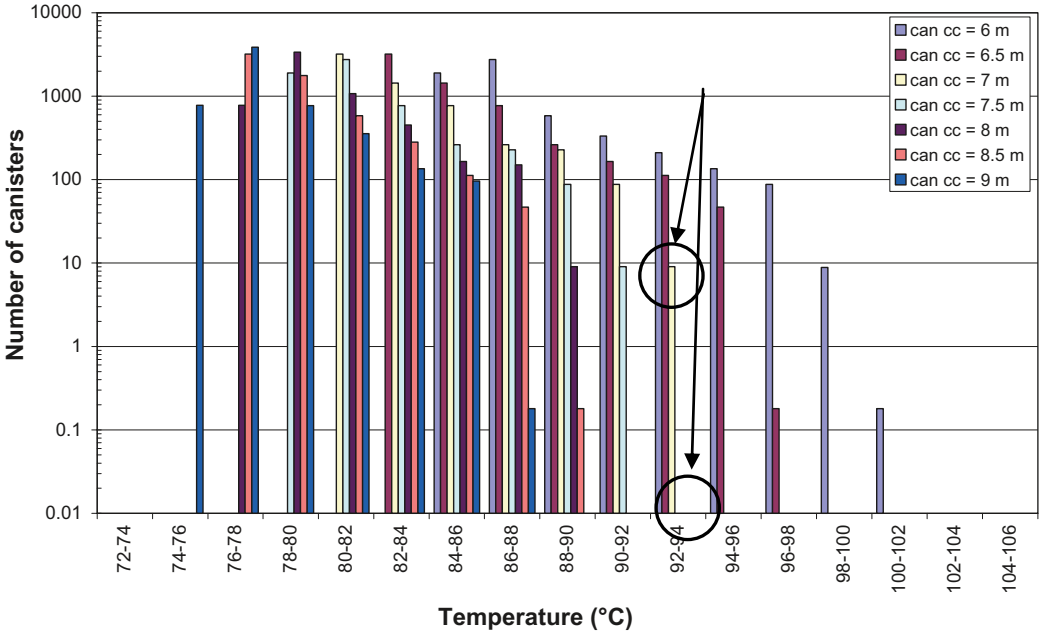

Figure D-10. *Rock domain RFM045: Initial power (all 6,000 canisters) = 1,700 W. In situ temperature (450 m) = 11.05°C. Correction for tail-effects. To bring the number of canisters with peak temperatures above the 92°C threshold below one, the spacing must be between 7 and 7.5 m (circled).*

Table D-1. Summary of results.

Rock domain	Trial spacing	Guess conductivity	Percentile of the rock conductivity distribution
RFM029	6.25	3.0 W/(m·K)	0.1
RFM045	7.25	2.6 W/(m·K)	1.6

D4 Summary

The scheme suggested here for obtaining first estimates of the canister spacing required to meet the 100°C criterion for all canisters deposited in a rock domain with non-uniform heat transport properties is approximate. The basis of the approach is to recognize that the temperature increase at the local canister can be separated into contributions that depend on properties averaged over very differently sized volumes.

For the two Forsmark rock domains, the best guess conductivity, i.e. the conductivity that should be picked from the analytically generated nomographic spacing-conductivity chart to establish the minimum spacing, corresponds to the 0.1–1.6 percentiles of the conductivity distributions. The difference between the two rock domains is due the difference in the shape of the low-conductivity tails. This demonstrates that there is no generally valid percentile that could be used directly to pick the best guess value.

The approach has not been tried on conductivity distributions that are fundamentally different from those of the two Forsmark rock domains. The selection of parameters in the correction expression may have to be modified and the outcome, i.e. the dimensioning percentiles, may turn out to be different, but the principles should be the same.

D5 References

Back P-E, Wrafter J, Sundberg J, Rosén L, 2007. Thermal properties. Site descriptive modelling. Forsmark – stage 2.2. SKB R-07-47, Svensk Kärnbränslehantering AB.

Itasca, 2005. FLAC. Fast Lagrangian Analysis of Continua. User's Guide. Itasca Consulting Group, Inc. Minneapolis.

Spalling

During the excavation phase and the subsequent heat release from the deposited canisters, high stresses will develop around the deposition holes and potentially cause spalling in the highest stressed parts, cf. /Hökmark et al. 2006/. Here, quarter-symmetric horizontal FLAC models are used to simulate heat transfer in deposition holes with and without spalled zones in order to examine the possible influence of spalling on the rock wall temperature.

The spalled area is typically notch-shaped, see Figure E-1 (left), and may have lower thermal conductivity than the surrounding intact rock. In the APSE experiment /Andersson 2007/, the mean breakout angle was 32° and the total volume of spalled rock was about 0.1 m^3. The FLAC model is shown in Figure E-1 (right).

In the FLAC model, the spalled area is 0.1 m deep and has a breakout angle of 30°. The material properties are presented in Table E-1. The thermal conductivity of the copper material has been reduced for numerical efficiency. Note that the copper shell is thicker (0.2 m) than in a real canister in order to compensate for the conductivity reduction. The thermal conductivity of the spalled zone is set to 0.5 W/(m·K), following the expression given by /Woodside and Messmer 1961/ and assuming that the spalled rock porosity is not likely to exceed 40%, and that the spalled rock is dry, cf. Figure E-2.

The canister's initial power per unit length is 367.4 W/m (corresponding to 1,837 W/canister). Decay is as described in Appendix B.

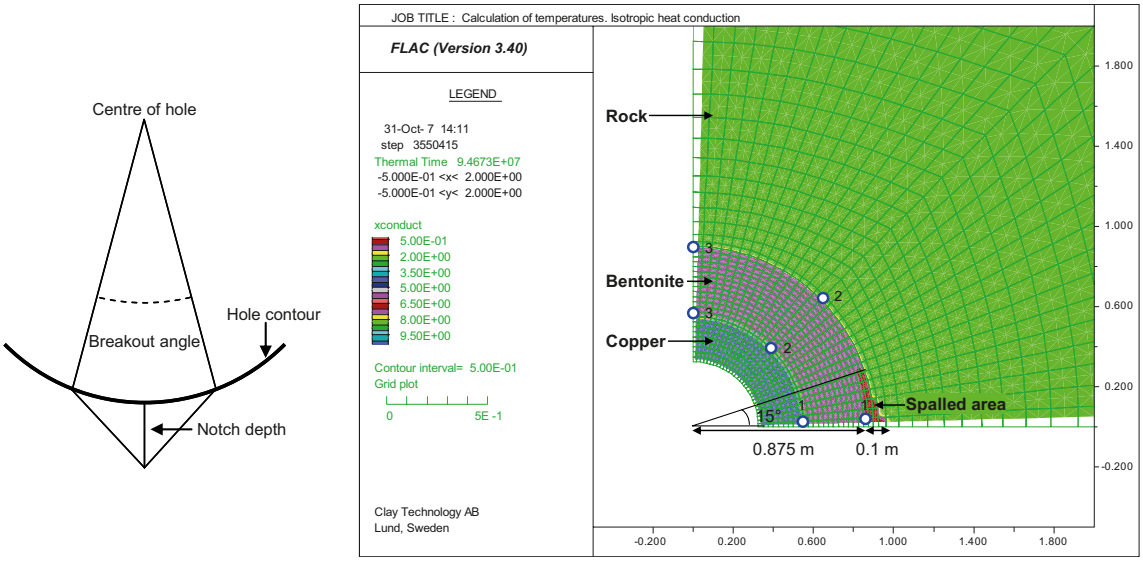

Figure E-1. *Left: Schematic view of shape of spalled area. Right: FLAC model of heat transport in deposition hole with notch-shaped shaped spalled zone. The temperature is monitored at three points at the canister/bentonite interface and at three points at the bentonite/rock interface.*

Table E-1. Material properties.

Material	Thermal conductivity [W/(m·K)]	Heat capacity [MJ/(m^3·K)]
Copper	3.0 (reduced for numerical efficiency)	3.48
Bentonite	1.0	5.00
Rock	2.30	2.08
	3.55	2.08
Spalled area	0.5	2.08

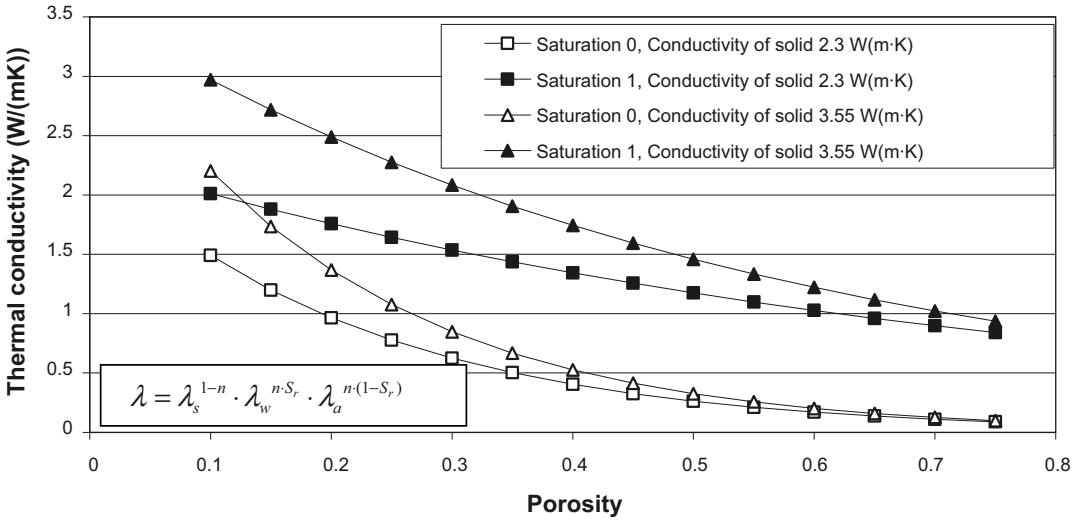

Figure E-2. *Thermal conductivity of porous medium as function of porosity (n) for different values of thermal conductivity of solid (λ_s), water (λ_w) and air (λ_a). Sr denotes degree of saturation. Expression from /Woodside and Messmer 1961/.*

Two different values of the rock thermal conductivity are tried: 2.30 W/(m·K) and 3.55 W/(m·K). The temperatures on the copper/bentonite interface and bentonite/rock interface are presented as functions of time in Figure E-3 and Figure E-4, respectively. The temperature at each point is compared with the corresponding value in a model with uniform thermal conductivity.

As seen in Figure E-3, the rock wall temperature in the spalled area (Point 1) increases by about 2.5°C compared with points outside this area as well as the case with uniform thermal conductivity.

The temperatures on the copper/bentonite interface, Figure E-4, vary by 0.1°C between Points 1 and 3. This small temperature difference is a result of the reduced value of the thermal conductivity of the copper material. The temperatures along the entire copper/bentonite interface are about 0.5°C higher in the spalled zone cases than in the cases with uniform thermal conductivity.

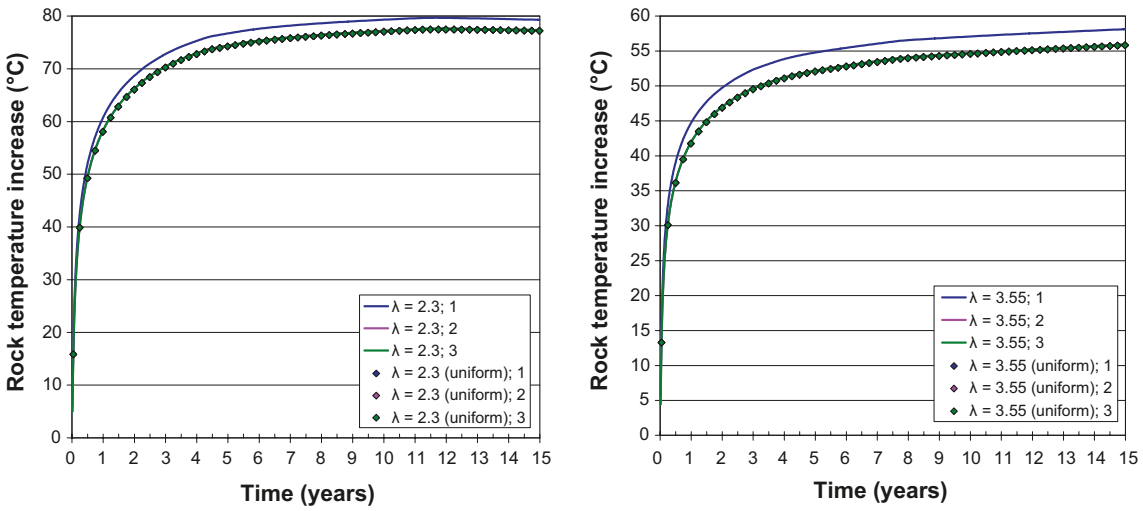

Figure E-3. *Bentonite/rock interface temperature increase for rock thermal conductivity 2.3 W/(m·K), left, and 3.55 W/(m·K), right. Solid lines represent models with spalled area, whereas the plot symbols represent models with uniform rock thermal conductivity.*

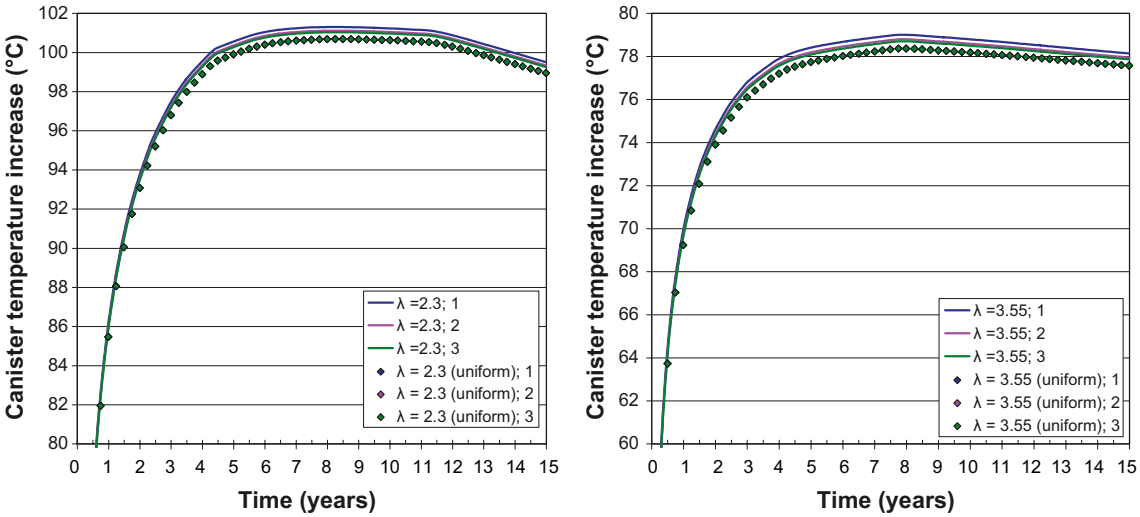

Figure E-4. *Canister/bentonite interface temperature increase for rock thermal conductivity 2.3 W/(m·K), left, and 3.55 W/(m·K), right. Solid lines represent models with spalled area, whereas the plot symbols represent models with uniform rock thermal conductivity.*

The temperatures calculated in the 2D models (and, consequently, the 0.5°C spalled zone effect) are greatly overestimated compared with the temperature distribution around a real cylindrical canister of finite length. The rock wall temperature increase for a real (individual) canister is about 40% of the increase found here (for comparable rock conductivities, cf. Figure E-3 and Figure 4-7 in the main text). This means that the spalled zone effect is about 0.2ºC. In practice it will be even smaller.

- Only parts of the wall are likely to spall, not the entire wall from top to bottom as implicitly assumed in the 2D representation and
- The spalled rock porosity is likely to be much smaller than 40%. /Andersson 2007/ found that the rock wall dilation was roughly 10% of the maximum notch depth, indicating that the spalled rock porosity is on the order of 10% and that the spalled rock conductivity should be about 1 W/(m·K) rather than 0.5 W/(m·K), cf. Figure E-2.

Because of the above, it is suggested that 0.1°C is a relevant estimate of the spalling effect, i.e. spalling is not expected to increase the canister temperature by more than 0.1°C.

References

Andersson C J, 2007. Äspö Hard Rock Laboratory. Äspö Pillar Stability Experiment, Final report. Rock mass response to coupled mechanical thermal loading. SKB TR-07-01, Svensk Kärnbränslehantering AB.

Hökmark H, Fälth B, Wallroth T, 2006. T-H-M couplings in rock. Overview of results of importance to the SR-Can safety assessment. SKB R-06-88, Svensk Kärnbränslehantering AB.

Woodside W, Messmer J M, 1961. Thermal conductivity of porous media. Journal of Applied Physics, vol 32, No 9.

Appendix F

Prototype Repository sensor readings

In deposition hole #6 in the Prototype Repository at the Äspö Hard Rock Laboratory, there is a 10 degree difference between thermocouple temperature readings and optic fibre temperature readings at the canister surface /Goudarzi and Johannesson 2006/ (Figure F-1, left). The optic fibre cable giving the lowest temperature failed some 300 days after test start. The signal from this particular cable did not differ by more than 4–5 degrees from the mid-height thermocouple results after 65 days (50 days of heating). It is proposed here that the thermocouple readings are correct and the optic fibre readings are overestimates. There are the following reasons:

- There is a significant difference between results obtained from different optic fibre cables installed in deposition hole #6 (cf. Figure F-1, left). This indicates that there is a general uncertainty in the calibration and/or in the cable function. Similar differences are found in hole #3.
- The Prototype thermocouples are of the same type and brand as those installed in the Temperature Buffer Test (TBT) experiment, conducted at the Äspö HRL. The spacing between thermocouples on the radial TBT temperature scan-lines is a few cm. The consistent results obtained from the individual thermocouples along the scan-lines, cf. Figure F-2 and /Goudarzi et al. 2007/, suggest that there is only little variability in the performance of this type of instrument.
- One additional (indirect) indication of the reliability of the thermocouple results is the behaviour of the thermocouple installed at the inner buffer boundary in hole #6. Some 170 days after test start this thermocouple seems to have displaced and got in contact with the canister surface (cf. Figure F-1, right). From day 170 and onwards this thermocouple and the one installed on the surface show practically identical temperatures. This strengthens the confidence in the thermocouple results.

Note that the thermocouple temperatures shown in Figure F-1 (right) after 65 days (50 days of heating) are identical to those shown in Figure 3-6 and Figure 3-7 in the main text.

Figure F-3 shows the way the Prototype thermocouples are attached to the canister surface. There does not appear to be any risk that the thermocouple could show any other temperature than that of the surface (for instance the air temperature a few mm outside the surface), as long as the protruding sensor head does not get in contact with the solid, conducting bentonite material.

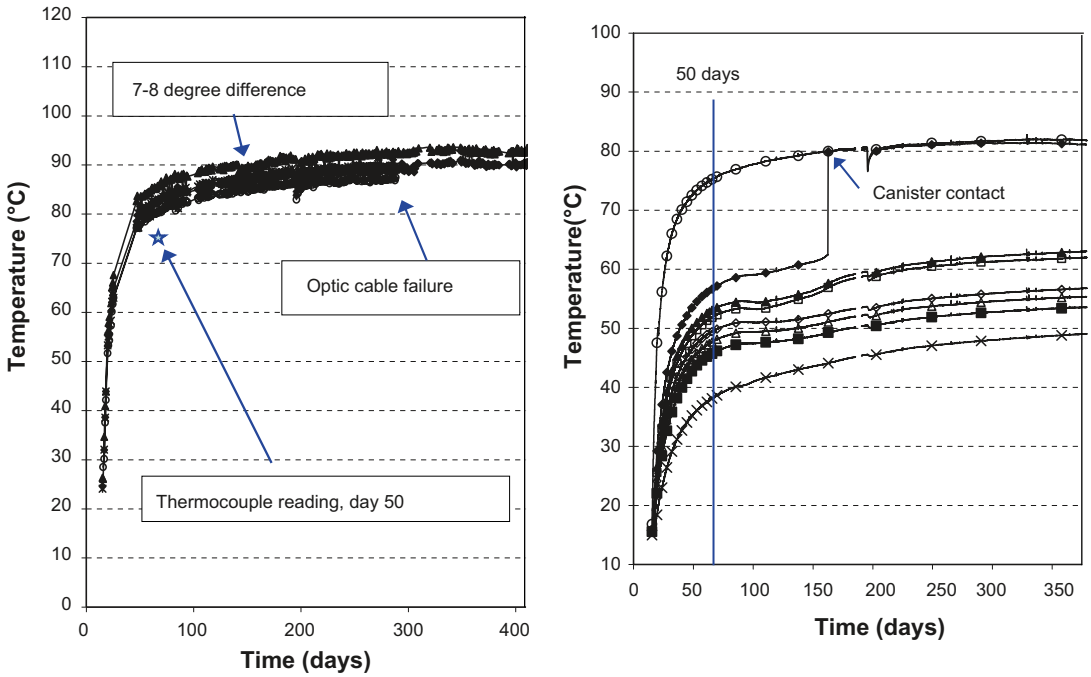

Figure F-1. *Left: Optic fibre results of max surface temperature. Optic fibre results are between 5 and 12 ºC higher than the thermocouple result. Right: Thermocouple readings at different radial distances from the canister surface. Both figures modified from /Goudarzi and Johannesson 2006/.*

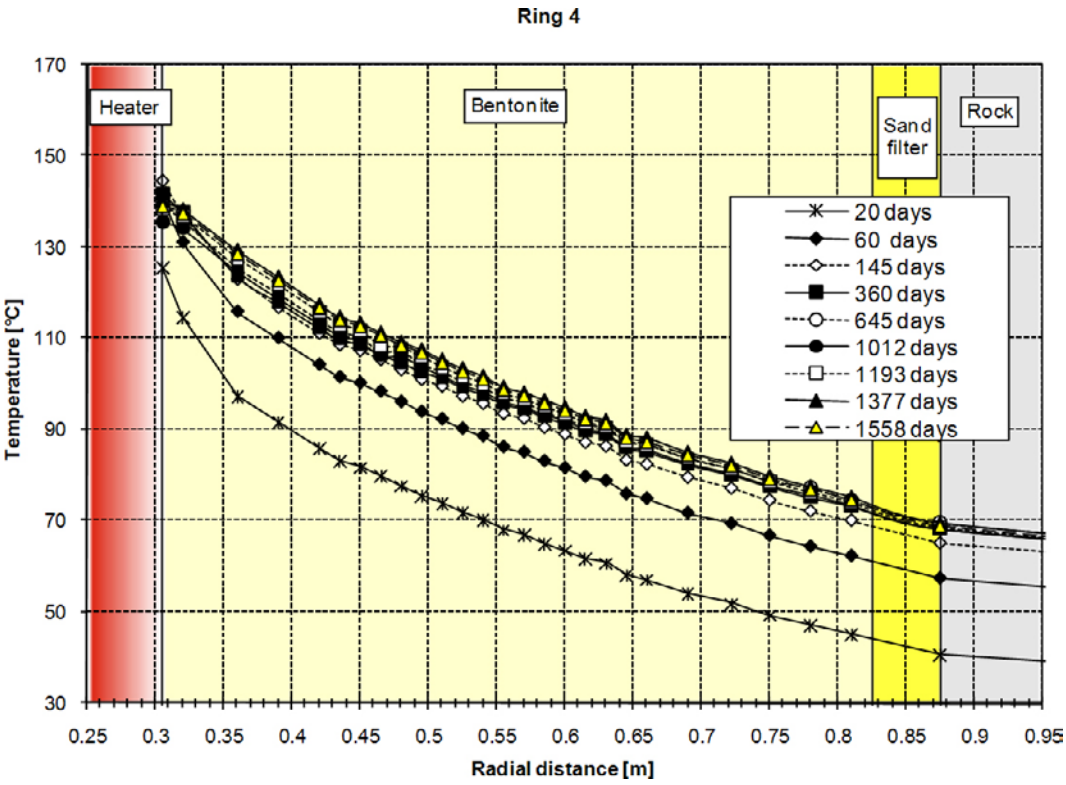

Figure F-2. *Thermocouple readings in TBT experiment at Äspö HRL. From /Goudarzi et al. 2007/.*

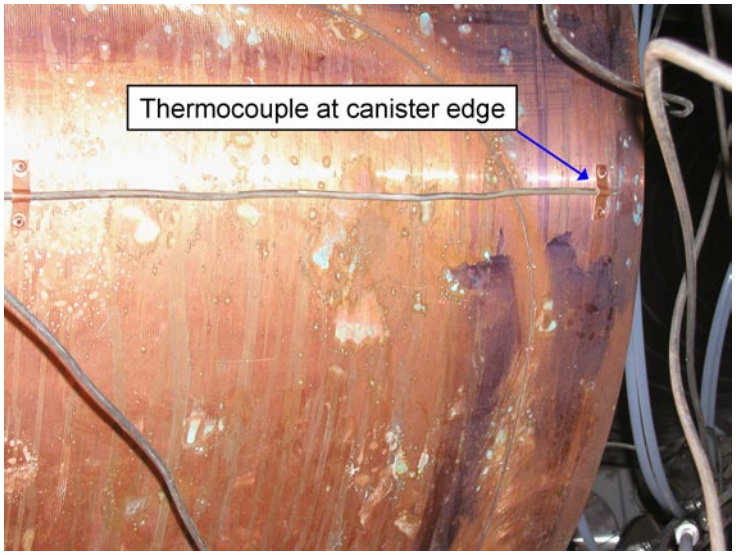

Figure F-3. *Thermocouple fixed to the canister surface.*

References

Goudarzi R, Börgesson L, Hökmark H, 2007. Äspö Hard Rock Laboratory. Temperature Buffer Test. Sensors data report (Period 030326–070701) Report No:10. SKB IPR-07-21, Svensk Kärnbränslehantering AB.

Goudarzi R, Johannesson L-E, 2006. Äspö Hard Rock Laboratory. Prototype Repository. Sensors data report (Period 010917–051201) Report No:14. SKB IPR-06-08, Svensk Kärnbränslehantering AB.